THE DEVELOPMENT AND APPLICATION OF CHEMICAL TOOLS TO STUDY QUORUM SENSING IN STAPHYLOCOCCI

By

Tian Yang

A dissertation submitted in partial fulfillment of

the requirement for the degree of

Doctor of Philosophy

(Chemistry)

at the

UNIVERSITY OF WISCONSIN – MADISON

2018

Date of final oral examination: January 10, 2018

The dissertation is submitted to the following members of the Final Oral Committee:

Helen E. Blackwell, Professor, Chemistry
Samuel H. Gellman, Professor, Chemistry
David M. Lynn, Professor, Chemical and Biological Engineering
Andrew R. Buller, Assistant Professor, Chemistry

THE DEVELOPMENT AND APPLICATION OF CHEMICAL TOOLS TO STUDY QUORUM SENSING IN STAPHYLOCOCCI

Tian Yang

Under the supervision of Professor Helen E. Blackwell

At the University of Wisconsin – Madison

ABSTRACT

Bacteria use quorum sensing (QS) to monitor their population density and coordinate group behaviors at high cell number. In the Gram-positive pathogens *Staphylococcus aureus* and *Staphylococcus epidermidis*, QS plays important roles in virulence regulation. Both pathogens use the accessory gene regulator (*agr*) system for QS. Central to the activation of the *agr* system is the interaction between the autoinducing peptide (AIP) signal and its cognate receptor AgrC. The *agr* system has received attention as a potential target for attenuating staphylococcal infections. However, the role of *agr* system in pathogenesis is complex, and more in-depth investigation is needed to assess its viability as a therapeutic target. Chemical modulators of the *agr* system could be valuable tools for such investigations.

While a number of synthetic ligands for the *agr* system in *S. aureus* have been developed, the majority of them are derived from *S. aureus* AIPs and possess drawbacks that limit their application in physiologically relevant settings. Chemical modulators targeting *S. epidermidis* QS are much fewer in number. The development of new and improved chemical tools is needed to better evaluate the impact of modulating staphylococcal QS in colonization and infection.

The investigations detailed in this dissertation focus on (i) chemical tools for the interception of *S. epidermidis* QS and (ii) strategies to render *S. aureus agr* modulators more amenable to biological applications. Towards the first goal, we performed the first structure-activity relationship (SAR) study of the three native *S. epidermidis* AIPs. In the process, we uncovered a number of *agr* modulators with varying activities and selectivities. Structural analyses of select

modulators allowed us to propose a model for receptor activation for one of *agr* systems in *S. epidermidis*, and aided us in the development of a first set of agonists capable of activating all *agr* systems in *S. epidermidis*. Towards the second goal, we modified known *agr* modulators or embeded these modulators in materials for sustained release in order to improve their solubilities and stabilities. Both approaches have enabled the application of *agr* modulators in biological studies. Together, this research represents a step forward in understanding QS signaling in staphylococci.

_____

Helen E. Blackwell

TABLE OF CONTENTS

ABSTRACT i

TABLE OF CONTENTS iii

LIST OF FIGURES AND TABLES vii

CHAPTER 1: Overview and Thesis Outline 1
1.1 Quorum sensing in staphylococci: overview 2
1.1.1 What is quorum sensing? 2
1.1.2 The accessory gene regulator quorum sensing system in staphylococci 4
1.1.3 The agr system plays important roles in regulating virulence of the human pathogens S. aureus and Staphylococcus epidermidis 6
1.1.4 Development of chemical modulators of the agr system 10
1.1.5 Limitations of AIP analogs as agr modulators and efforts to overcome them 11
1.1.6 Competition between staphylococcal species and the role of the agr system 12
1.2 Efforts to expand, improve, and apply the chemical toolset for targeting quorum sensing in staphylococci 13
1.2.1 Overview 13
1.2.2 Development of novel AgrC modulators in S. epidermidis 14
1.2.3 Strategies to improve AgrC modulators in S. aureus 15
1.3 Dissertation scope 16
1.3.1 Chapter 2: Staphylococcus epidermidis Autoinducing Peptide I Structure-Function Analyses Reveals Motifs Critical for Modulation of AgrC Receptors 16
1.3.2 Chapter 3: Structural Characterization of Peptidic Modulators of the Staphylococcus epidermidis Quorum Sensing Receptor AgrC-I 17
1.3.3 Chapter 4: Development of Synthetic Pan-Group Agonists of the Quorum Sensing Receptor AgrC in Staphylococcus epidermidis 18
1.3.4 Chapter 5: Highly Stable, Amide-Bridged Autoinducing Peptide Analogues that Strongly Inhibit the AgrC Quorum Sensing Receptor in Staphylococcus aureus . 19
1.3.5 Chapter 6: Non-Woven Polymer Nanofiber Coatings that Inhibit Quorum Sensing in Staphylococcus aureus: Toward New Non-Bactericidal Approaches to Infection Control 19
1.3.6 Appendix I: Investigation of the role of agr interference in competition between Staphylococcus aureus and Staphylococcus epidermidis in lab media 20
1.4 References 22

CHAPTER 2: *Staphylococcus epidermidis Autoinducing Peptide I Structure-Function Analyses Reveals Motifs Critical for Modulation of AgrC Receptors 31*
2.1 Abstract 32
2.2 Introduction 33
2.3 Results and Discussion 37
2.3.1 AIP-I SARs revealed through alanine and D-amino acid scans 37
2.3.2 SAR studies direct the design of second-generation AIP-I analogs 41
2.3.3 Agr group-selective inhibition in S. epidermidis by certain AIP analogs 44
2.3.4 Potent pan-group inhibitors of the agr system in S. epidermidis 46
2.3.5 Species-selective agr inhibition between S. epidermidis Group-I and S. aureus . 47
2.3.6 Modulation of biofilm formation in S. epidermidis Group-I using non-native AIPs . 48

2.4 Summary 51
2.5 Methods 53
2.5.1 Biological reagents, strains, and general methods 53
2.5.2 Peptide synthesis 54
2.5.3 Fluorescence reporter assay protocol 54
2.5.4 Crystal violet biofilm assay protocol 55
2.6 Supplementary Information 55
2.6.1 Chemical reagents and instrumentation 55
2.6.2 Peptide synthesis 56
2.6.3 HPLC traces for S. epidermidis AIPs and AIP analogs 58
2.6.4 S. epidermidis AgrC fluorescence dose response curves 66
2.7 Acknowledgements 78
2.8 References 79

CHAPTER 3: Structural Characterization of Peptidic Modulators of the *Staphylococcus epidermidis* Quorum Sensing Receptor AgrC-I 85
3.1 Abstract 86
3.2 Introduction 87
3.3 Results and Discussion 90
3.3.1 Selection of S. epidermidis AIP-I analogs 90
3.3.2 NMR analyses 91
3.3.3 Structural comparison of AIP-I to AIP-I V3A 91
3.3.4 Structural comparison of AgrC-I agonists with increasing potency 94
3.3.5 Comparison between the most potent AgrC-I agonist and antagonist 96
3.4 Summary 97
3.5 Methods 99
3.5.1 Chemical reagents and peptide synthesis 99
3.5.2 NMR methods and spectra analyses 99
3.6 Supplementary Information 100
3.6.1 NMR spectra 100
3.6.2 Chemical shift assignments 115
3.6.3 Constraint summaries 117
3.6.4 Structure ensembles 117
3.7 Acknowledgements 119
3.8 References 120

CHAPTER 4: Development of Synthetic Pan-Group Agonists of the Quorum Sensing Receptor AgrC in *Staphylococcus epidermidis* 125
4.1 Abstract 126
4.2 Introduction 127
4.3 Results and Discussion 130
4.3.1 Preliminary SARs of AIP-II and AIP-III 131
4.3.2 Incorporation of AgrC-I activating motifs into AIP-II scaffold 138
4.3.3 Activities of AIPII9aaP4Vtail AIPIring analogs 143
4.3.4 Activities of AIPII9aaP4V analogs 145
4.3.5 Optimization of the AIPII9aatail AIPIring scaffold 147
4.4 Summary 148
4.5 Methods 150
4.5.1 Biological reagents, strains, and general methods 150
4.5.2 Chemical reagents and instrumentation 150
4.5.3 Peptide synthesis 151

4.5.4 Fluorescence reporter assay 152
4.6 Supplementary Information 153
4.6.1 MS and HPLC data 153
4.6.2 HPLC traces for S. epidermidis AIP analogs 156
4.6.3 S. epidermidis AgrC fluorescence dose-response curves 172
4.7 Acknowledgements 190
4.8 References 192

CHAPTER 5: Highly Stable, Amide-Bridged Autoinducing Peptide Analogues that Strongly Inhibit the AgrC Quorum Sensing Receptor in *Staphylococcus aureus* 197
5.1 Abstract 198
5.2 Introduction 199
5.3 Results and Discussion 200
5.4 Methods 208
5.4.1 Chemical reagents and instrumentation 208
5.4.2 Peptide synthesis and purification 209
5.4.3 Biological reagents and strain information 211
5.4.4 Compound handling protocol 212
5.4.5 Fluorescence assay protocol 212
5.4.6 β-lactamase assay protocol 212
5.4.7 Peptide stability assay 213
5.4.8 General NMR methods 214
5.5 Supplementary Information 215
5.5.1 HPLC traces for AIP-III analogues 215
5.5.2 MS/MS analysis of select AIP-III analogues 217
5.5.3 Calculated log P values for representative peptides 218
5.5.4 Fluorescence antagonism dose response curves 219
5.5.5 Peptide stability studies 223
5.5.6 NMR chemical shift assignments, numbers of assigned ROEs, and RMSD values 225 224
5.5.7 Additional images of calculated peptide structures 225
5.6 Acknowledgements 228
5.7 References 229

CHAPTER 6: Non-Woven Polymer Nanofiber Coatings that Inhibit Quorum Sensing in *Staphylococcus aureus*: Toward New Non-Bactericidal Approaches to Infection Control 233
6.1 Abstract 234
6.2 Introduction 235
6.3 Results and Discussion 238
*6.3.1 Fabrication of Nanofiber Mats Containing Synthetic Peptide QSIs **1** and $\mathbf{1}_{FL}$ 238*
6.3.2 Characterization of QSI Release Profiles 241
6.3.3 QSI-Loaded Nanofiber Mats Inhibit QS in S. aureus 243
6.3.4 QSI-Loaded Nanofiber Mats Inhibit QS-controlled Hemolysis in Solution and at Surfaces 245
6.4 Summary 249
6.5 Methods 251
6.5.1 Materials 251
6.5.2 Instrumentation and Related Considerations 251
6.5.3 Biological Reagents and Strain Information 252
6.5.4 Fabrication of Non-Woven Nanofiber Mats 252
6.5.5 Characterization of Peptide Release Kinetics 252

6.5.6 Release of Peptides for Liquid Culture Assays *253*
6.5.7 GFP Reporter Assays *253*
6.5.8 Hemolysis Assays *254*
6.6 Supplementary Information 255
6.7 Acknowledgements 257
6.8 References 258

CHAPTER 7: Thesis Summary and Future Directions 264
7.1 Summary 265
7.2 Development of *S. epidermidis* pan-group agonists with improved efficacy 266
7.3 Application of QS inhibitor embedded electrospun nanofiber coatings in animal models of *S. aureus* infections 267
7.4 Expansion into other Gram-positive organisms 267
7.5 References 269

APPENDIX I: Investigation of the Role of *agr* Interference in Competition between *Staphylococcus aureus* and *Staphylococcus epidermidis* in Lab Media 270
Appendix I.1 Abstract 271
Appendix I.2 Introduction 272
Appendix I.3 Results and discussion 274
Appendix I.4 Conclusion and future direction 278
Appendix I.5 Methods 279
Appendix I.6 References 280

LIST OF FIGURES AND TABLES

CHAPTER 1: Overview and Thesis Outline 1
Figure 1.1. Diagram of a generic QS circuit 3
Figure 1.2. Scheme of the *agr* QS circuit 5
Figure 1.3. Primary structures of the native AIPs identified to date for (A) *S. aureus* and (B) *S. epidermidis* 6
Figure 1.4. Schematic of the biofilm lifecycle and the roles of the *agr* system 8

CHAPTER 2: *Staphylococcus epidermidis* Autoinducing Peptide I Structure-Function Analyses Reveals Motifs Critical for Modulation of AgrC Receptors 31
Figure 2.1. The *agr* QS system in *S. epidermidis* and associated AIP signals 34
Table 2.1. IC_{50} and EC_{50} values for alanine and D-amino acid scan analogs of *S. epidermidis* AIP-I in AgrC-I determined using a fluorescence reporter strain 39
Table 2.2. IC_{50} and EC_{50} values of second-generation AIP analogs in *S. epidermidis* AgrC-I determined using a fluorescence reporter strain 42
Figure 2.2. Pan-group activity profiles of selected *S. epidermidis* AIP-I analogs in *S. epidermidis* 45
Figure 2.3. AgrC antagonism dose response curves and IC_{50} values for (A) AIP-I D1AS6AV3A and (B) AIP-I D1AS6AV3AA5S in the *S. epidermidis* Group-I–III GFP reporter strains 47
Figure 2.4. Effects of selected AIP analogs on the AgrC-I receptor in *S. epidermidis* Group-I and the AgrC I–IV receptors in *S. aureus* Groups-I–IV 48
Figure 2.5. (Top) Biofilm antagonism dose response curves for S. epidermidis AIP-I and AIP-I D1AS6A against S. epidermidis Group-I RP62A strain as determined by CV staining (see Methods for assay procedure). (Bottom) Representative image of the CV assay with S. epidermidis AIP-I and AIP-I D1AS6A over a range of concentrations 50
Figure 2.6. Summary of the key SAR trends for activation of *S. epidermidis* AgrC-I by AIP-I as revealed by the reporter assays in this study 52
Table 2.3. MS and HPLC data for the native *S. epidermidis* AIPs and AIP analogs in this study. EM = exact mass. Rt = retention time 57
Table 2.4. IC_{50} values, EC_{50} values, and 95% confidence ranges for the active alanine and D-amino acid scan analogs of AIP-I in AgrC-I determined using fluorescence reporter strains 71
Table 2.5. IC_{50} values, EC_{50} values, and 95% confidence ranges for the second-generation *S. epidermidis* AIP analogs in AgrC-I determined using fluorescence reporter strains 72
Table 2.6. IC_{50} values and 95% confidence ranges for the potent pan-group *S. epidermidis agr* inhibitors against AgrC-II and AgrC-III determined using fluorescence reporter strains 73
Figure 2.7. Effects of alanine and D-amino acid analogs of *S. epidermidis* AIP-I on *S. epidermidis* AgrCs I–III at 10 μM as determined using fluorescence reporter strains 73
Figure 2.8. Effects of the second-generation *S. epidermidis* AIP analogs and *S. aureus* AIP-III D4A on *S. epidermidis* AgrCs I–III at 10 μM as determined using fluorescence reporter strains 74
Figure 2.9. Effects of selected *S. epidermidis* AIP analogs and *S. aureus* AIP-III D4A on *S.*

epidermidis AgrCs I–III as determined using fluorescence reporter strains 75
Figure 2.10. Effects of selected *S. epidermidis* AIP analogs and *S. aureus* AIP-III D4A on *S. aureus* AgrCs I–IV as determined using fluorescence reporter strains 76
Figure 2.11. *S. epidermidis* biofilm growth inhibition dose response curves for (A) AIP-I and (B) AIP-I D1AS6A 77
Figure 2.12. Single-concentration *S. epidermidis* biofilm growth inhibition assay data 78

CHAPTER 3: Structural Characterization of Peptidic Modulators of the *Staphylococcus epidermidis* Quorum Sensing Receptor AgrC-I 85
Figure 3.1. Primary structures of *S. epidermidis* AIP-I and its analogs that are characterized in this study 89
Table 3.1. Cell-based reporter activities of the peptides evaluated in this study against AgrC-I 90
Figure 3.2. Average heavy atom structures of (A) AIP-I and (B) AIP-I V3A derived from the ensemble of 20 lowest energy structures of each peptide 92
Figure 3.3. Average heavy atom structures of (A) AIP-I, (B) AIP-I D1A, and (C) AIP-I D1AS6A derived from the ensemble of 20 lowest energy structures of each peptide 94
Figure 3.4. Average heavy atom structures of (A) AIP-I D1AS6A (most potent AgrC-I agonist) and (B) AIP-I D1AS6AV3A (most potent AgrC-I antagonist) derived from the ensemble of 20 lowest energy structures of each peptide 97
Figure 3.5. Model for AgrC-I activation by AIP-I 98
Table 3.2. Assignments for AIP-I 115
Table 3.3. Assignments for AIP-I V3A 116
Table 3.4. Assignments for AIP-I D1A 116
Table 3.5. Assignments for AIP-I D1AS6A 116
Table 3.6. Assignments for AIP-I D1AS6AV3A 117
Table 3.7. Number of assigned ROEs for each peptide 117
Figure 3.6. Heavy atom ensemble of the 20 lowest-energy structures for AIP-I 117
Figure 3.7. Heavy atom ensemble of the 20 lowest-energy structures for AIP-I V3A 118
Figure 3.8. Heavy atom ensemble of the 20 lowest-energy structures for AIP-I D1A 118
Figure 3.9. Heavy atom ensemble of the 20 lowest-energy structures for AIP-I D1AS6A 118
Figure 3.10. Heavy atom ensemble of the 20 lowest-energy structures for AIP-I D1AS6AV3A 119

CHAPTER 4: Development of Synthetic Pan-Group Agonists of the Quorum Sensing Receptor AgrC in *Staphylococcus epidermidis* 125
Figure 4.1. The *agr* system and the associated AIP signals of *S. epidermidis* 128
Table 4.1. Activities of the alanine and D-amino acid scan analogs of *S. epidermidis* AIP-II against AgrC-II as determined using a fluorescence reporter strain 133
Table 4.2. IC_{50} and EC_{50} values for alanine and D-amino acid scan analogs of *S. epidermidis* AIP-III against AgrC-III as determined using the fluorescence reporter strain . 134
Figure 4.2 Summary of the known SAR trends for the activation of the three AgrC receptors by their cognate AIPs 138
Table 4.3. IC_{50} (shown in red) and EC_{50} (shown in green) values for potential pan-group agonist analogs of *S. epidermidis* AIP against the known AgrC receptors (AgrC-I–III) as determined using fluorescence reporter strains 140
Figure 4.3 Scaffolds of interest identified from the first attempt of designing pan-group agonists for the *agr* system of *S. epidermidis* 143

Table 4.4. IC_{50} (shown in red) and EC_{50} (shown in green) values for analogs of the AIPII9aaP4Vtail AIPIring scaffold against the known AgrC receptors (AgrC-I–III) as determined using fluorescence reporter strains 144
Table 4.5. IC_{50} (shown in red) and EC_{50} (shown in green) values for analogs of the AIPII9aaP4V scaffold against the known AgrC receptors (AgrC-I–III) as determined using fluorescence reporter strains 146
Table 4.6. IC_{50} (shown in red) and EC_{50} (shown in green) values for analogs of the AIPII9aatail AIPIring scaffold against the known AgrC receptors (AgrC-I–III) as determined using fluorescence reporter strains 147
Table 4.7. MS and HPLC data for the *S. epidermidis* AIP-II analogs synthesized in this study. EM = exact mass. Rt = retention time 153
Table 4.8. MS and HPLC data for the *S. epidermidis* AIP-III analogs synthesized in this study. EM = exact mass. Rt = retention time 154
Table 4.9. MS and HPLC data for the *S. epidermidis* AIP analogs synthesized for pan-group agonist evaluation. EM = exact mass. Rt = retention time. α = L-2-Aminobutyric acid 155
Table 4.10. IC_{50} values, EC_{50} values, and 95% confident intervals for the active analogs assayed for AIP-III SAR characterization, as determined using the fluorescence reporter strain for Group III 189
Table 4.11. IC_{50} (shown in red) and EC_{50} (shown in green) values for the additional analogs synthesized based on the AIPII9aaP4V scaffold against the known AgrC receptors (AgrC-I–III) as determined using fluorescence reporter strains 190

CHAPTER 5: Highly Stable, Amide-Bridged Autoinducing Peptide Analogues that Strongly Inhibit the AgrC Quorum Sensing Receptor in *Staphylococcus aureus* 197
Figure 5.1. Structures of a native AIP (AIP-III), an inhibitor derived therefrom (AIP-III D4A), and a representative scaffold studied herein (AIP-III D4A Amide) 199
Table 5.1. Peptides evaluated in this study 201
Table 5.2. IC_{50} values of the amide-bridged AIP analogs against AgrCs I–IV determined using *S. aureus* fluorescence reporter strains 203
Figure 5.2. A) Heavy atom lowest energy structure of AIP-III Amide. B) Overlay of AIP-III Amide (cyan) and AIP-III (tan) structures 204
Figure 5.3. A) Heavy atom lowest energy structure of AIP-III D4A Amide. B) Overlay of AIP-III D4A Amide (cyan) and AIP-III D4A (tan) structures 205
Figure 5.4. A) Heavy atom lowest energy structure of tAIP-III D2A Amide. Space-filling models of B) tAIP-III D2A, C) tAIP-III D2A Amide and D) tAIP-III D2A Amide (showing the alternate triangular knob) displaying hydrophobic (yellow) and hydrophilic (green) surfaces 205
Figure 5.5. Peptide stability studies as monitored by HPLC 208
Figure 5.6. Solid-phase synthetic route to amide-bridged AIP-III analogues 211
Table 5.3. *S. aureus* strains used in this study listed according to group 212
Table 5.4 MS and HPLC data for AIP-III analogues in this study. EM = Exact Mass 215
Figure 5.7. Positive ion MS/MS analysis of AIP-III Amide 217
Figure 5.8. Positive ion MS/MS analysis of AIP-III D4A Amide 218
Table 5.5. Complete set of IC_{50} values and 95% confidence ranges for the amide-bridged AIP analogues and control AIPs against AgrC I–IV as determined using the *S. aureus* fluorescence reporter strains 223
Table 5.6. Chemical shift assignments for AIP-III Amide 225
Table 5.7. Chemical shift assignments for AIP-III D4A Amide 225
Table 5.8. Chemical shift assignments for tAIP-III D2A Amide 225
Table 5.9. Number of assigned ROEs and RMSD values for each peptide 225

Figure 5.9. Images of the heavy atom 10-structure ensembles for A) AIP-III Amide; B) AIP-III D4A Amide; and C) tAIP-III D2A Amide 226
Figure 5.10. Images of the heavy atom lowest energy structures for A) AIP-III Amide; and B) AIP-III D4A Amide showing the distance between Leu7 and Ile1 227
Figure 5.11. Space-filling models of A) AIP-III D4A and B) AIP-III D4A Amide displaying hydrophobic (yellow) and hydrophilic (green) surfaces 227

CHAPTER 6: Non-Woven Polymer Nanofiber Coatings that Inhibit Quorum Sensing in *Staphylococcus aureus*: Toward New Non-Bactericidal Approaches to Infection Control 233
Figure 6.1. (A,B) Representative SEM images of electrospun PLGA nanofibers loaded with peptide **1** (A) or peptide $\mathbf{1}_{FL}$ (B). (C,D) Representative fluorescence microscopy images of electrospun PLGA nanofibers loaded with non-fluorescence peptide **1** (C) or fluorescently-labeled peptide $\mathbf{1}_{FL}$ (D) 240
Figure 6.2. Plot showing the release of peptide $\mathbf{1}_{FL}$ from PLGA nanofiber mats versus time upon incubation in PBS at 37 °C 242
Figure 6.3. Plot showing the fluorescence of a GFP reporter strain of *S. aureus*, normalized to positive media control, versus time fro the incubation of substrates coated with nanofiber mats 244
Figure 6.4. Inhibition of hemolysis by group-I *S. aureus* promoted by QSI released from substrates coated with electrospun PLGA nanofiber mats 247
Figure 6.5. (Left) Histogram showing the distribution of fiber diameters for samples of electrospun nanofiber mats. (Right) Representative SEM image of control PLGA nanofibers (no peptide) 255
Figure 6.6. Plot showing the optical densities of bacterial cultures in the GFP reporter assays used to obtain the results shown in Figure 6.3 256
Figure 6.7. Plot showing the optical densities of bacterial cultures in the liquid-phase hemolysis inhibition assays used to obtain the results shown in Figure 6.4A 256

APPENDIX I: Investigation of the Role of *agr* Interference in Competition between *Staphylococcus aureus* and *Staphylococcus epidermidis* in Lab Media 270
Figure Appendix I.1. Primary structures of the native AIPs identified in (A) *S. aureus* and (B) *S. epidermidis* and the (C) AIP analogs used in this work 273
Figure Appendix I.2. Cfu counts of *S. aureus* and *S. epidermidis* planktonic and biofilm growth from co-culture experiments 275
Figure Appendix I.3. Cfu counts of *S. aureus* and *S. epidermidis* planktonic and biofilm growth from co-culture experiments performed in minimal media 277

CHAPTER 1:

Overview and Thesis Outline

1.1 Quorum sensing in staphylococci: overview

1.1.1 What is quorum sensing?

Once thought to only engage in individualistic behaviors important for self-survival, bacteria have since been shown to be social organisms that coordinate with others in the community and cooperate in group-beneficial tasks *(1, 2)*. The primary mechanism by which this coordination is achieved is a small chemical mediated communication process known as quorum sensing (QS) *(1, 3-5)*. While the exact nature of the "quorum" that the bacteria sense is not well defined, with Popat *et al.* recently describing QS as environmental sensing at the collective level (or emergent sensing) *(2)*, generally speaking, QS coordinate bacteria behaviors as a function of population density *(3-5)*.

QS was first described in the Gram-negative bacterium *Vibrio fischeri*, a marine organism frequently found in symbiosis with the Hawaiian bobtail squid (*Euprymna scolopes*) *(6)*. Intrigued by the bioluminescence phenotype being only observed at high bacteria cell density, Eberhard and coworkers characterized the small molecule, an *N*-acylated homoserine lactone, that allows *V. fischeri* to collectively induce the expression of bioluminescence related genes at high cell density *(7)*. Subsequent studies led to the identification of LuxR/I QS system that is responsible for the synthesis and recognition of the signaling molecule in *V. fischeri (4, 5)*. Since then, a wide variety of bacteria species with diverse chemical signals and distinct QS systems have been identified *(3-5, 8)*. Despite the differences among the known QS systems, they all share the following general characteristics (Figure 1.1): (i) the production of QS signals that are secreted or diffuse into the extracellular milieu; (ii) as population density increases so does the concentration of the signaling molecules; (iii) once a threshold concentration of the signal is reached, the signals can effectively bind their cognate receptors and trigger changes in gene expressions typically associated with cooperative behaviors; and (iv) auto-induction of the QS system to facilitate a concerted response in the population *(1, 4, 5, 8, 9)*.

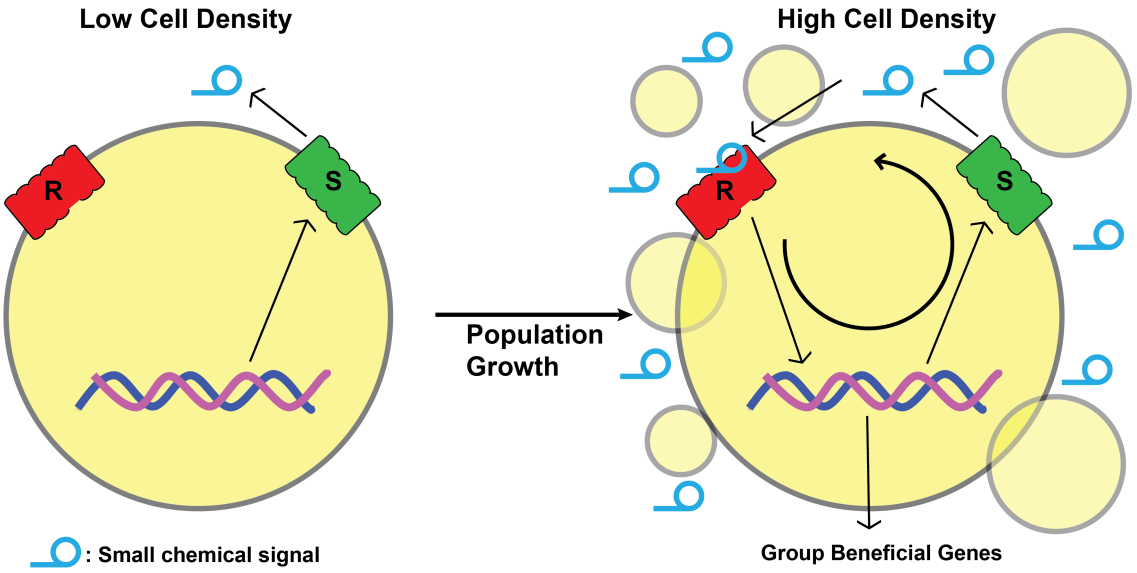


Figure 1.1: Diagram of a generic QS circuit. Signal synthase (**S**) produces small chemical signals are accumulate in the extracellular milieu. At low cell density, no productive binding occurs between signal and its receptor (**R**). As population density increases, so does the concentration of the signal molecules. At threshold concentration, the signal binds effectively to **R** and changes expression of genes typically involved in group beneficial behaviors. The QS circuit itself is also upregulated to form a positive feedback loop.

QS is an integral component of the global gene regulatory networks in bacteria, and it is involved the regulation of an estimated 5 to 25% of the genes based the bacteria genomes sequenced *(10)*. Behaviors and processes under the regulation of QS are diverse as well, with activities ranging from nutrient catabolism and competence to motility and biofilm formation *(2, 9)*. For many pathogenic bacteria, the QS regulon also includes virulence factor production and secretion *(2, 5, 9, 11)*. With the growing concern over the rise of antibiotic resistances, anti-virulence strategies have emerged as an alternative to, or a complement of, traditional antimicrobials in limiting infections, and QS is a prime target for such approach *(2, 9, 10, 12)*. Since the QS system and its regulon generally are not considered essential genes, modulation of the QS system could reduce the virulence of a pathogen without placing a strong selective pressure for resistance development and spreading that are typically seen with traditional

antibiotics *(2, 9, 10, 12)*. Consequently, understanding QS has gained significant interests as an avenue to identify novel opportunities to combat bacterial infections.

1.1.2 The accessory gene regulator quorum sensing system in staphylococci

The LuxR/I system and its *N*-acylated homoserine lactone signal molecule found in *V. fischeri* represents the canonical QS system for the Gram-negative bacteria, with homologous systems identified in a variety of Gram-negative organisms *(1, 5, 8)*. For Gram-positive bacteria however, the primary QS signals are peptide based, and one of the better-characterized QS systems among Gram-positive bacteria is the accessory gene regulator (agr) system found in the staphylococci, which has been most studied in the opportunistic human pathogen *Staphylococcus aureus (5, 9, 13-16)*. The *agr* system consists of four components (AgrA-D) expressed from the *agr* locus and a thiolactone containing macrocyclic peptide called autoinducing peptide (or AIP) as the signaling molecule (Figure 1.2) *(13-15, 17, 18)*. AgrD, the peptide precursor for the mature AIP signal, is processed and secreted in part by the transmembrane endopeptidase AgrB *(19, 20)*. AIP accumulates in the extracellular milieu, and, as the bacteria population density increases, so does the concentration of the AIP. Once a threshold concentration is reached, AIP can interact productively with the cognate receptor AgrC, a transmembrane histidine kinase *(21)*. AgrC exists as preformed dimer, and the successful binding of AIP at each monomer triggers *trans*-autophosphorylation of the receptor in a non-cooperative manner *(22)*. Phosphorylated AgrC then transfers the phosphate group to the response regulator AgrA, which in turn can bind to the promoter regions on the chromosome and drive gene expressions *(22)*. One main output from the *agr* system is the RNAIII molecule transcribed from the P3 promoter. RNAIII is the main effector molecule of the *agr* system, which controls the expression of a number of genes either via direct RNA-mediated post-transcriptional regulation or via RNAIII-dependent inhibition of the Rot repressor *(15, 23)*. Other outputs include the expression of the *agr* locus from the P2 promoter, leading to an auto-

inductive circuit of the *agr* system *(24)*, and the production of phenol-soluble modulins, a group of small amphipathic peptides shown to play important roles in staphylococcal colonization and virulence, from the psm promoters *(25-27)*.

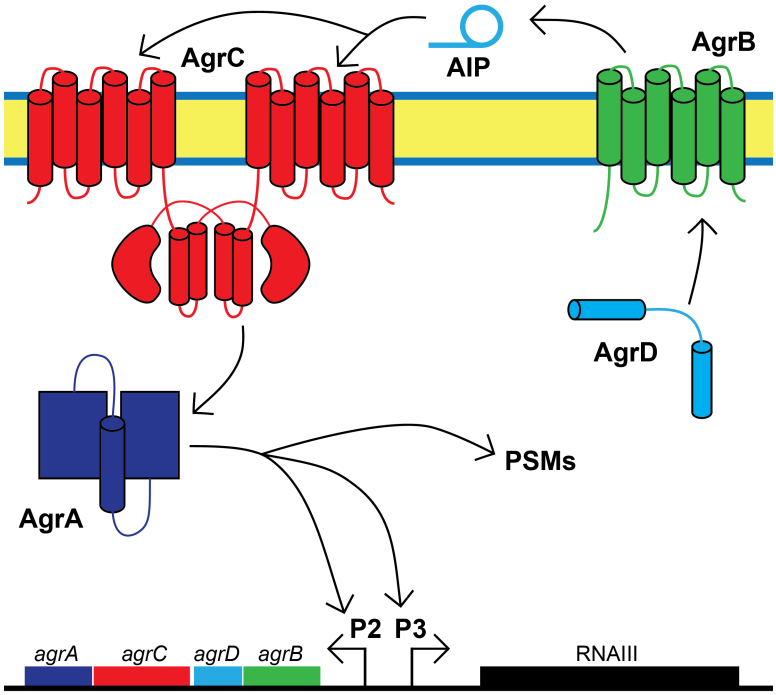


Figure 1.2: Scheme of the *agr* QS circuit. AgrD is processed and secreted by AgrB as the mature signal peptide (called autoinducing peptide, or AIP). Once the concentration of AIP is sufficiently high, AIP can bind to the transmembrane receptor AgrC. AIP-bound AgrC undergoes *trans*-autophosphorylation, and then transfer the phosphate group to AgrA. Phosphorylated AgrA then binds to the promoter regions to induce transcription. Transcript from P2 promoters encodes the entire *agr* locus, whereas transcripts from P3 and psm promoters are RNAIII and PSMs, respectively. RNAIII is the main effector molecule of the *agr* system. PSMs are important to the colonization and virulence of staphylococci.

For many staphylococcal species, multiple variants of the *agr* system can exist within a species due to a hypervariable region between the 3' end of the *agrB* gene and the 5' end of the *agrC* gene (which also includes the *agrD* gene) *(15)*. This variation has led to the categorization of different *agr* specificity groups, where each group has an AIP with a unique sequence and the AgrB and AgrC proteins with the corresponding changes needed for synthesis and detection of that specific AIP *(15)*. Thus, while any isolated strain only possesses one *agr* system for QS, multiple signal-receptor pairs can be used for QS in a species of Staphylococcus. For *S. aureus,*

four *agr* specificity groups have been identified to date (Figure 1.3A) *(15)*. Interestingly, the different *agr* systems within a staphylococcal species are not “blind” to the non-cognate AIPs. Instead, some of these systems have shown to exhibit cross-group inhibitory activities, where the AIP of one group not only can activate the cognate AgrC receptor but also inhibit the non-cognate receptor from a different group of the same species *(15, 21)*. The physiological significance of this *agr* interference phenomenon, however, is not well characterized and requires further investigation.

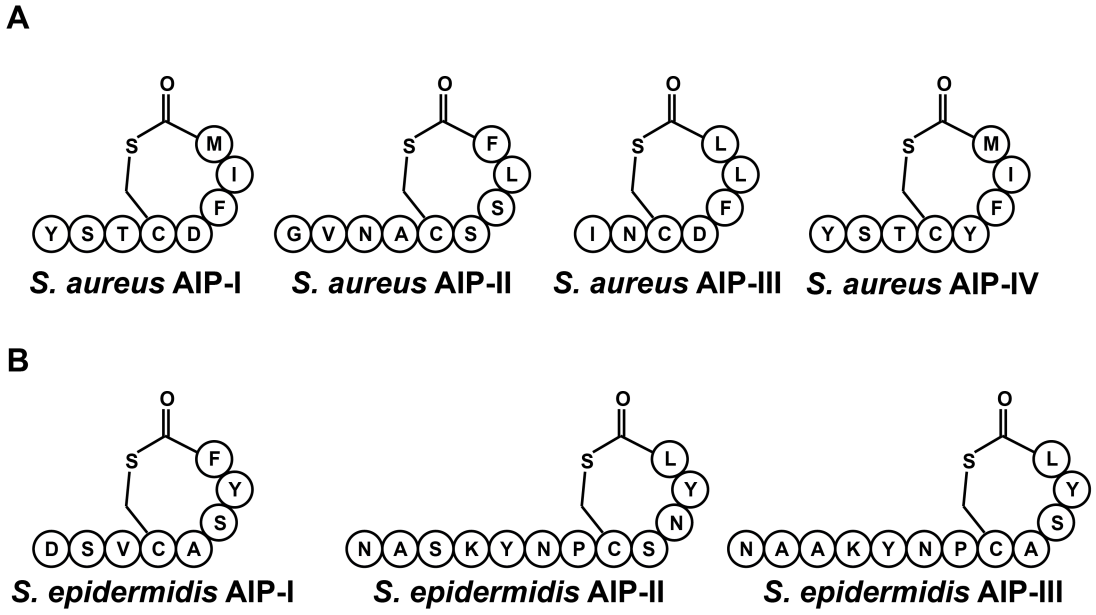


Figure 1.3: Primary structures of the native AIPs identified to date for (A) *S. aureus* and (B) *S. epidermidis*.

1.1.3 The agr system plays important roles in regulating virulence of the human pathogens S. aureus and Staphylococcus epidermidis

Similar to the QS systems from a number of pathogens, the *agr* QS system is also heavily involved in the infectivity of the staphylococcal pathogens *(9, 15, 16, 18, 28, 29)*. In particular, understanding the roles of the *agr* systems in regulating virulence of *S. aureus* and *Staphylococcus epidermidis* has received considerable interest. Both species are opportunistic human pathogens that are frequently found on human epithelia and mucosal membrane, and,

together, they are the leading the cause of nosocomial infections *(30, 31)*. Infections by both bacteria are difficult to treat due to the growing resistances to antibiotics and the ability to form biofilm, making these infections a significant burden on public health *(30-35)*.

S. aureus has been the subject of extensive investigation, due in part to the impressive arsenal of virulence factors the bacterium possesses. This arsenal, which includes an array of toxin, degradative enzymes, and immune evasion mechanisms *(18, 35, 36)*, allows *S. aureus* to overcome host immune system and cause a wide variety of acute and chronic infections, some of which can be life threatening, and the *agr* system is a major regulator of its expression *(15, 18, 31, 36)*. Especially in acute infections, studies using animal models of different types of infections have demonstrated the necessity of activation of the *agr* system in disease progression *(18)*. More recently, hypervirulent strains of antimicrobial resistant *S. aureus* capable of infecting otherwise healthy individuals have emerged and spread quickly, and infections by these strains, known as the community-associated methicillin-resistance *Staphylococcus aureus* (CA-MRSA) are of great clinical concern *(15, 37-39)*. While the mechanisms for the hypervirulence and the rapid expansion are not fully understood, for the epidemic CA-MRSA strain USA300, these properties are likely a result of the upregulation of virulence factors by the elevated activity of its *agr* system, further highlighting the importance of the *agr* system in infectivity of the *S. aureus (15, 38, 39)*.

In contrast to *S. aureus*, *S. epidermidis* is less likely to cause life-threatening infections, as it does not have the repertoire of toxins that *S. aureus* possesses *(30)*. Nevertheless, in part due to it being part of the human skin microflora, *S. epidermidis* is a leading causative agent of medical device-associated infections *(30, 33, 40-43)*. The formation of robust biofilm and the resistance to antibiotics by *S. epidermidis* cause the *S. epidermidis* infections particularly difficult to eradicate, making the removal of the infected devices necessary and the infections costly *(30, 34, 44-46)*. Despite a less impressive arsenal of virulence factors, the *agr* system still plays an important role in the pathogenesis of *S. epidermidis (25, 26, 47-49)*. Specifically, an

active *agr* system provides *S. epidermidis* with significantly more protection against defense mechanisms deployed by the host innate immune system *(47, 48)*, and the virulence factors induced by the *agr* system promote dissemination and tissue infiltration of *S. epidermidis* during device-associated infections *(48, 50-52)*.

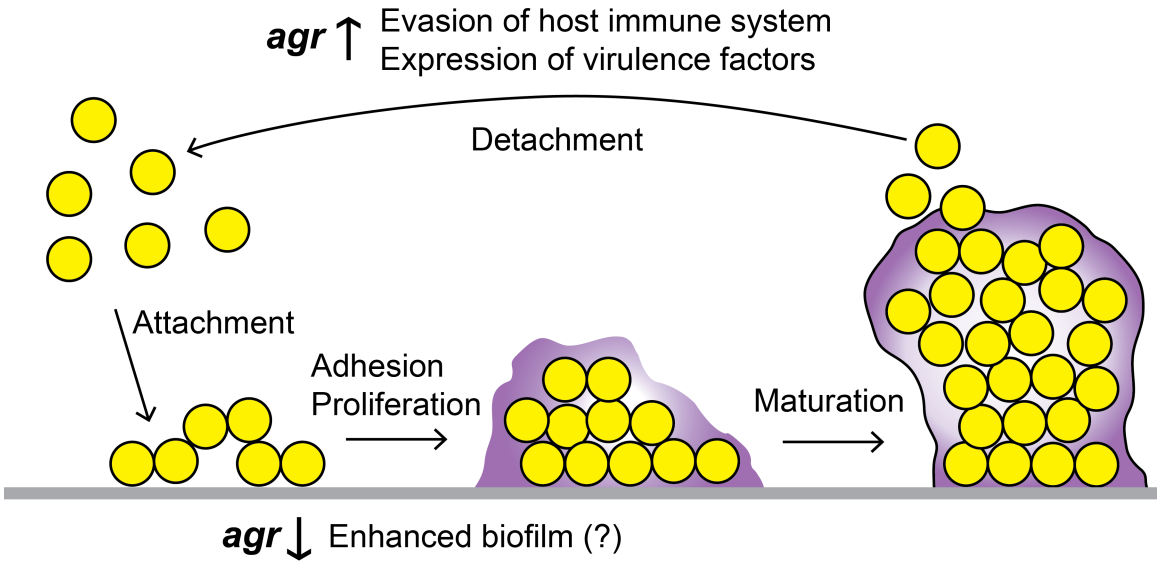


Figure 1.4: Schematic of the biofilm lifecycle and the roles of the *agr* system. The biofilm lifecycle can be divided into four stages: attachment of planktonic bacteria to biotic or abiotic surfaces; adhesion and proliferation of the initial sessile colony; maturation of the biofilm structure; and dispersion of bacteria from the biofilm colony to colonize new environments. The *agr* system's role in the maturation and detachment stage is well established, but the impact of the system in early stages of biofilm is not well understood.

In both *S. aureus* and *S. epidermidis*, the *agr* system is also involved in the regulation of biofilm formation (Figure 1.4), an important virulent phenotype typically associated with chronic infections and, for *S. epidermidis*, the primary mechanism by which the infection is established *(18, 30, 34, 36, 47, 52-55)*. In addition to facilitating the bacteria attachment to an abiotic surface (i.e. a medical device), which can help the bacteria to bypass the skin barrier and enter the host body, biofilm also protects the bacteria from antibiotics and host immune system *(32, 34, 36, 44, 54, 56)*. The biofilm lifecycle can be roughly divided into four stages: attachment, adhesion and proliferation, maturation, and detachment *(15, 57)*. The role for the *agr* system is well established for the final two stages of this lifecycle, where the *agr* system is activated to produce

the proteases and surfactants necessary for structuring the biofilm, allowing further growth of the biofilm community and the dispersal of the bacteria to establish new colonies *(18, 36, 51, 52, 54)*. The impact of the *agr* system on early stages of biofilm formation is not as well understood and may differ between the two bacteria. For example, in *S. epidermidis* strains that form biofilm containing polysaccharide intercellular adhesin (PIA) as a structural component, the *agr* system negatively regulates the expression of the AtlE protein, an adhesion factor important for the attachment stage of biofilm growth *(58, 59)*. However, this *agr*-dependent regulation of Atl protein is not observed for *S. aureus* strains that form PIA-dependent biofilm *(60)*. Moreover, both bacteria can form PIA-independent biofilms, and the role of the *agr* system in the early stages of forming these biofilms is not clear *(15, 61)*. Nevertheless, the established *agr*-mediated biofilm dispersal mechanism, along with the observations that *agr* dysfunction can enhance biofilm formation, suggests that activation of the *agr* system can reduce biofilm accumulation on surfaces and potentially render the dispersed bacteria more susceptible to antibiotics and host immune defenses *(18, 50, 52, 54, 62-64)*.

The dichotomy of the *agr* regulation on virulent phenotypes in *S. aureus* and *S. epidermidis* presents a conundrum for targeting the *agr* system as a strategy for attenuating virulence and limiting infectivity *(18, 36, 54)*. While inhibition of the *agr* system may limit the production of toxins and prevent the bacteria from escaping the immune system and spreading from the site of infection, an inactive *agr* system could lead to stronger biofilm build-up and more persistent infections. To further complicate the matter, the effect of the *agr* system activation and inhibition on biofilm formation or bacteria colonization on biotic surfaces can differ from that on abiotic surfaces *(65, 66)*. In addition, the impact of *agr* inactivation in chronic *S. aureus* infections, which are typically associated with biofilm-like growth, is infection dependent *(36, 54)*. Lastly, even though low level of expression of the *agr* system is generally observed during chronic infections *(54)*, for *S. epidermidis* at least, these infections do not appear to select for *agr*-negative phenotype *(46)*, suggesting that the presence of an active *agr* system may be

important for the infection *(36, 54)*. Taken together, the role of the *agr* system during a staphylococcal infection is complex, and more in-depth investigation of how the *agr* system contributes to the pathogenesis of *S. aureus* and *S. epidermidis* in the various types of infections are needed.

1.1.4 Development of chemical modulators of the agr system

Given the significance of the *agr* system in virulence regulation for *S. aureus* and *S. epidermidis*, various chemical strategies to modulate the *agr* system have been developed in recent years. While quorum quenching methods based on signal peptide sequestration *(67)*, inhibition of signal synthesis *(68)*, and disruption of AgrA-DNA interactions have been developed for *S. aureus (69)*, the majority of the modulators of the *S. aureus agr* system target the AgrC receptor and interfere with the signal-receptor interactions *(70-81)*. Inspired by the observation that the inhibition of an *agr* system with a non-cognate AIP (or *agr* interference, as described above) can successfully reduce skin abscess formation by *S. aureus* in a murine infection model *(70, 82)*, a number of studies, including the ones from our group, have characterized the structure-activity relationships (SARs) of the AIP:AgrC interactions in *S. aureus* and developed multiple AIP analogs capable of inhibiting the AgrC receptors from all *agr* systems (pan-group antagonists) in *S. aureus* with high potency *(70-74, 76, 77, 79-81)*. These chemical strategies allow for modulating *S. aureus agr* system with spatial and temporal control *(83-85)*, making them powerful tools for better understanding the role of the *agr* system during an infection and for assessing the viability of targeting *agr* system to limit infectivity.

In contrast, the AIP:AgrC interactions in *S. epidermidis* are not as well characterized. The first AIP (AIP-I) of *S. epidermidis* was identified by Otto and co-workers in 1998, and they demonstrated that the thioester lactone of the macrocycle and the three exocyclic residues are required for receptor activation *(86)*. Since then, two other AIPs (AIP-II and AIP-III) have been found, and their structures were only recently elucidated (Figure 1.3B) *(87, 88)*. No SAR

characterization has been performed for AIP-II and AIP-III. The limited SAR study has resulted in no non-native AgrC activators and inhibitors being reported for *S. epidermidis*. Given the success of the SAR studies in *S. aureus*, a systematic SAR characterization of all three AIPs in *S. epidermidis* will likely improve our understanding of the AIP:AgrC interactions in staphylococci and generate potent modulators of the *agr* systems in *S. epidermidis*.

1.1.5 Limitations of AIP analogs as agr modulators and efforts to overcome them

Although the AIP-based AgrC inhibitors exhibit high potency, they have few drawbacks. Notably, the thioester lactone present in these analogs, which is required for receptor activation by the native AIPs *(70, 86)*, has low stability in aqueous media *(82)*, while the hydrophobic bulk of these AIPs limit their solubility in aqueous solutions. Furthermore, though the impact of serum proteins on AIP analogs has not bee explored, studies with native *S. aureus* AIPs have shown that serum, more specifically apolipoprotein B in the serum, is capable of AIP sequestration *(89, 90)*. If this effect were applicable to AIP analogs, a very likely possibility given the structural similarities, using AIP analogs to control the *agr* system *in vivo* would be hindered by the low bioavailability. Finally, the current strategy for producing these AIP analogs is largely based on solid-phase peptide synthesis. While effective, the excess reagents typically needed for efficient peptide synthesis make large-scale synthesis of the AIP analogs cost-inefficient *(81)*.

Consequently, improvements on existing AIP-based AgrC modulators are needed to make them more amenable to applications in biologically relevant settings. Towards that effort, our group recently reported the first 3-dimensional structural characterization of the native *S. aureus* AIPs and their analogs *(91, 92)*. Comparison of AgrC activators and inhibitors allowed us to identify structural motifs important for receptor inhibition, and our studies provided the first structural support for the current model of AIP:AgrC interactions in *S. aureus*. Insights obtained from the structural studies can be used to guide the design of minimized AIP scaffolds, or even non-AIP-based scaffolds, that maintain the necessary features for inhibiting the AgrC receptors.

An alternative method to overcome the limitations of the existing AgrC modulators is the use of material-based approach to deliver these modulators to the sites of interest, which can prevent unnecessary exposure of the modulators to aqueous environments and avoid the need of high compound concentration *(93, 94)*. As an example, in collaboration with Lynn group, we have exploited the properties of nanoporous, polymer-based superhydrophobic coatings to enable loading and sustained release of a potent AgrC inhibitor of *S. aureus* into an aqueous media that modulated *agr*-associated phenotypes for at least 40 days *(94)*. Given the instability of the thioester lactone, the observation of bioactive compounds after 40 days suggests that embedding the inhibitor in the material protected the inhibitor from hydrolysis, thus overcoming the water-lability of the inhibitor and prolonging its lifetime. Other methods incorporating AIPs to different surfaces also have been reported *(93, 95)*, and this material-based approach represent an exciting avenue for applying these AgrC modulators in medically relevant settings to assess the impact of *agr* modulation on staphylococcal infections.

1.1.6 Competition between staphylococcal species and the role of the agr system

Beyond the impact on virulence regulation and pathogenesis, the *agr* systems in *staphylococci* are hypothesized to also play a role in colonization *(27, 30, 36)*. In agreement with this hypothesis, a recent study of *S. epidermidis* found the *agr* system to be necessary for skin colonization *(88)*. Interestingly, *agr* interference (first mentioned above) is not limited to the different *agr* specificity groups within a species, but also exists between the *agr* systems of different staphylococcal species *(96-100)*. Taken into account the similar environment niches colonized by the staphylococcal species and the association of infections with specific *agr* specificity groups, *agr* interference is hypothesized to provide competitive advantages for establishing infections and colonization *(101)*.

Supporting the hypothesis that *agr* interference is plays a role in establishing infections, recent studies using different infection models have shown either the attenuation of *S. aureus*

virulence via co-infection with non-pathogenic staphylococcal species or fitness advantage of *S. aureus* strains conferred by *agr* interference *(99-101)*. However, the clinical significance of *agr* interference has not been conclusively shown *(102, 103)*. Consequently, additional studies are necessary to better understand in the relevance of *agr* interference, and chemical modulators that target different *agr* systems with selectivity would serve as promising tools for such studies.

Similarly, the relevance of *agr* interference in colonization has not been conclusively shown. Although studies have identified commensal staphylococcal species, including *S. epidermidis*, that provide protection of host from *S. aureus* colonization via secreted products *(104-107)*, characterization of the *agr* systems of staphylococcal isolates from human microflora has not revealed any influence of *agr* interference on colonization *(108)*. Nevertheless, with the identification of *agr*-regulated products being implicated in successful skin colonization of commensal staphylococcal species, the *agr* system likely plays an important role in survival within a competitive host environment *(100)*. Moreover, a recent study showed that *agr*-regulated products from *S. epidermidis* exerted selective antimicrobial actions against *S. aureus*, further highlighting the likely importance of the *agr* system in the protection against *S. aureus* colonization by the commensal staphylococcal species *(104)*. While a much better understanding of the role of the *agr* system in colonization of different staphylococcus species is necessary, modulation of the *agr* systems from the commensal staphylococci may provide an attractive approach to leverage the protective properties of these commensals against colonization of the more pathogenic *S. aureus (100)*.

1.2 Efforts to expand, improve, and apply the chemical toolset for targeting quorum sensing in staphylococci

1.2.1 Overview

The complex role of the *agr* system in staphylococcal lifestyles warrants more in-depth investigation, particularly in relation to the impact the *agr* system has on the pathogenesis of *S.*

aureus and *S. epidermidis*. Chemical modulators of *agr* systems can serve as powerful tools for better understanding the importance of the *agr* systems in various settings and assessing the viability of the *agr* system as a target for therapeutic purposes. To date, with the exception of *S. aureus*, characterization of the *agr* systems and the development of modulators have been limited. In addition, although the *agr* modulators in *S. aureus* have been shown to successfully limit *S. aureus* virulence in *in vitro* experiments and in animal infection models, many of these modulators have notable weaknesses and will benefit from improvements. My work detailed in this document will focus on the efforts on developing new and improved *agr* modulators for both *S. aureus* and *S. epidermidis*. In addition, I have contributed to the development of a novel delivery method of *agr* modulators, which is a step forward in designing innovative systems for application of QS modulators in biologically relevant settings.

1.2.2 Development of novel AgrC modulators in S. epidermidis

S. epidermidis is previously thought to be an innocuous commensal of the human epithelia, but it has since been shown to be an important nosocomial pathogen. The primary QS circuit, the *agr* system, was shown to be implicated in the pathogenesis of *S. epidermidis*, and it could be a viable target for strategies to limit infectivity. The activity of the *agr* system is mediated in part by the interaction between the signal peptide (AIP) and the cognate receptor AgrC, and interfering with this interaction is an effective approach to control the activity of the *agr* system. Previous studies in *S. aureus* characterizing the SAR of signal:receptor interactions of the *agr* systems have identified a number of potent modulators of the AgrC receptors. However, such SAR characterization is very limited for the *agr* systems in *S. epidermidis*. Chapter 2 and first half of Chapter 4 detail the first systematic SAR characterizations for all three native AIPs identified for *S. epidermidis agr* system. Not only did we gain insights into the interactions of the AIPs and their receptors, we were able to uncover the first set of non-native AIP analogs capable of modulating the AgrC receptors of *S. epidermidis*. Structural comparison of activators

and inhibitors against one of the AgrC receptor (AgrC-I) in *S. epidermidis*, as documented in Chapter 3, has allowed us to identify key structural motifs important for activation and inhibition of *S. epidermidis* AgrC-I and provided structural support for the SARs delineated in earlier studies.

Inspired the identification of structural motif for AgrC-I activation, we built upon the known SARs of *S. epidermidis* AIP:AgrC interactions to design AIP analogs capable of activating all three AgrC receptors of *S. epidermidis*. AIP analog with this "pan-group agonist" activity has never been identified in prior studies with AIPs of *S. aureus* and *S. epidermidis*, and the development of one could be valuable for reducing biofilm formation, a key virulent phenotype for both pathogens. As described in the second half of Chapter 4, we have uncovered three peptides, from a limited set of AIP analogs, with agonistic activities towards all three AgrC receptors in *S. epidermidis*. Despite the need for improvement of their efficacy, these three peptides represent the first known AIP analogs capable of pan-group agonism in a single staphylococcal species. The pan-group agonists, along with the AgrC modulators uncovered in Chapter 2, represent new tools for assessing the impact of targeting QS in limiting *S. epidermidis* infectivity.

During our SAR characterization of *S. epidermidis* AIP-I:AgrC-I interactions, we identified a small group of AgrC inhibitors showing some degree of receptor selectivity. This finding has provided us with chemical tools to probe the potential role of *agr* interference in competition between *S. epidermidis* and *S. aureus*. Effort towards that goal is documented in Appendix I.

1.2.3 Strategies to improve AgrC modulators in S. aureus

In contrast to *S. epidermidis*, *S. aureus* and its *agr* systems have received considerable attention, and characterization of the AIP:AgrC interactions in *S. aureus* has laid foundation for understanding AgrC activation and inhibition by AIPs. Different aspects of the *agr* systems have been targeted for modulating the activity of the *agr* systems, but the majority of the *agr*

modulators uncovered to date focus on blocking the AIP:AgrC interaction and they are mostly analogs derived from the native AIPs. While these AgrC modulators have potency, they have few drawbacks. Notably, the instability of the thioester lactone and low solubility in aqueous media could hinder the application of these modulators in more biologically relevant settings. By replacing the thioester lactone with a lactam, we show in Chapter 5 that two of the most potent AgrC modulators can be made more stable and soluble without significant sacrifice of their potencies. Structural characterization of the lactam analogs confirmed our proposed model for AgrC inhibition, suggesting that the model can be used to guide the design for AgrC inhibitors with improved properties.

Our group, in collaboration with the Lynn group, has successfully developed material-based approach to deliver QS modulators with diverse compound release profiles and material properties. In particular, our use of superhydrophobic coatings for long-term release of an AIP-derived AgrC inhibitor protected the inhibitor from hydrolysis and enabled the *agr* modulation for up to 40 days. This material-based approach represents another method of overcoming the drawbacks of the AIP-derived AgrC modulators, and we exploit the method again in Chapter 6, where we used electrospun nanofiber to efficiently load and release peptidic AgrC inhibitor in bioactive form for up to two weeks. In addition to preserving the AgrC inhibitor for sustained activity, the relative ease of depositing the electrospun nanofiber on diverse surfaces, including on the gauze-like non-woven mesh, could allow for the AgrC inhibitors to be embedded in medically-relevant surfaces and provides a different avenue for applying AgrC inhibitors in future *S. aureus* infection studies.

1.3 Dissertation scope

1.3.1 Chapter 2: Staphylococcus epidermidis Autoinducing Peptide I Structure-Function Analyses Reveals Motifs Critical for Modulation of AgrC receptors

S. epidermidis is recently identified as an important nosocomial pathogen due to its ubiquity in the human flora and ability to form robust biofilm. Playing an important role in the infectivity of *S. epidermidis* is the *agr* QS system. Activity of the *agr* system is mediated in part by the binding of the signal peptide (AIP) to its cognate AgrC receptor. Despite the implication of the *agr* system in virulence regulation, questions remain about the role of QS in *S. epidermidis* infections and survival in competitive host environment, and chemical modulators of the *agr* system could provide novel insights. The AIP ligands provides an initial scaffold for the development of such probes; however, little is know about the SAR for AgrC activation by the cognate AIP. In Chapter 2, we performed the first SAR analyses of an *S. epidermidis* AIP using systematic alanine and D-amino acid scans of AIP-I. The results from our SAR characterization allowed us to design and identify the first set of potent, pan-group inhibitors against all three AgrC receptors found in *S. epidermidis*. We also uncovered a number of AIP analogs showing selective inhibition of AgrC receptor in either specific *S. epidermidis agr* groups or in *S. aureus*. Lastly, we identified a non-native AgrC-I agonist that inhibited *S. epidermidis* biofilm growth *in vitro* with a higher potency and efficacy than the native AIP-I. Together, these synthetic analogs represent new and readily accessible tools for probing the roles of QS in *S. epidermidis* colonization and infections.

1.3.2 Chapter 3: Structural Characterization of Peptidic Modulators of the Staphylococcus epidermidis Quorum Sensing Receptor AgrC-I

Our systematic SAR characterization for the *S. epidermidis* AIP-I:AgrC-I interaction revealed important residues for receptor binding and activation and led to the identification of the first set of non-native AIP analogs capable of modulating the activity of the AgrC receptor (Chapter 2). However, lack of structural data limited the understanding of the chemical features important to receptor activation and inhibition. In Chapter 3, we used solution-phase two-dimensional NMR spectroscopy to visualize the three-dimensional (3D) structures of AIP-I and its analogs.

Structural comparisons of agonists and antagonists revealed key structural motifs important for AgrC-I activation and provided support for the known SARs derived from cell-based assays. The 3D structural analyses not only improved our understanding of the AIP:AgrC interactions in *S. epidermidis*, but can facilitate the design of new *agr* modulators with enhanced activities.

1.3.3 Chapter 4: Development of Synthetic Pan-Group Agonists of the Quorum Sensing Receptor AgrC in Staphylococcus epidermidis

Biofilm formation is the primary mechanism by which *S. epidermidis* establishes device-associated infections. Although the role of the *agr* system in early stages of biofilm formation is not well understood, the intentional activation of the *agr* system using exogenous native AIP has been shown to reduce biofilm growth. To date, three different *agr* specificity groups (Group I-III) have been identified in *S. epidermidis*, each using a unique AIP (AIP-I–III), and these AIPs can exhibit cross-group inhibitory activities. The development of synthetic agonists capable of activating the receptors from all three *agr* groups would allow for the assessment of *agr* activation as a viable strategy for promoting dispersal of *S. epidermidis* biofilm. Such pan-group agonists are yet to be identified, in part due to the lack of information on the SARs for AIP-II and AIP-III. We carried out the first systematic SAR characterization of *S. epidermidis* AIP-II and AIP-III in Chapter 4, which revealed key residues important for receptor activation in Group II and III. Building on these new SAR data and those reported for AIP-I (Chapter 2 and 3), we designed and identified the first set of pan-group agonists for the *agr* system in *S. epidermidis*. These AIP analogs, along with additional SARs uncovered in this chapter, provide scaffolds for additional structural characterization and further optimization to yield more efficacious pan-group agonists. These pan-group agonists represent new tools for evaluating the impact of targeting QS in limiting *S. epidermidis* infectivity.

1.3.4 Chapter 5: Highly Stable, Amide-Bridged Autoinducing Peptide Analogues that Strongly Inhibit the AgrC Quorum Sensing Receptor in Staphylococcus aureus

The common human pathogen *S. aureus* is a leading cause for nosocomial infections. With the emergence of methicillin-resistance *S. aureus* (MRSA) and the expansion of MRSA infection from hospital settings to infections of otherwise healthy human, *S. aureus* infections are of great clinical concern. QS plays a vital role in regulating the production of virulence factors and establishing infections, and blocking QS pathways has attracted considerable interest as an approach to suppress virulence in *S. aureus*. Towards this goal, a number of studies have identified potent inhibitors of the *S. aureus agr* system derived from the native AIPs. More recently, our group developed analogs of *S. aureus* AIP-III that inhibit AgrC receptors and attenuate virulence phenotypes with high potencies. However, application of these compounds is limited by the hydrolytically unstable thioester they contain and their low aqueous solubilities. In Chapter 5, we report the development of AIP analogs with enhanced hydrolytic stabilities and solubilities by replacing the thioester with an amide linkage, without significantly sacrificing their potencies as AgrC receptor inhibitors in all four *agr* specificity groups of *S. aureus*. The improved properties of these amide-bridged analogs make them powerful new tools for the study of QS in *S. aureus*, especially in biologically relevant environments.

1.3.5 Chapter 6: Non-Woven Polymer Nanofiber Coatings that Inhibit Quorum Sensing in Staphylococcus aureus: Toward New Non-Bactericidal Approaches to Infection Control

In Chapter 6, we report the fabrication and biological evaluation of non-woven polymer nanofiber coatings that inhibit QS and virulence in *S. aureus*. We demonstrate that a potent and non-bactericidal AIP-derived QS inhibitor (QSI) in *S. aureus* can be loaded into degradable polymer nanofibers by electrospinning, and that this approach can deposit QSI-loaded nanofiber coatings onto model non-woven mesh substrates. QSI was release over approximately three weeks when these materials were incubated in physiological buffer, and retained its biological

activity and strongly inhibited *agr*-based QS in a GFP reporter strain of *S. aureus* for at least 14 days without promoting cell death. These materials also inhibited production of hemolysins, a QS-controlled virulence phenotype, and reduced the lysis of erythrocytes when placed in contact with wild-type *S. aureus* growing on surfaces. The sustained activity of the QSI, which contains a hydrolytically unstable thioester linkage, suggests that the nanofiber coatings also offer protection for the QSI from hydrolytic degradation. This approach is modular, and can be used with many different polymers, active agents, and processing parameters to fabricate nanofiber coatings on surfaces important in healthcare contexts. The QSI-based strategies reported here also provide springboards for the development of new anti-infective materials and novel treatment strategies that target virulence as opposed to growth in *S. aureus*. This approach also provides porous scaffolds for cell culture that could prove useful in future studies on the influence of QS modulation on the development and structure of bacterial communities.

1.3.6 Appendix I: Investigation of the role of agr interference in competition between Staphylococcus aureus and Staphylococcus epidermidis in lab media

The *agr* QS systems in human pathogen *S. aureus* and *S. epidermidis* have been shown to play vital roles in their infectivity. Important to the activation of the *agr* system is the binding of the receptor AgrC and its cognate AIP signal. To date, four and three different receptor-signal pairs have been identified for *S. aureus* and *S. epidermidis*, respectively. These different pairs are categorized as *agr* specificity groups, and the AIP of one group can exhibit cross-group or cross-species inhibitory activities towards non-cognate AgrC receptors. This phenomenon, dubbed *agr* interference, is hypothesized to play a role in establishing infections and colonization, but the *in vivo* studies have not provided conclusive support for the hypothesis. In Chapter 2, we reported AIP analogs capable of inhibiting AgrC receptors from selective specificity groups or staphylococcal species. In Appendix I, we document the attempt to use the species-selective AgrC inhibitors to probe whether *agr* interference plays a role in competition

between *S. aureus* and *S. epidermidis*. Our initial attempt shows that, in lab media, *agr* interference does not appear to have an impact. However, investigation of *agr* interference in settings where *agr* systems likely play important roles is needed to better test the hypothesis on *agr* interference.

1.4 References

1. Williams, P. (2007) Quorum sensing, communication and cross-kingdom signalling in the bacterial world, *Microbiology 153*, 3923-3938.

2. Popat, R., Cornforth, D. M., McNally, L., and Brown, S. P. (2015) Collective sensing and collective responses in quorum-sensing bacteria, *J. R. Soc. Interface. 12*.

3. Hastings, J. W., and Greenberg, E. P. (1999) Quorum sensing: the explanation of a curious phenomenon reveals a common characteristic of bacteria, *J. Bacteriol. 181*, 2667-2668.

4. Camilli, A., and Bassler, B. L. (2006) Bacterial small-molecule signaling pathways, *Science 311*, 1113-1116.

5. Waters, C. M., and Bassler, B. L. (2005) Quorum sensing: cell-to-cell communication in bacteria, *Annu. Rev. Cell Dev. Biol. 21*, 319-346.

6. Nealson, K. H., and Hastings, J. W. (1979) Bacterial bioluminescence: its control and ecological significance, *Microbiol Rev. 43*, 496-518.

7. Eberhard, A., Burlingame, A. L., Eberhard, C., Kenyon, G. L., Nealson, K. H., and Oppenheimer, N. J. (1981) Structural identification of autoinducer of *Photobacterium fischeri* luciferase, *Biochemistry 20*, 2444-2449.

8. Williams, P., Winzer, K., Chan, W. C., and Camara, M. (2007) Look who's talking: communication and quorum sensing in the bacterial world, *Philos. Trans. R. Soc. Lond. B Biol. Sci. 362*, 1119-1134.

9. Rutherford, S. T., and Bassler, B. L. (2012) Bacterial quorum sensing: its role in virulence and possibilities for its control, *Cold Spring Harb. Perspect. Med. 2*.

10. Joint, I., Allan Downie, J., and Williams, P. (2007) Bacterial conversations: talking, listening and eavesdropping. An introduction, *Philos. Trans. R. Soc. Lond. B Biol. Sci. 362*, 1115-1117.

11. Antunes, L. C., Ferreira, R. B., Buckner, M. M., and Finlay, B. B. (2010) Quorum sensing in bacterial virulence, *Microbiology 156*, 2271-2282.

12. Laxminarayan, R., Duse, A., Wattal, C., Zaidi, A. K., Wertheim, H. F., Sumpradit, N., Vlieghe, E., Hara, G. L., Gould, I. M., Goossens, H., Greko, C., So, A. D., Bigdeli, M., Tomson, G., Woodhouse, W., Ombaka, E., Peralta, A. Q., Qamar, F. N., Mir, F., Kariuki, S., Bhutta, Z. A., Coates, A., Bergstrom, R., Wright, G. D., Brown, E. D., and Cars, O. (2013) Antibiotic resistance-the need for global solutions, *Lancet Infect. Dis. 13*, 1057-1098.

13. Lyon, G. J., and Novick, R. P. (2004) Peptide signaling in *Staphylococcus aureus* and other Gram-positive bacteria, *Peptides 25*, 1389-1403.

14. Novick, R. P., and Geisinger, E. (2008) Quorum sensing in staphylococci, *Annu. Rev. Genet. 42*, 541-564.

15. Thoendel, M., Kavanaugh, J. S., Flack, C. E., and Horswill, A. R. (2011) Peptide signaling in the staphylococci, *Chem. Rev. 111*, 117-151.

16. Gray, B., Hall, P., and Gresham, H. (2013) Targeting agr- and agr-Like quorum sensing systems for development of common therapeutics to treat multiple gram-positive bacterial infections, *Sensors (Basel) 13*, 5130-5166.

17. George, E. A., and Muir, T. W. (2007) Molecular mechanisms of agr quorum sensing in virulent staphylococci, *ChemBioChem 8*, 847-855.

18. Le, K. Y., and Otto, M. (2015) Quorum-sensing regulation in staphylococci-an overview, *Front. Microbiol. 6*, 1174.

19. Ji, G., Beavis, R. C., and Novick, R. P. (1995) Cell density control of staphylococcal virulence mediated by an octapeptide pheromone, *Proc. Natl. Acad. Sci. USA 92*, 12055-12059.

20. Kavanaugh, J. S., Thoendel, M., and Horswill, A. R. (2007) A role for type I signal peptidase in *Staphylococcus aureus* quorum sensing, *Mol. Microbiol. 65*, 780-798.

21. Ji, G., Beavis, R., and Novick, R. P. (1997) Bacterial interference caused by autoinducing peptide variants, *Science 276*, 2027-2030.

22. Wang, B., Zhao, A., Novick, R. P., and Muir, T. W. (2014) Activation and inhibition of the receptor histidine kinase AgrC occurs through opposite helical transduction motions, *Mol. Cell 53*, 929-940.

23. Novick, R. P., Ross, H. F., Projan, S. J., Kornblum, J., Kreiswirth, B., and Moghazeh, S. (1993) Synthesis of staphylococcal virulence factors is controlled by a regulatory RNA molecule, *EMBO J. 12*, 3967-3975.

24. Queck, S. Y., Jameson-Lee, M., Villaruz, A. E., Bach, T. H., Khan, B. A., Sturdevant, D. E., Ricklefs, S. M., Li, M., and Otto, M. (2008) RNAIII-independent target gene control by the agr quorum-sensing system: insight into the evolution of virulence regulation in *Staphylococcus aureus*, *Mol. Cell 32*, 150-158.

25. Vuong, C., Durr, M., Carmody, A. B., Peschel, A., Klebanoff, S. J., and Otto, M. (2004) Regulated expression of pathogen-associated molecular pattern molecules in *Staphylococcus epidermidis*: quorum-sensing determines pro-inflammatory capacity and production of phenol-soluble modulins, *Cell. Microbiol. 6*, 753-759.

26. Cheung, G. Y., Joo, H. S., Chatterjee, S. S., and Otto, M. (2014) Phenol-soluble modulins - critical determinants of staphylococcal virulence, *FEMS Microbiol. Rev. 38*, 698-719.

27. Otto, M. (2014) Phenol-soluble modulins, *Int. J. Med. Microbiol. 304*, 164-169.

28. Otto, M. (2004) Quorum-sensing control in Staphylococci -- a target for antimicrobial drug therapy?, *FEMS Microbiol. Lett. 241*, 135-141.

29. Gordon, C. P., Williams, P., and Chan, W. C. (2013) Attenuating *Staphylococcus aureus* virulence gene regulation: a medicinal chemistry perspective, *J. Med. Chem. 56*, 1389-1404.

30. Otto, M. (2009) *Staphylococcus epidermidis*--the 'accidental' pathogen, *Nat. Rev. Microbiol. 7*, 555-567.

31. Wang, B., and Muir, T. W. (2016) Regulation of Virulence in *Staphylococcus aureus*: Molecular Mechanisms and Remaining Puzzles, *Cell Chem. Biol. 23*, 214-224.

32. Costerton, J. W., Stewart, P. S., and Greenberg, E. P. (1999) Bacterial biofilms: a common cause of persistent infections, *Science 284*, 1318-1322.

33. Rogers, K. L., Fey, P. D., and Rupp, M. E. (2009) Coagulase-negative staphylococcal infections, *Infect. Dis. Clin. North Am. 23*, 73-98.

34. Sabate Bresco, M., Harris, L. G., Thompson, K., Stanic, B., Morgenstern, M., O'Mahony, L., Richards, R. G., and Moriarty, T. F. (2017) Pathogenic Mechanisms and Host Interactions in *Staphylococcus epidermidis* Device-Related Infection, *Front. Microbiol. 8*, 1401.

35. Khan, B. A., Yeh, A. J., Cheung, G. Y., and Otto, M. (2015) Investigational therapies targeting quorum-sensing for the treatment of *Staphylococcus aureus* infections, *Expert Opin. Investig. Drugs 24*, 689-704.

36. Kavanaugh, J. S., and Horswill, A. R. (2016) Impact of Environmental Cues on Staphylococcal Quorum Sensing and Biofilm Development, *J. Biol. Chem. 291*, 12556-12564.

37. Pang, Y. Y., Schwartz, J., Thoendel, M., Ackermann, L. W., Horswill, A. R., and Nauseef, W. M. (2010) agr-Dependent interactions of *Staphylococcus aureus* USA300 with human polymorphonuclear neutrophils, *J. Innate. Immun. 2*, 546-559.

38. Joo, H. S., Cheung, G. Y., and Otto, M. (2011) Antimicrobial activity of community-associated methicillin-resistant *Staphylococcus aureus* is caused by phenol-soluble modulin derivatives, *J. Biol. Chem. 286*, 8933-8940.

39. Otto, M. (2010) Basis of virulence in community-associated methicillin-resistant *Staphylococcus aureus*, *Annu. Rev. Microbiol. 64*, 143-162.

40. von Eiff, C., Peters, G., and Heilmann, C. (2002) Pathogenesis of infections due to coagulase-negative staphylococci, *Lancet Infect. Dis. 2*, 677-685.

41. Vuong, C., and Otto, M. (2002) *Staphylococcus epidermidis* infections, *Microb. Infect. 4*, 481-489.

42. McCann, M. T., Gilmore, B. F., and Gorman, S. P. (2008) *Staphylococcus epidermidis* device-related infections: pathogenesis and clinical management, *J. Pharm. Pharmacol. 60*, 1551-1571.

43. Mertens, A., and Ghebremedhin, B. (2013) Genetic determinants and biofilm formation of clinical *Staphylococcus epidermidis* isolates from blood cultures and indwelling devises, *Eur. J. Microbiol. Immunol. (Bp) 3*, 111-119.

44. Schommer, N. N., Christner, M., Hentschke, M., Ruckdeschel, K., Aepfelbacher, M., and Rohde, H. (2011) *Staphylococcus epidermidis* uses distinct mechanisms of biofilm formation to interfere with phagocytosis and activation of mouse macrophage-like cells 774A.1, *Infect. Immun. 79*, 2267-2276.

45. Claessens, J., Roriz, M., Merckx, R., Baatsen, P., Van Mellaert, L., and Van Eldere, J. (2015) Inefficacy of vancomycin and teicoplanin in eradicating and killing *Staphylococcus epidermidis* biofilms in vitro, *Int. J. Antimicrob. Agents 45*, 368-375.

46. Harris, L. G., Dudley, E., Rohde, H., Frommelt, L., Siemssen, N., Wilkinson, T. S., and Mack, D. (2017) Limitations in the use of PSMgamma, agr, RNAIII, and biofilm formation as biomarkers to define invasive *Staphylococcus epidermidis* from chronic biomedical device-associated infections, *Int. J. Med. Microbiol. 307*, 382-387.

47. Kong, K. F., Vuong, C., and Otto, M. (2006) Staphylococcus quorum sensing in biofilm formation and infection, *Int. J. Med. Microbiol. 296*, 133-139.

48. Yao, Y., Vuong, C., Kocianova, S., Villaruz, A. E., Lai, Y., Sturdevant, D. E., and Otto, M. (2006) Characterization of the *Staphylococcus epidermidis* accessory-gene regulator response: quorum-sensing regulation of resistance to human innate host defense, *J. Infect. Dis. 193*, 841-848.

49. Wang, C., Li, M., Dong, D., Wang, J., Ren, J., Otto, M., and Gao, Q. (2007) Role of ClpP in biofilm formation and virulence of *Staphylococcus epidermidis*, *Microb. Infect. 9*, 1376-1383.

50. Wang, R., Khan, B. A., Cheung, G. Y., Bach, T. H., Jameson-Lee, M., Kong, K. F., Queck, S. Y., and Otto, M. (2011) *Staphylococcus epidermidis* surfactant peptides promote biofilm maturation and dissemination of biofilm-associated infection in mice, *J. Clin. Invest. 121*, 238-248.

51. Otto, M. (2013) Staphylococcal infections: mechanisms of biofilm maturation and detachment as critical determinants of pathogenicity, *Annu. Rev. Med. 64*, 175-188.

52. Le, K. Y., Dastgheyb, S., Ho, T. V., and Otto, M. (2014) Molecular determinants of staphylococcal biofilm dispersal and structuring, *Front. Cell. Infect. Microbiol. 4*, 167.

53. Yarwood, J. M., Bartels, D. J., Volper, E. M., and Greenberg, E. P. (2004) Quorum Sensing in *Staphylococcus aureus* Biofilms, *J. Bacteriol. 186*, 1838-1850.

54. Paharik, A. E., and Horswill, A. R. (2016) The Staphylococcal Biofilm: Adhesins, Regulation, and Host Response, *Microbiol Spectr. 4*.

55. Mack, D., Davies, A. P., Harris, L. G., Rohde, H., Horstkotte, M. A., and Knobloch, J. K. (2007) Microbial interactions in *Staphylococcus epidermidis* biofilms, *Anal. Bioanal. Chem. 387*, 399-408.

56. Hoiby, N., Ciofu, O., Johansen, H. K., Song, Z. J., Moser, C., Jensen, P. O., Molin, S., Givskov, M., Tolker-Nielsen, T., and Bjarnsholt, T. (2011) The clinical impact of bacterial biofilms, *Int. J. Oral. Sci. 3*, 55-65.

57. O'Toole, G., Kaplan, H. B., and Kolter, R. (2000) Biofilm formation as microbial development, *Annu. Rev. Microbiol. 54*, 49-79.

58. Vuong, C., Gerke, C., Somerville, G. A., Fischer, E. R., and Otto, M. (2003) Quorum-sensing control of biofilm factors in *Staphylococcus epidermidis*, *J. Infect. Dis. 188*, 706-718.

59. Buttner, H., Mack, D., and Rohde, H. (2015) Structural basis of *Staphylococcus epidermidis* biofilm formation: mechanisms and molecular interactions, *Front. Cell. Infect. Microbiol. 5*, 14.

60. Vuong, C., Saenz, H. L., Gotz, F., and Otto, M. (2000) Impact of the agr quorum-sensing system on adherence to polystyrene in *Staphylococcus aureus*, *J. Infect. Dis. 182*, 1688-1693.

61. Schaeffer, C. R., Woods, K. M., Longo, G. M., Kiedrowski, M. R., Paharik, A. E., Buttner, H., Christner, M., Boissy, R. J., Horswill, A. R., Rohde, H., and Fey, P. D. (2015) Accumulation-associated protein enhances *Staphylococcus epidermidis* biofilm formation under dynamic conditions and is required for infection in a rat catheter model, *Infect. Immun. 83*, 214-226.

62. Davies, D. (2003) Understanding biofilm resistance to antibacterial agents, *Nat. Rev. Drug Discov. 2*, 114-122.

63. Boles, B. R., and Horswill, A. R. (2008) Agr-mediated dispersal of *Staphylococcus aureus biofilms*, *PLoS Pathog. 4*, e1000052.

64. Lauderdale, K. J., Malone, C. L., Boles, B. R., Morcuende, J., and Horswill, A. R. (2010) Biofilm dispersal of community-associated methicillin-resistant *Staphylococcus aureus* on orthopedic implant material, *J. Orthop. Res. 28*, 55-61.

65. Beenken, K. E., Mrak, L. N., Griffin, L. M., Zielinska, A. K., Shaw, L. N., Rice, K. C., Horswill, A. R., Bayles, K. W., and Smeltzer, M. S. (2010) Epistatic relationships between sarA and agr in *Staphylococcus aureus* biofilm formation, *PLoS One 5*, e10790.

66. Shenkman, B., Varon, D., Tamarin, I., Dardik, R., Peisachov, M., Savion, N., and Rubinstein, E. (2002) Role of agr (RNAIII) in *Staphylococcus aureus* adherence to fibrinogen, fibronectin, platelets and endothelial cells under static and flow conditions, *J. Med. Microbiol. 51*, 747-754.

67. Kirchdoerfer, R. N., Garner, A. L., Flack, C. E., Mee, J. M., Horswill, A. R., Janda, K. D., Kaufmann, G. F., and Wilson, I. A. (2011) Structural basis for ligand recognition and discrimination of a quorum-quenching antibody, *J. Biol. Chem. 286*, 17351-17358.

68. Todd, D. A., Parlet, C. P., Crosby, H. A., Malone, C. L., Heilmann, K. P., Horswill, A. R., and Cech, N. B. (2017) Signal Biosynthesis Inhibition with Ambuic Acid as a Strategy To Target Antibiotic-Resistant Infections, *Antimicrob. Agents Chemother. 61*.

69. Sully, E. K., Malachowa, N., Elmore, B. O., Alexander, S. M., Femling, J. K., Gray, B. M., DeLeo, F. R., Otto, M., Cheung, A. L., Edwards, B. S., Sklar, L. A., Horswill, A. R., Hall, P. R., and Gresham, H. D. (2014) Selective chemical inhibition of agr quorum sensing in *Staphylococcus aureus* promotes host defense with minimal impact on resistance, *PLoS Pathog. 10*, e1004174.

70. Mayville, P., Ji, G., Beavis, R., Yang, H., Goger, M., Novick, R. P., and Muir, T. W. (1999) Structure-activity analysis of synthetic autoinducing thiolactone peptides from *Staphylococcus aureus* responsible for virulence, *Proc. Natl. Acad. Sci. USA 96*, 1218-1223.

71. Lyon, G. J., Mayville, P., Muir, T. W., and Novick, R. P. (2000) Rational design of a global inhibitor of the virulence response in *Staphylococcus aureus*, based in part on localization of the site of inhibition to the receptor-histidine kinase, AgrC, *Proc. Natl. Acad. Sci. USA 97*, 13330-13335.

72. P, M., Affas, Z., Reynolds, C., Holden, M. T., Wood, S. J., Saint, S., Cockayne, A., Hill, P. J., Dodd, C. E., Bycroft, B. W., Chan, W. C., and Williams, P. (2001) Structure, activity and evolution of the group I thiolactone peptide quorum-sensing system of *Staphylococcus aureus*, *Mol. Microbiol. 41*, 503-512.

73. Lyon, G. J., Wright, J. S., Muir, T. W., and Novick, R. P. (2002) Key determinants of receptor activation in the agr autoinducing peptides of *Staphylococcus aureus*, *Biochemistry 41*, 10095-10104.

74. Scott, R. J., Lian, L. Y., Muharram, S. H., Cockayne, A., Wood, S. J., Bycroft, B. W., Williams, P., and Chan, W. C. (2003) Side-chain-to-tail thiolactone peptide inhibitors of the staphylococcal quorum-sensing system, *Bioorg. Med. Chem. Lett. 13*, 2449-2453.

75. Fowler, S. A., Stacy, D. M., and Blackwell, H. E. (2008) Design and synthesis of macrocyclic peptomers as mimics of a quorum sensing signal from *Staphylococcus aureus*, *Org. Lett. 10*, 2329-2332.

76. George, E. A., Novick, R. P., and Muir, T. W. (2008) Cyclic peptide inhibitors of staphylococcal virulence prepared by Fmoc-based thiolactone peptide synthesis, *J. Am. Chem. Soc. 130*, 4914-4924.

77. Tal-Gan, Y., Stacy, D. M., Foegen, M. K., Koenig, D. W., and Blackwell, H. E. (2013) Highly potent inhibitors of quorum sensing in *Staphylococcus aureus* revealed through a systematic synthetic study of the group-III autoinducing peptide, *J. Am. Chem. Soc. 135*, 7869-7882.

78. Nielsen, A., Mansson, M., Bojer, M. S., Gram, L., Larsen, T. O., Novick, R. P., Frees, D., Frokiaer, H., and Ingmer, H. (2014) Solonamide B inhibits quorum sensing and reduces *Staphylococcus aureus* mediated killing of human neutrophils, *PLoS One 9*, e84992.

79. Tal-Gan, Y., Stacy, D. M., and Blackwell, H. E. (2014) N-Methyl and peptoid scans of an autoinducing peptide reveal new structural features required for inhibition and activation of AgrC quorum sensing receptors in *Staphylococcus aureus*, *Chem. Commun. (Camb.) 50*, 3000-3003.

80. Johnson, J. G., Wang, B., Debelouchina, G. T., Novick, R. P., and Muir, T. W. (2015) Increasing AIP Macrocycle Size Reveals Key Features of agr Activation in *Staphylococcus aureus*, *ChemBioChem 16*, 1093-1100.

81. Vasquez, J. K., Tal-Gan, Y., Cornilescu, G., Tyler, K. A., and Blackwell, H. E. (2017) Simplified AIP-II Peptidomimetics Are Potent Inhibitors of *Staphylococcus aureus* AgrC Quorum Sensing Receptors, *ChemBioChem 18*, 413-423.

82. Wright, J. S., 3rd, Jin, R., and Novick, R. P. (2005) Transient interference with staphylococcal quorum sensing blocks abscess formation, *Proc. Natl. Acad. Sci. USA 102*, 1691-1696.

83. Amara, N., Krom, B. P., Kaufmann, G. F., and Meijler, M. M. (2011) Macromolecular inhibition of quorum sensing: enzymes, antibodies, and beyond, *Chem. Rev. 111*, 195-208.

84. Galloway, W. R., Hodgkinson, J. T., Bowden, S., Welch, M., and Spring, D. R. (2012) Applications of small molecule activators and inhibitors of quorum sensing in Gram-negative bacteria, *Trends Microbiol. 20*, 449-458.

85. Praneenararat, T., Palmer, A. G., and Blackwell, H. E. (2012) Chemical methods to interrogate bacterial quorum sensing pathways, *Org. Biomol. Chem. 10*, 8189-8199.

86. Otto, M., Sussmuth, R., Jung, G., and Gotz, F. (1998) Structure of the pheromone peptide of the *Staphylococcus epidermidis* agr system, *FEBS Lett. 424*, 89-94.

87. Carmody, A. B., and Otto, M. (2004) Specificity grouping of the accessory gene regulator quorum-sensing system of *Staphylococcus epidermidis* is linked to infection, *Arch. Microbiol. 181*, 250-253.

88. Olson, M. E., Todd, D. A., Schaeffer, C. R., Paharik, A. E., Van Dyke, M. J., Buttner, H., Dunman, P. M., Rohde, H., Cech, N. B., Fey, P. D., and Horswill, A. R. (2014) *Staphylococcus epidermidis* agr quorum-sensing system: signal identification, cross talk, and importance in colonization, *J. Bacteriol. 196*, 3482-3493.

89. Yarwood, J. M., McCormick, J. K., Paustian, M. L., Kapur, V., and Schlievert, P. M. (2002) Repression of the *Staphylococcus aureus* accessory gene regulator in serum and in vivo, *J. Bacteriol. 184*, 1095-1101.

90. Peterson, M. M., Mack, J. L., Hall, P. R., Alsup, A. A., Alexander, S. M., Sully, E. K., Sawires, Y. S., Cheung, A. L., Otto, M., and Gresham, H. D. (2008) Apolipoprotein B Is an innate barrier against invasive *Staphylococcus aureus* infection, *Cell Host Microbe 4*, 555-566.

91. Tal-Gan, Y., Ivancic, M., Cornilescu, G., Cornilescu, C. C., and Blackwell, H. E. (2013) Structural characterization of native autoinducing peptides and abiotic analogues reveals key features essential for activation and inhibition of an AgrC quorum sensing receptor in *Staphylococcus aureus*, *J. Am. Chem. Soc. 135*, 18436-18444.

92. Tal-Gan, Y., Ivancic, M., Cornilescu, G., and Blackwell, H. E. (2016) Characterization of structural elements in native autoinducing peptides and non-native analogues that permit

the differential modulation of AgrC-type quorum sensing receptors in *Staphylococcus aureus*, *Org. Biomol. Chem. 14*, 113-121.

93. Kim, M. K., Zhao, A., Wang, A., Brown, Z. Z., Muir, T. W., Stone, H. A., and Bassler, B. L. (2017) Surface-attached molecules control *Staphylococcus aureus* quorum sensing and biofilm development, *Nat. Microbiol. 2*, 17080.

94. Kratochvil, M. J., Tal-Gan, Y., Yang, T., Blackwell, H. E., and Lynn, D. M. (2015) Nanoporous Superhydrophobic Coatings that Promote the Extended Release of Water-Labile Quorum Sensing Inhibitors and Enable Long-Term Modulation of Quorum Sensing in *Staphylococcus aureus*, *ACS Biomater. Sci. Eng. 1*, 1039-1049.

95. Broderick, A. H., Stacy, D. M., Tal-Gan, Y., Kratochvil, M. J., Blackwell, H. E., and Lynn, D. M. (2014) Surface coatings that promote rapid release of peptide-based AgrC inhibitors for attenuation of quorum sensing in *Staphylococcus aureus*, *Adv. Healthc. Mater. 3*, 97-105.

96. Otto, M., Sussmuth, R., Vuong, C., Jung, G., and Gotz, F. (1999) Inhibition of virulence factor expression in *Staphylococcus aureus* by the *Staphylococcus epidermidis* agr pheromone and derivatives, *FEBS Lett. 450*, 257-262.

97. Otto, M. (2001) *Staphylococcus aureus* and *Staphylococcus epidermidis* peptide pheromones produced by the accessory gene regulator agr system, *Peptides 22*, 1603-1608.

98. Otto, M., Echner, H., Voelter, W., and Gotz, F. (2001) Pheromone cross-inhibition between *Staphylococcus aureus* and *Staphylococcus epidermidis*, *Infect. Immun. 69*, 1957-1960.

99. Canovas, J., Baldry, M., Bojer, M. S., Andersen, P. S., Grzeskowiak, P. K., Stegger, M., Damborg, P., Olsen, C. A., and Ingmer, H. (2016) Cross-Talk between *Staphylococcus aureus* and Other Staphylococcal Species via the agr Quorum Sensing System, *Front. Microbiol. 7*, 1733.

100. Paharik, A. E., Parlet, C. P., Chung, N., Todd, D. A., Rodriguez, E. I., Van Dyke, M. J., Cech, N. B., and Horswill, A. R. (2017) Coagulase-Negative Staphylococcal Strain Prevents *Staphylococcus aureus* Colonization and Skin Infection by Blocking Quorum Sensing, *Cell Host Microbe 22*, 746-756 e745.

101. Fleming, V., Feil, E., Sewell, A. K., Day, N., Buckling, A., and Massey, R. C. (2006) Agr interference between clinical *Staphylococcus aureus* strains in an insect model of virulence, *J. Bacteriol. 188*, 7686-7688.

102. Goerke, C., Kummel, M., Dietz, K., and Wolz, C. (2003) Evaluation of intraspecies interference due to agr polymorphism in *Staphylococcus aureus* during infection and colonization, *J. Infect. Dis. 188*, 250-256.

103. Kahl, B. C., Becker, K., Friedrich, A. W., Clasen, J., Sinha, B., Von Eiff, C., and Peters, G. (2003) agr-dependent bacterial interference has no impact on long-term colonization of *Staphylococcus aureus* during persistent airway infection of cystic fibrosis patients, *J. Clin. Microbiol. 41*, 5199-5201.

104. Cogen, A. L., Yamasaki, K., Sanchez, K. M., Dorschner, R. A., Lai, Y., MacLeod, D. T., Torpey, J. W., Otto, M., Nizet, V., Kim, J. E., and Gallo, R. L. (2010) Selective antimicrobial action is provided by phenol-soluble modulins derived from *Staphylococcus epidermidis*, a normal resident of the skin, *J. Invest. Dermatol. 130*, 192-200.

105. Iwase, T., Uehara, Y., Shinji, H., Tajima, A., Seo, H., Takada, K., Agata, T., and Mizunoe, Y. (2010) *Staphylococcus epidermidis* Esp inhibits *Staphylococcus aureus* biofilm formation and nasal colonization, *Nature 465*, 346-349.

106. Zipperer, A., Konnerth, M. C., Laux, C., Berscheid, A., Janek, D., Weidenmaier, C., Burian, M., Schilling, N. A., Slavetinsky, C., Marschal, M., Willmann, M., Kalbacher, H., Schittek, B., Brotz-Oesterhelt, H., Grond, S., Peschel, A., and Krismer, B. (2016) Human commensals producing a novel antibiotic impair pathogen colonization, *Nature 535*, 511-516.

107. Nakatsuji, T., Chen, T. H., Narala, S., Chun, K. A., Two, A. M., Yun, T., Shafiq, F., Kotol, P. F., Bouslimani, A., Melnik, A. V., Latif, H., Kim, J. N., Lockhart, A., Artis, K., David, G., Taylor, P., Streib, J., Dorrestein, P. C., Grier, A., Gill, S. R., Zengler, K., Hata, T. R., Leung, D. Y., and Gallo, R. L. (2017) Antimicrobials from human skin commensal bacteria protect against *Staphylococcus aureus* and are deficient in atopic dermatitis, *Sci. Transl. Med. 9*.

108. Lina, G., Boutite, F., Tristan, A., Bes, M., Etienne, J., and Vandenesch, F. (2003) Bacterial Competition for Human Nasal Cavity Colonization: Role of Staphylococcal agr Alleles, *Appl. Environ. Microbiol. 69*, 18-23.

CHAPTER 2:

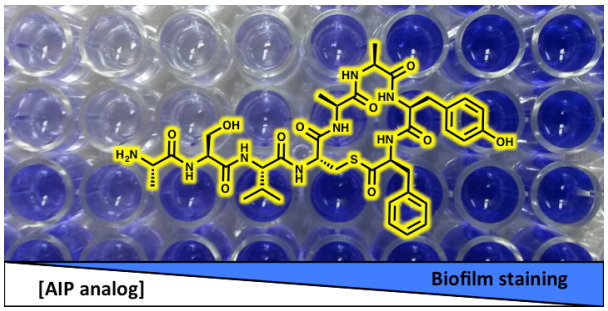
Staphylococcus epidermidis Autoinducing Peptide I Structure-Function Analyses Reveals Motifs Critical for Modulation of AgrC Receptors

Contribution: T. Yang designed the experiments, synthesized the peptides, performed biological assays and wrote the manuscript. Y. Tal-Gan assisted in peptide synthesis. A. E. Paharik constructed the fluorescence reporter strains for biological assays. A. R. Horswill contributed to reporter strain constructions and manuscript preparation. H. E. Blackwell guided the project and assisted in manuscript preparation.

*This chapter is published under the same title; *ACS. Chem. Biol.,* **2016**, *11*, 1982-1991.

Copyright 2016 American Chemical Society.

2.1 Abstract



Staphylococcus epidermidis is frequently implicated in medical device infections due to its ubiquity in the skin flora and formation of robust biofilms. The accessory gene regulator (*agr*) quorum sensing (QS) system plays prominently in the establishment of biofilms and infection by this bacterium. *Agr* activation is mediated by the binding of a peptide signal (or autoinducing peptide, AIP) to its cognate AgrC receptor. Many questions remain about the role of QS in *S. epidermidis* infections, as well as in mixed-microbe populations on a host, and chemical modulators of its *agr* system could provide novel insights. The AIP ligand provides an initial scaffold for the development of such probes; however, the structure-activity relationships (SARs) for activation of *S. epidermidis* AgrC receptors by AIPs are largely unknown. Herein, we report the first SAR analyses of an *S. epidermidis* AIP by performing systematic alanine and D-amino acid scans of the *S. epidermidis* AIP-I. Based on these results, we designed and identified potent, pan-group inhibitors of the AgrC receptors in the three *S. epidermidis agr* groups, as well as a set of AIP-I analogs capable of selective AgrC inhibition in either specific *S. epidermidis agr* groups or in another common Staphylococcal species, *S. aureus*. Lastly, we uncovered a non-native peptide agonist of AgrC-I that can strongly inhibit *S. epidermidis* biofilm growth with a higher potency and efficacy than that of native AIP-I. Together, these synthetic analogs represent new and readily accessible probes for investigating the roles of QS in *S. epidermidis* colonization and infections.

2.2 Introduction

Staphylococcus epidermidis is a ubiquitous commensal colonizer of human epithelia *(1)*. Previously thought to be innocuous, *S. epidermidis* recently has been identified as an important nosocomial pathogen *(2, 3)*. In particular, *S. epidermidis* is a leading causative agent in infections associated with indwelling medical devices, which is directly related to its ubiquity and propensity to form biofilms on abiotic surfaces *(3-6)*. The barrier provided by this biofilm lifestyle, combined with growing resistance to antibiotics, make *S. epidermidis* infections especially recalcitrant to traditional antimicrobial treatments and, consequently, a serious problem to public health *(2, 3, 6-8)*.

Playing an important role in the virulence of *S. epidermidis* is its quorum sensing (QS) system *(9-13)*. QS is a cell-cell communication process that allows bacteria to sense population density and coordinate gene expression to control group behavior at high cell numbers *(14, 15)*. The primary QS circuit in *S. epidermidis* is the accessory gene regulator (*agr*) system, which was first characterized and has been most studied to date in the related human pathogen *Staphylococcus aureus (16-18)*. The *agr* system consists of four components (AgrA–D) that are encoded by the *agr* locus (Figure 2.1) *(16-19)*. AgrD is a propeptide containing the sequence of the mature autoinducing peptide (or AIP) signal, and it is processed and secreted by the integral membrane endopeptidase AgrB *(20, 21)*. Once reaching a threshold extracellular concentration (produced by a “quorate” population of cells), the AIP is sensed by a two-component system comprised of AgrC and AgrA. Productive binding of the AIP to AgrC, a transmembrane receptor histidine kinase, triggers its subsequent dimerization and *trans*-autophosphorylation *(22, 23)*; the activated AgrC then phosphorylates the response regulator AgrA. Phosphorylated AgrA next dimerizes, binds the P2 and P3 promoters, and upregulates the transcription of the *agr* locus and RNAIII, respectively. RNAIII serves as the main effector of the *agr* system, and thereby, many virulence phenotypes in *S. epidermidis (24)*. Phosphorylated AgrA also directly activates the production of a group of small amphipathic peptides known as phenol-soluble modulins

(PSMs), which are key virulence factors for both the biofilm life cycle and survival in infected hosts *(11, 25)*.

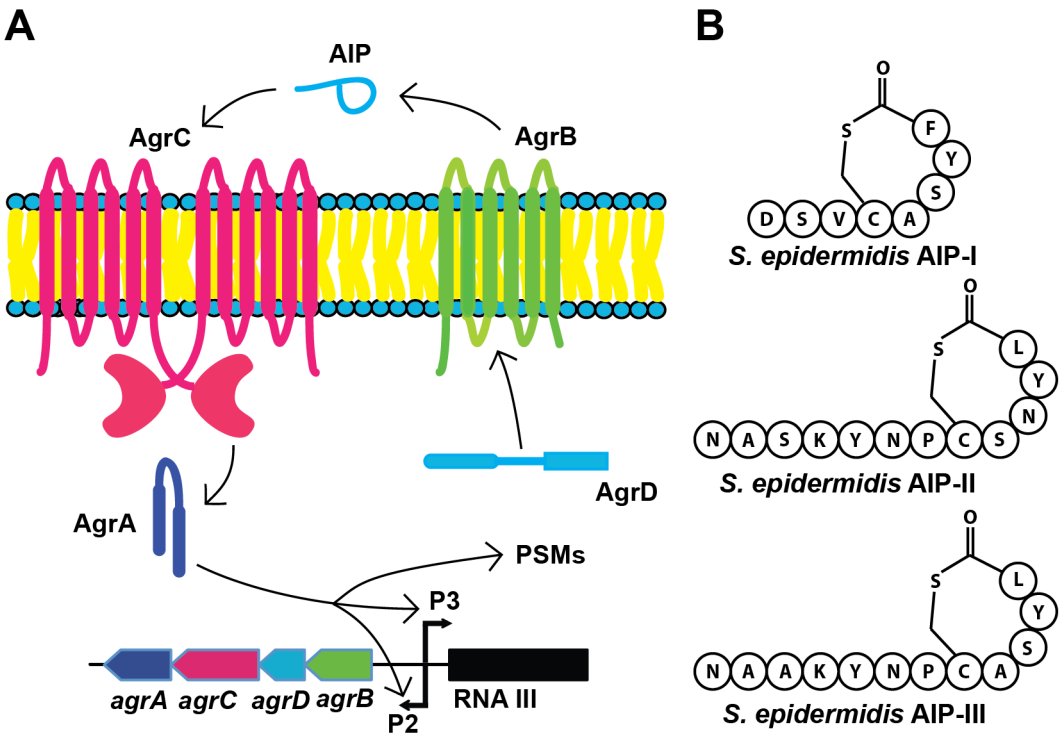


Figure 2.1: The *agr* QS system in *S. epidermidis* and associated AIP signals. (A) Simplified schematic of the *agr* system. Propeptide AgrD is processed and secreted by the integral membrane endopeptidase AgrB to generate the mature autoinducing peptide (AIP) signal. Once a threshold extracellular concentration of AIP is reached, the AgrC receptor binds to its cognate AIP and homodimerizes. Activation of AgrC, a transmembrane histidine kinase, by AIP leads to AgrC *trans*-autophosphorylation, which then phosphorylates the response regulator AgrA. The phosphorylated AgrA subsequently activates transcription from the P2, P3, and PSM promoters. P2 encodes the four components of the *agr* system, whereas P3 drives the expression of RNAIII, the main effector molecule of the *agr* system. (B) Primary structures of the three AIP signals (I–III) corresponding to the three *S. epidermidis agr* Groups (I–III).

The formation of a robust biofilm is the primary mechanism by which *S. epidermidis* causes infections on medical implants *(3)*. A number of studies have identified the polysaccharide intercellular adhesin (PIA) as being a critical structural component of the biofilm *(26)*. In *S. epidermidis* strains that produce PIA, the *agr* system is involved in many of the distinct stages of biofilm formation *(10, 27, 28)*. Specifically, the *agr* system negatively regulates the expression of

the surface-attached AtlE protein *(29)*, an important adhesion factor in the attachment phase of biofilm growth, and positively regulates the production of PSMs and proteases that facilitate the detachment of bacteria from biofilm *(11, 30, 31)*. Consequently, intentional *activation* of the *agr* system could provide an alternative approach of limiting *S. epidermidis* infection by reducing biofilm growth *(32)*, especially considering that *S. epidermidis*, unlike *S. aureus*, does not possess a vast repertoire of damaging toxins under QS control *(3, 18)*. Furthermore, this approach could be combined with administration of antibiotics to potentiate the effectiveness of such drugs *(4, 32)*. In contrast, other studies have proposed that inhibition, as opposed to activation, of the *agr* system can also attenuate virulence, despite the concern over the enhanced accumulation of biofilm observed in *S. epidermidis agr* mutants *(28, 33, 34)*. For example, Otto and co-workers, using *agr*-null strains of *S. epidermidis,* have demonstrated that the presence of an active *agr* system offers the bacterium significantly more protection against antimicrobial peptides and oxidative stress, both of which are defense mechanisms against infections employed by the innate immune system *(10, 13)*. The *agr* system has also been shown to promote bacteria dissemination and tissue infiltration during device-related infections *(13, 30, 31, 35)*. Further, a recent report by Olson et al. revealed the *agr* system to be necessary for optimal skin colonization *(36)*. Lastly, there is growing appreciation that many *S. epidermidis* clinical isolates from implant infections do not have the genes to make PIA *(37-39)*, but these strains still build a biofilm *(40)*. The role the *agr* system plays in the early stages of biofilm development in these PIA-negative strains is unclear. Combined, these studies and others highlight the complex roles played by the *agr* system in the lifestyle of *S. epidermidis*. Therefore, while the *agr* system is an attractive target for controlling the virulence of *S. epidermidis*, further fundamental studies are required to assess when and how the *agr* system should be modulated (either via activation or inhibition) to attenuate infection.

Similar to *S. aureus*, the *agr* system is not identical within the *S. epidermidis* species. Based upon the primary structures of the three reported AIP signals (I–III) (Figure 2.1B), *S. epidermidis*

can be classified into three *agr* specificity groups referred to as Groups-I–III *(36, 41)*. Interestingly, the *agr* systems of these groups are known to interact with each other, a phenomenon called *agr* interference that was first described in *S. aureus (18, 42-44)*. In *S. epidermidis*, the *agr* system of Group-I is significantly inhibited by the AIP-II and –III signals, whereas Groups-II and -III are inhibited by AIP-I *(36)*. In addition, *agr* interference has also been identified between *S. epidermidis* Group-I and *S. aureus* Groups-I–IV, two species that colonize similar environmental niches on the human body *(45-47)*. These cross-inhibitory activities of the *agr* systems between different specificity groups and species have been hypothesized to play a role in competition for colonization and establishing infections *(18, 46, 48)*. However, *in vivo* studies have not provided conclusive support for such hypothesis *(48, 49)*. Additional studies are therefore necessary to elucidate the biological significance of *agr* interference, if any.

Chemical methods to modulate QS in bacteria have attracted considerable interest over the past decade, due in part to the temporal and spatial control they can provide and their often ready applicability to biologically relevant environments *(50-52)*. The development of chemical probes capable of modulating the *S. epidermidis agr* system could provide valuable tools for better understanding the role of the *agr* system in colonization and infection by this common bacterium. Both *agr* agonists and antagonists are of interest, given the dynamic and complex role played by QS during *S. epidermidis* infection. Moreover, identification of modulators that can selectively target a specific *agr* group or Staphylococcal species in a mixed bacteria population would provide promising tools to investigate the role of QS in the interplay between different *agr* groups or species. Prior studies by our lab and others have focused on the structure-activity relationships (SARs) for AIP:AgrC interactions in *S. aureus*, and have uncovered a number of potent, non-native *S. aureus* AgrC inhibitors in the process *(43, 53-61)*. Little is known, however, about the SARs of AIP:AgrC interactions in *S. epidermidis*. Earlier work by Otto and co-workers has shown that the thioester linkage and the three-amino acid exocyclic tail of AIP-I (Figure 2.1B) are required for AgrC-I activation, as they found the

hydrolyzed acyclic AIP-I, AIP-I analogs with exocyclic tails either one amino acid shorter or longer, and AIP-I analogs with a lactam or a lactone in place of the thioester were all inactive in cell-based AgrC-I activation assays *(47, 62)*. However, to our knowledge, no non-native AgrC agonists and antagonists have been reported for *S. epidermidis* to date.

Herein, we report a systematic analysis of the *S. epidermidis* AIP-I structure and delineate key SARs for AgrC-I activation by this ligand. We used these SAR data to develop a series of AIP-I analogs that strongly antagonize or agonize the AgrC-I receptor. Several of these ligands were capable of either pan-group or group-selective AgrC receptor inhibition in *S. epidermidis*. In turn, other peptides were found to be species selective, and could be applied to selectively modulate either *S. epidermidis* or *S. aureus* AgrC receptors. Notably, one of our non-native AgrC-I agonists was found to strongly inhibit *S. epidermidis* biofilm growth, with a higher potency and efficacy than that of native AIP-I. These new compounds represent the first synthetic modulators of AgrC in *S. epidermidis* and constitute powerful new tools to elucidate the complex roles of the *agr* QS system in this emerging pathogen.

2.3 Results and Discussion

2.3.1 AIP-I SARs revealed through alanine and D-amino acid scans.

Our SAR investigation began by systematically replacing each amino acid of the *S. epidermidis* AIP-I with either alanine or the corresponding D-amino acid to explore the roles of each side chain and stereocenter in the interaction between AIP-I and AgrC-I (note, Cys4 was not mutated to Ala due to its essentiality for macrocycle formation, and Ala5 did not require alanine replacement). The initial set of 14 analogs (listed in Table 2.1) was synthesized using solid-phase peptide chemistry and purified to homogeneity using our previously established HPLC methods *(59)*. We tested each analog for its ability to modulate the activity of the AgrC-I receptor using a wild-type *S. epidermidis* Group-I fluorescence reporter strain (see Methods). This strain contained a reporter plasmid encoding a *gfp* gene fused to the P3 promoter found

upstream of RNAIII *(36)*. Under high cell-density conditions, activation of the AgrC-I receptor by the endogenously produced AIP-I leads to phosphorylation of AgrA, which then binds the P3 promoter and activates *gfp* expression. The level of GFP fluorescence can therefore be quantified as a measurement of the extent of AgrC-I activation (note, this strain then fluoresces in the absence of added AIP-I at high densities). AgrC-I antagonism was measured by testing AIP-I analogs alone, while AgrC-I agonism was measured in the presence of a known strong AgrC-I inhibitor, *S. epidermidis* AIP-II, to block activation of AgrC-I by endogenously produced AIP-I. For comparison, we also evaluated the activities of the native *S. epidermidis* AIPs (I–III) and *S. aureus* AIPs (I–IV), as well as *S. aureus* AIP-III D4A, the most potent pan-group inhibitor of *S. aureus agr* systems that we have reported to date *(59)*. The native AIPs served as important controls for our fluorescence reporter assays, as their effects on AgrC-I activation by AIP-I in *S. epidermidis* have been described previously *(36, 45)*; the activity of the lead *S. aureus agr* inhibitor, AIP-III D4A, in *S. epidermidis* was unknown. Compounds demonstrating appreciable antagonism or agonism of AgrC-I in these assays were subjected to dose-response analyses, which permitted calculation of IC_{50} and EC_{50} values. The assay data for the alanine and D-amino acid AIP-I analogs and the control AIPs in AgrC-I are summarized in Table 2.1.

Table 2.1: IC_{50} and EC_{50} values for alanine and D-amino acid scan analogs of *S. epidermidis* AIP-I in AgrC-I determined using a fluorescence reporter strain.[a] Shaded cells represent control peptides.

Peptide Name	Sequence	IC_{50} (nM)	EC_{50}[b] (nM)
AIP-I D1A	A-S-V-(C-A-S-Y-F)	-	49.3
AIP-I S2A	D-A-V-(C-A-S-Y-F)	-	>1000
AIP-I V3A	D-S-A-(C-A-S-Y-F)	51.9	-
AIP-I S6A	D-S-V-(C-A-A-Y-F)	-	71.0
AIP-I Y7A	D-S-V-(C-A-S-A-F)		Inactive[c]
AIP-I F8A	D-S-V-(C-A-S-Y-A)		Inactive[c]
AIP-I D-D1	DD-S-V-(C-A-S-Y-F)	-	>1000
AIP-I D-S2	D-DS-V-(C-A-S-Y-F)	192[d]	
AIP-I D-V3	D-S-DV-(C-A-S-Y-F)	>1000	-
AIP-I D-C4	D-S-V-(DC-A-S-Y-F)		Inactive[c]
AIP-I D-A5	D-S-V-(C-DA-S-Y-F)		Inactive[c]
AIP-I D-S6	D-S-V-(C-A-DS-Y-F)	-	>1000
AIP-I D-Y7	D-S-V-(C-A-S-DY-F)		Inactive[c]
AIP-I D-F8	D-S-V-(C-A-S-Y-DF)	-	>1000
AIP-I	D-S-V-(C-A-S-Y-F)	-	196
AIP-II	N-A-S-K-Y-N-P-(C-S-N-Y-L)	9.64	-
AIP-III	N-A-A-K-Y-N-P-(C-A-S-Y-L)	34.3	-
S. aureus AIP-I	Y-S-T-(C-D-F-I-M)		Inactive[c]
S. aureus AIP-II	G-V-N-A-(C-S-S-L-F)	62.9	-
S. aureus AIP-III	I-N-(C-D-F-L-L)		Inactive[c]
S. aureus AIP-IV	Y-S-T-(C-Y-F-I-M)	>1000	-
S. aureus AIP-III D4A	I-N-(C-A-F-L-L)		Inactive[c]

[a] See Methods for details of the reporter strain and assay procedures. See Supplementary Information for peptide MS and HPLC characterization data, dose response curves, and 95% confidence intervals (CI) for IC_{50} and EC_{50} values. [b] Activation dose response curves were performed in the presence of 50 nM *S. epidermidis* AIP-II (an inhibitor) to block activation of AgrC-I by endogenously produced AIP-I. [c] Dose response curves revealed neither agonism nor antagonism over the concentration range tested. [d] Maximum inhibition did not exceed 60%.

The activities of the native *S. epidermidis* and *S. aureus* AIPs were congruent with previous reports, with the exception of *S. aureus* AIP-II. *S. aureus* AIP-II was previously reported to be inactive toward *S. epidermidis* AgrC-I *(46)*, but behaved as a relatively strong AgrC-I antagonist in our assay. This difference may be attributable to variances in the assay protocol and the strain used *(46)*. Interestingly, we found *S. aureus* AIP-III D4A, our potent pan-group inhibitor in

S. aureus, to be largely inactive in *S. epidermidis* Group-I, suggesting that this peptide could be used as a species-specific *agr* inhibitor in *S. aureus*. We return to this possibility below.

Turning to the alanine and D-amino acid scans of AIP-I, several interesting trends in the SAR of the AIP-I:AgrC-I interaction were revealed (Table 2.1). Previous SAR studies of *S. aureus* AIPs have shown that activation of an AgrC receptor by its cognate AIP likely involves two main steps: (i) initial binding of the AIP to AgrC (i.e., AIP "recognition") that is mediated largely by the macrocycle and bulky, hydrophobic endocyclic residues, and (ii) subsequent activation of AgrC via interactions with the exocyclic tail region of the bound AIP *(55, 61, 63)*. Consistent with these previous studies, replacement of either of the two hydrophobic residues (Tyr7 and Phe8) in the macrocycle of the *S. epidermidis* AIP-I with alanine resulted in a complete loss of activity in AgrC-I. Furthermore, the substitution of Tyr7 with the corresponding D-amino acid (i.e., AIP-I D-Y7) also caused a complete loss of activity, demonstrating the stringent requirement of this residue for AIP-I recognition by AgrC-I. AIP-I D-F8, however, maintained agonistic activity, albeit with lower potency relative to AIP-I, suggesting that the spatial configuration at this position plays less of a role in AIP-I:AgrC-I interactions in comparison to the composition of the side chain. Also in agreement with prior observations of AgrC receptor activation by receptor bound AIPs *(16, 55)*, alanine or D-amino acid replacements at residue Val3 in the exocyclic tail region converted AIP-I into a moderate or weak antagonist, respectively, demonstrating that Val3 likely plays an important role in AgrC-I activation. Replacing the nearby residue Ser2 with an alanine caused a decrease in agonistic activity, indicating that Ser2 contributes to AgrC-I activation by AIP-I. In addition, substitution with the D-amino acid counterpart at Ser2 yielded a weak AgrC-I antagonist, suggesting that the orientation of the residue at this position may influence the presentation of the key activating residue, Val3.

Converting both Cys4 and Ala5 residues to their D-isomers caused a complete loss of activity. Given the locations of these two stereocenters relative to the key thioester linkage

forming the macrocycle, this loss of activity could be the result of either a stringent requirement for the correct local stereochemistry at these two positions for AIP-I recognition or a global shift in the macrocycle conformation that prevents proper interaction between the key hydrophobic residues and AgrC-I. Additional structural studies are needed to provide a more definitive explanation for these observed effects. Perhaps the most intriguing finding in these initial AIP-I scans was that substitution of either Asp1 in the exocyclic tail or Ser6 in the macrocycle with alanine *increased* the agonistic activity of AIP-I on AgrC-I (by 2–4-fold). This observation is, to our knowledge, the first report that two residues in a native AIP allow for suboptimal activation of its cognate AgrC receptor. Previous SAR studies in *S. aureus* have identified only one residue in a single native AIP (*S. aureus* AIP-II) where a mutation yielded an analog with an increased agonistic activity relative to the starting structure (the extent of this increase was not reported) *(16)*. Replacement of Asp1 and Ser6 with their D-Amino acid counterparts reduced, but did not abolish, the agonistic activity of AIP-I. Together, these SAR trends suggest that the spatial configuration of these two residues contribute to the productive binding of AIP-I to its receptor, while the side chain composition of these residues appear to hinder optimal AIP-I:AgrC-I interactions (relative to alanine analogs).

2.3.2 SAR studies direct the design of second-generation AIP-I analogs.

A second set of *S. epidermidis* AIP-I analogs was next designed and synthesized to further examine the SAR trends revealed by the alanine and D-Amino acid analogs, and to potentially generate more potent modulators of AgrC-I. This set of analogs included peptides with substitutions at Ala5 (a position inaccessible through the alanine scan), combinatorial alanine modifications, and truncations to the exocyclic tail. In addition, a series of *S. epidermidis* AIP-II analogs with decreasing length of the exocyclic tail were also synthesized. These latter peptides were designed to explore the use of the AIP-II scaffold for AgrC-I inhibition, as the native AIP-II demonstrated the strongest inhibitory potency of our first-generation analogs and control

peptides (see Table 2.1). The structures of the second-generation analogs are shown in Table 2.2, and their associated activities in *S. epidermidis* AgrC-I were assessed using the fluorescence reporter assay introduced above.

Table 2.2: IC_{50} and EC_{50} values of second-generation AIP analogs in *S. epidermidis* AgrC-I determined using a fluorescence reporter strain.[a]

Peptide Name	Sequence	IC_{50} (nM)	EC_{50}[b] (nM)
AIP-I A5Y	D-S-V-(C-Y-S-Y-F)	95.4	-
AIP-I A5S	D-S-V-(C-S-S-Y-F)	135[c,d]	
AIP-I V3AA5Y	D-S-A-(C-Y-S-Y-F)	59.6	-
AIP-I V3AA5S	D-S-A-(C-S-S-Y-F)	29.4	-
AIP-I D1AS6A	A-S-V-(C-A-A-Y-F)	-	10.3
tAIP-I	Ac-(C-A-S-Y-F)	192	-
AIP-I D1AS6AV3A	A-S-A-(C-A-A-Y-F)	2.84	-
AIP-I D1AS6AV3AA5S	A-S-A-(C-S-A-Y-F)	2.08	-
AIP-II 11aa	A-S-K-Y-N-P-(C-S-N-Y-L)	5.43	-
AIP-II 10aa	S-K-Y-N-P-(C-S-N-Y-L)	5.29	-
AIP-II 9aa	K-Y-N-P-(C-S-N-Y-L)	2.83	-
AIP-II 8aa	Y-N-P-(C-S-N-Y-L)	6.08	-
AIP-II 7aa	N-P-(C-S-N-Y-L)	721	-
tAIP-II	Ac-(C-S-N-Y-L)	>1000	-

[a] See Methods for details of the reporter strain and assay procedures. See Supplementary Information for peptide MS and HPLC characterization data, dose response curves, and 95% confidence intervals (CI) for IC_{50} and EC_{50} values. [b] Activation dose response curves were performed in the presence of 50 nM *S. epidermidis* AIP-II (an inhibitor) to block activation of AgrC-I by endogenously produced AIP-I. [c] Maximum inhibition did not exceed 75%. [d] Two different AIP-I A5S analogs were isolated that exhibited differing activities; IC_{50} value listed is derived from the antagonism dose response curves for A5S-1 (see text). Ac: acetylated N-terminus

To assess the role of the Ala5 side chain in the AIP-I:AgrC-I interaction, we replaced Ala5 with either serine or tyrosine. These modifications were selected based on the primary structures of the native *S. aureus* and *S. epidermidis* AIPs that were found to exhibit inhibitory activities against AgrC-I (Table 2.1). Specifically, with the exception of *S. epidermidis* AIP-III having an alanine, all other native AIPs active in AgrC-I possess either a serine or a tyrosine at the second endocyclic position. We found substitution of Ala5 with a tyrosine yielded a weak

AgrC-I antagonist (Table 2.2), whereas substitution with a serine surprisingly produced two peptide products of the correct mass with differing activities (A5S-1 and A5S-2). Analog A5S-1 behaved as a weak inhibitor against AgrC-I, while A5S-2 displayed a non-monotonic dose response that indicated very weak inhibition at low concentrations yet activation at higher concentrations (see Supporting Information). When either the A5Y or A5S modification was combined with the inhibitory modification V3A, the resulting analogs, AIP-I V3AA5Y and AIP-I V3AA5S, exhibited similar inhibitory activities as the parent compound AIP-I V3A. One possible explanation for these observations is that the modifications at Ala5 influence the orientation of the activating residue Val3, leading to varying degrees of AgrC-I activation. When the activating valine is replaced with an alanine, the mutations of Ala5 have little to no effect on the activity of the resulting analogs. The chemical difference between the two AIP-I A5S analogs remains unclear, but we speculate that the two peptides are conformational isomers; efforts to elucidate the structural differences are ongoing.

Next, we tested additional AIP-I analogs with multiple alanine modifications to examine whether their modulatory effects on AgrC-I could be additive. Replacing both Asp1 and Ser6 residues with alanine generated an analog with enhanced agonistic activity in AgrC-I relative to the parent single alanine mutants (Table 2.2). This observation led to us testing the hypothesis that introduction of the inhibitory modification V3A to the D1AS6A analog, an AIP-I analog that presumably associates strongly with AgrC-I, could produce an AgrC-I *antagonist* with increased potency. Indeed, the resulting analog – AIP-I D1AS6AV3A – was one of the most potent AgrC-I antagonists identified in this study (IC_{50} = ~2 nM). A similar analog AIP-I D1AS6AV3AA5S, which contained an additional mutation (A5S) that could potentially further enhance AgrC-I binding, exhibited analogous potency as the parent triple mutant. Overall, the activities of these AIP-I analogs with combinatorial alanine mutations strengthened the SAR trends delineated in our first set of AIP-I analogs. Specifically, their activities confirmed that Val3 is the essential residue for activation of AgrC-I and that the side chains of residues Asp1 and Ser6 play a

negative role in the AIP-I:AgrC-I interaction. The importance of the exocyclic tail portion of AIP-I (which includes Val3) for AgrC-I activation was further confirmed by the weak inhibitory activity observed for the truncated analog of AIP-I (tAIP-I; Table 2.2). This observation was again consistent with prior SAR studies in *S. aureus*, where AIP macrocycles without exocyclic tails were shown to be sufficient for receptor recognition but not receptor activation, and thus acted as competitive AgrC inhibitors *(16, 55, 64)*.

The last group of peptides examined was the AIP-II analogs with varying lengths of the exocyclic tail (Table 2.2). Notably, both the native *S. epidermidis* AIP-II and AIP-III signals have markedly longer exocyclic tails relative to other structurally characterized AIPs, and understanding the role of this structural feature, for receptor activation or inhibition, is of fundamental interest *(36)*. The AIP-II analogs in this study were designed to determine whether the primary structure of AIP-II could be reduced, while maintaining the high potency of its inhibitory activity toward AgrC-I. Removing one amino acid at a time from the N-terminus of AIP-II (Table 2.2, Rows 9–13), we found that an AIP-II analog with only three amino acids left in the exocyclic tail (AIP-II 8aa) still exhibited inhibitory activity toward AgrC-I with potency similar to the parent AIP-II. Further removal of amino acids from the N-terminus (as in AIP-II 7aa and tAIP-II) caused a dramatic reduction in inhibitory activity. Since AIP-II 8aa has the same number of residues as the most potent AIP-I analogs introduced above, optimization of this AIP-II scaffold using the SAR trends uncovered herein could yield interesting AgrC-I modulators exhibiting strong activities.

2.3.3 Agr group-selective inhibition in S. epidermidis by certain AIP analogs.

As shown in Table 2.1, we found the native AIP-II and AIP-III signals of *S. epidermidis* both inhibit AgrC-I, congruent with the results of Olson et al. *(36)*. However, the biological significance of this *agr* interference remains unclear, although it has been hypothesized to potentially play a role in competition between different groups in a mixed bacteria milieu *(18)*.

Developing chemical modulators that target a specific *agr* group and are inactive toward the others could provide valuable tools for investigating the hypothesis of *agr* interference. To this end, we screened all of the AIP analogs introduced above in GFP reporter strains of Groups-II and -III *S. epidermidis* to complement the Group-I *S. epidermidis* data in Tables 2.1 and 2.2 (see Methods; Figures 2.7 and 2.8). The only AIP-I analog to show moderate group selectivity was AIP-I Y7A, which was inactive against Group-I but inhibited AgrC-II and –III to ~50% (Figures 2.7 and 2.8). More interestingly, two AIP-II analogs, tAIP-II and AIP-II 8aa, were shown to be strongly selective against Group-I and -II at 10 μM (inhibiting to ~75%) but were inactive against Group-III (Figure 2.2A).

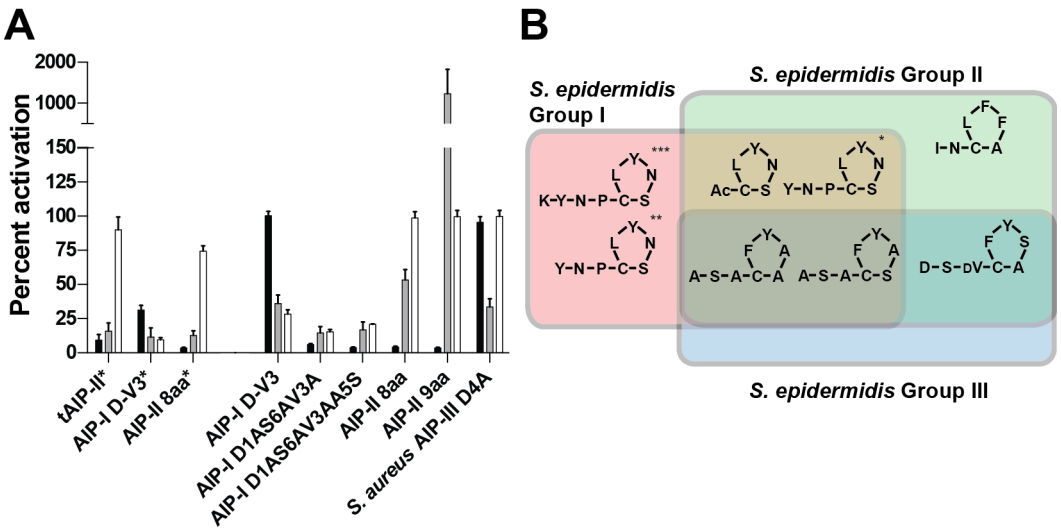


Figure 2.2: Pan-group activity profiles of selected *S. epidermidis* AIP-I analogs in *S. epidermidis*. (A) Effects of AIP-I analogs on AgrC-I–III as determined by fluorescence reporter strains (see Methods for details of strains and assay procedures). Compounds were tested at either 10 μM (indicated with *) or 100 nM. Black: Group-I; Gray: Group-II; White: Group-III. (B) Venn diagram summarizing *agr* group selectivity profiles for AgrC inhibition by AIP analogs in *S. epidermidis*. AIP-II 8aa shows differential selectivity at *10 μM and at **100 nM. ***Compound is an agonist of AgrC-II (see text).

We next screened a subset of peptides in these cross-group screens at a lower concentration to better gauge their relative activities (1 μM or 100 nM; Figure 2.2A, Figure 2.9). At the lower concentration, AIP-I D-V3 remained an antagonist against Group-II and Group-III

but lost its inhibitory activity toward Group-I (Figure 2.2A). Conversely, AIP-II 8aa remained active toward Group-I at 100 nM, whereas its inhibitory activity against Group-II decreased, making the activity of this analog more Group-I specific. AIP-II 9aa and *S. aureus* AIP-III D4A also exhibited group-selective activities, with AIP-II 9aa being inactive toward Group-III and *S. aureus* AIP-III D4A inhibiting exclusively Group-II. We note, however, that while AIP-II 9aa only inhibited Group-I, AIP-II 9aa was also a highly active *agonist* for Group-II. These selectively profiles are significant, as few *agr* group selective probes have been reported in any Staphylococcal species *(60)*, and none have been reported in *S. epidermidis*. Accordingly, these peptides represent a valuable new suite of chemical probes, and hold promise for examining the role of *agr*-based QS competition between any two *agr*-groups of *S. epidermidis* grown together. For example, by using AIP-II 8aa to target Group-I, *S. aureus* AIP-III D4A to target Group-II, or AIP-I D-V3 to target Group-III, a single *agr* system can be selectively inhibited in a bacterial population containing two different specificity groups (Figure 2.2B). We predict that further SAR studies of the AIP-II and AIP-III scaffolds may generate additional peptides with complementary group-selective activities.

2.3.4 Potent pan-group inhibitors of the agr system in S. epidermidis.

During our efforts to identify *agr*-group selective modulators, we noticed that AIP-I D1AS6AV3A and AIP-I D1AS6AV3AA5S, two of the most potent inhibitors that we identified in AgrC-I, also strongly inhibited AgrC-II and AgrC-III at 100 nM (Figure 2.2). To determine whether these two analogs were equally potent against AgrC-II and -III, we performed dose response antagonism assays on these analogs. The IC_{50} values obtained for AIP-I D1AS6AV3A and AIP-I D1AS6AV3AA5S against AgrC-II and -III were both in the subnanomolar to low nanomolar range and comparable to their IC_{50} values in AgrC-I (Figure 2.3). These two analogs represent, to the best of our knowledge, the first potent pan-group inhibitors of the *agr* system in *S. epidermidis*. Complementary to the selective probes described above, AIP-I D1AS6AV3A

and AIP-I D1AS6AV3AA5S should prove useful in a range of fundamental and applied studies, perhaps most so in those where *agr* inhibition in all three groups of *S. epidermidis* is required.

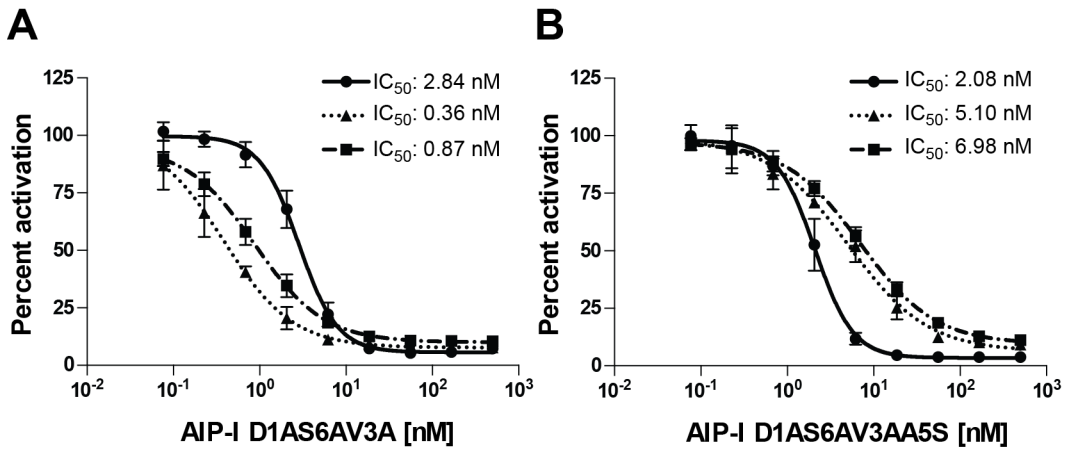


Figure 2.3. AgrC antagonism dose response curves and IC_{50} values for (A) AIP-I D1AS6AV3A and (B) AIP-I D1AS6AV3AA5S in the *S. epidermidis* Group-I–III GFP reporter strains. Circles: Group-I; triangles: Group-II; squares: Group-III. See Methods for strains and assay procedures.

2.3.5 Species-specific agr inhibition between S. epidermidis Group-I and S. aureus.

The *S. epidermidis* AIP-I is also known to inhibit the *agr* system in *S. aureus*. Similar to the cross-group inhibition observed between different *agr* groups of the same species, this *cross-species* inhibitory effect has no known biological role but is hypothesized to provide a competitive advantage on a host *(18, 46)*. Thus, we sought to examine the AIP analogs described herein to identify potential species-specific inhibitors that target either *S. epidermidis* Group-I or *S. aureus* Groups-I–IV. As noted in the discussions above, *S. aureus* AIP-III D4A, our most potent pan-group inhibitor against *S. aureus*, was inactive against *S. epidermidis* Group-I at 100 nM (Figure 2.4). We expanded our search and screened all of the AIP analogs reported herein capable of inhibiting the *agr* system in *S. epidermidis* Group-I for activity against the *agr* systems of *S. aureus* Groups-I–IV using analogous GFP reporter constructs (see Methods). We identified three peptides (Figure 2.4 and Figure 2.10), chief among them AIP-II 8aa, that selectively inhibited the *agr* system in *S. epidermidis* Group-I without significantly

affecting *agr* activity in *S. aureus* Groups-I–IV. Another analog, AIP-II 9aa, was shown to be largely an inhibitor specific to *S. epidermidis* Group-I, with only weak inhibitory activity in *S. aureus* Group-III. These two analogs, together with *S. aureus* AIP-III D4A, represent the first set of *species-specific*, chemical modulators targeting the *agr* systems of either *S. epidermidis* or *S. aureus*.

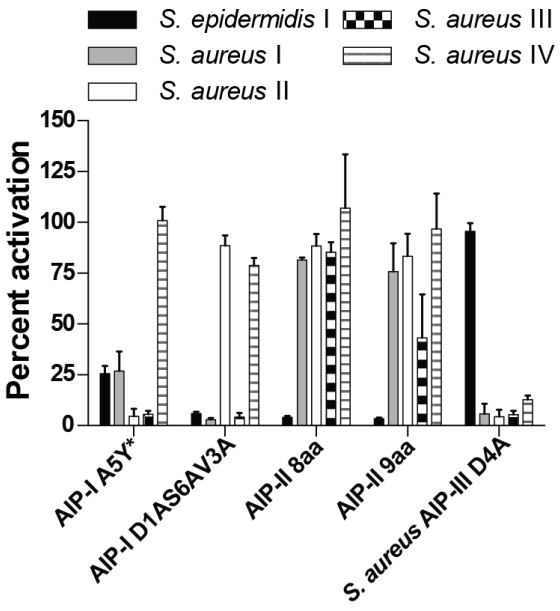


Figure 2.4. Effects of selected AIP analogs on the AgrC-I receptor in *S. epidermidis* Group-I and the AgrC I–IV receptors in *S. aureus* Groups-I–IV. Compounds tested at 100 nM unless otherwise noted. * Compound tested at 1 μM. See Methods for details of strains and assay procedures.

2.3.6 Modulation of biofilm formation in S. epidermidis Group-I using non-native AIPs.

As described above, the use of fluorescence reporter strains allowed for the rapid screening of AIP analogs and the identification of AgrC modulators with varying activities. However, the responses from an artificial reporter gene system may not translate to effects on relevant QS phenotypes. As a validation for the physiological relevance of the new AgrC modulators uncovered in this study, we assessed the ability of select non-native AIPs to modulate biofilm formation by *S. epidermidis* Group-I using the PIA-producing strain RP62A in a crystal violet

(CV) static biofilm assay (see Methods). Again, biofilm formation is the most important virulence phenotype associated with infection by *S. epidermidis*, and previous reports have established that its *agr* system plays an important role in biofilm formation (see above) *(10, 35)*. In particular, activation of the *agr* system is believed to disperse biofilm, thereby preventing the accumulation of sessile bacteria on a surface. We therefore hypothesized that addition of native AIP-I (an AgrC agonist) would inhibit *S. epidermidis* biofilm growth, and in agreement with a similar study in *S. aureus (32)*, static biofilm assays in 96-well microtiter plates in the presence of exogenous AIP-I showed substantial biofilm reduction (by ~60%, IC_{50} = 99 nM; Figure 2.5). We then tested AIP-I D1AS6A, the AIP-I analog identified with enhanced agonistic activity in AgrC-I relative to AIP-I, for modulation of *S. epidermidis* biofilm formation, and in agreement with its effect on the fluorescent reporter strain, this analog also decreased biofilm formation under similar conditions. In fact, it had overall enhanced efficacy and potency relative to AIP-I (~80% inhibition, IC_{50} = 18 nM; Figure 2.5). These matching activity trends provide support for the use of fluorescent reporter strains in identifying *S. epidermidis* AgrC modulators with physiological relevance. Moreover, our results with AIP-I D1AS6A provide the first non-native AIP analog, to our knowledge, that can strongly inhibit *S. epidermidis* biofilm growth.

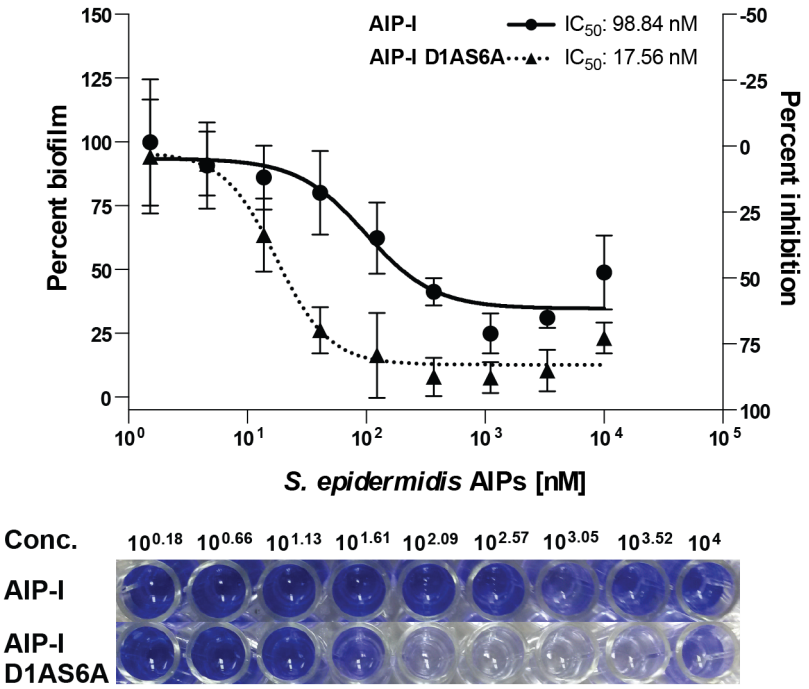


Figure 2.5. (Top) Biofilm antagonism dose response curves for *S. epidermidis* AIP-I and AIP-I D1AS6A against *S. epidermidis* Group-I RP62A strain as determined by CV staining (see Methods for assay procedure). Dose response curves shown represent the average of at least 4 biological replicates. (Bottom) Representative image of the CV assay with *S. epidermidis* AIP-I and AIP-I D1AS6A over a range of concentrations. Blue color correlates with biofilm growth.

While agonists of the *agr* system can decrease biofilm growth, *agr* system antagonists are generally expected to promote biofilm accumulation. Indeed, as discussed above, this relationship between the *agr* system and biofilm has raised concern over the merit of inhibiting QS in *S. epidermidis* (and related staphylococcal species) as a method of reducing virulence *(28, 34)*. To our surprise, however, exposing *S. epidermidis* Group-I to our nanomolar AgrC-I inhibitor (AIP-I D1AS6AV3AA5S) at 10 μM did not increase biofilm growth as expected in the static biofilm assay (Figure 2.12). Instead, the inhibitor did not alter, and perhaps even decreased, biofilm growth. While the CV assay is a relatively rudimentary method to monitor biofilm formation and the results obtained could be specific to our experimental conditions, we believe these results reflect the complex roles played by the *agr* system during biofilm formation in *S. epidermidis*. We suspect that the lack of stimulation in biofilm accumulation by the

antagonist is a result of the proficiency of *S. epidermidis* RP62A in PIA production, which could have maximized the formation of biofilm even in the absence of an exogenous AgrC antagonist. Inhibition of the *agr* system in a PIA-negative *S. epidermidis* strain could yield a more dramatic impact on biofilm formation. Additional investigation is certainly needed to better assess this hypothesis and the general consequences of modulating QS during *S. epidermidis* colonization. The new modulators reported in the current study could be useful tools for such an endeavor.

2.4 Summary

Infections by *S. epidermidis* have become a significant public health problem *(2, 3, 6-8)*. Current treatment options are limited, as like many other common pathogens, *S. epidermidis* is increasingly antibiotic resistant and can establish robust biofilms *(3-6, 8)*. The *agr* QS system is extensively involved in the pathogenesis of *S. epidermidis* infection, making this system a potentially attractive target for an alternative anti-infective strategy. However, the roles of the *agr* system in the infection process and biofilm formation are complex and dynamic. Chemical probes that interfere with the *S. epidermidis agr* system could pave a route toward a deeper understanding of how and when QS should be modulated to attenuate virulence. We report the first such compounds herein.

In this study, we prepared a series of non-native analogs of *S. epidermidis* AIP-I and performed the first systematic SAR analysis of this AIP scaffold for activation of AgrC-I (key SARs highlighted in Figure 2.6). This analysis had several important outcomes. First, it revealed two hydrophobic, endocyclic residues (Tyr7 and Phe8) that, in addition to the thioester linkage and Ala5, are essential for AgrC-I recognition. We also found that the exocyclic residue Val3 is critical for AgrC-I activation, and more interestingly, the Asp1 and Ser6 residues allow for submaximal activation of AgrC-I and actually could be mutated to augment the agonistic potencies of AIP-I analogs.

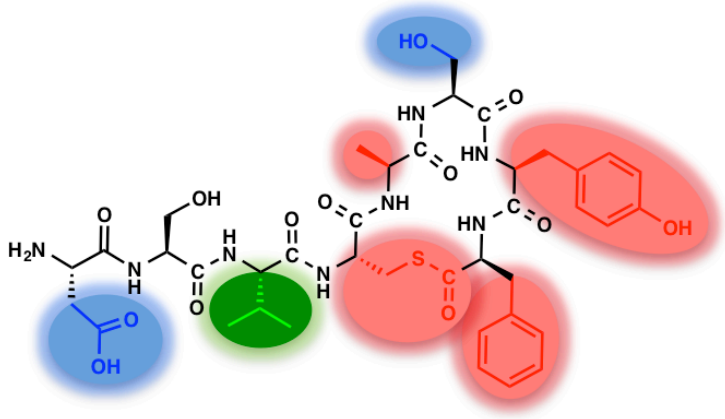


Figure 2.6: Summary of the key SAR trends for activation of *S. epidermidis* AgrC-I by AIP-I as revealed by the reporter assays in this study. Red: essential for AgrC receptor recognition. Green: essential for AgrC receptor activation. Blue: detrimental to AgrC receptor activation. Remaining residues contribute but are not critical to receptor recognition.

Second, our studies revealed several highly potent, non-native AgrC modulators, including the first pan-group AgrC inhibitors for *S. epidermidis* (AIP-I D1AS6AV3A and AIP-I D1AS6AV3AA5S). We also discovered a non-native agonist of AgrC-I (AIP-I D1AS6A) with improved potency over the native AIP-I and demonstrated that this analog was capable of strongly inhibiting *S. epidermidis* biofilm growth, an important virulence phenotype (at least) partially controlled by the *agr* system. This result suggests that the AgrC-I modulators reported herein can be used to alter QS-controlled virulence phenotypes in *S. epidermidis*. Moreover, AIP-I D1AS6A, to the best of our knowledge, represents the first non-native AIP analog with anti-biofilm activity in any staphylococcal species. Co-administration of this peptide with various antibiotics to examine whether *S. epidermidis* biofilm removal can improve the effectiveness of antibiotics would be an interesting experimental path forward, and is currently underway in our laboratories. As our most potent AgrC-I inhibitor (AIP-I D1AS6AV3AA5S) also slightly inhibited biofilm formation, examining its effects on biofilm growth and morphology in the presence of antibiotics would also be valuable. Looking to the future, applying AIP-I D1AS6AV3AA5S in various infection models at different stages of colonization could better illuminate the role of *agr*-

type QS in *S. epidermidis* infections and allow us to assess the viability of targeting QS in this pathogen as a possible anti-infective treatment.

Third and to close, this study has provided the first set of AgrC inhibitors that, at the concentrations tested, are selective either for particular *S. epidermidis* specificity groups or for a staphylococcal species (i.e., *S. epidermidis* or *S. aureus*). These new group and species selective AgrC inhibitors now can be utilized to selectively target an *agr* system in a mixed bacteria population and investigate the hypothesis of *agr* interference *(18, 42-44)*. Preliminary efforts toward this goal are ongoing in our laboratories and will be reported in due course. Overall, we predict that these peptide tools and the insights that they provide will open new avenues of investigation for QS in *Staphylococci* and could provide a pathway, with further development, toward new chemical strategies to attenuate infection.

2.5 Methods

2.5.1 Biological reagents, strains, and general methods

All standard reagents were purchased from commercial sources and used according to enclosed instructions. The *S. epidermidis* fluorescence reporter strains AH3408 (Group-I), AH3567 (Group-II), and AH3409 (Group-III) were cultured in Tryptic Soy Broth (TSB, from Sigma) augmented with 10 μg mL^{-1} of erythromycin *(36)*. The *S. epidermidis* wild-type strain RP62A (Group-I) was cultured in TSB (from Sigma or EMD Millipore). The *S. aureus* fluorescence reporter strains AH1677 (Group-I), AH430 (Group-II), AH1747 (Group-III), and AH1872 (Group-IV) were cultured in Brain Heart Infusion (BHI, from Teknova) augmented with 10 μg mL^{-1} of chloramphenicol *(65)*. All cultures were grown at 37 °C with shaking (200 rpm) unless noted otherwise. Absorbance and fluorescence measurements were obtained using a Biotek Synergy 2 microplate reader operating Gen5 data analysis software. IC_{50} values and EC_{50} values were determined from sigmoidal curve fits using GraphPad Prism software (v. 6.0).

2.5.2 Peptide synthesis

S. epidermidis AIP analogs were synthesized on solid-phase resin, purified by preparative high performance liquid chromatography (HPLC), and characterized using our previously reported methods *(59)*. See Supplementary Information for mass spectrometry (MS) and HPLC characterization data for the peptides in this study, as well as additional information on reagents and instrumentation used in peptide synthesis.

2.5.3 Fluorescence reporter assay protocol

For AgrC antagonism assays, peptide stock solutions in DMSO (1 mM) were serially diluted with DMSO (either 1:3 or 1:10), and 2 μL aliquots of the diluted solutions were added to each of the wells in a black 96-well polystyrene microtiter plate (Costar). Each peptide solution was tested in triplicate. As a negative control, 2 μL of DMSO was included. An overnight culture of the *S. epidermidis* or *S. aureus* fluorescence reporter strain was diluted 1:50 with fresh media, and 198 μL of the diluted culture were added to each of the wells of the microtiter plate containing peptide. Plates were then incubated at 37 °C for 24 h. Fluorescence (EX 500 nm / EM 540 nm) and OD_{600} of each well was measured using a plate reader, and the fluorescence values were normalized to the DMSO control. For *S. epidermidis* AgrC-I agonism assays, an additional 2 μL of *S. epidermidis* AIP-II stock solution was added to the wells to a final concentration of 50 nM, in order to block AgrC-I activation by endogenously produced AIP-I. The remaining steps of the fluorescence assay were the same as above.

For single-concentration fluorescence reporter assays, 2 μL of the peptide stock solutions were added to the wells in a black 96-well microtiter plate to a final concentration of 10 μM, 1 μM, or 100 nM. The remaining steps of the fluorescence assay were the same as above.

2.5.4 Crystal violet biofilm assay protocol

Peptide stock solutions were serially diluted with DMSO (1:3), and 2 μL of the diluted solutions were added to each of the wells in a clear, flat-bottom, 96-well polystyrene microtiter plate (Costar). Each solution was tested in triplicate. As a negative control, 2 μL of DMSO was included. An overnight culture of *S. epidermidis* RP62A was diluted 1:100 with fresh TSB (EMD Millipore) augmented with 0.5% (w/v) glucose, and 198 μL of the diluted culture were added to each of the wells of the microtiter plate containing peptides. Bacteria were incubated at 37 °C for 24 h under static conditions. Quantification of the amount of biofilm formed using crystal violet (CV) assays was performed according to previously reported protocols *(66)*. For single-concentration CV assays, 2 μL of the peptide stock solutions were added to the wells to a final concentration of 10 μM. The remaining steps of the biofilm assay were the same as above.

2.6 Supplementary Information

2.6.1 Chemical reagents and instrumentation

Chemical reagents, resin, and solvents were purchased from commercial sources (Sigma-Aldrich and Chem-Impex International) and used as obtained, with the exception of anhydrous dichloromethane (CH_2Cl_2), which was kept dry using molecular sieves. Water (18 MΩ) was purified using a Barnstead Nanopure (Thermo Scientific).

Reverse-phase high performance liquid chromatography (RP-HPLC) was performed using a Shimadzu system equipped with a SLC-10Avp controller, a LC-10AT pump, a FCV-ALvp solvent mixer, and a SPC-10MAvp UV/Vis diode array detector. Preparative RP-HPLC work was performed on a semi-preparative Phenomenex Gemini C18 column (5 μm, 10 x 250 mm^2, 110 Å), and analytical RP-HPLC work was performed on an analytical Phenomenex Gemini C18 column (5 μm, 4.6 x 250 mm^2, 110 Å). The RP-HPLC conditions were as follows: flow rate = 5 mL min^{-1} for semi-preparative work and 1 mL min^{-1} for analytical work; mobile phase A = 18 MΩ

water + 0.1% trifluoroacetic acid (TFA); mobile phase B = acetonitrile + 0.1% TFA. Linear peptides were purified using a linear gradient (80% → 50% A over 30 min). Cyclic peptides were purified using a linear gradient (80% → 65% A over 27 min). Peptide purity was determined using a linear gradient (90% → 5% A over 27 min) and integrating peaks detected at 220 nm.

A Micromass LCT ESI-TOF mass spectrometer (Waters) was used to obtain Exact Mass (EM) measurements for all peptides. The samples were sprayed with a sample cone voltage of 20 V.

2.6.2 Peptide synthesis

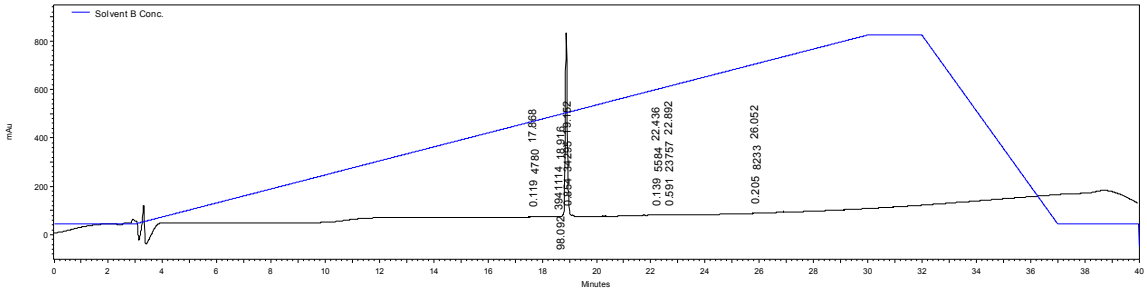
S. epidermidis AIPs and analogs were synthesized using our previously reported solid-phase synthesis and macrocyclization methods *(59)*. Briefly, linear peptide was synthesized on Boc-protected, amino acid pre-loaded 4-hydroxymethyl-phenylacetamidomethyl resin using standard Fmoc/tBu solid-phase synthesis protocols. The linear protected peptide was cleaved under anhydrous conditions using ethanethiol activated by dimethylaluminum chloride, and then treated with TFA to effect deprotection. The resulting linear peptide-thioester was purified by preparative RP-HPLC before being subjected macrocyclization. Upon macrocyclization completion, cyclic peptide was purified by preparative RP-HPLC, and its identity and purity were confirmed by exact mass (EM) measurement and analytical RP-HPLC, respectively. Purified cyclic peptide product was lyophilized prior to analysis in biological assays. See below for EM and HPLC characterization data for all of the peptides in this study. The native S. aureus AIPs I–IV and AIP-III D4A were previously prepared in our laboratory1 and were not re-synthesized for the current study.

Table 2.3: MS and HPLC data for the native *S. epidermidis* AIPs and AIP analogs in this study. EM = exact mass. Rt = retention time.

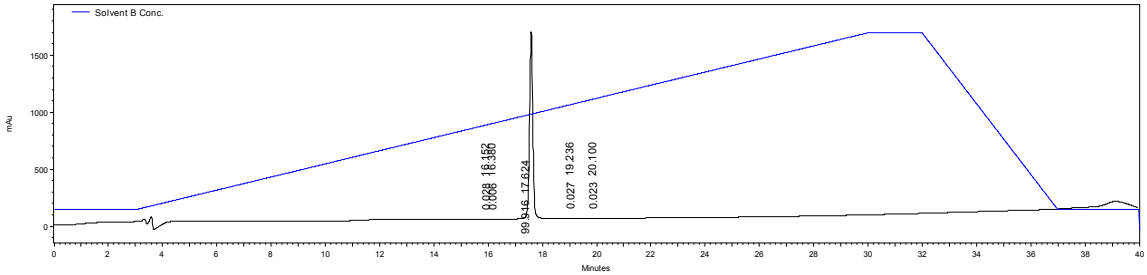
Peptide name	Structure	Calc. EM	Obs. EM	Rt (min)	% Purity
AIP-I	D-S-V-(C-A-S-Y-F)	873.3448	873.3456	18.9	>98
AIP-II	N-A-S-K-Y-N-P-(C-S-N-Y-L)	678.3056 $[M+2H]^{2+}$	678.3058 $[M+2H]^{2+}$	17.6	>99
AIP-III	N-A-A-K-Y-N-P-(C-A-S-Y-L)	648.8053 $[M+2H]^{2+}$	648.8043 $[M+2H]^{2+}$	18.0	>99
AIP-I D1A	A-S-V-(C-A-S-Y-F)	829.3550	829.3538	17.9	>99
AIP-I S2A	D-A-V-(C-A-S-Y-F)	857.3499	857.3494	18.1	>97
AIP-I V3A	D-S-A-(C-A-S-Y-F)	845.3135	845.3126	18.3	>99
AIP-I S6A	D-S-V-(C-A-A-Y-F)	857.3499	857.3495	19.7	>97
AIP-I Y7A	D-S-V-(C-A-S-A-F)	781.3186	781.3186	16.5	>97
AIP-I F8A	D-S-V-(C-A-S-Y-A)	797.3135	797.3135	15.5	>99
AIP-I D-D1	DD-S-V-(C-A-S-Y-F)	873.3448	873.3442	22.5	>97
AIP-I D-S2	D-DS-V-(C-A-S-Y-F)	873.3448	873.3458	19.9	>96
AIP-I D-V3	D-S-DV-(C-A-S-Y-F)	873.3448	873.3448	21.6	>97
AIP-I D-C4	D-S-V-(DC-A-S-Y-F)	873.3448	873.3455	23.0	>96
AIP-I D-A5	D-S-V-(C-DA-S-Y-F)	873.3448	873.3452	23.2	>94
AIP-I D-S6	D-S-V-(C-A-DS-Y-F)	873.3448	873.3447	22.5	>94
AIP-I D-Y7	D-S-V-(C-A-S-DY-F)	873.3448	873.3447	22.6	>92
AIP-I D-F8	D-S-V-(C-A-S-Y-DF)	873.3448	873.3447	22.5	>98
AIP-I A5Y	D-S-V-(C-Y-S-Y-F)	965.3710	965.3712	19.5	>98
AIP-I A5S-1	D-S-V-(C-S-S-Y-F)	889.3397	889.3372	18.5	>98
AIP-I A5S-2	D-S-V-(C-S-S-Y-F)	889.3397	889.3372	18.6	>96
AIP-I V3AA5Y	D-S-A-(C-Y-S-Y-F)	937.3397	937.3399	17.9	>99
AIP-I V3AA5S	D-S-A-(C-S-S-Y-F)	861.3084	861.3065	16.8	>98
AIP-I D1AS6A	A-S-V-(C-A-A-Y-F)	813.3600	813.3604	18.1	>99
tAIP-I	Ac-(C-A-S-Y-F)	614.2280	614.2279	18.9	>99
AIP-I D1AS6AV3A	A-S-A-(C-A-A-Y-F)	785.3287	785.3284	17.6	>99
AIP-I D1AS6AV3AA5S	A-S-A-(C-S-A-Y-F)	801.3237	801.3239	17.1	>99
AIP-II 11aa	A-S-K-Y-N-P-(C-S-N-Y-L)	1241.5620	1241.562	17.7	>99
AIP-II 10aa	S-K-Y-N-P-(C-S-N-Y-L)	1170.5249	1170.5249	17.3	>99
AIP-II 9aa	K-Y-N-P-(C-S-N-Y-L)	1083.4928	1083.4962	16.5	>99
AIP-II 8aa	Y-N-P-(C-S-N-Y-L)	955.3979	955.4007	17.3	>99
AIP-II 7aa	N-P-(C-S-N-Y-L)	792.3346	792.3314	16.5	>99
tAIP-II	Ac-(C-S-N-Y-L)	623.2494	623.2491	17.7	>99

2.6.3 HPLC traces for S. epidermidis AIPs and AIP analogs

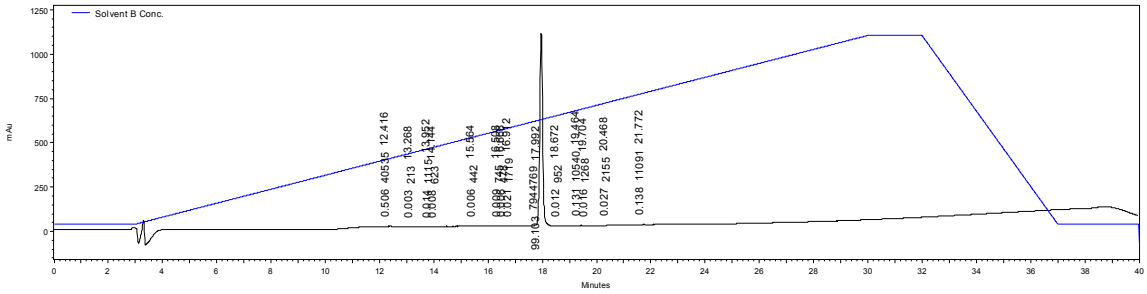
AIP-I



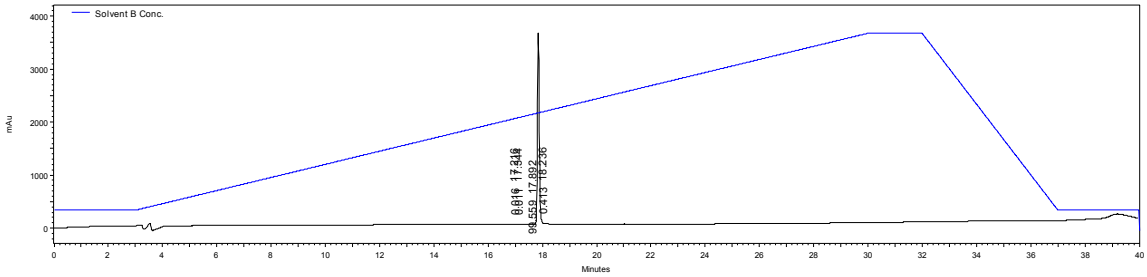
AIP-II



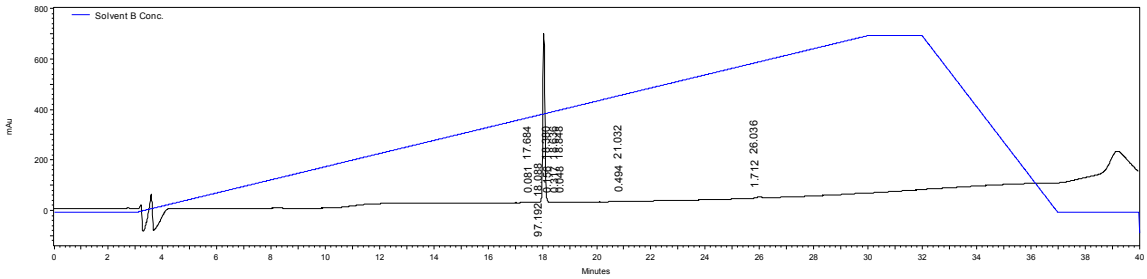
AIP-III



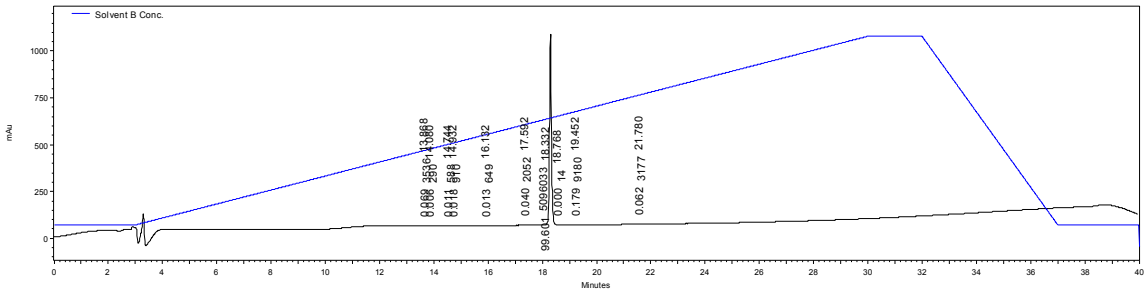
AIP-I D1A



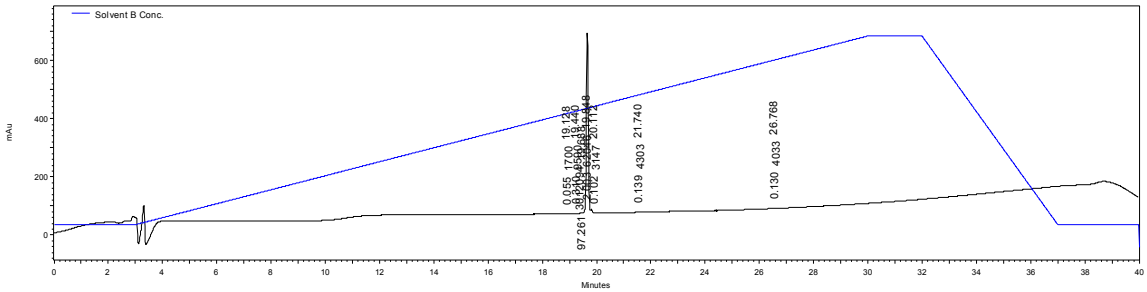
AIP-I S2A



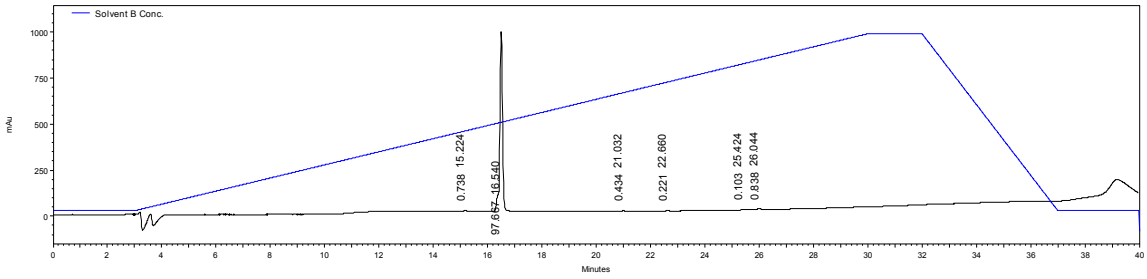
AIP-I V3A



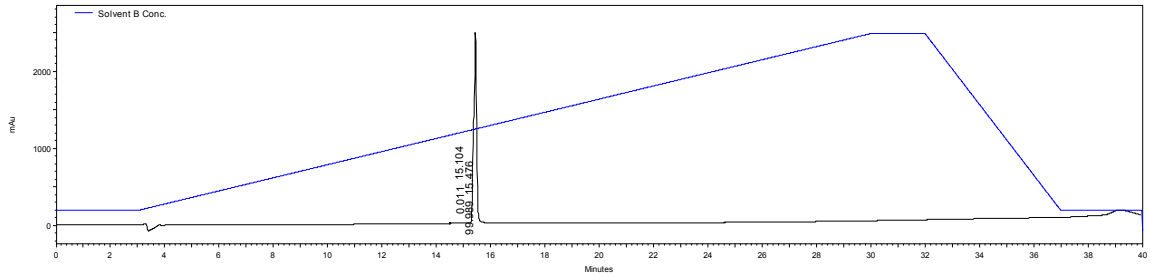
AIP-I S6A



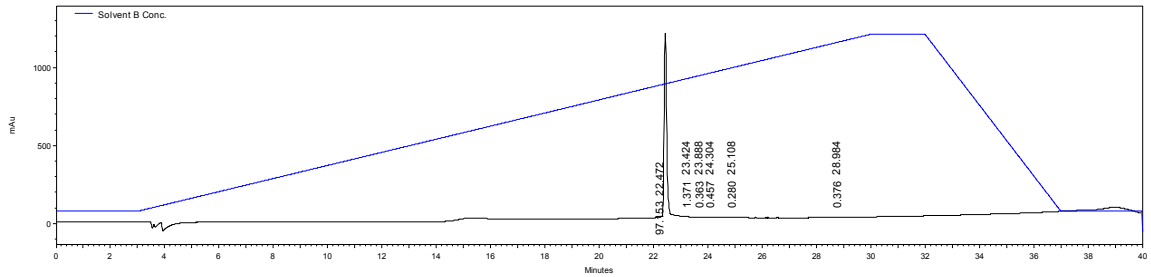
AIP-I Y7A



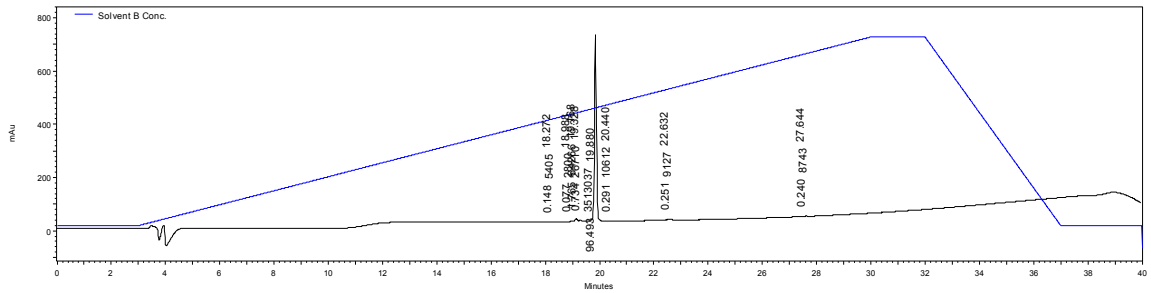
AIP-I F8A



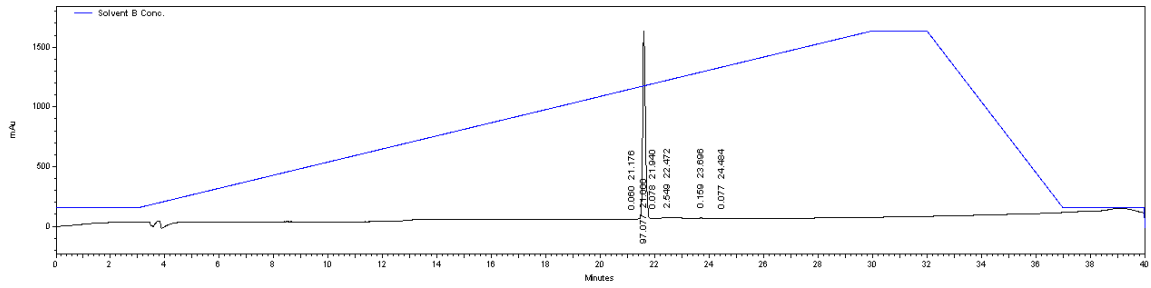
AIP-I D-D1



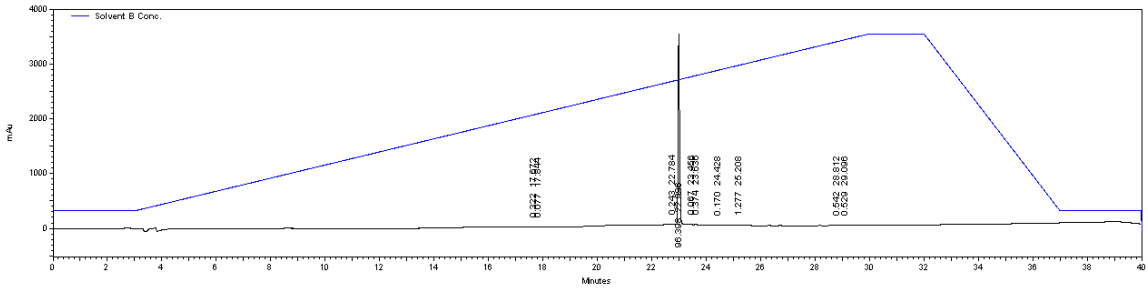
AIP-I D-S2



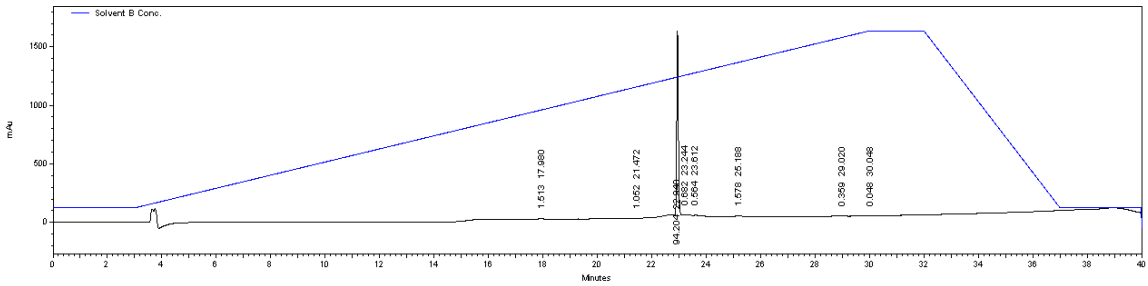
AIP-I D-V3



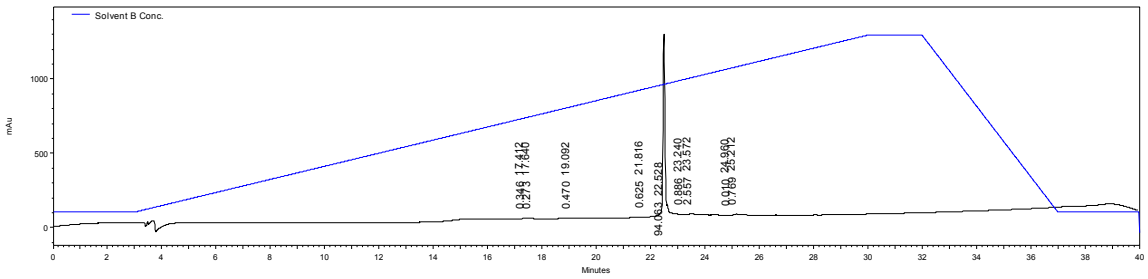
AIP-I D-C4



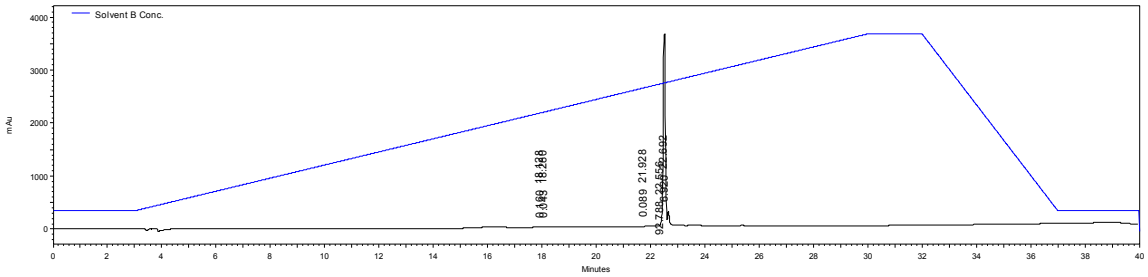
AIP-I D-A5



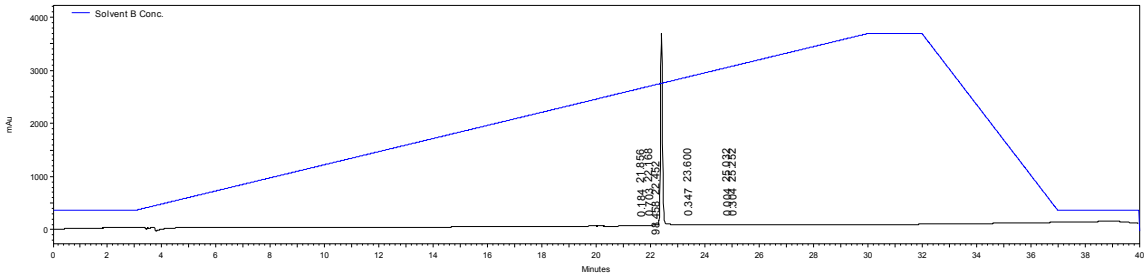
AIP-I D-S6



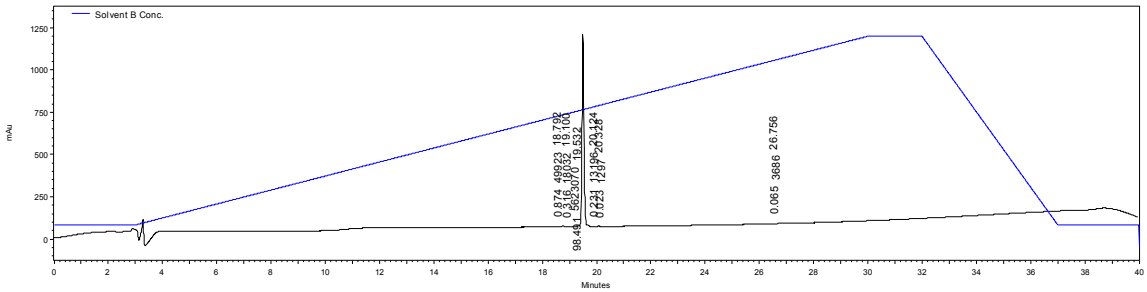
AIP-I D-Y7



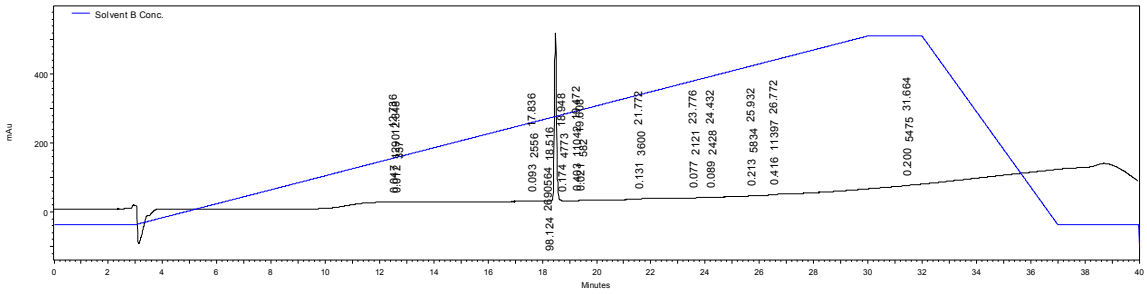
AIP-I D-F8



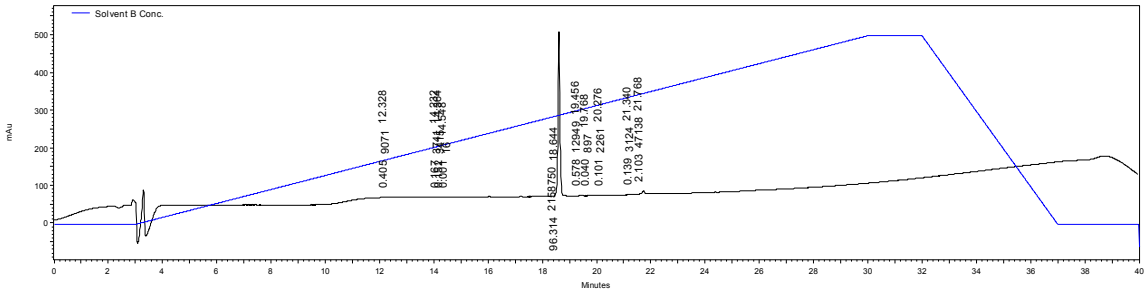
AIP-I A5Y



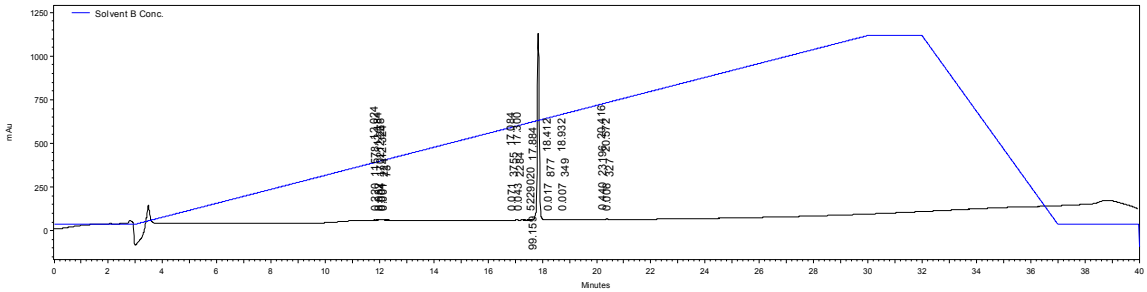
AIP-I A5S-1



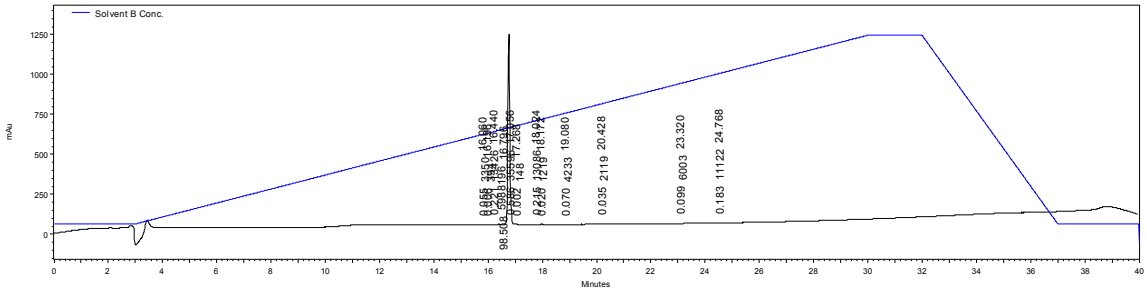
AIP-I A5S-2



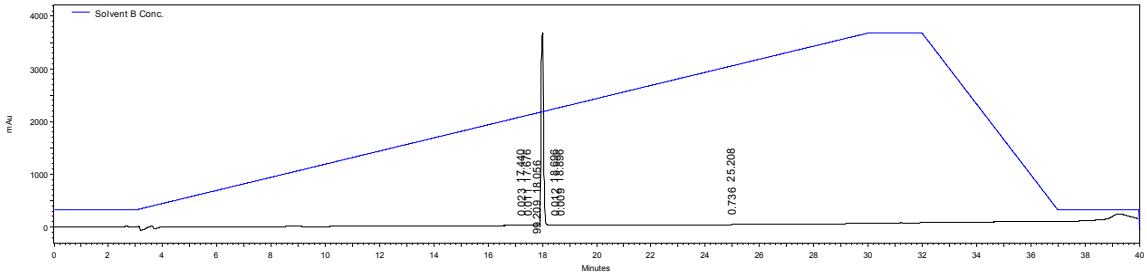
AIP-I V3AA5Y



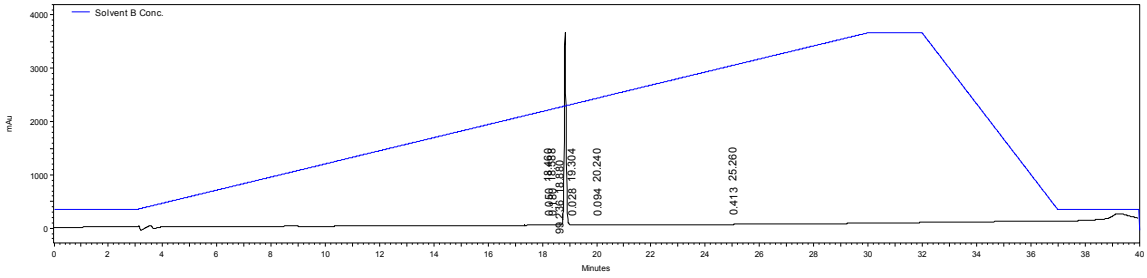
AIP-I V3AA5S



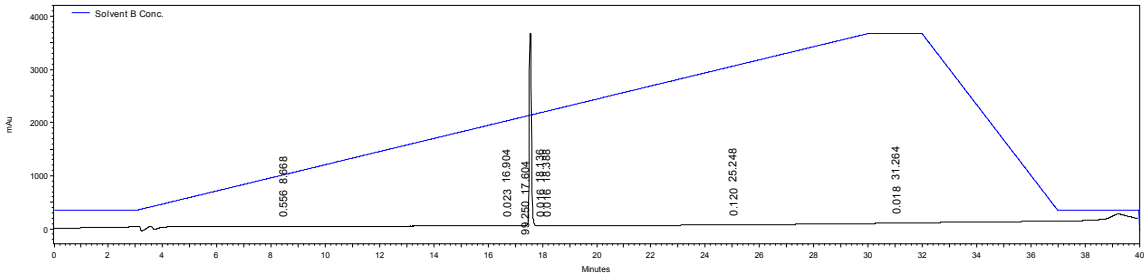
AIP-I D1AS6A



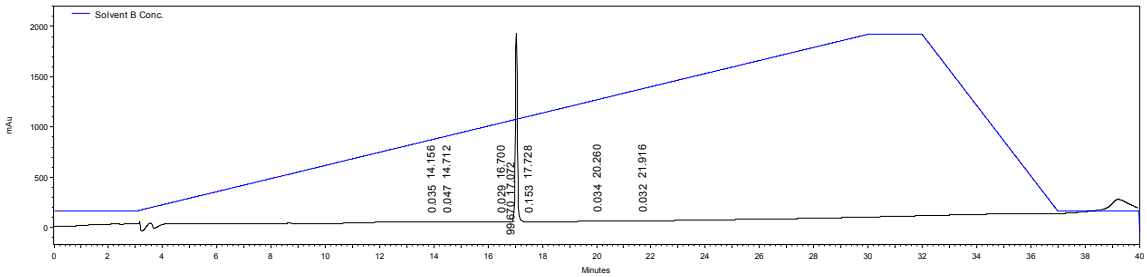
tAIP-I



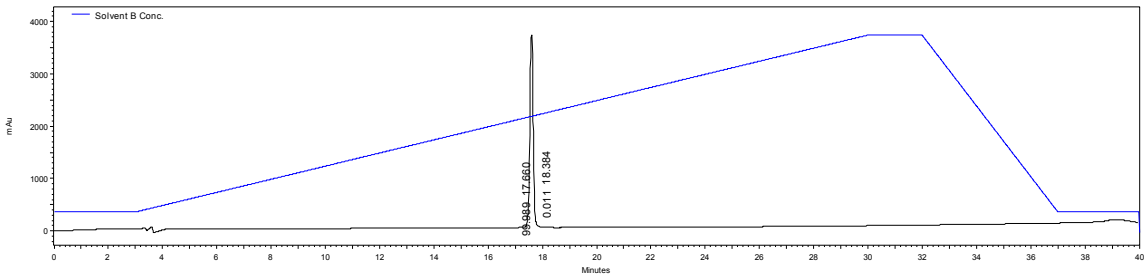
AIP-I D1AS6AV3A



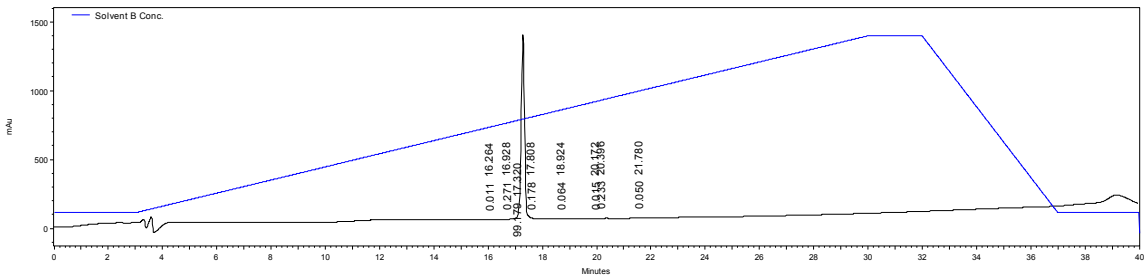
AIP-I D1AS6AV3AA5S



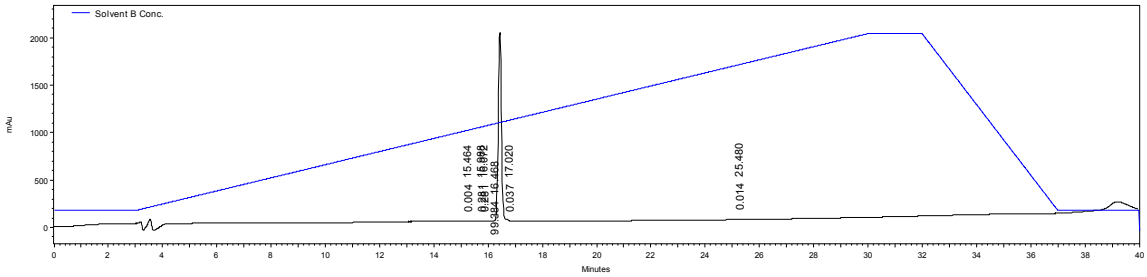
AIP-II 11aa



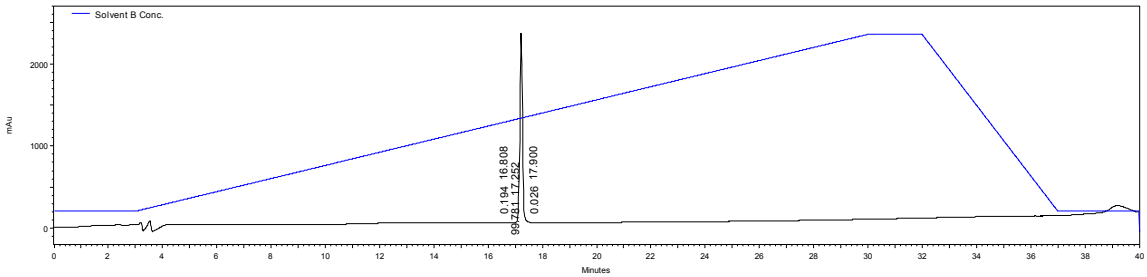
AIP-II 10aa



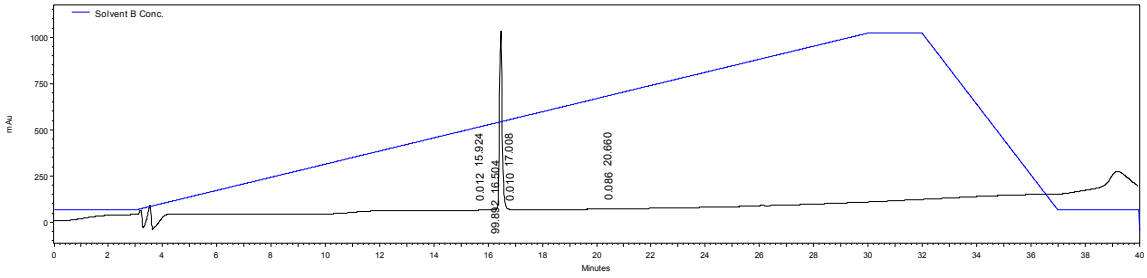
AIP-II 9aa



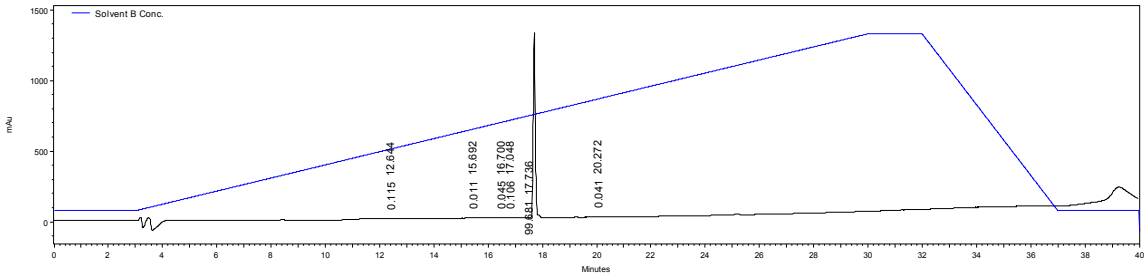
AIP-II 8aa



AIP-II 7aa



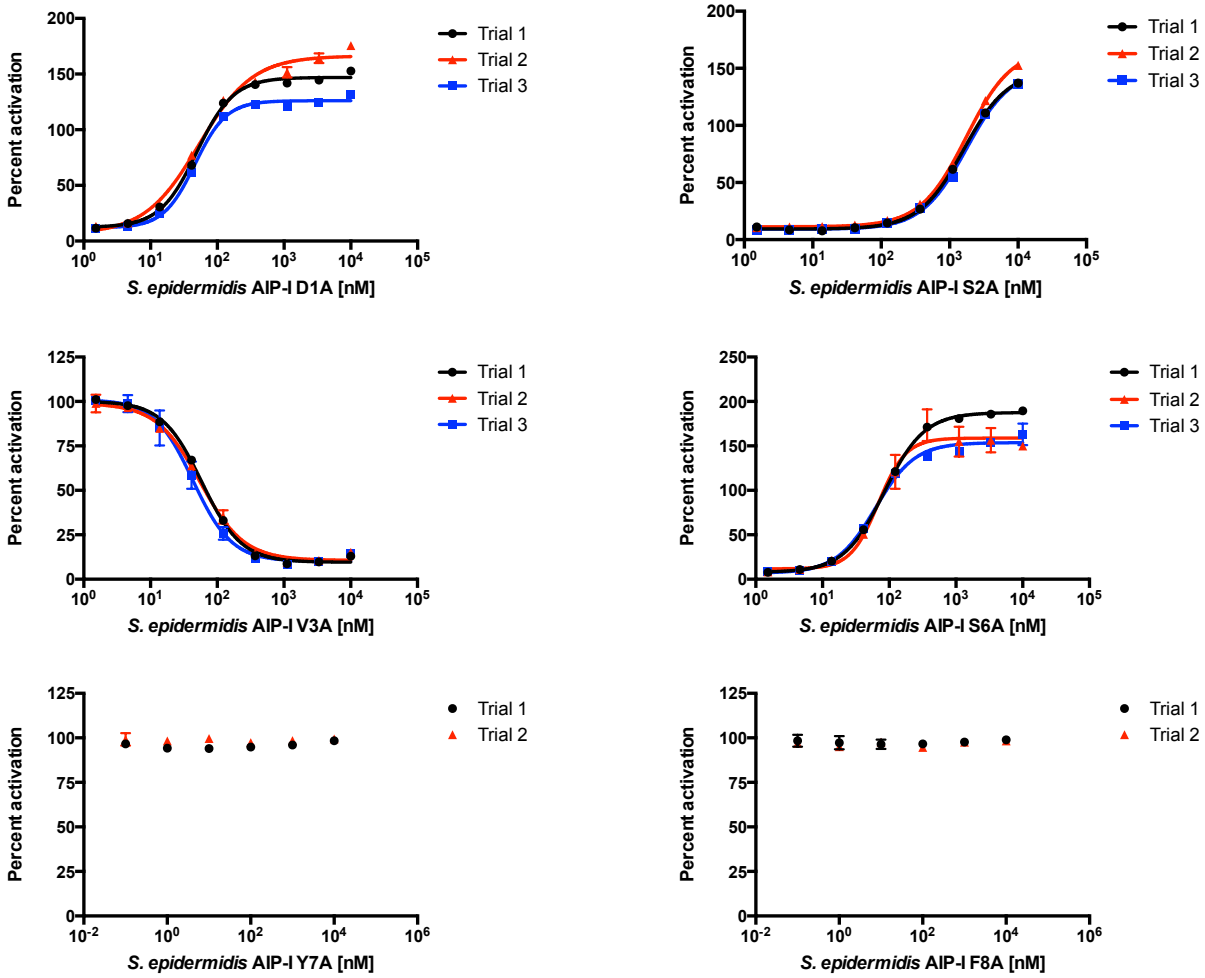
tAIP-II

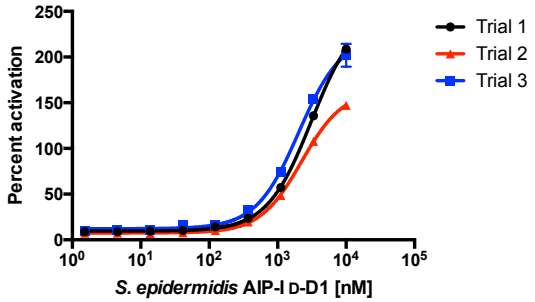


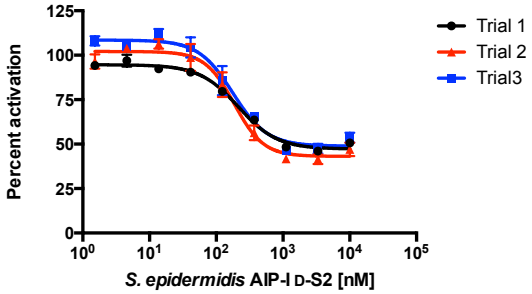
2.6.4 S. epidermidis AgrC fluorescence dose response curves

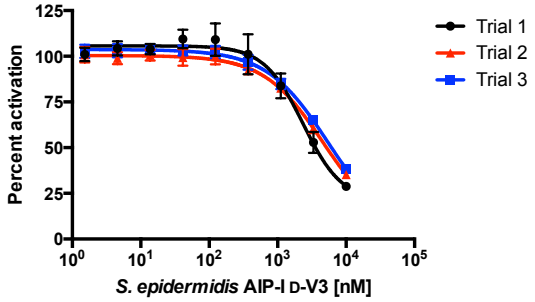
The analogs were screened over varying concentrations in the S. epidermidis fluorescence reporter strains for AgrC receptor agonism and antagonism (see main text for details of strains and protocols). For AgrC-I agonism dose response assays, 50 nM S. epidermidis AIP-II was introduced to all wells to block AgrC-I activation due to endogenously produced AIP-I. Curves for each of the three biological replicates (Trials 1–3) are shown; error bars represent standard deviation of triplicate values. Percent activation was normalized to a DMSO control.

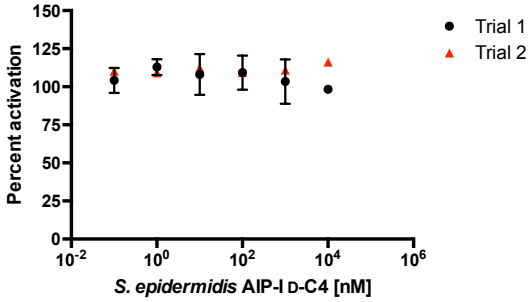
S. epidermidis AH3408 (Group-I):

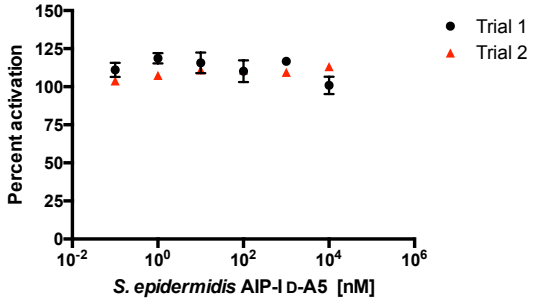


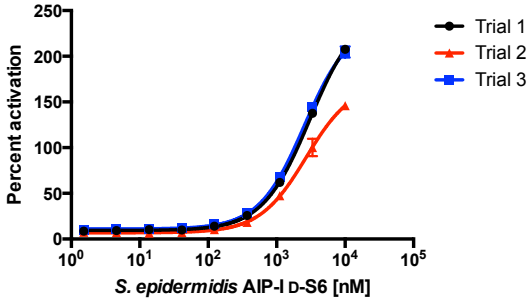

Percent activation
Trial 1
Trial 2
Trial 3
S. epidermidis AIP-I D-D1 [nM]

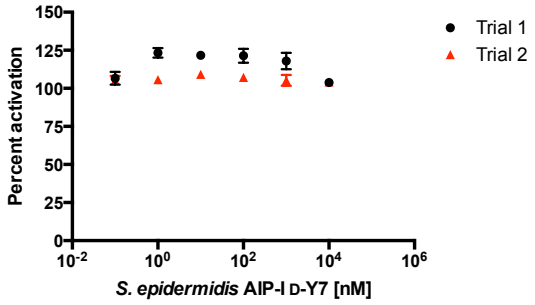

Percent activation
Trial 1
Trial 2
Trial3
S. epidermidis AIP-I D-S2 [nM]

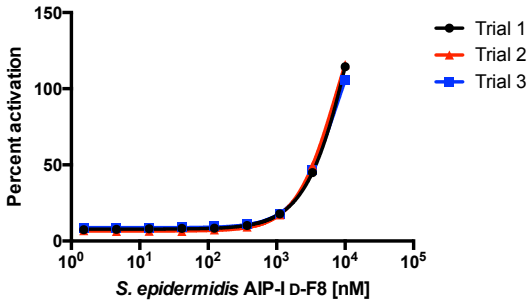

Percent activation
Trial 1
Trial 2
Trial 3
S. epidermidis AIP-I D-V3 [nM]

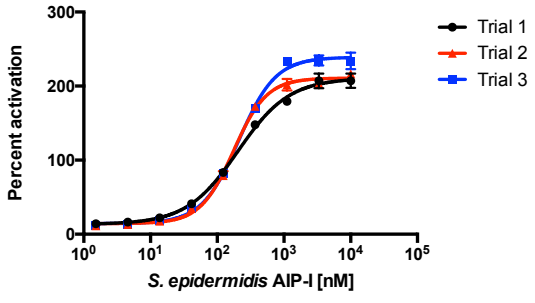

Percent activation
Trial 1
Trial 2
S. epidermidis AIP-I D-C4 [nM]

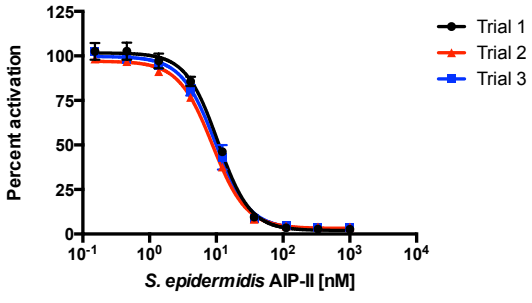

Percent activation
Trial 1
Trial 2
S. epidermidis AIP-I D-A5 [nM]

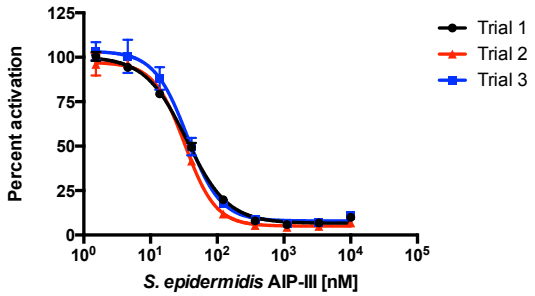

Percent activation
Trial 1
Trial 2
Trial 3
S. epidermidis AIP-I D-S6 [nM]

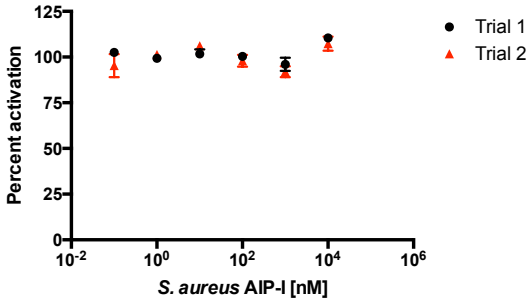

Percent activation
Trial 1
Trial 2
S. epidermidis AIP-I D-Y7 [nM]

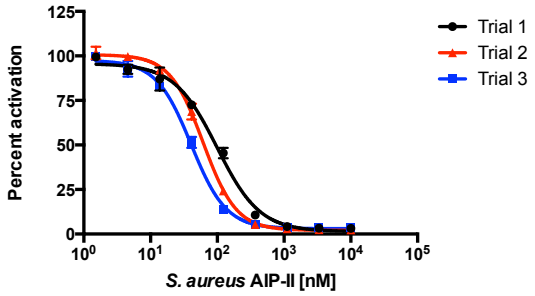

Percent activation
Trial 1
Trial 2
Trial 3
S. epidermidis AIP-I D-F8 [nM]

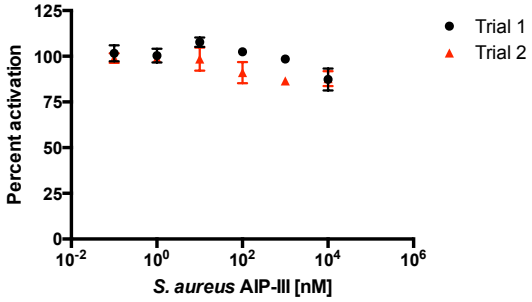

Percent activation
Trial 1
Trial 2
Trial 3
S. epidermidis AIP-I [nM]

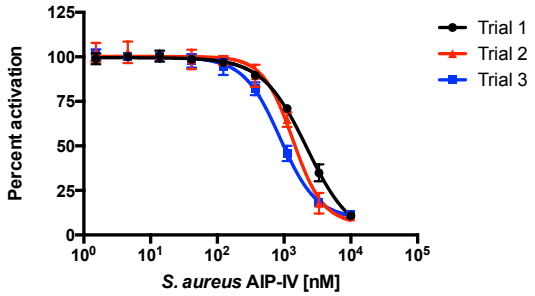

Percent activation
Trial 1
Trial 2
Trial 3
S. epidermidis AIP-II [nM]

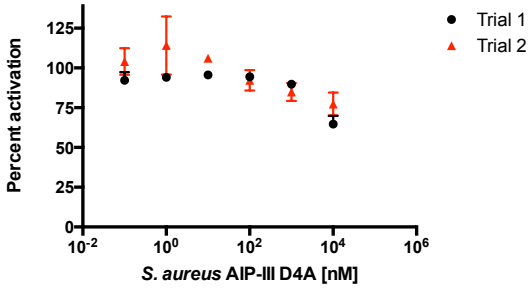

Percent activation
Trial 1
Trial 2
Trial 3
S. epidermidis AIP-III [nM]

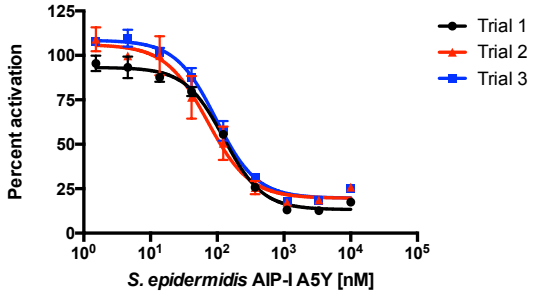

Percent activation
Trial 1
Trial 2
S. aureus AIP-I [nM]

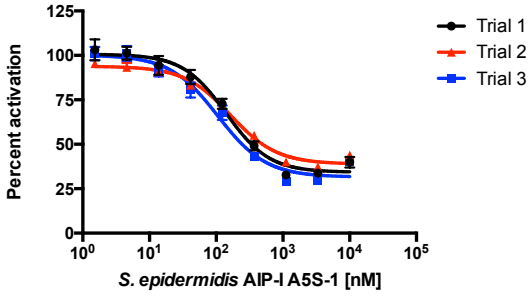

Percent activation
Trial 1
Trial 2
Trial 3
S. aureus AIP-II [nM]

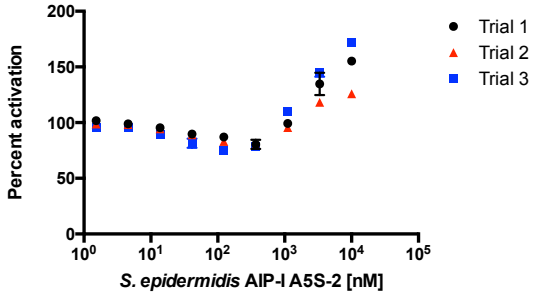

Percent activation
Trial 1
Trial 2
S. aureus AIP-III [nM]

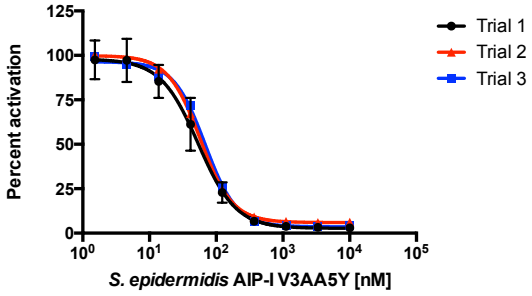

Percent activation
Trial 1
Trial 2
Trial 3
S. aureus AIP-IV [nM]

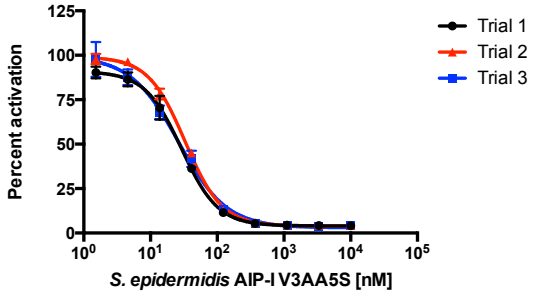

Percent activation
Trial 1
Trial 2
S. aureus AIP-III D4A [nM]

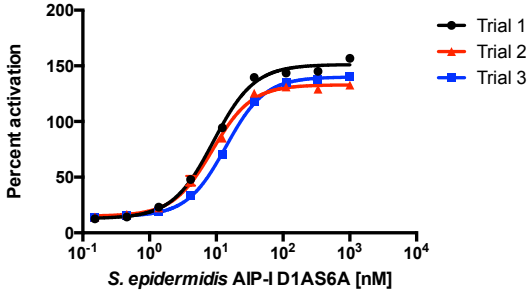

Percent activation
Trial 1
Trial 2
Trial 3
S. epidermidis AIP-I A5Y [nM]

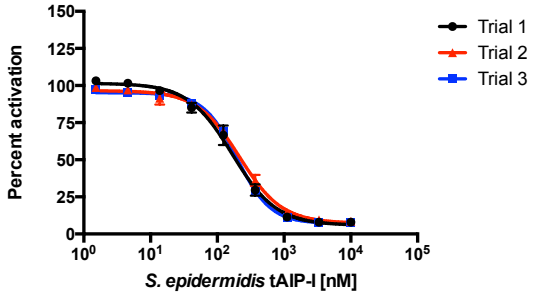

Percent activation
Trial 1
Trial 2
Trial 3
S. epidermidis AIP-I A5S-1 [nM]

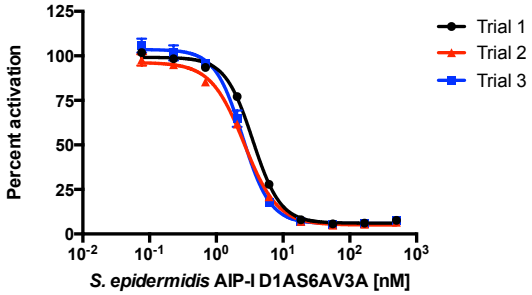

Percent activation
Trial 1
Trial 2
Trial 3
S. epidermidis AIP-I A5S-2 [nM]

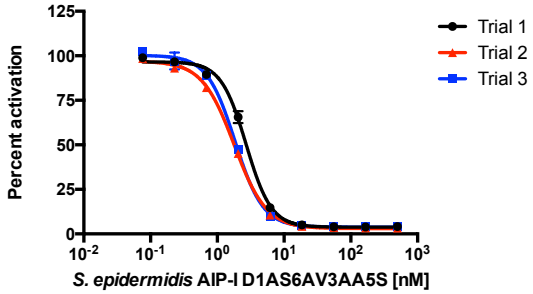

Percent activation
Trial 1
Trial 2
Trial 3
S. epidermidis AIP-I V3AA5Y [nM]

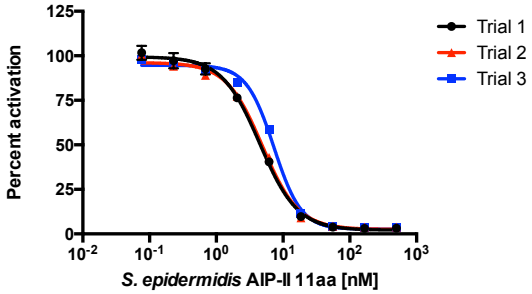

Percent activation
125
100
75
50
25
0
10^0 10^1 10^2 10^3 10^4 10^5
S. epidermidis AIP-I V3AA5S [nM]
Trial 1
Trial 2
Trial 3

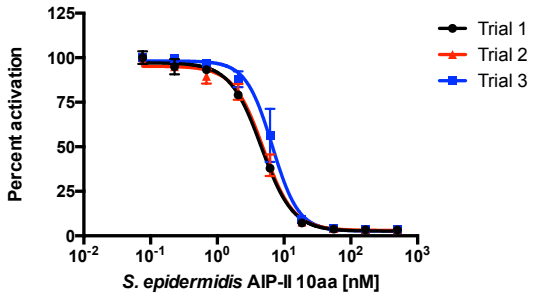

Percent activation
200
150
100
50
0
10^{-1} 10^0 10^1 10^2 10^3 10^4
S. epidermidis AIP-I D1AS6A [nM]
Trial 1
Trial 2
Trial 3

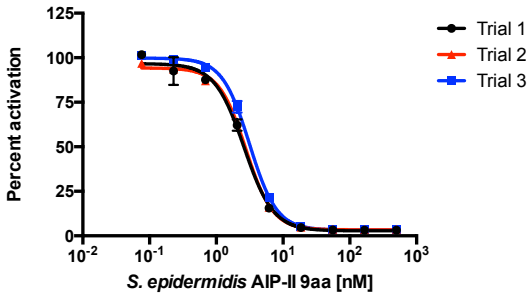

Percent activation
150
125
100
75
50
25
0
10^0 10^1 10^2 10^3 10^4 10^5
S. epidermidis tAIP-I [nM]
Trial 1
Trial 2
Trial 3

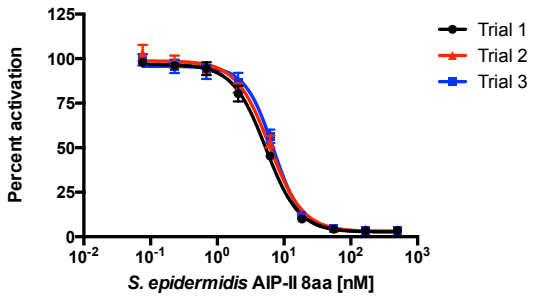

Percent activation
125
100
75
50
25
0
10^{-2} 10^{-1} 10^0 10^1 10^2 10^3
S. epidermidis AIP-I D1AS6AV3A [nM]
Trial 1
Trial 2
Trial 3

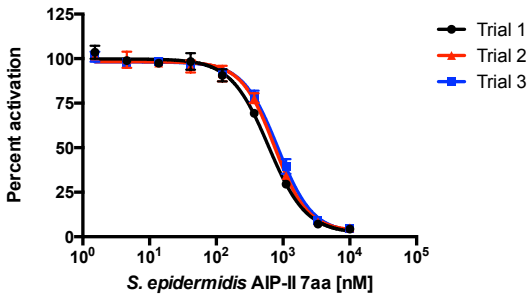

Percent activation
125
100
75
50
25
0
10^{-2} 10^{-1} 10^0 10^1 10^2 10^3
S. epidermidis AIP-I D1AS6AV3AA5S [nM]
Trial 1
Trial 2
Trial 3

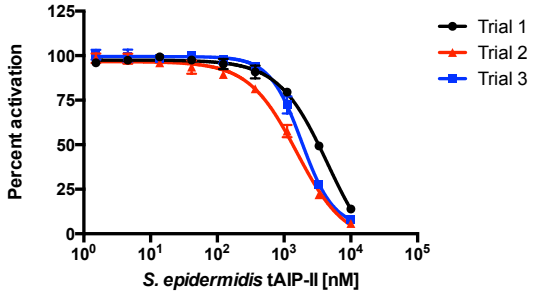

Percent activation
125
100
75
50
25
0
10^{-2} 10^{-1} 10^0 10^1 10^2 10^3
S. epidermidis AIP-II 11aa [nM]
Trial 1
Trial 2
Trial 3


Percent activation
125
100
75
50
25
0
10^{-2} 10^{-1} 10^0 10^1 10^2 10^3
S. epidermidis AIP-II 10aa [nM]
Trial 1
Trial 2
Trial 3

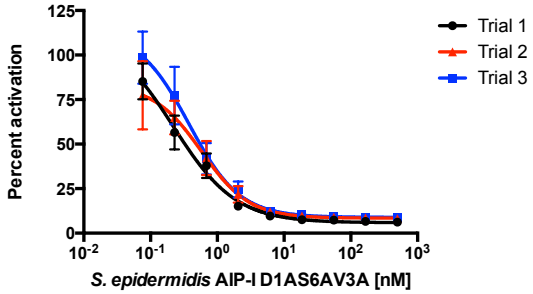

Percent activation
125
100
75
50
25
0
10^{-2} 10^{-1} 10^0 10^1 10^2 10^3
S. epidermidis AIP-II 9aa [nM]
Trial 1
Trial 2
Trial 3

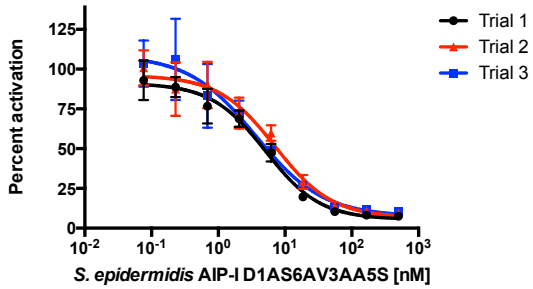

Percent activation
125
100
75
50
25
0
10^{-2} 10^{-1} 10^0 10^1 10^2 10^3
S. epidermidis AIP-II 8aa [nM]
Trial 1
Trial 2
Trial 3


Percent activation
125
100
75
50
25
0
10^0 10^1 10^2 10^3 10^4 10^5
S. epidermidis AIP-II 7aa [nM]
Trial 1
Trial 2
Trial 3

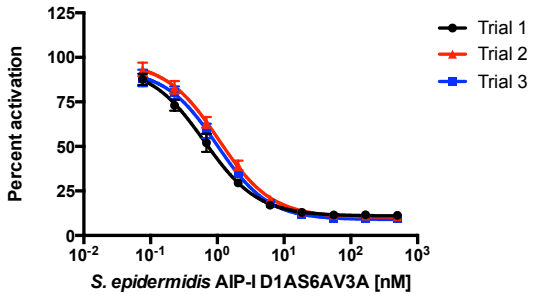


S. epidermidis AH3567 (Group-II):





S. epidermidis AH3408 (Group-III):



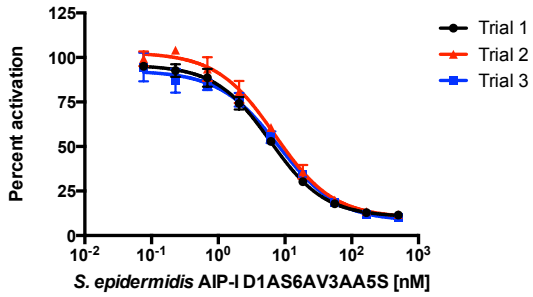


Table 2.4: IC_{50} values, EC_{50} values, and 95% confidence ranges for the active alanine and D-amino acid scan analogs of AIP-I in AgrC-I determined using fluorescence reporter strains.[a] Shaded cells represent control peptides.

Peptide name	Sequence	IC_{50} (nM)	EC_{50} (nM)[b]
AIP-I D1A	A-S-V-(C-A-S-Y-F)	-	49.3 (43.3 – 56.2)
AIP-I S2A	D-A-V-(C-A-S-Y-F)	-	>1000
AIP-I V3A	D-S-A-(C-A-S-Y-F)	51.9 (37.9 – 71.0)	-
AiP-I S6A	D-S-V-(C-A-A-Y-F)	-	71.0 (52.8 – 95.4)
AIP-I D-D1	DD-S-V-(C-A-S-Y-F)	-	>1000
AIP-I D-S2	D-DS-V-(C-A-S-Y-F)	192[c] (159 – 233)	
AIP-I D-V3	D-S-DV-(C-A-S-Y-F)	>1000	-
AIP-I D-S6	D-S-V-(C-A-DS-Y-F)	-	>1000
AIP-I D-F8	D-S-V-(C-A-S-Y-DF)	-	>1000
AIP-I	D-S-V-(C-A-S-Y-F)	-	196 (162 – 238)
AIP-II	N-A-S-K-Y-N-P-(C-S-N-Y-L)	9.64 (7.99 – 11.6)	-
AIP-III	N-A-A-K-Y-N-P-(C-A-S-Y-L)	34.3 (31.4 - 37.4)	-
S. aureus AIP-II	G-V-N-A-(C-S-S-L-F)	62.9 (26.1 – 151)	-
S. aureus AIP-IV	Y-S-T-(C-Y-F-I-M)	>1000	-

[a] See main text for details of the reporter strains and assay procedures. See above for MS and HPLC characterization data and dose response curves. All IC_{50} and EC_{50} values are obtained from three biological replicates. [b] Activation dose response curves were performed in the presence of 50 nM *S. epidermidis* AIP-II to block AgrC-I activation caused by endogenously produced AIP-I. [c] Maximum inhibition did not exceed 60%.

Table 2.5: IC_{50} values, EC_{50} values, and 95% confidence ranges for the second-generation *S. epidermidis* AIP analogs in AgrC-I determined using fluorescence reporter strains.[a]

Peptide name	Sequence	IC_{50} (nM)	EC_{50} (nM)[b]
AIP-I A5Y	D-S-V-(C-Y-S-Y-F)	95.4 (54.9 – 166)	-
AIP-I A5S	D-S-V-(C-S-S-Y-F)	135[c,d] (87.6 – 207)	
AIP-I V3AA5Y	D-S-A-(C-Y-S-Y-F)	59.6 (46.8 – 75.8)	-
AIP-I V3AA5S	D-S-A-(C-S-S-Y-F)	29.4 (23.6 – 36.6)	-
AIP-I D1AS6A	A-S-V-(C-A-A-Y-F)	-	10.3 (6.18 – 17.2)
tAIP-I	Ac-(C-A-S-Y-F)	192 (150 – 245)	-
AIP-I D1AS6AV3A	A-S-A-(C-A-A-Y-F)	2.84 (1.95 – 4.11)	-
AIP-I D1AS6AV3AA5S	A-S-A-(C-S-A-Y-F)	2.08 (1.32 – 3.26)	-
AIP-II 11aa	A-S-K-Y-N-P-(C-S-N-Y-L)	5.43 (3.26 – 9.03)	-
AIP-II 10aa	S-K-Y-N-P-(C-S-N-Y-L)	5.29 (3.56 – 7.87)	-
AIP-II 9aa	K-Y-N-P-(C-S-N-Y-L)	2.83 (2.34 – 3.42)	-
AIP-II 8aa	Y-N-P-(C-S-N-Y-L)	6.08 (4.70 – 7.86)	-
AIP-II 7aa	N-P-(C-S-N-Y-L)	721 (525 – 991)	-
tAIP-II	Ac-(C-S-N-Y-L)	>1000	-

[a] See main text for details of the reporter strains and assay procedures. See above for MS and HPLC characterization data and dose response curves. All IC_{50} and EC_{50} values are obtained from three biological replicates. [b] Activation dose response curves were performed in the presence of 50 nM *S. epidermidis* AIP-II to block AgrC-I activation caused by endogenously produced AIP-I. [c] Maximum inhibition did not exceed 75%. [d] Two different AIP-I A5S analogs with the same molecular weight (AIP-I A5S-1 and AIP-I A5S-2) were isolated from the synthesis that showed different activities; IC_{50} value listed is derived from the antagonism dose response curves for A5S-1 (see main text).

Table 2.6: IC_{50} values and 95% confidence ranges for the potent pan-group *S. epidermidis agr* inhibitors against AgrC-II and AgrC-III determined using fluorescence reporter strains.[a]

Peptide Name	Sequence	AgrC-II IC_{50} (nM)	AgrC-III IC_{50} (nM)
AIP-I D1AS6AV3A	A-S-A-(C-A-A-Y-F)	0.36 (0.14 – 0.96)	0.87 (0.51 – 1.47)
AIP-I D1AS6AV3AA5S	A-S-A-(C-S-A-Y-F)	5.10 (2.64 – 9.84)	6.98 (5.23 – 9.32)

[a] See main text for details of the reporter strains and assay procedures. See above for MS and HPLC characterization data and dose response curves. All IC_{50} values are obtained from three biological replicates.

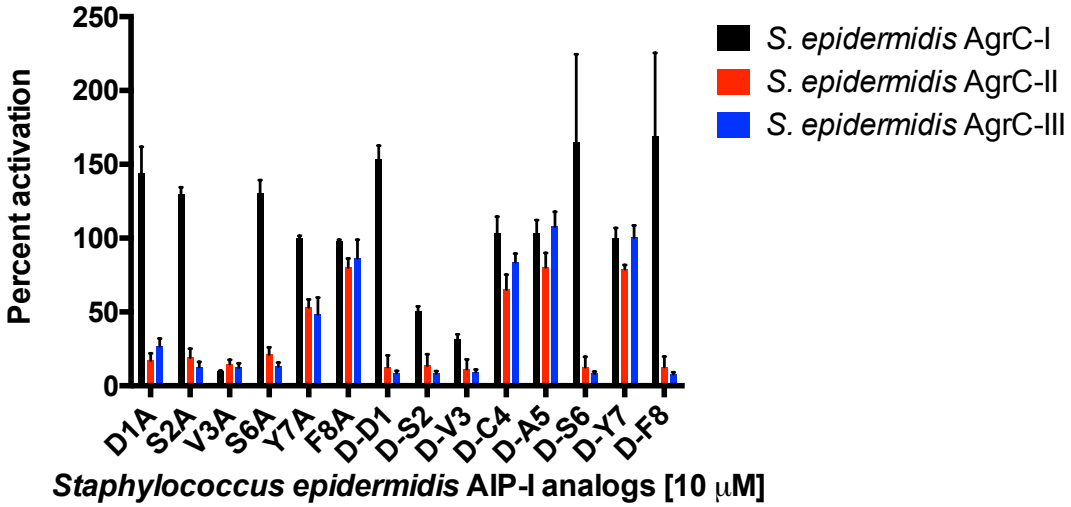


Figure 2.7: Effects of alanine and D-amino acid analogs of *S. epidermidis* AIP-I on *S. epidermidis* AgrCs I–III at 10 μM as determined using fluorescence reporter strains. Error bars represent the standard deviation of measurements from three biological replicates. See main text for details of the reporter strains and assay procedures.

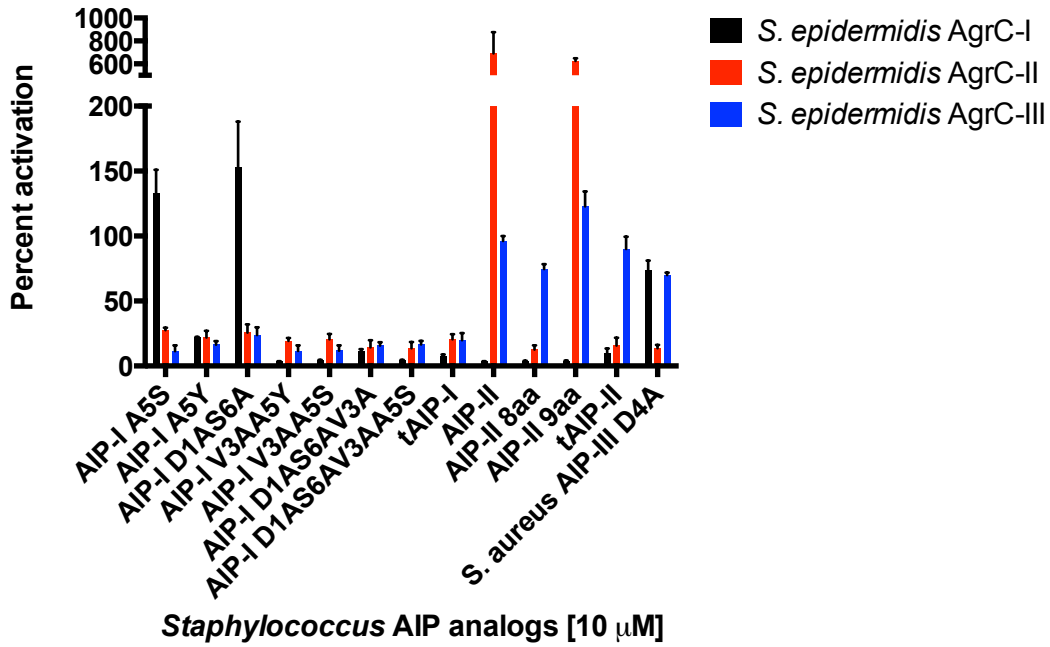


Figure 2.8*:* Effects of the second-generation *S. epidermidis* AIP analogs and *S. aureus* AIP-III D4A on *S. epidermidis* AgrCs I–III at 10 μM as determined using fluorescence reporter strains. Error bars represent the standard deviation of measurements from three biological replicates. See main text for details of the reporter strains and assay procedures.

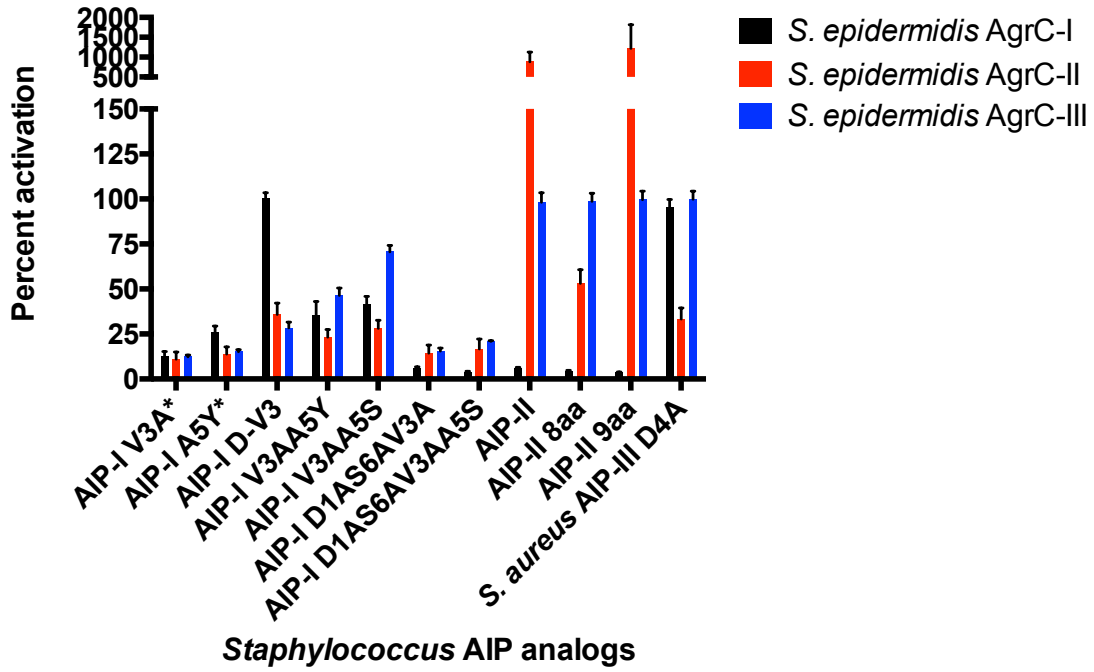


Figure 2.9: Effects of selected *S. epidermidis* AIP analogs and *S. aureus* AIP-III D4A on *S. epidermidis* AgrCs I–III as determined using fluorescence reporter strains. Compounds were tested at 100 nM unless otherwise noted. Error bars represent the standard deviation of measurements from three biological replicates. * Compound tested at 1 μM. See main text for details of the reporter strains and assay procedures.

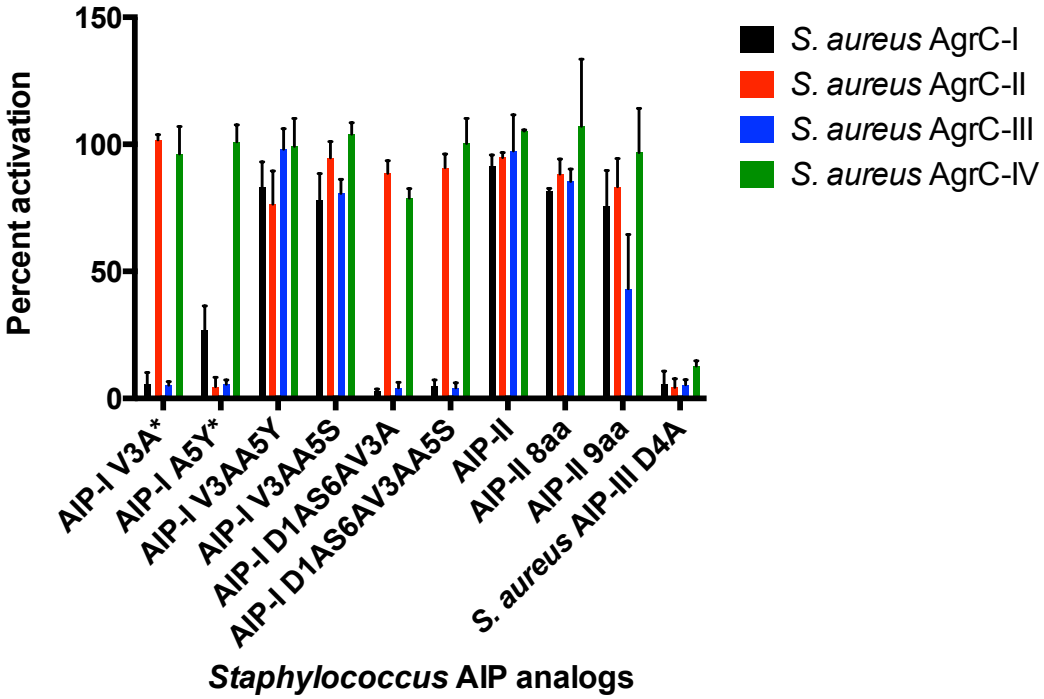


Figure 2.10: Effects of selected *S. epidermidis* AIP analogs and *S. aureus* AIP-III D4A on *S. aureus* AgrCs I–IV as determined using fluorescence reporter strains. Compounds were tested at 100 nM unless otherwise noted. Error bars represent the standard deviation of measurements from three biological replicates. * Compound was tested at 1 μM. See main text for details of the reporter strains and assay procedures.

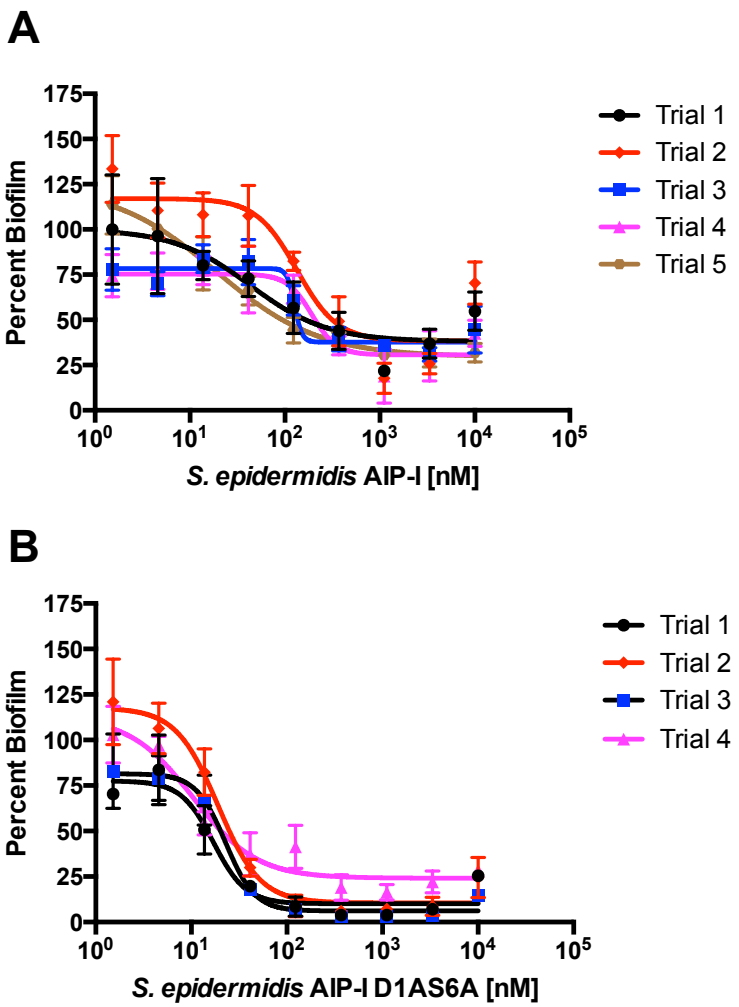


Figure 2.11: *S. epidermidis* biofilm growth inhibition dose response curves for (A) AIP-I and (B) AIP-I D1AS6A. Peptides were screened over varying concentrations in (wild-type) *S. epidermidis* Group-I RP62A after 24 h in at least four separate experiments. Biofilm growth was measured by staining with crystal violet (CV). Error bars represent the standard deviation of triplicate values from each experiment. Percent of biofilm formation was normalized to a DMSO control. See main text for details of the strain and assay procedure.

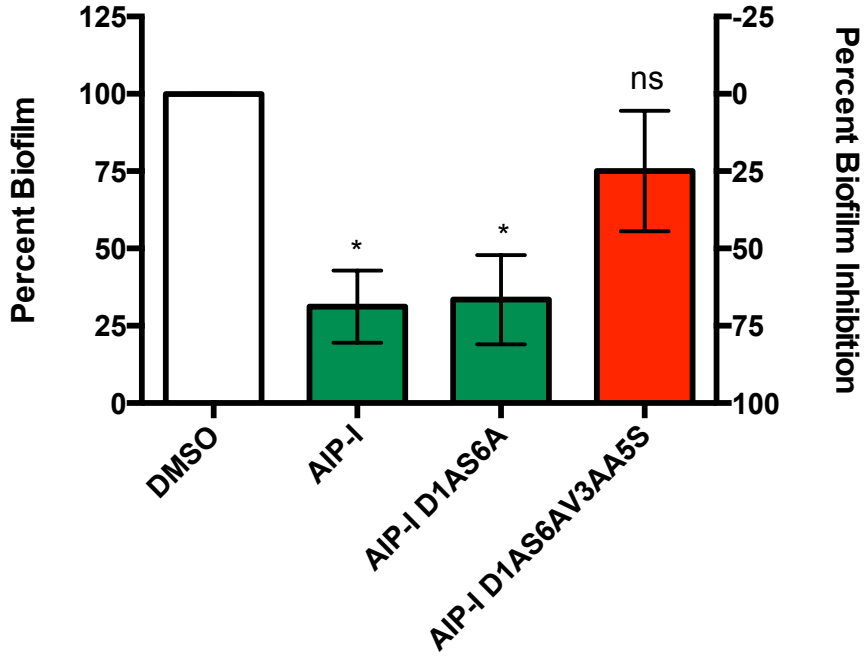


Figure 2.12: Single-concentration *S. epidermidis* biofilm growth inhibition assay data. Selected peptides were tested for effects on biofilm formation in (wild-type) *S. epidermidis* Group-I RP62A at 10 μM after 24 h. Green: AgrC-I agonist; red: AgrC-I antagonist. Biofilm growth was measured by staining with crystal violet (CV). Data shown represent the average and the standard deviation of three biological replicates. P-values were calculated using an unpaired *t*-test compared to a no-peptide DMSO control. * = $P < 0.05$; ns = not significant. See main text for details of the strain and assay procedure.

2.7 Acknowledgements

Financial support for this work was provided by the Office of Naval Research (N00014-14-1-0791) and the Burroughs Wellcome Fund (to H.E.B) and a Merit Award (I01 BX002711) from the Department of Veteran Affairs (to A.R.H). T.Y. was supported in part by the UW–Madison NIH Biotechnology Training Program (T32 GM08349), and A.E.P was supported by an American Heart Association predoctoral fellowship. MS instrumentation at UW–Madison is supported by the NIH (1S10 0D020022) and a generous gift from Paul J. Bender.

2.8 References

1. Vuong, C., and Otto, M. (2002) *Staphylococcus epidermidis* infections, *Microb. Infect. 4*, 481-489.

2. von Eiff, C., Peters, G., and Heilmann, C. (2002) Pathogenesis of infections due to coagulase-negative staphylococci, *Lancet Infect. Dis. 2*, 677-685.

3. Otto, M. (2009) *Staphylococcus epidermidis*--the 'accidental' pathogen, *Nat. Rev. Microbiol. 7*, 555-567.

4. McCann, M. T., Gilmore, B. F., and Gorman, S. P. (2008) *Staphylococcus epidermidis* device-related infections: pathogenesis and clinical management, *J. Pharm. Pharmacol. 60*, 1551-1571.

5. Mertens, A., and Ghebremedhin, B. (2013) Genetic determinants and biofilm formation of clinical *Staphylococcus epidermidis* isolates from blood cultures and indwelling devises, *Eur. J. Microbiol. Immunol. (Bp) 3*, 111-119.

6. Rogers, K. L., Fey, P. D., and Rupp, M. E. (2009) Coagulase-negative staphylococcal infections, *Infect. Dis. Clin. North Am. 23*, 73-98.

7. Costerton, J. W., Stewart, P. S., and Greenberg, E. P. (1999) Bacterial biofilms: a common cause of persistent infections, *Science 284*, 1318-1322.

8. Claessens, J., Roriz, M., Merckx, R., Baatsen, P., Van Mellaert, L., and Van Eldere, J. (2015) Inefficacy of vancomycin and teicoplanin in eradicating and killing *Staphylococcus epidermidis* biofilms in vitro, *Int. J. Antimicrob. Agents 45*, 368-375.

9. Cheung, G. Y., Joo, H. S., Chatterjee, S. S., and Otto, M. (2014) Phenol-soluble modulins - critical determinants of staphylococcal virulence, *FEMS Microbiol. Rev. 38*, 698-719.

10. Kong, K. F., Vuong, C., and Otto, M. (2006) Staphylococcus quorum sensing in biofilm formation and infection, *Int. J. Med. Microbiol. 296*, 133-139.

11. Vuong, C., Durr, M., Carmody, A. B., Peschel, A., Klebanoff, S. J., and Otto, M. (2004) Regulated expression of pathogen-associated molecular pattern molecules in *Staphylococcus epidermidis*: quorum-sensing determines pro-inflammatory capacity and production of phenol-soluble modulins, *Cell. Microbiol. 6*, 753-759.

12. Wang, C., Li, M., Dong, D., Wang, J., Ren, J., Otto, M., and Gao, Q. (2007) Role of ClpP in biofilm formation and virulence of *Staphylococcus epidermidis*, *Microb. Infect. 9*, 1376-1383.

13. Yao, Y., Vuong, C., Kocianova, S., Villaruz, A. E., Lai, Y., Sturdevant, D. E., and Otto, M. (2006) Characterization of the *Staphylococcus epidermidis* accessory-gene regulator response: quorum-sensing regulation of resistance to human innate host defense, *J. Infect. Dis. 193*, 841-848.

14. Camilli, A., and Bassler, B. L. (2006) Bacterial small-molecule signaling pathways, *Science 311*, 1113-1116.

15. Rutherford, S. T., and Bassler, B. L. (2012) Bacterial quorum sensing: its role in virulence and possibilities for its control, *Cold Spring Harb. Perspect. Med. 2*, a012427.

16. Lyon, G. J., and Novick, R. P. (2004) Peptide signaling in *Staphylococcus aureus* and other Gram-positive bacteria, *Peptides 25*, 1389-1403.

17. Novick, R. P., and Geisinger, E. (2008) Quorum sensing in staphylococci, *Annu. Rev. Genet. 42*, 541-564.

18. Thoendel, M., Kavanaugh, J. S., Flack, C. E., and Horswill, A. R. (2011) Peptide signaling in the staphylococci, *Chem. Rev. 111*, 117-151.

19. George, E. A., and Muir, T. W. (2007) Molecular mechanisms of agr quorum sensing in virulent staphylococci, *ChemBioChem 8*, 847-855.

20. Ji, G., Beavis, R. C., and Novick, R. P. (1995) Cell density control of staphylococcal virulence mediated by an octapeptide pheromone, *Proc. Natl. Acad. Sci. USA 92*, 12055-12059.

21. Kavanaugh, J. S., Thoendel, M., and Horswill, A. R. (2007) A role for type I signal peptidase in *Staphylococcus aureus* quorum sensing, *Mol. Microbiol. 65*, 780-798.

22. Wang, B., Zhao, A., Novick, R. P., and Muir, T. W. (2014) Activation and inhibition of the receptor histidine kinase AgrC occurs through opposite helical transduction motions, *Mol. Cell 53*, 929-940.

23. George Cisar, E. A., Geisinger, E., Muir, T. W., and Novick, R. P. (2009) Symmetric signalling within asymmetric dimers of the *Staphylococcus aureus* receptor histidine kinase AgrC, *Mol. Microbiol. 74*, 44-57.

24. Novick, R. P., Ross, H. F., Projan, S. J., Kornblum, J., Kreiswirth, B., and Moghazeh, S. (1993) Synthesis of staphylococcal virulence factors is controlled by a regulatory RNA molecule, *EMBO J. 12*, 3967-3975.

25. Otto, M. (2014) Phenol-soluble modulins, *Int. J. Med. Microbiol. 304*, 164-169.

26. Buttner, H., Mack, D., and Rohde, H. (2015) Structural basis of *Staphylococcus epidermidis* biofilm formation: mechanisms and molecular interactions, *Front. Cell. Infect. Microbiol. 5*, 14.

27. Otto, M. (2004) Virulence factors of the coagulase-negative staphylococci, *Front. Biosci. 9*, 841-863.

28. Mack, D., Davies, A. P., Harris, L. G., Rohde, H., Horstkotte, M. A., and Knobloch, J. K. (2007) Microbial interactions in *Staphylococcus epidermidis* biofilms, *Anal. Bioanal. Chem. 387*, 399-408.

29. Vuong, C., Gerke, C., Somerville, G. A., Fischer, E. R., and Otto, M. (2003) Quorum-sensing control of biofilm factors in *Staphylococcus epidermidis*, *J. Infect. Dis. 188*, 706-718.

30. Wang, R., Khan, B. A., Cheung, G. Y., Bach, T. H., Jameson-Lee, M., Kong, K. F., Queck, S. Y., and Otto, M. (2011) *Staphylococcus epidermidis* surfactant peptides promote biofilm maturation and dissemination of biofilm-associated infection in mice, *J. Clin. Invest. 121*, 238-248.

31. Le, K. Y., Dastgheyb, S., Ho, T. V., and Otto, M. (2014) Molecular determinants of staphylococcal biofilm dispersal and structuring, *Front. Cell. Infect. Microbiol. 4*, 167.

32. Boles, B. R., and Horswill, A. R. (2008) Agr-mediated dispersal of *Staphylococcus aureus* biofilms, *PLoS Pathog. 4*, e1000052.

33. Vuong, C., Kocianova, S., Yao, Y., Carmody, A. B., and Otto, M. (2004) Increased colonization of indwelling medical devices by quorum-sensing mutants of *Staphylococcus epidermidis* in vivo, *J. Infect. Dis. 190*, 1498-1505.

34. Otto, M. (2004) Quorum-sensing control in Staphylococci -- a target for antimicrobial drug therapy?, *FEMS Microbiol. Lett. 241*, 135-141.

35. Otto, M. (2013) Staphylococcal infections: mechanisms of biofilm maturation and detachment as critical determinants of pathogenicity, *Annu. Rev. Med. 64*, 175-188.

36. Olson, M. E., Todd, D. A., Schaeffer, C. R., Paharik, A. E., Van Dyke, M. J., Buttner, H., Dunman, P. M., Rohde, H., Cech, N. B., Fey, P. D., and Horswill, A. R. (2014) *Staphylococcus epidermidis* agr quorum-sensing system: signal identification, cross talk, and importance in colonization, *J. Bacteriol. 196*, 3482-3493.

37. Klug, D., Wallet, F., Kacet, S., and Courcol, R. J. (2003) Involvement of adherence and adhesion *Staphylococcus epidermidis* genes in pacemaker lead-associated infections, *J. Clin. Microbiol. 41*, 3348-3350.

38. Hellmark, B., Soderquist, B., Unemo, M., and Nilsdotter-Augustinsson, A. (2013) Comparison of *Staphylococcus epidermidis* isolated from prosthetic joint infections and commensal isolates in regard to antibiotic susceptibility, agr type, biofilm production, and epidemiology, *Int. J. Med. Microbiol. 303*, 32-39.

39. Lianhua, Y., Yunchao, H., Guangqiang, Z., Kun, Y., Xing, L., and Fengli, G. (2014) The effect of iatrogenic *Staphylococcus epidermidis* intercellar adhesion operon on the formation of bacterial biofilm on polyvinyl chloride surfaces, *Surg. Infect. (Larchmt) 15*, 768-773.

40. Schaeffer, C. R., Woods, K. M., Longo, G. M., Kiedrowski, M. R., Paharik, A. E., Buttner, H., Christner, M., Boissy, R. J., Horswill, A. R., Rohde, H., and Fey, P. D. (2015) Accumulation-associated protein enhances *Staphylococcus epidermidis* biofilm formation under dynamic conditions and is required for infection in a rat catheter model, *Infect. Immun. 83*, 214-226.

41. Carmody, A. B., and Otto, M. (2004) Specificity grouping of the accessory gene regulator quorum-sensing system of *Staphylococcus epidermidis* is linked to infection, *Arch. Microbiol. 181*, 250-253.

42. Ji, G., Beavis, R., and Novick, R. P. (1997) Bacterial interference caused by autoinducing peptide variants, *Science 276*, 2027-2030.

43. Mayville, P., Ji, G., Beavis, R., Yang, H., Goger, M., Novick, R. P., and Muir, T. W. (1999) Structure-activity analysis of synthetic autoinducing thiolactone peptides from *Staphylococcus aureus* responsible for virulence, *Proc. Natl. Acad. Sci. USA 96*, 1218-1223.

44. Wright, J. S., 3rd, Jin, R., and Novick, R. P. (2005) Transient interference with staphylococcal quorum sensing blocks abscess formation, *Proc. Natl. Acad. Sci. USA 102*, 1691-1696.

45. Otto, M. (2001) *Staphylococcus aureus* and *Staphylococcus epidermidis* peptide pheromones produced by the accessory gene regulator agr system, *Peptides 22*, 1603-1608.

46. Otto, M., Echner, H., Voelter, W., and Gotz, F. (2001) Pheromone cross-inhibition between *Staphylococcus aureus* and *Staphylococcus epidermidis*, *Infect. Immun. 69*, 1957-1960.

47. Otto, M., Sussmuth, R., Vuong, C., Jung, G., and Gotz, F. (1999) Inhibition of virulence factor expression in *Staphylococcus aureus* by the *Staphylococcus epidermidis* agr pheromone and derivatives, *FEBS Lett. 450*, 257-262.

48. Fleming, V., Feil, E., Sewell, A. K., Day, N., Buckling, A., and Massey, R. C. (2006) Agr interference between clinical *Staphylococcus aureus* strains in an insect model of virulence, *J. Bacteriol. 188*, 7686-7688.

49. Lina, G., Boutite, F., Tristan, A., Bes, M., Etienne, J., and Vandenesch, F. (2003) Bacterial Competition for Human Nasal Cavity Colonization: Role of Staphylococcal agr Alleles, *Appl. Environ. Microbiol. 69*, 18-23.

50. Amara, N., Krom, B. P., Kaufmann, G. F., and Meijler, M. M. (2011) Macromolecular inhibition of quorum sensing: enzymes, antibodies, and beyond, *Chem. Rev. 111*, 195-208.

51. Galloway, W. R., Hodgkinson, J. T., Bowden, S., Welch, M., and Spring, D. R. (2012) Applications of small molecule activators and inhibitors of quorum sensing in Gram-negative bacteria, *Trends Microbiol. 20*, 449-458.

52. Praneenararat, T., Palmer, A. G., and Blackwell, H. E. (2012) Chemical methods to interrogate bacterial quorum sensing pathways, *Org. Biomol. Chem. 10*, 8189-8199.

53. McDowell, P., Affas, Z., Reynolds, C., Holden, M. T., Wood, S. J., Saint, S., Cockayne, A., Hill, P. J., Dodd, C. E., Bycroft, B. W., Chan, W. C., and Williams, P. (2001) Structure, activity and evolution of the group I thiolactone peptide quorum-sensing system of *Staphylococcus aureus*, *Mol. Microbiol. 41*, 503-512.

54. Lyon, G. J., Mayville, P., Muir, T. W., and Novick, R. P. (2000) Rational design of a global inhibitor of the virulence response in *Staphylococcus aureus*, based in part on localization of the site of inhibition to the receptor-histidine kinase, AgrC, *Proc. Natl. Acad. Sci. USA 97*, 13330-13335.

55. Lyon, G. J., Wright, J. S., Muir, T. W., and Novick, R. P. (2002) Key determinants of receptor activation in the agr autoinducing peptides of *Staphylococcus aureus*, *Biochemistry 41*, 10095-10104.

56. Scott, R. J., Lian, L. Y., Muharram, S. H., Cockayne, A., Wood, S. J., Bycroft, B. W., Williams, P., and Chan, W. C. (2003) Side-chain-to-tail thiolactone peptide inhibitors of the staphylococcal quorum-sensing system, *Bioorg. Med. Chem. Lett. 13*, 2449-2453.

57. George, E. A., Novick, R. P., and Muir, T. W. (2008) Cyclic peptide inhibitors of staphylococcal virulence prepared by Fmoc-based thiolactone peptide synthesis, *J. Am. Chem. Soc. 130*, 4914-4924.

58. Fowler, S. A., Stacy, D. M., and Blackwell, H. E. (2008) Design and synthesis of macrocyclic peptomers as mimics of a quorum sensing signal from *Staphylococcus aureus*, *Org. Lett. 10*, 2329-2332.

59. Tal-Gan, Y., Stacy, D. M., Foegen, M. K., Koenig, D. W., and Blackwell, H. E. (2013) Highly potent inhibitors of quorum sensing in *Staphylococcus aureus* revealed through a systematic synthetic study of the group-III autoinducing peptide, *J. Am. Chem. Soc. 135*, 7869-7882.

60. Tal-Gan, Y., Stacy, D. M., and Blackwell, H. E. (2014) N-Methyl and peptoid scans of an autoinducing peptide reveal new structural features required for inhibition and activation of AgrC quorum sensing receptors in *Staphylococcus aureus*, *Chem. Commun. (Camb.) 50*, 3000-3003.

61. Johnson, J. G., Wang, B., Debelouchina, G. T., Novick, R. P., and Muir, T. W. (2015) Increasing AIP Macrocycle Size Reveals Key Features of agr Activation in *Staphylococcus aureus*, *ChemBioChem 16*, 1093-1100.

62. Otto, M., Sussmuth, R., Jung, G., and Gotz, F. (1998) Structure of the pheromone peptide of the *Staphylococcus epidermidis* agr system, *FEBS Lett. 424*, 89-94.

63. Khan, B. A., Yeh, A. J., Cheung, G. Y., and Otto, M. (2015) Investigational therapies targeting quorum-sensing for the treatment of *Staphylococcus aureus* infections, *Expert Opin. Investig. Drugs 24*, 689-704.

64. Tal-Gan, Y., Ivancic, M., Cornilescu, G., Cornilescu, C. C., and Blackwell, H. E. (2013) Structural characterization of native autoinducing peptides and abiotic analogues reveals key features essential for activation and inhibition of an AgrC quorum sensing receptor in *Staphylococcus aureus*, *J. Am. Chem. Soc. 135*, 18436-18444.

65. Kirchdoerfer, R. N., Garner, A. L., Flack, C. E., Mee, J. M., Horswill, A. R., Janda, K. D., Kaufmann, G. F., and Wilson, I. A. (2011) Structural basis for ligand recognition and discrimination of a quorum-quenching antibody, *J. Biol. Chem. 286*, 17351-17358.

66. Kratochvil, M. J., Tal-Gan, Y., Yang, T., Blackwell, H. E., and Lynn, D. M. (2015) Nanoporous Superhydrophobic Coatings that Promote the Extended Release of Water-Labile Quorum Sensing Inhibitors and Enable Long-Term Modulation of Quorum Sensing in *Staphylococcus aureus*, *ACS Biomater. Sci. Eng. 1*, 1039-1049.

CHAPTER 3:

Structural Characterization of Peptidic Modulators of the *Staphylococcus epidermidis* Quorum Sensing Receptor AgrC-I

Contributions: T. Yang and J. K. Vasquez designed the experiments and performed NMR analyses. T. Yang prepared the manuscript. J. K. Vasquez performed the NMR experiments and assisted with writing. G. Cornilescu assisted with the NMR experiments. H. E. Blackwell guided the project and assisted with manuscript preparation.

*This chapter is being prepared as a manuscript intended for publication under the same title.

3.1 Abstract

Staphylococcus epidermidis is one of the leading causes for nosocomial infections, and the infections are recalcitrant to traditional therapies due to emerging antibiotics resistance and formation of robust biofilms. Playing an important role in the regulation of virulence is the accessory gene regulator (*agr*) quorum sensing (QS) system. The interaction between a macrocyclic peptide signal (dubbed as autoinducing peptide or AIP) and its cognate transmembrane receptor (AgrC) is responsible for the activation of the *agr* system, and non-native ligands capable of disrupting this interaction are of interest as probes for assessing the *agr* system as a potential target for attenuating infections. We recently reported the first systematic structure-activity relationships (SARs) characterization for the AIP-I:AgrC-I interaction, and uncovered the first set of non-native AIP analogs that modulate the activity of the AgrC receptor. However, lack of structural data limited the understanding of the chemical features important to receptor activation and inhibition. Herein, we report the first three-dimensional structural analysis of AIP-I and its analogs using NMR spectroscopy. Structural comparisons of agonists and antagonists revealed key features important for AgrC-I activation and support the known SARs derived from cell-based assays. The results from the present study not only improve our understanding of the AIP:AgrC interactions in *S. epidermidis*, but also facilitate the design of new *agr* modulators with enhanced activities.

3.2 Introduction

Staphylococcus epidermidis, a ubiquitous colonizer of the human epithelia *(1)*, is an important nosocomial pathogen *(2, 3)*, and it is a leading cause for biomedical device-associated infections due to its propensity to form robust biofilms on abiotic surfaces *(3-8)*. This biofilm lifestyle, combined with the emergence of antibiotic resistances, makes treating *S. epidermidis* infections with traditional antimicrobials difficult *(2, 3, 6, 9-11)*. Playing an important role in the pathogenesis of *S. epidermidis* infections is the accessory gene regulator (*agr*) system *(12-17)*, a cell-cell communication system that allows the bacteria to sense population density and coordinate gene expressions in a process known as quorum sensing (QS) *(18, 19)*. This communication is mediated in part by the peptidic signaling molecule termed autoinducing peptide (AIP) *(20-23)*. As the bacteria population density increases, so does the concentration of AIP. Once a threshold concentration is reached, AIP can productively bind with its cognate receptor AgrC, a transmembrane histidine kinase, which initiates the signaling cascade that leads to changes in gene expression.

Since a number of the genes associated with *S. epidermidis* virulence are under the control of QS *(11, 13, 14, 24-28)*, targeting the *agr* system can be an attractive approach for controlling *S. epidermidis* infection *(25, 29-32)*. Such effort has been undertaken extensively toward *Staphylococcus aureus*, a better-studied human pathogen closely related to *S. epidermidis*, and prior studies by our lab and others have uncovered several potent, non-native antagonists of the *agr* system in *S. aureus (33-47)*. More recently, our lab has conducted the first systematic analysis of the structure-activity relationships (SARs) for the interaction between *S. epidermidis* AIP-I and its cognate receptor AgrC-I *(48)*, and we reported the discovery of the first set of non-native AIP analogs that are capable of potently activating or inhibiting the *agr* system in *S. epidermidis* (Figure 3.1). While we gained valuable information regarding the roles of side chain functional groups and the stereochemistry of the amino acids in the interaction between the native signal peptide and its receptor, the lack of three-dimensional (3-D) structural information

limited our understanding of how the different amino acid substitutions introduced to the native agonist AIP-I altered the signal activities, as well as the chemical features crucial to the activation and inhibition of AgrC-I. Detailed structural analyses of AIP-I and its analogs therefore would not only enhance our understanding of the SARs of the AIP-I:AgrC-I interaction, but also facilitate the design of a new generation of AgrC modulators with improved properties or interesting activities. To date, only the solution-phase structure of AIP-I has been reported in a mixed-solvent system *(49)*, and the analysis of the structure is focused on the motifs important for interaction with the *S.aureus* AgrC receptor, not with *S. epidermidis* AgrC-I. No structural information on *S. epidermidis* AIP-I analogs, to the best of our knowledge, has been reported.

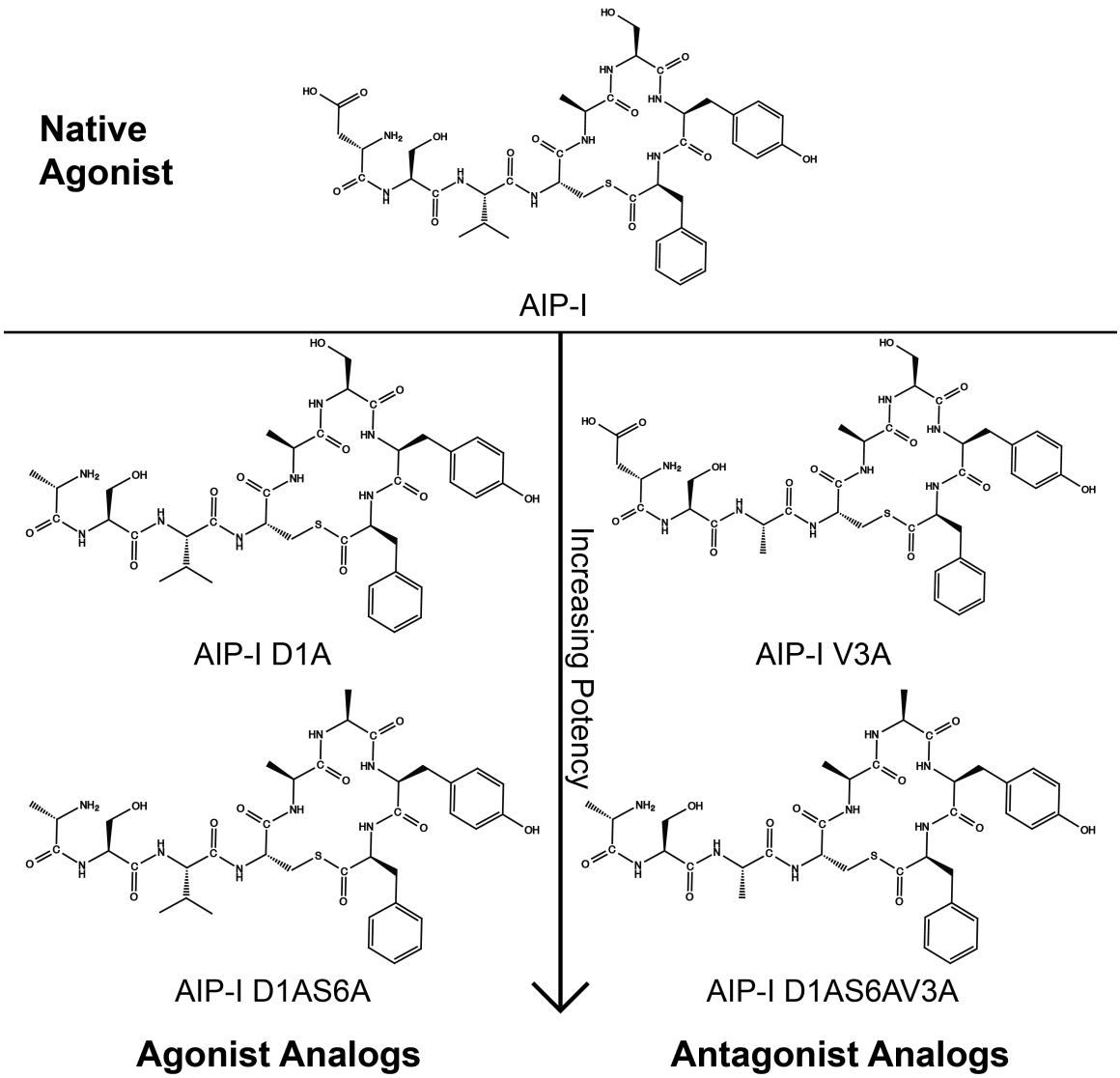


Figure 3.1: Primary structures of *S. epidermidis* AIP-I and its analogs that are characterized in this study.

Herein, we report the first characterization of the 3-D solution-phase structures of *S. epidermidis* AIP-I analogs. Structural comparison of these analogs to the native signal AIP-I confirmed our previous hypotheses on the key features important to AgrC-I binding and activation. In addition, the structural analyses generated new hypotheses on the modularity of the receptor-activation motif and receptor-binding motif of AIP-I, which will guide the design of new peptidic analogs that could possess unique activities.

3.3 Results and Discussion

3.3.1 Selection of S. epidermidis AIP-I analogs.

To help elucidate the structural features important for activation and inhibition of *S. epidermidis* AgrC-I, in addition to the native signal AIP-I, we chose to characterize the structures for four non-native *S. epidermidis* AIP-I analogs with a range of activities (Figure 3.1). First, we selected a moderate antagonist, AIP-I V3A, where a single mutation to the native peptide signal switched the activity from agonism to antagonism. Comparison between AIP-I V3A and AIP-I would help explain the role of the Val residue in receptor activation. Next, two agonist analogs with enhanced potency, AIP-I D1A and AIP-I D1AS6A, were analyzed to better understand how the Ala substitutions increased the potency of the native agonist, as well as to highlight the structural motifs crucial to receptor activation. Lastly, we chose one of the most potent antagonists against AgrC-I, AIP-I D1AS6AV3A, which would provide insights into the chemical features important to receptor inhibition. The biological activities of these analogs as well as AIP-I have been characterized previously using a *S. epidermidis* GFP reporter strain *(48)*, and the results are summarized in Table 3.1. We would like to note that the *S. epidermidis* AIP-I is the first ligand of this class of system to have two residues that lead to suboptimal activation of its cognate AgrC receptor, and multiple non-native ligands designed by our laboratory are more than an order of magnitude more potent than the native ligand as agonists against AgrC-I *(48)*.

Table 3.1: Cell-based reporter activities of the peptides evaluated in this study against AgrC-I[a]

Peptide name	Sequence	IC_{50}[b] (CI)	EC_{50}[b] (CI)
AIP-I	D-S-V-(C-A-S-Y-F)	-	196 nM (162 – 238)
AIP-I D1A	A-S-V-(C-A-S-Y-F)	-	49.3 nM (43.3 – 56.2)
AIP-I D1AS6A	A-S-V-(C-A-A-Y-F)	-	10.3 nM (6.18 – 17.2)
AIP-I V3A	D-S-A-(C-A-S-Y-F)	51.9 nM (37.9 – 71.0)	-
AIP-I D1AS6AV3A	A-S-A-(C-A-A-Y-F)	2.84 nM (1.95 – 4.11)	-

[a] Values are from ref 48. [b] CI = 95% confidence interval.

3.3.2 NMR analyses.

To characterize the 3-D structures of AIP-I and AIP-I analogs, we utilized NMR spectroscopy, which was previously used by our lab to study the structures of *agr* modulators in *S. aureus (43, 49, 50).* All 1-D and 2-D (TOCSY and ROESY) NMR spectra were obtained on a 750 MHz spectrometer at ambient temperature in either H_2O/D_2O (95:5) or H_2O/CD_3CN (87.5:12.5), and subsequently analyzed using MestReNova 10 NMR processing software. The 1-D proton and 2-D TOCSY spectra were used to determine chemical shifts of the proton resonances and assisted in the sequential assignments of proton resonances to each amino acid residue. The internuclear proton distances derived from the 2-D ROESY spectra were used to calculate and refine 3-D structures with the Xplor-NIH software, and the ensemble of the 20 lowest energy structures obtained was used to determine the most representative low energy structure (see Supplementary Information for the ensembles). Although the organic solvent acetonitrile needed for the NMR experiments was absent in the biological assays, previous structure studies of *S. aureus agr* modulators found that the presence of small amount of acetonitrile did not cause significant change to structures obtained in pure water *(43)*.

3.3.3 Structural comparison of AIP-I to AIP-I V3A.

We first focused on the comparison between the native signal peptide AIP-I, an agonist, and AIP-I V3A, an antagonist arose from a single amino acid substitution (Figure 3.2). Prior SAR studies of the AIP:AgrC interactions in both *S. aureus* and *S. epidermidis* have identified the macrocycle, and in particular the endocyclic hydrophobic residues, of the signal peptide to be important for receptor binding, and a hydrophobic binding pocket on the receptor AgrC has been proposed to be involved in AIP recognition *(36, 42, 48, 50, 51)*. In agreement with these results, the structure of AIP-I shows the side chains of both endocyclic hydrophobic residues (Phe8 and Tyr7) oriented away from one face of the macrocycle to form a more hydrophobic side (Figure

3.2A and C). Interestingly, the ensemble of the lowest energy structures for AIP-I is quite disordered, likely due to the overall more hydrophilic nature of the peptide. However, the macrocycle portion of the peptide shows much less deviation among the structures (Figure 3.6), underscoring the importance of the arrangements of the hydrophobic residues in the macrocycle for receptor binding. Protruding towards the same hydrophobic side is the side chain of residue Val3, a key activation residue identified in the prior SAR study of *S. epidermidis* AIP-I. Despite the exocyclic tail region being disordered, the positioning of residue Val3 relative to the macrocycle is very well conserved among the structures of the ensemble (Figure 3.6B), suggesting that the orientation of Val3 is likely important for receptor activation.

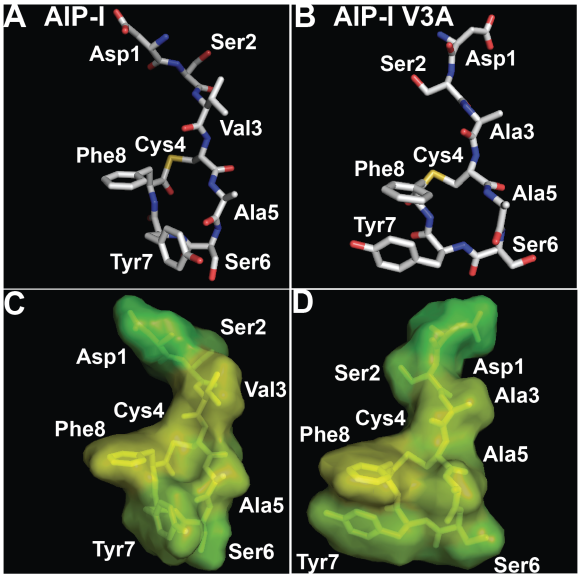


Figure 3.2: Average heavy atom structures of (A) AIP-I and (B) AIP-I V3A derived from the ensemble of 20 lowest energy structures of each peptide. Carbon is shown in silver, oxygen in red, nitrogen in blue, and sulfur in yellow. Surface plots of (C) AIP-I and (D) AIP-I V3A. Yellow indicates more hydrophobic surfaces, and green indicates more hydrophilic surfaces.

The ensemble of the lowest energy structures for AIP-I V3A is also disordered, but like AIP-I, the structures of the macrocycle are highly consistent (Figure 3.7). Also similar to the structure of AIP-I, the hydrophobic residues (Phe8 and Tyr7) of AIP-I V3A are extended towards one face of the macrocycle to create a hydrophobic surface (Figure 3.2B and D). In addition, while the branched hydrophobic side chain of residue Val3 is replaced with a methyl group in AIP-I V3A,

the orientation of the Ala side chain relative to the macrocycle is still conserved (Figure 3.2A-B and Figure 3.7B), though to a lesser extent than that of the Val residue in AIP-I. One major difference between AIP-I V3A and AIP-I is the orientation of residue Tyr7. Compared to that of AIP-I, the side chain of Tyr7 in AIP-I V3A is rotated about 180°, causing the hydroxyl group on the tyrosine to point away from the proposed hydrophobic surface. While this difference in Tyr7 orientation between the two structures could be significant to ligand activities, we believe the difference is more likely a result of the uncertainty in calculating internuclear distances due to spin diffusion and not responsible for the switch from agonist to antagonist caused by the Val and Ala mutation (we will return to this point in the following section). Due to the disordered nature of the exocyclic tail in both AIP-I and AIP-I V3A, the differences for residues Asp1 and Ser2 in the average structures of the two peptides are not meaningful, and the two residues likely can adopt whichever positions necessary for proper interaction with the receptor. Therefore, the structures for AIP-I and AIP-I V3A overall are fairly similar, and we propose that the lack of the branched hydrophobic side chain of residue Val3 to be the primary cause for switching AIP-I from an agonist to an antagonist.

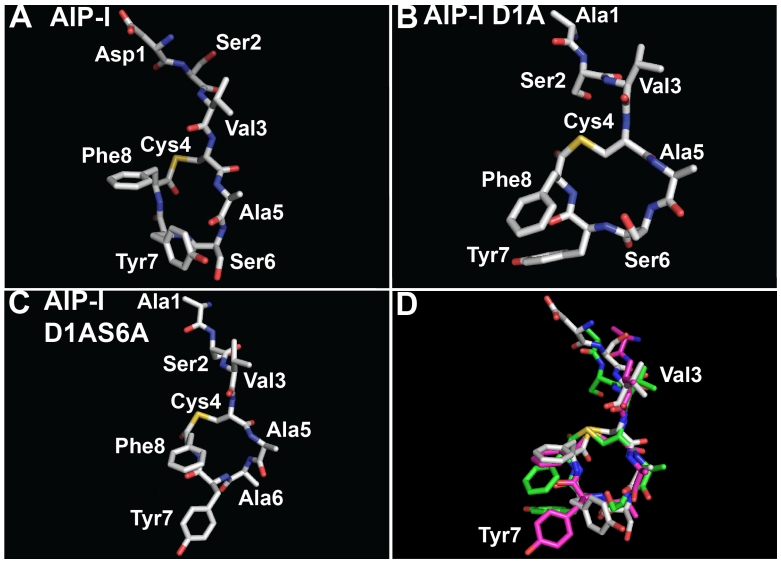


Figure 3.3: Average heavy atom structures of (A) AIP-I, (B) AIP-I D1A, and (C) AIP-I D1AS6A derived from the ensemble of 20 lowest energy structures of each peptide. Carbon is shown in silver, oxygen in red, nitrogen in blue, and sulfur in yellow. (D) Overlay of the structures of all three agonists. AIP-I is in silver, AIP-I D1A is in green, and AIP-I D1AS6A is in magenta.

3.3.4 Structural comparison of AgrC-I agonists with increasing potency.

To further our understanding of the structural features important for AgrC-I activation, we characterized the structures for two non-native agonists of AgrC-I, AIP-I D1A and AIP-I D1AS6A (Figure 3.3). Both analogs are more potent agonists than the native agonist, with AIP-I D1AS6A being the most potent non-native agonist targeting *S. epidermidis* AgrC-I uncovered to date. Despite the close to 20-fold difference in potency, all three agonists adopt similar structures, with the well-defined macrocycles and the side chain of residue Val3 positioned on the same side of the macrocycle as the endocyclic hydrophobic residues (Figure 3.3D). Neither the Asp1 to Ala1 mutation nor the Ser6 to Ala6 mutation significantly altered overall structure of the peptides, though the unstructured exocyclic tail region of AIP-I makes the analysis on the structural effect of the Asp1 to Ala1 mutation difficult. The most striking difference among the three structures is the orientation of Tyr7 residue, which varies greatly from structure to structure. While the substitution of residue Ser6 with Ala could impact the orientation of Tyr7, the greater shift in the position of Tyr7 is found between AIP-I and AIP-I D1A, two peptides with

the same amino acid sequence for the macrocycle. Furthermore, no through-space proton-proton interactions were observed in 2-D ROESY between residue Asp1 or Ala1 and the macrocycle in either structures. Lastly, residue Tyr7 in AIP-I D1A actually adopts two different orientations in the ensemble of the lowest energy structures (Figure 3.8), where a minority of the structures positions Tyr7 more closely to that of AIP-I structures. Although obtaining NMR spectra for AIP-I D1A was difficult, and thus caution needs to be exercised when drawing conclusions about structural features, taken all together the different orientations of Tyr7 are unlikely to be the cause for the differences in potency observed for these peptides. Instead, the constraint allowance we assigned for the calculated internuclear distances, which was done to account for spin diffusion, along with the limitations of signal intensity in the 2-D ROESY spectra caused by the peptide solubility limit (see Supplementary Information for NMR spectra), allowed a degree of conformational variability of residues (more so for the native AIP-I) in the peptide structures when analyzing with Xplor.

In addition to determining the structural features important for AgrC-I activation, we also looked for possible explanation for the increases in potency caused by the introduction of the Ala substitutions. Given that the overall structures of all three peptides are quite similar, the increases in potency could be a result of removal of unfavorable interactions with the AgrC-I receptor. Specifically, residue Ser6 resides in the hydrophobic face that is proposed to be important for receptor binding, and the removal of the more polar hydroxyl group in the side chain could improve the non-polar interactions between the peptide and the receptor. A similar explanation could also apply to residue Asp1, though a non-polar binding site for the N-terminal residue of the exocyclic tail of an AIP is much more speculative.

We would like to note, however, that the ensembles of the structures for AIP-I D1A (backbone atom RMSD: 0.29Å) and AIP-I D1AS6A (backbone atom RMSD: 0.26Å) are much more ordered than that of AIP-I (backbone atom RMSD: 1.01Å). Assuming that the orientations adopted by the exocyclic tail region of AIP-I D1A and AIP-I D1AS6A are favorable for receptor

binding, then the more structured exocyclic tail of AIP-I D1A and AIP-I D1AS6A would incur a lower entropic cost when binding to AgrC-I. Even though the ensembles of AIP-I D1A and AIP-I D1AS6A being more structured could be explained by the observation that both peptides are more water-soluble than AIP-I and thus allow subtler internuclear proton-proton interactions to be detected (Table 3.7), we could not definitely rule out entropic cost as a factor in the increase in potency for both peptides. Additional AIP-I analogs need to be designed and studied to better understand how the Ala substitutions increase the agonist potency.

3.3.5 Comparison between the most potent AgrC-I agonist and antagonist.

Based on the structural analyses from before, we propose that 1) the macrocycle contains a hydrophobic face, formed by the endocyclic hydrophobic residues, that is crucial for receptor binding, 2) the macrocycle orients the nearest exocyclic residue Val3 such that the side chain protrudes towards the same hydrophobic face, 3) the branched hydrophobic motif of the Val3 side chain forms important interactions with the receptor in order to activate the receptor, and 4) the remaining exocyclic tail forms additional contacts with the receptor to improve receptor binding. To strengthen our model for AgrC-I activation, we sought to compare the structures of our most potent agonist, AIP-I D1AS6A, and most potent antagonist, AIP-I D1AS6AV3A (Figure 3.4). In agreement with our model and similar to our analysis for the comparison between AIP-I and AIP-I V3A, the major structural difference between AIP-I D1AS6A and AIP-I D1AS6AV3A is the presence and absence of the Val3 side chain (Figure 3.4C and D). Furthermore, unlike the previous comparisons, the orientation of Tyr7 in both structures is much more comparable, supporting our previous assertions that the differences in Tyr7 orientation are unlikely to be responsible for the differences in peptide activities (Figure 3.4C and D). Additionally, these peptides were present in sufficiently high concentrations in solution to make NOE constraint violations with a much higher degree of confidence relative to any molecules studied with an Asp at the N-terminal position (Table 3.7), thus providing more accurate representations of the

structures of AgrC-I agonist and antagonist and strengthening our model for AgrC-I activation and inhibition. We also would like to highlight that the positioning of Val3 and Ala3 in AIP-I D1AS6A and AIP-I D1AS6AV3A, respectively, does not differ by much. We hypothesize that the relative orientation of Val3 to the macrocycle, which we propose to be important for receptor activation, may not be dictated significantly by the specific interactions between the macrocycle and the branched hydrophobic side chain of Val3. Our hypothesis means that Val, and only Val positioned properly right next to the ring, is crucial for activation. Consequently, introducing a Val residue next to a different AIP macrocycle could possibly allow the new AIP to activate *S. epidermidis* AgrC-I, as long as the exocyclic residue nearest to the macrocycle is oriented properly.

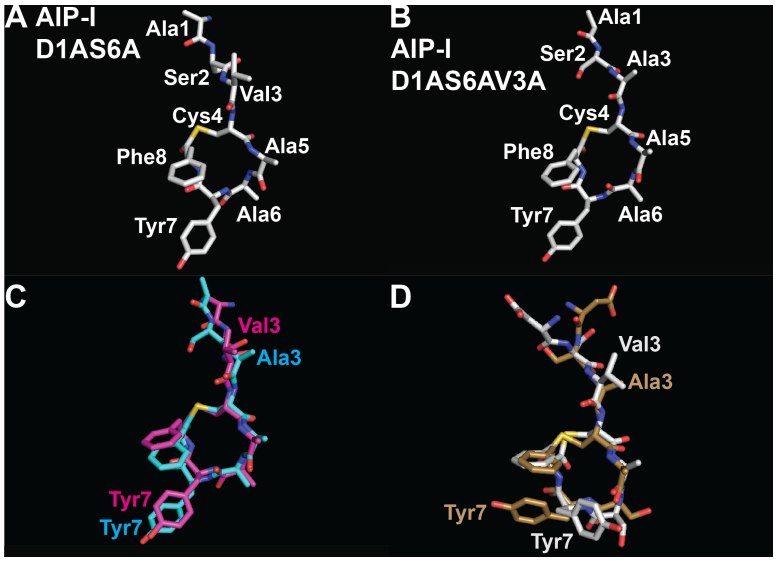


Figure 3.4: Average heavy atom structures of (A) AIP-I D1AS6A (most potent AgrC-I agonist) and (B) AIP-I D1AS6AV3A (most potent AgrC-I antagonist) derived from the ensemble of 20 lowest energy structures of each peptide. Carbon is shown in silver, oxygen in red, nitrogen in blue, and sulfur in yellow. (C) Overlay of the structures of both peptides. AIP-I D1AS6A is in magenta and AIP-I D1AS6AV3A is in cyan. Key residues discussed in text are labeled with color matching the structure of each peptide. (D) Overlay of AIP-I (native agonist in silver) and AIP-I V3A (moderate antagonist in tan). Key residues discussed in text are labeled with color matching the structure of each peptide.

3.4 Summary

In order to gain more insight into how *S. epidermidis* AIP-I and its analogs activate and inhibit *S. epidermidis* AgrC-I, we determined the 3-D solution-phase structures of the native AIP signal and 4 analogs with varying activities. Structural comparisons of different agonists and antagonists revealed chemical features important to AgrC-I activation (Figure 3.5). Specifically, we propose that the macrocycle exhibits a hydrophobic face that facilitates receptor binding, and that a branched hydrophobic group, oriented properly by the macrocycle, is the essential factor for receptor activation. Removal of the branched hydrophobic group, while maintaining the important features of the macrocycle, results in an AgrC-I antagonist. In addition, the exocyclic tail forms additional contacts with the receptor to improve the AIP-I:AgrC-I interaction. The proposed model is in agreement with the activities of the AIP analogs observed in the cell-based reporter assay, thus providing the first structural data to support the SAR characterization derived from the cell-based study.

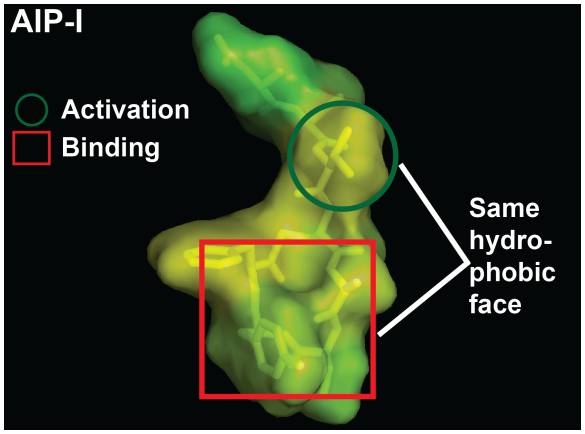


Figure 3.5: Model for AgrC-I activation by AIP-I. The macrocyclic hydrophobic residues form a hydrophobic face important for receptor binding. The valine residue, with a branched hydrophobic motif in the side chain, is properly oriented relative the macrocycle and necessary for receptor activation. Absence of the activation motif results in an inhibitor of AgrC-I.

In addition to AIP-I and AgrC-I, two other signal-receptor pairs exist in *S. epidermidis*, namely AIP-II/AgrC-II and AIP-III/AgrC-III, and each signal has a unique amino acid sequence *(30, 52)*. Interestingly, both AIP-II and AIP-III are capable of inhibiting AgrC-I, while AIP-I is an inhibitor against both AgrC-II and AgrC-III *(30, 48)*. To further test our model for AgrC-I

activation and inhibition, as well as to better understand the AIP:AgrC interactions for all systems in *S. epidermidis*, structural studies with AIP-II, AIP-III, and their analogs of interest, are needed. Efforts toward this goal are currently underway.

Lastly, because the primary mechanism by which *S. epidermidis* causes infection is biofilm formation and the activation of the *agr* system can reduce biofilm accumulation *(12, 25, 27, 29)*, designing AIP analogs that can activate all three AgrC receptors in *S. epidermidis* would be of great interest. Our structural study suggests that, while the branched hydrophobic side chain of residue Val3 is crucial for receptor activation, the proper orientation of this side chain may not be dictated by any specific interactions between the side chain and the macrocycle. Consequently, we hypothesize that a Val residue, or another amino acid with similar side chain group, could be introduced into the AIP-II or AIP-III scaffold, turning the resulting peptide into an activator for multiple AgrC receptors. Experiments toward testing this hypothesis and developing agonists against multiple *S. epidermidis* AgrC receptors are underway as well.

3.5 Methods

3.5.1 Chemical reagents and peptide synthesis

All reagents and solvents were purchased from Sigma-Aldrich or Chem-Impex and used as obtained. Water (18 MΩ) was purified using a Barnstead Nanopure from Thermo Scientific. All peptides analyzed in this study were previously synthesized in our laboratory *(48)*, and all were purified to homogeneity using established reverse-phase high performance liquid chromatography methods using a Kromasil Eternity C_{18} column.

3.5.2 NMR methods and spectra analyses

NMR experiments (1-D proton, 2-D TOCSY, and 2-D ROESY) and subsequent analyses of the spectral data were carried out using our previously reported method *(43)*. Briefly, peptides were dissolved in H_2O:D_2O (95:5), except for AIP-I which was dissolved in H_2O:CD_3CN

(87.5:12.5), to a concentration of at least 0.7 mM. All NMR spectra were obtained on a 750 MHz spectrometer using standard pulse sequences at ambient temperature. Chemical shifts were referenced to H_2O at 4.79 ppm or CD_3CN at 1.94 ppm. See Supplementary Information for selected parameters for the NMR experiments.

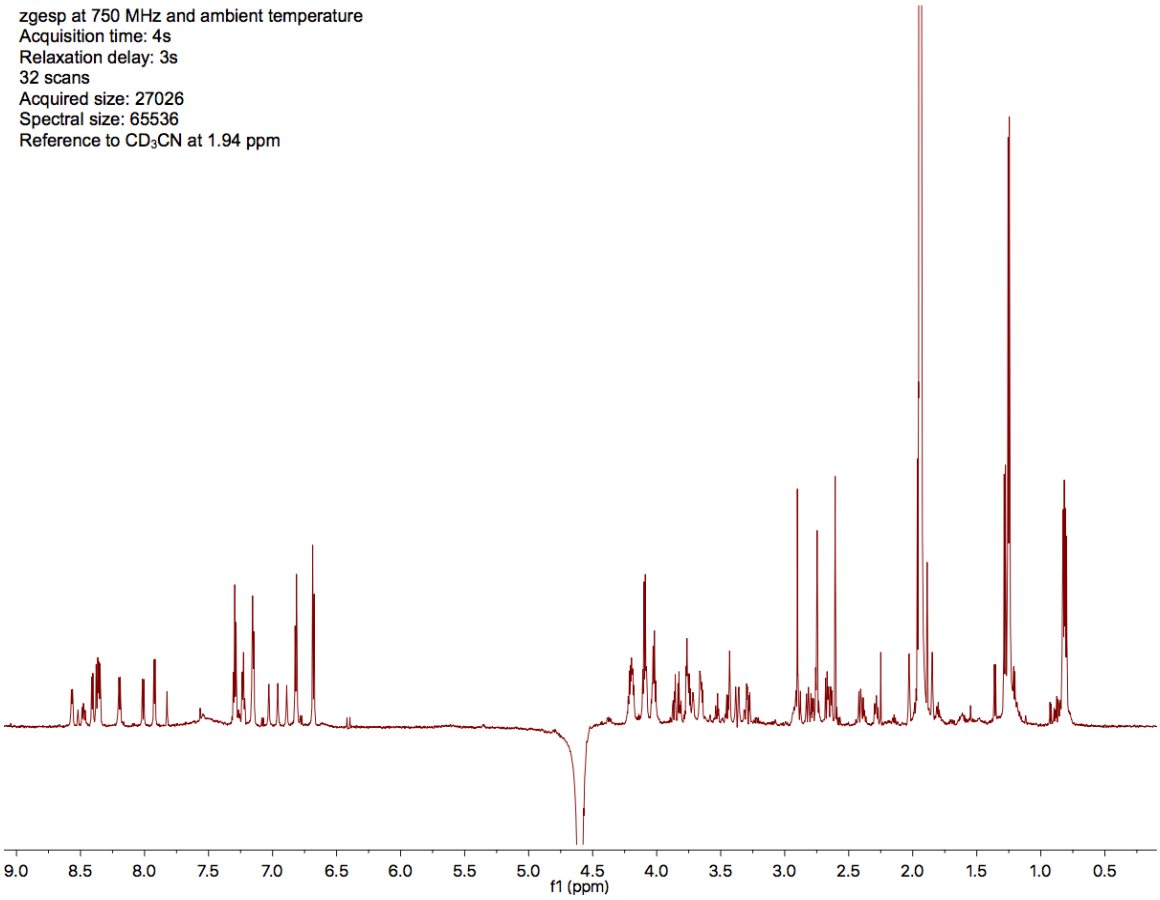
All spectra were analyzed using MestReNova 10 NMR processing software. Resonance assignments for each peptide, calculations of interproton distance restraints from ROESY crosspeak volumes, and the three-dimensional structure calculations and refinements were completed according to the established protocols. Representative spectra, chemical shift assignments, and summary of the constraints are provided in the Supplementary Information. An average structure for each peptide was determined from an ensemble of the 20 lowest-energy structures obtained by high-temperature annealing in NIH-Xplor, with an initial higher constraint allowance (±20%) used to determine initial structures, and a greater refinement to more accurately show the interpretation of the spectra of ±10% for constraint allowance so a more representative structure could be obtained. Visual analysis and presentation of the peptide structures were performed with PyMOL.

3.6 Supplementary Information

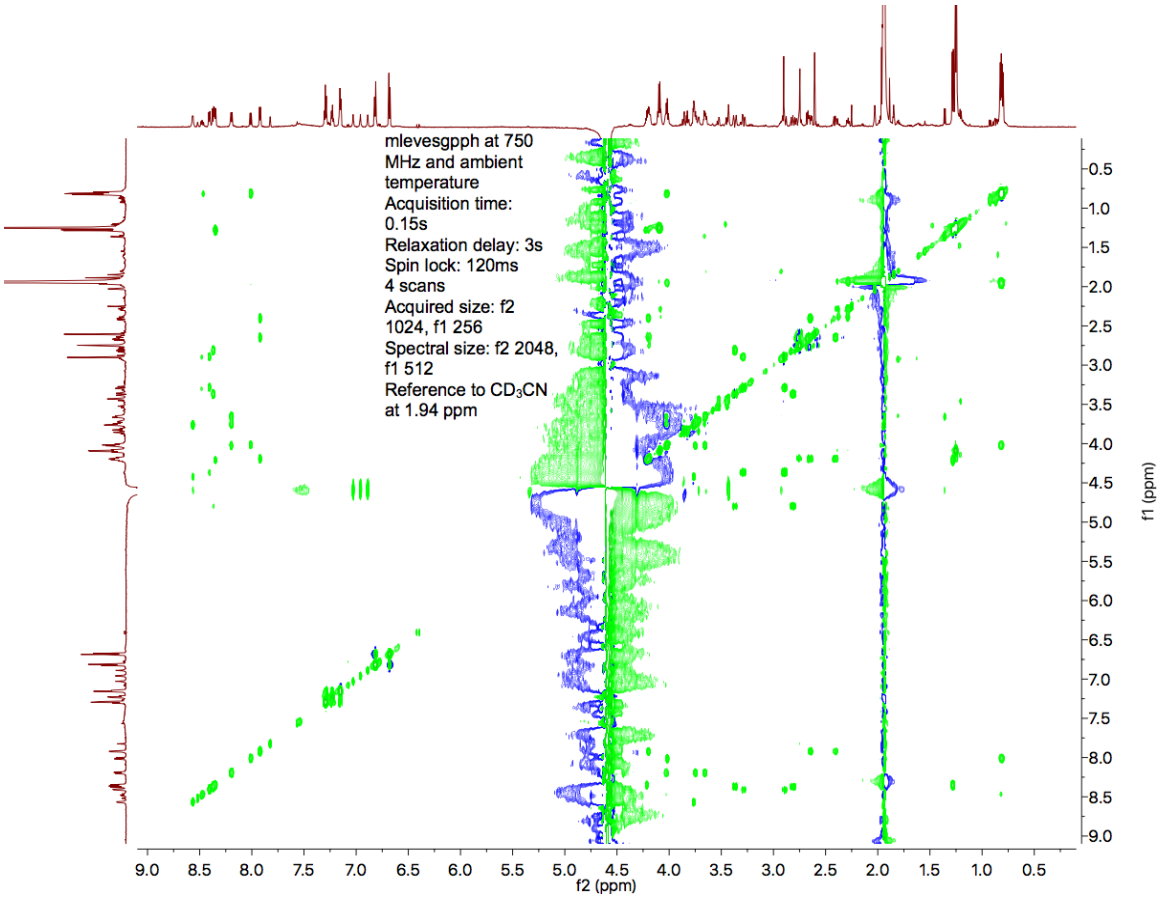
3.6.1 NMR spectra

One-dimensional proton, two-dimensional TOCSY, and two-dimensional ROESY NMR experiments were performed for each peptide as described in the main text. Selected parameters for each experiment are included in each spectrum. For the 2-D experiments, blue indicates negative peak intensity and green indicates positive peak intensity.

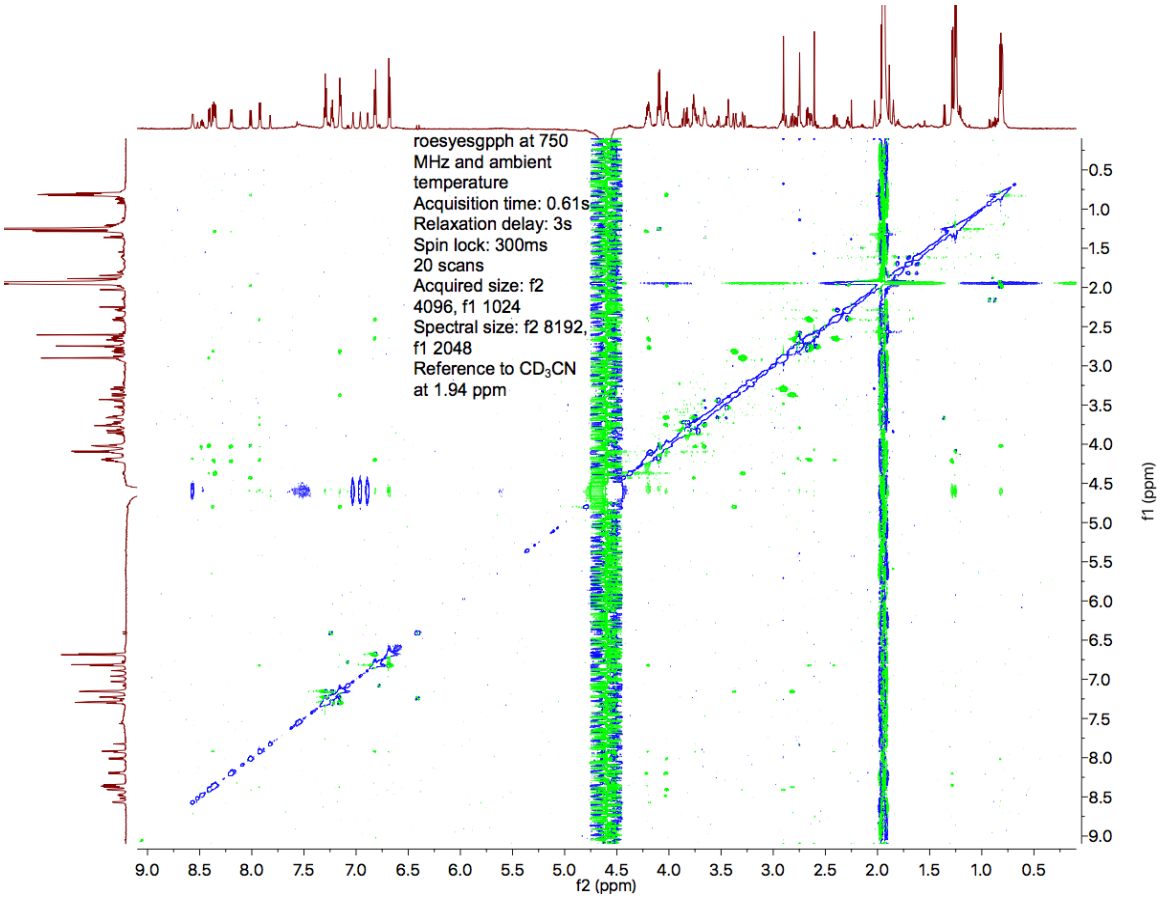
AIP-I ^{1}H NMR spectrum



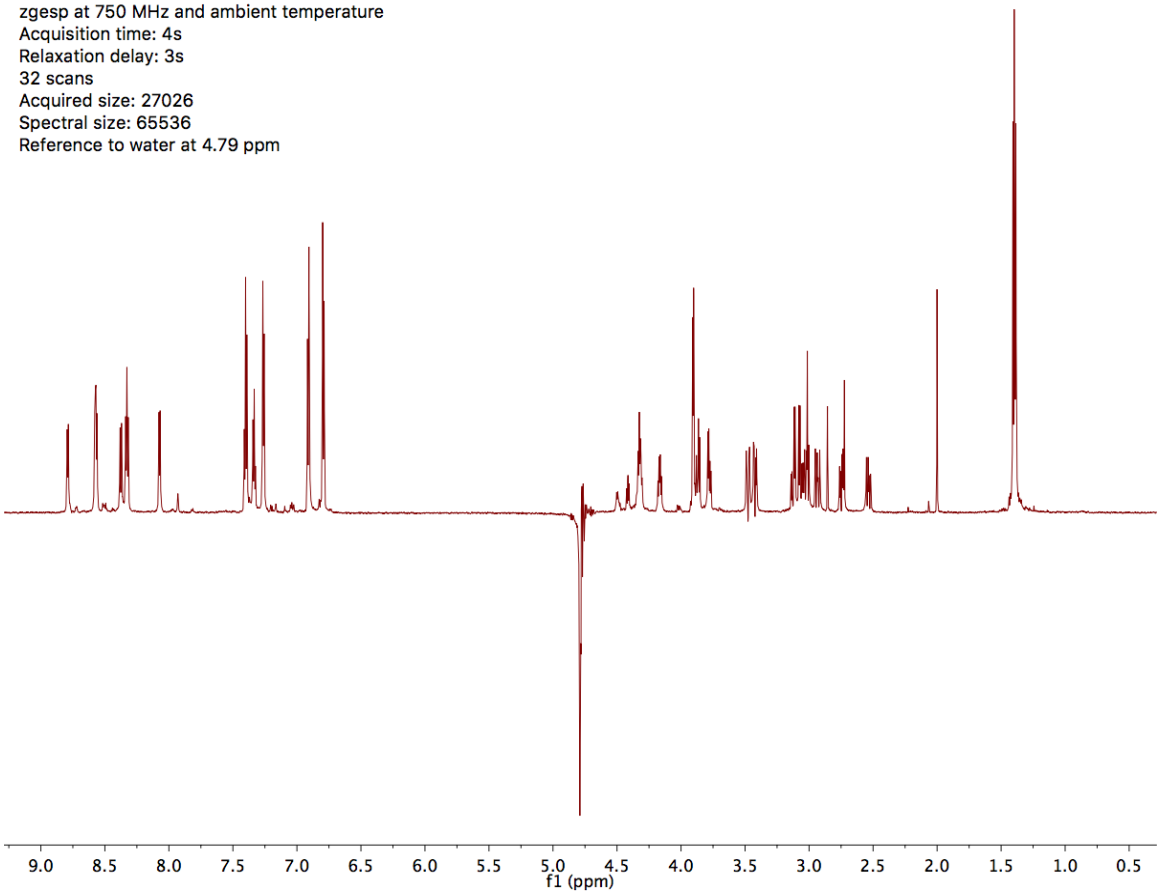
AIP-I TOCSY spectrum



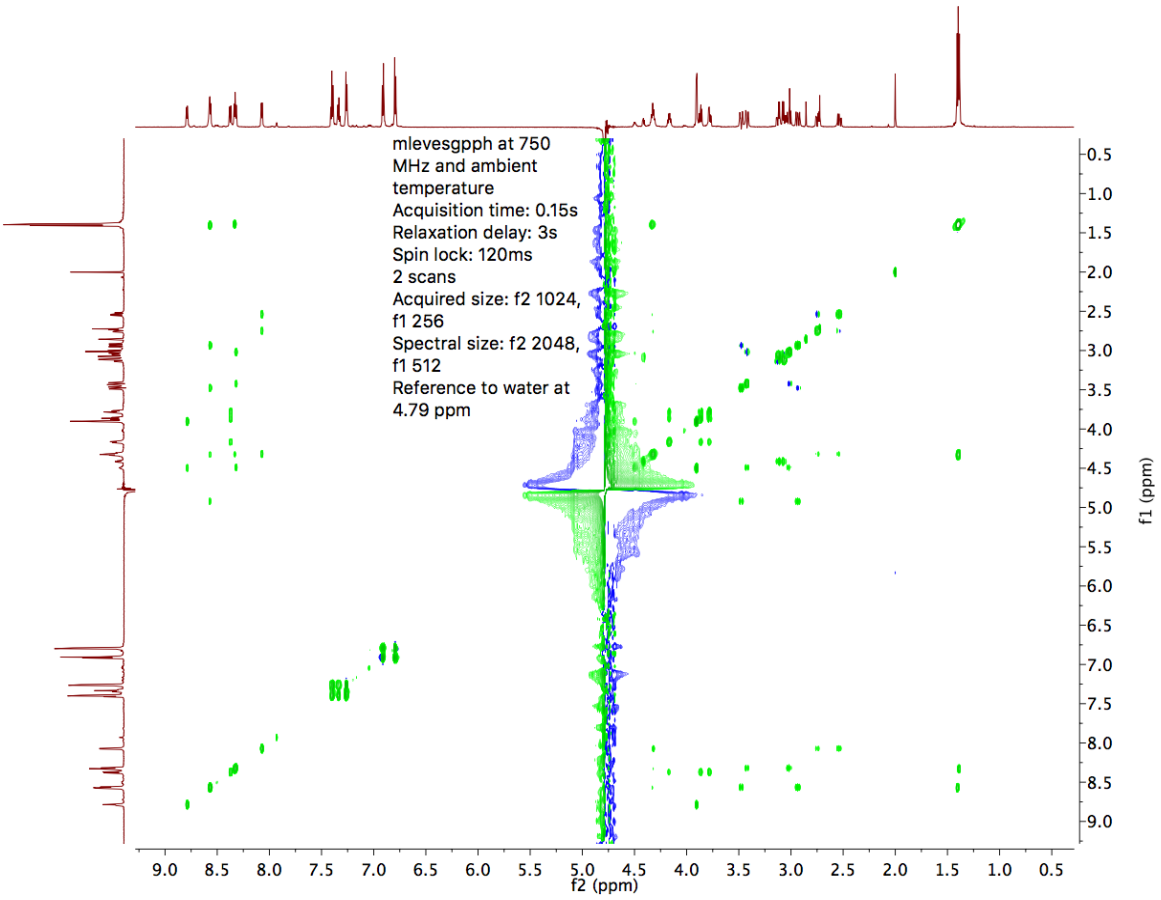
AIP-I ROESY spectrum



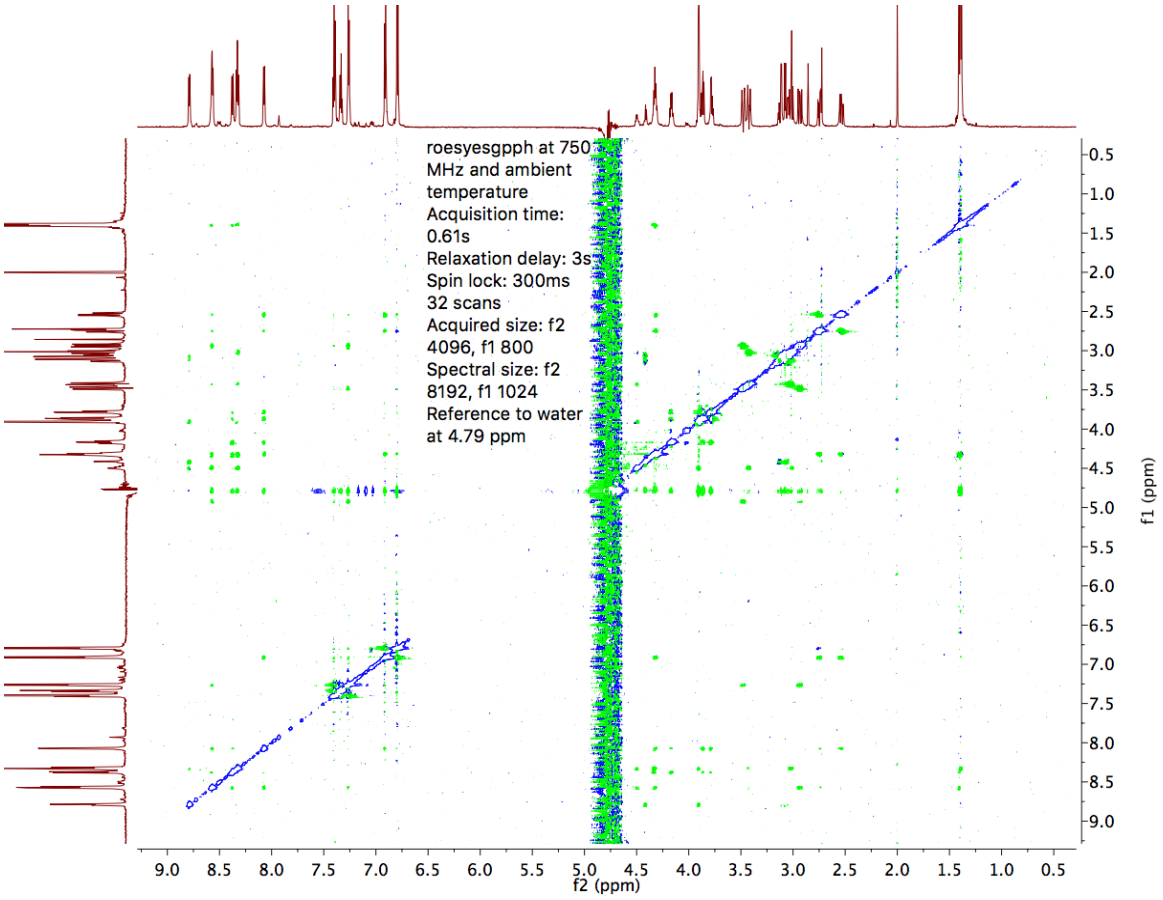
AIP-I V3A ^{1}H spectrum



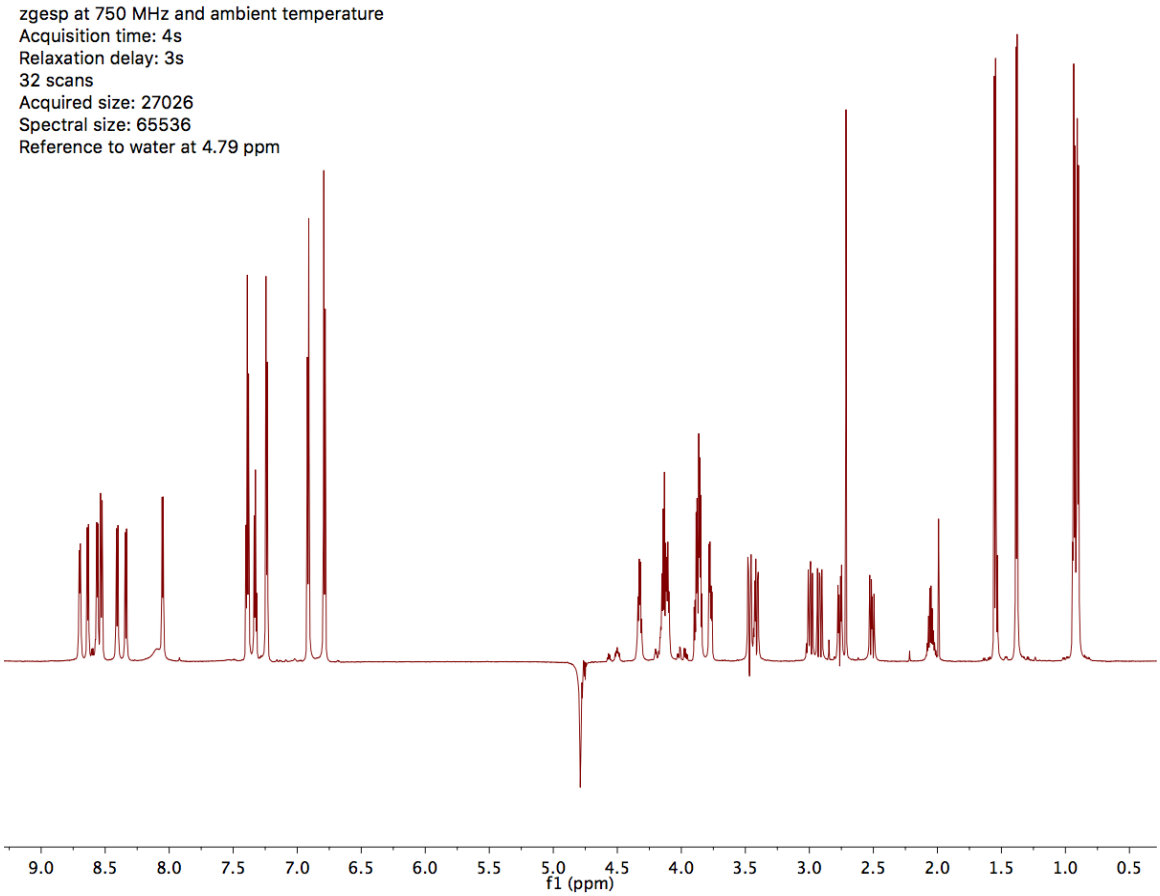
AIP-I V3A TOCSY spectrum



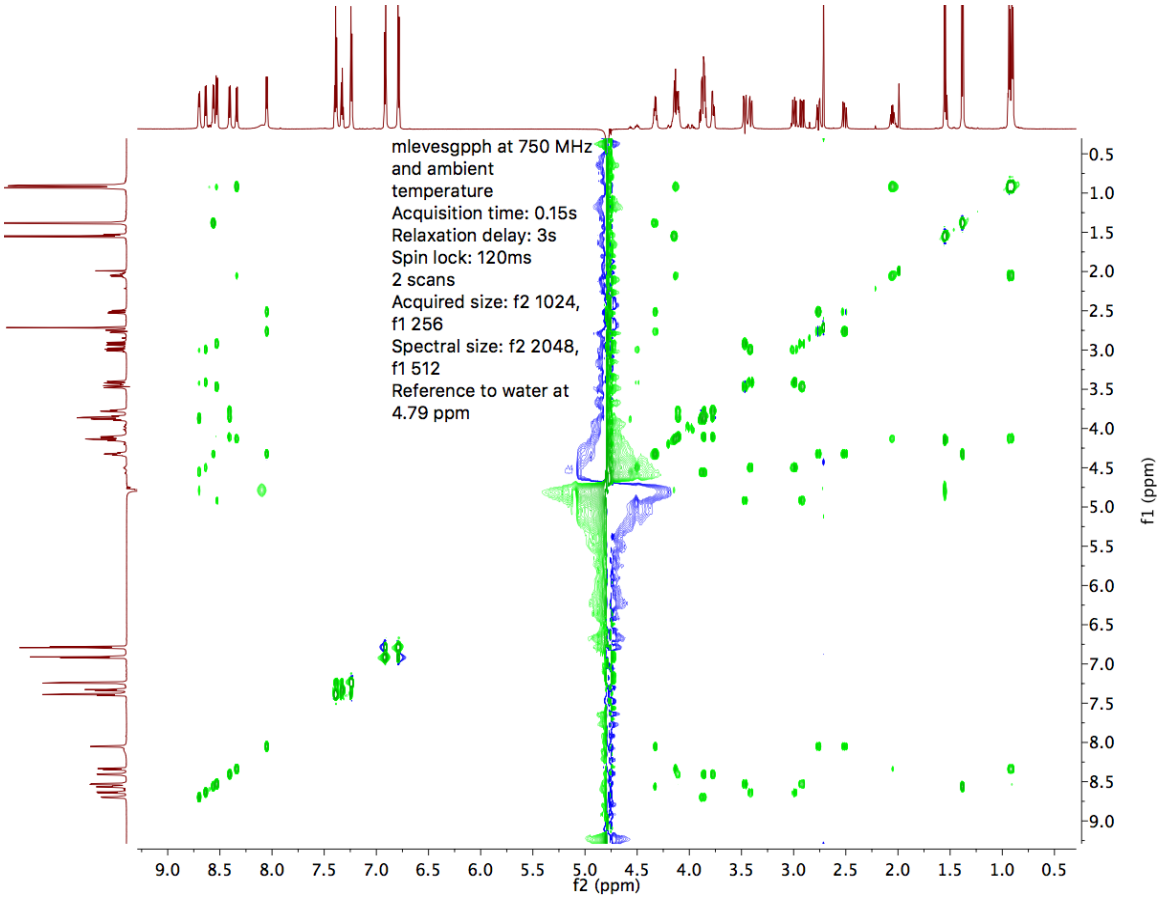
AIP-I V3A ROESY spectrum



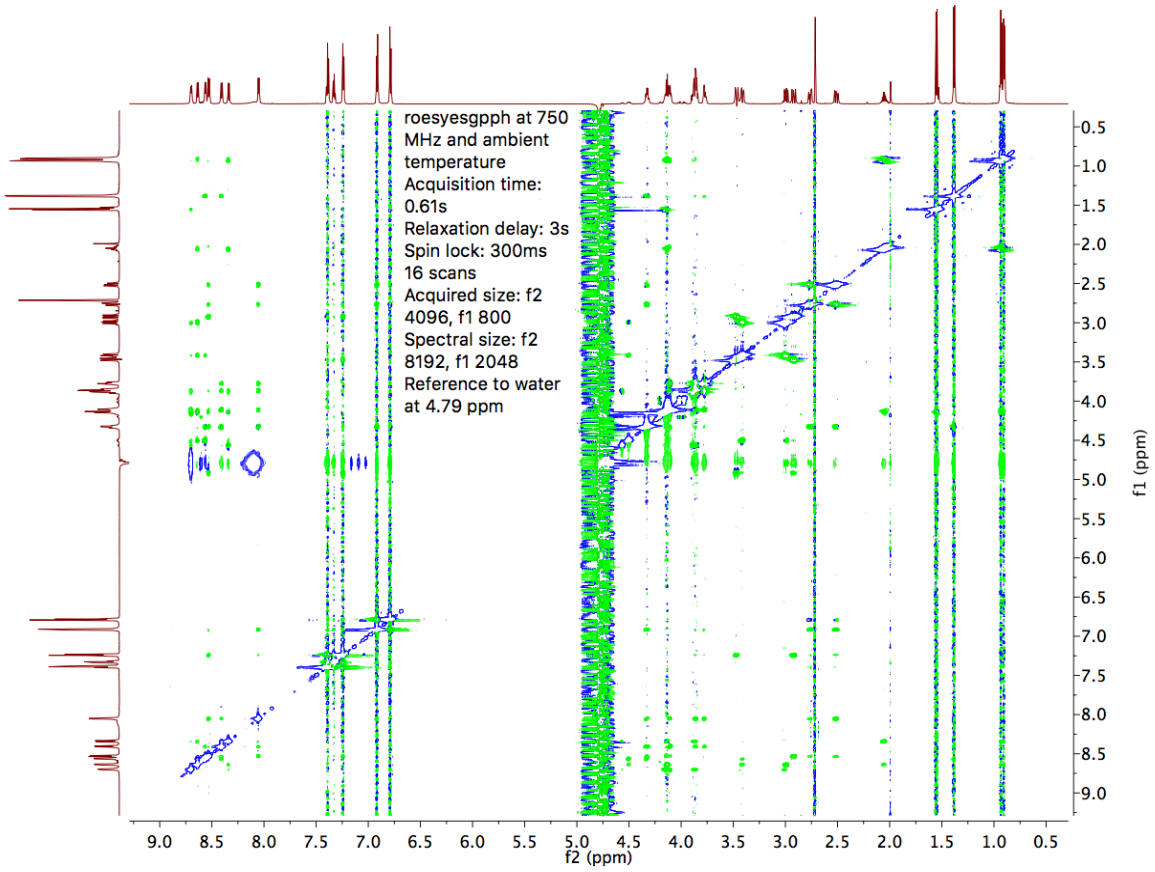
AIP-I D1A ^{1}H spectrum



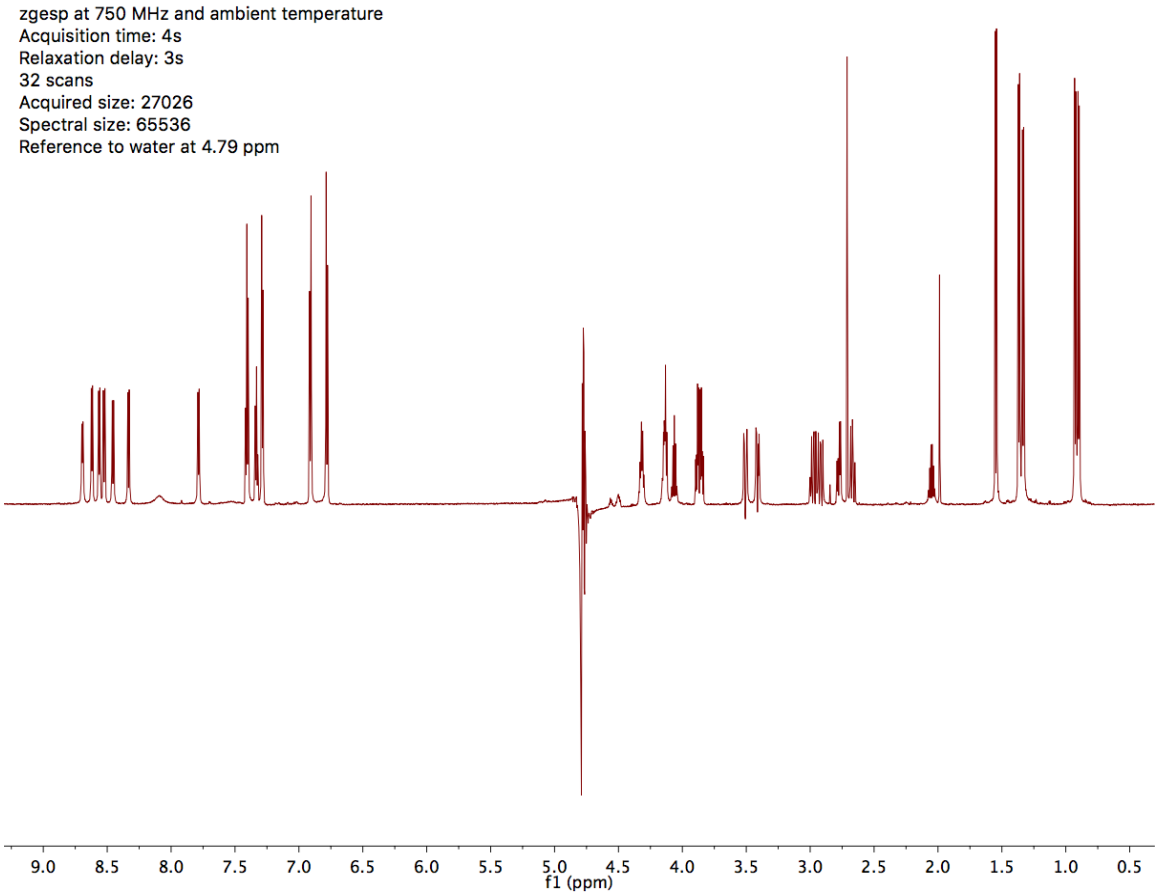
AIP-I D1A TOCSY spectrum



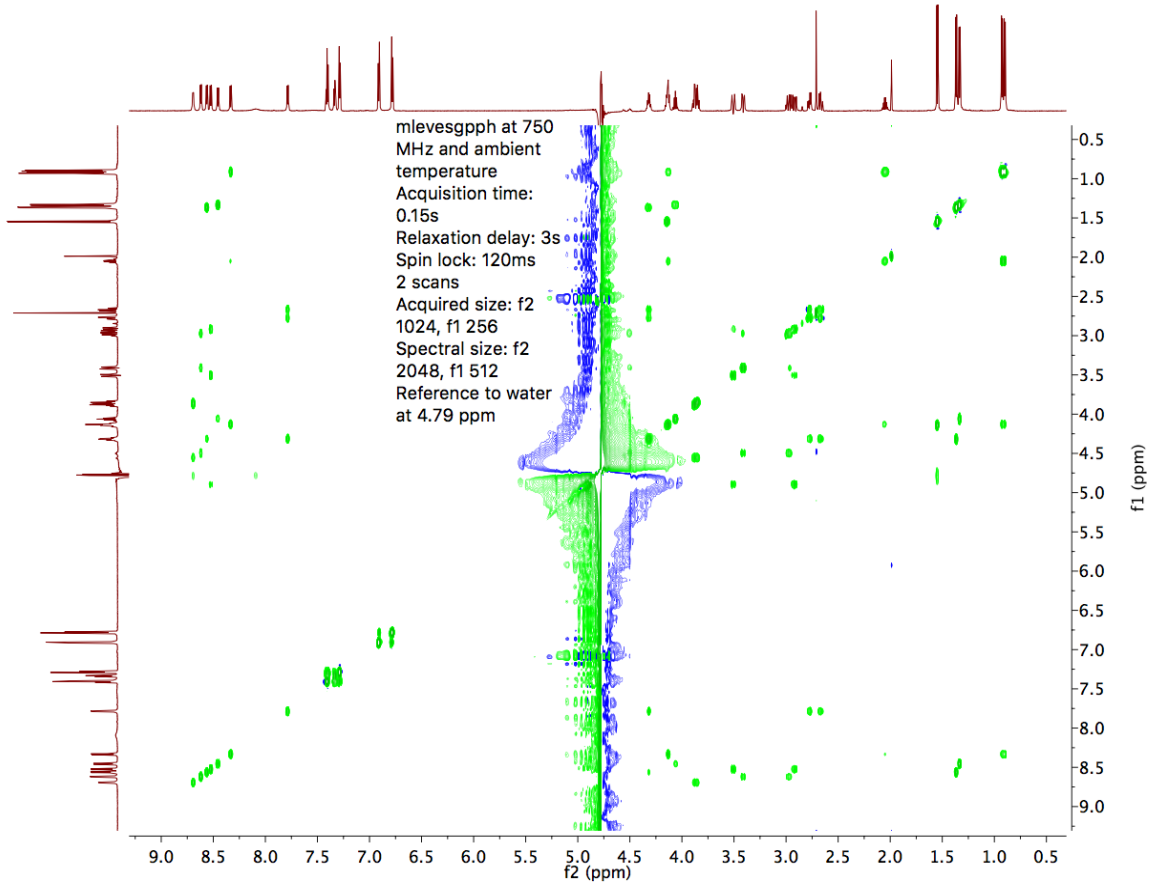
AIP-I D1A ROESY spectrum



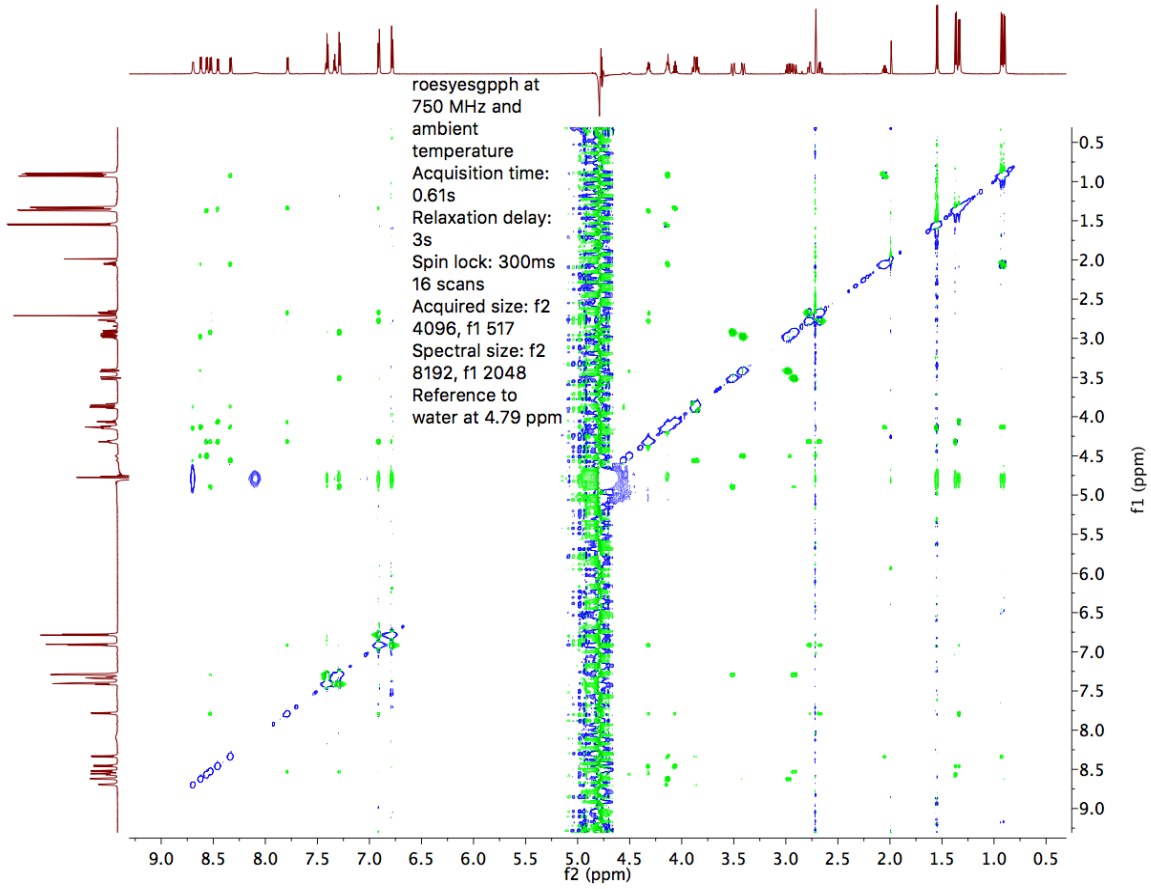
AIP-I D1AS6A ^{1}H spectrum



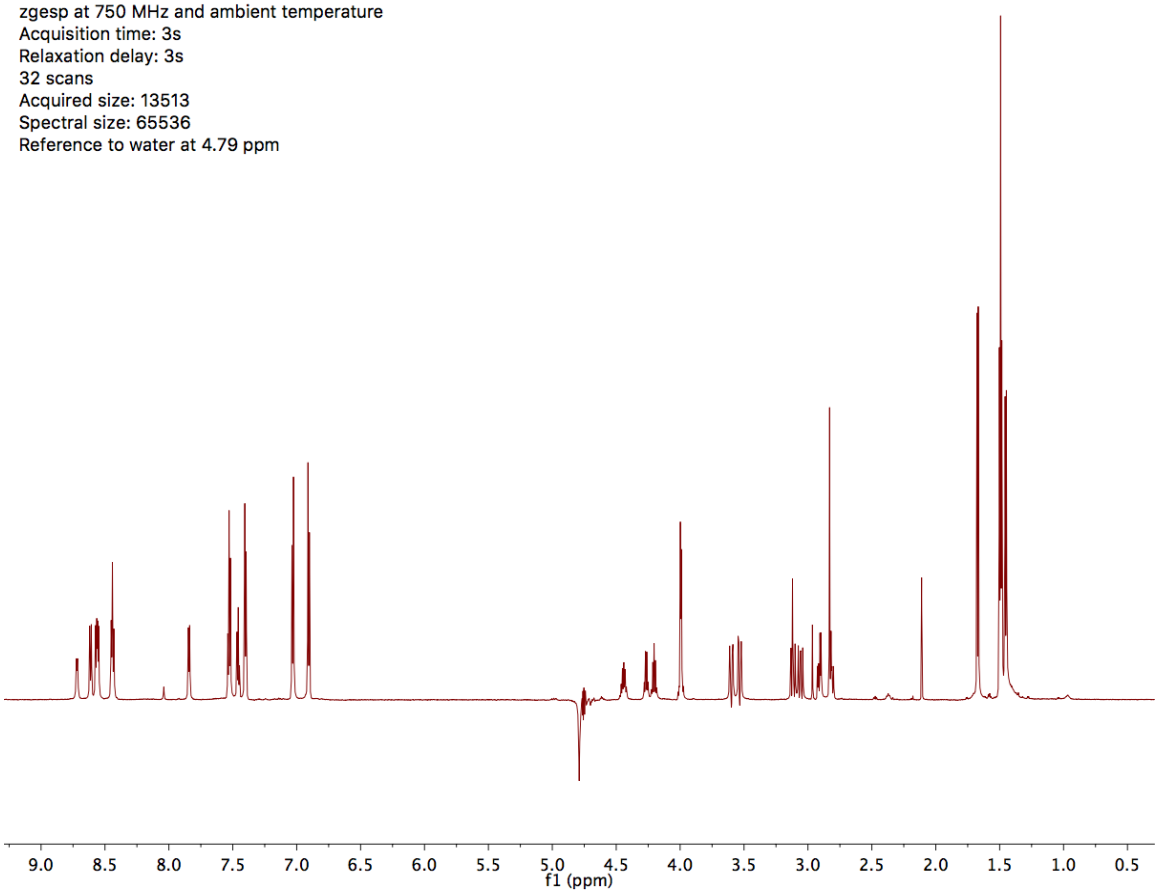
AIP-I D1AS6A TOCSY spectrum



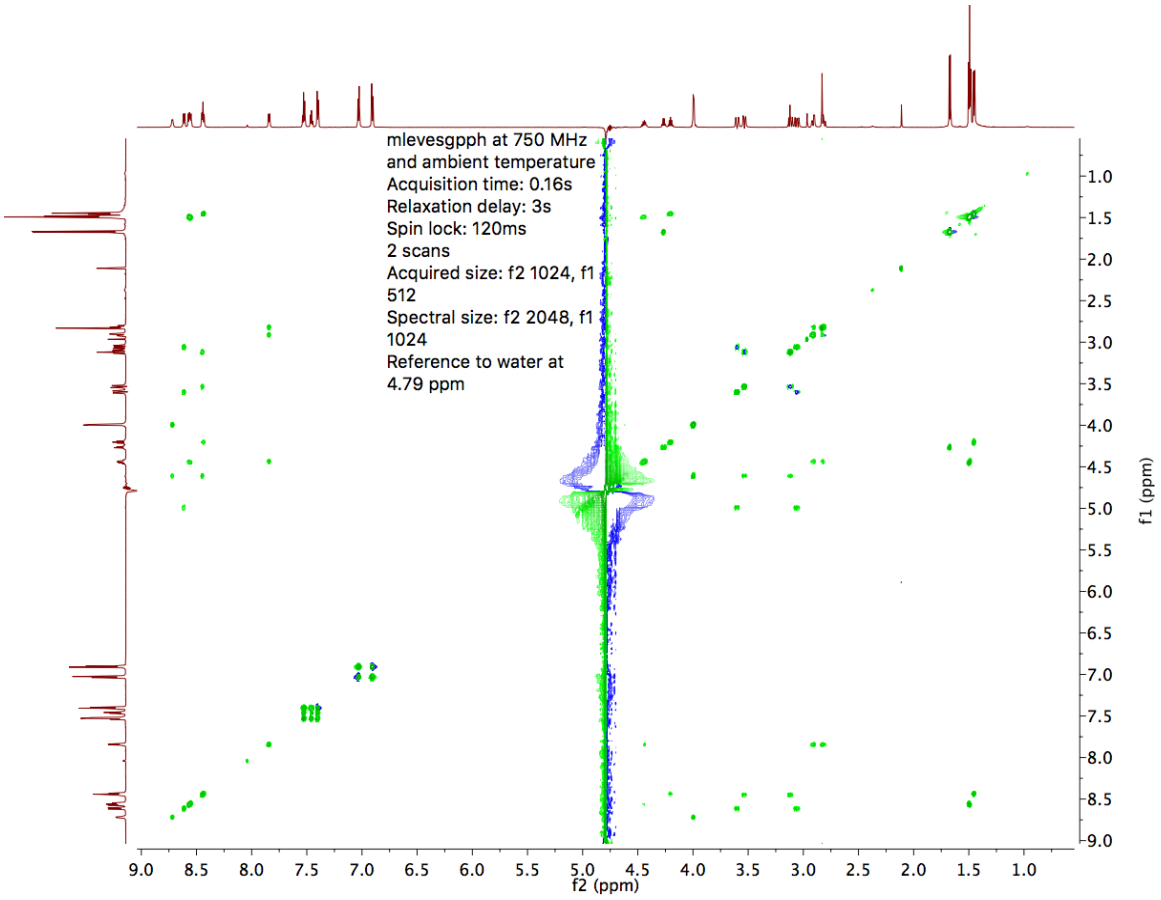
AIP-I D1AS6A ROESY spectrum



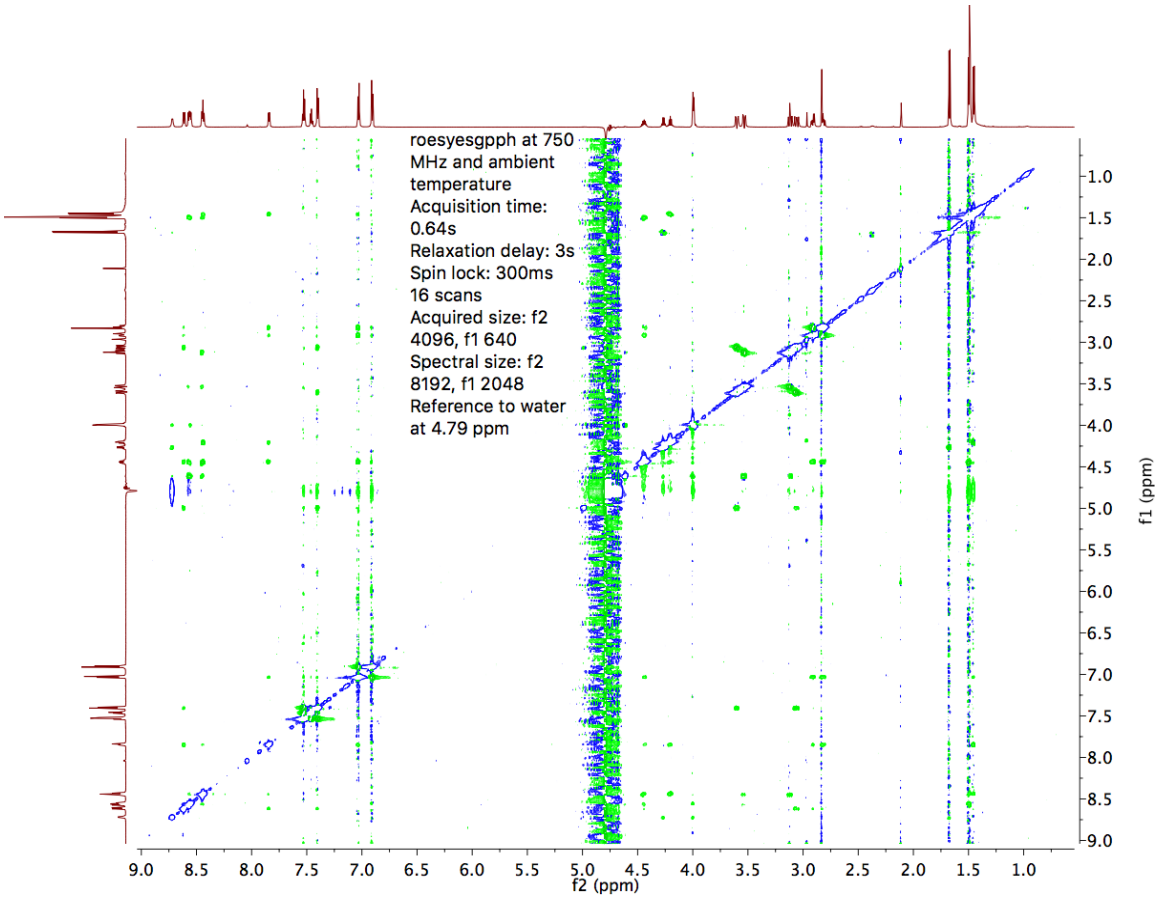
AIP-I D1AS6AV3A ^{1}H spectrum



AIP-I D1AS6AV3A TOCSY spectrum



AIP-I D1AS6AV3A ROESY spectrum



3.6.2 Chemical shift assignments

Table 3.2: Assignments for AIP-I

Residue	HN (ppm)	Hα (ppm)	Hβ (ppm)	Others (ppm)
Asp1		4.19	2.75, 2.75	
Ser2	8.57	4.42	3.76, 3.76	
Val3	8.01	4.01	1.97	Hγ 0.80, 0.82
Cys4	8.41	4.37	2.89, 3.28	
Ala5	8.35	4.21	1.28	
Ser6	8.19	4.02	3.65, 3.75	
Tyr7	7.92	4.19	2.40, 2.64	Hδ 6.82; Hε 6.68
Phe8	8.37	4.80	2.82, 3.37	Hδ 7.15; Hε 7.30; Hζ 7.23

Table 3.3: Assignments for AIP-I V3A

Residue	HN (ppm)	Hα (ppm)	Hβ (ppm)	Others (ppm)
Asp1		4.42	3.06, 3.13	
Ser2	8.79	4.50	3.91, 3.91	
Ala3	8.33	4.33	1.39	
Cys4	8.32	4.50	3.02, 3.42	
Ala5	8.58	4.33	1.40	
Ser6	8.38	4.17	3.78, 3.87	
Tyr7	8.07	4.32	2.54, 2.75	Hδ 6.91; Hε 6.79
Phe8	8.57	4.92	2.93, 3.48	Hδ 7.26; Hε 7.40; Hζ 7.33

Table 3.4: Assignments for AIP-I D1A

Residue	HN (ppm)	Hα (ppm)	Hβ (ppm)	Others (ppm)
Ala1		4.15	1.55	
Ser2	8.70	4.56	3.85, 3.89	
Val3	8.34	4.13	2.06	Hγ 0.90, 0.93
Cys4	8.64	4.50	2.99, 3.41	
Ala5	8.56	4.33	1.38	
Ser6	8.41	4.11	3.77, 3.86	
Tyr7	8.05	4.33	2.51, 2.76	Hδ 6.92; Hε 6.79
Phe8	8.53	4.91	2.92, 3.47	Hδ 7.24; Hε 7.39; Hζ 7.33

Table 3.5: Assignments for AIP-I D1AS6A

Residue	HN (ppm)	Hα (ppm)	Hβ (ppm)	Others (ppm)
Ala1		4.14	1.55	
Ser2	8.69	4.56	3.85, 3.89	
Val3	8.33	4.13	2.05	Hγ 0.90, 0.93
Cys4	8.62	4.50	2.97, 3.41	
Ala5	8.56	4.32	1.37	
Ala6	8.46	4.06	1.33	
Tyr7	7.79	4.32	2.67, 2.78	Hδ 6.91; Hε 6.78
Phe8	8.52	4.89	2.92, 3.51	Hδ 7.29; Hε 7.41; Hζ 7.33

Table 3.6: Assignments for AIP-I D1AS6AV3A

Residue	HN (ppm)	Hα (ppm)	Hβ (ppm)	Others (ppm)
Ala1		4.27	1.67	
Ser2	8.72	4.61	3.99, 4.00	
Ala3	8.55	4.45	1.50	
Cys4	8.45	4.61	3.12, 3.53	
Ala5	8.57	4.44	1.49	
Ala6	8.44	4.20	1.45	
Tyr7	7.84	4.44	2.82, 2.91	Hδ 7.03; Hε 6.91
Phe8	8.61	4.99	3.06, 3.60	Hδ 7.40; Hε 7.53; Hζ 7.46

3.6.3 Constraint summaries

Table 3.7: Number of assigned ROEs for each peptide

Peptide	Total ROEs	Intra-residue ROEs	Inter-residue ROEs		
			i – i+1	*i – i+2*	other
AIP-I	59	38	19	1	1
AIP-I V3A	73	43	29	0	1
AIP-I D1A	114	49	54	8	3
AIP-I D1AS6A	92	47	43	0	2
AIP-I D1AS6AV3A	89	43	38	3	5

3.6.4 Structure ensembles

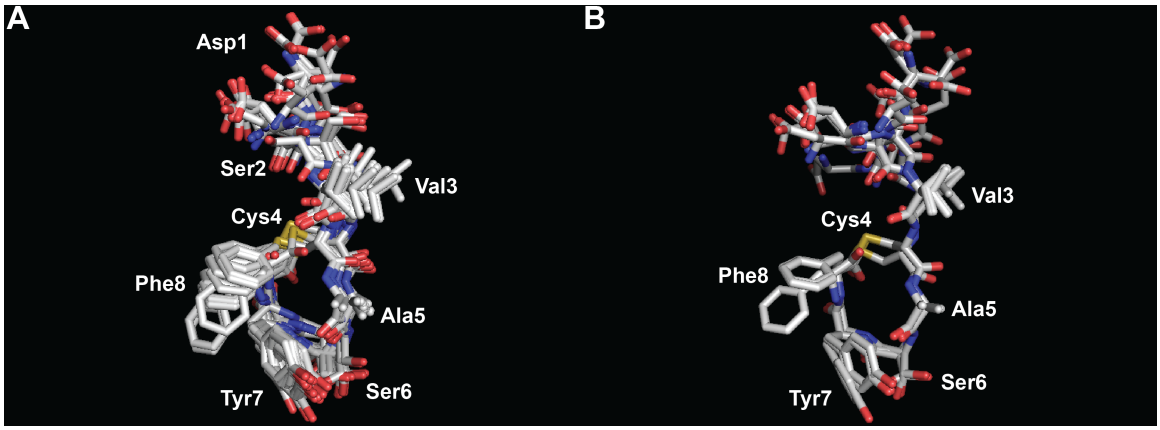


Figure 3.6 Heavy atom ensemble of the 20 lowest-energy structures for AIP-I. (A) Structures aligned to minimize RMSD for all residues. Backbone RMSD from average = 1.01Å, heavy atom RMSD from average = 1.73Å. (B) Structures aligned to minimize RMSD for only the macrocycle residues.

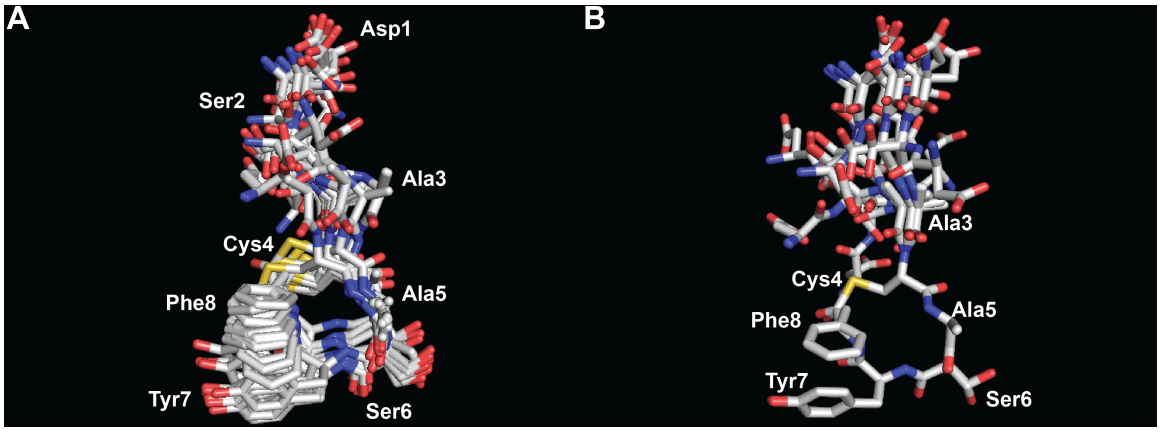


Figure 3.7 Heavy atom ensemble of the 20 lowest-energy structures for AIP-I V3A. (A) Structures aligned to minimize RMSD for all residues. Backbone RMSD from average = 1.13Å, heavy atom RMSD from average = 1.70Å. (B) Structures aligned to minimize RMSD for only the macrocycle residues.

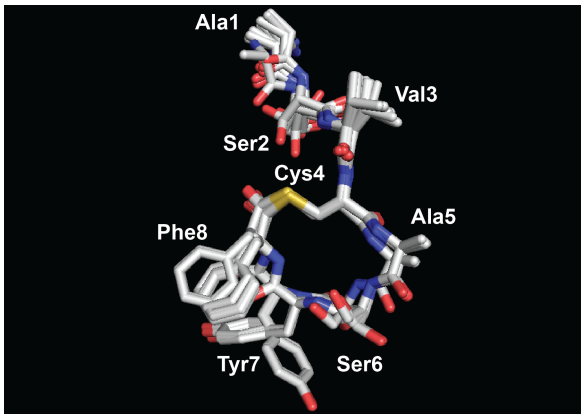


Figure 3.8 Heavy atom ensemble of the 20 lowest-energy structures for AIP-I D1A. Backbone RMSD from average = 0.29Å, heavy atom RMSD from average = 1.18Å.

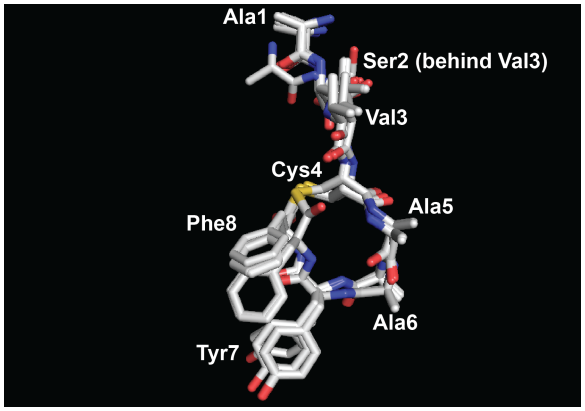


Figure 3.9 Heavy atom ensemble of the 20 lowest-energy structures for AIP-I D1AS6A. Backbone RMSD from average = 0.26Å, heavy atom RMSD from average = 0.91Å.

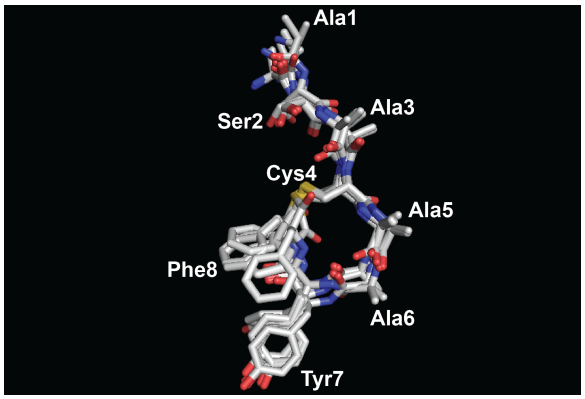


Figure 3.10 Heavy atom ensemble of the 20 lowest-energy structures for AIP-I D1AS6AV3A. Backbone RMSD from average = 0.35Å, heavy atom RMSD from average = 0.88Å.

3.7 Acknowledgements

Financial support for this work was provided by the Office of Naval Research (N00014-14-1-0791) and the Burroughs Wellcome Fund. T.Y. was supported in part by the UW – Madison NIH Biotechnology Training Program (T32 GM08349). J.K.V. was supported in part by the UW – Madison NIH Chemistry-Biology Interface Training Program (T32 GM008505 and the UW – Madison Office of the Vice Chancellor for Research and Graduate Education (with funding from the Wisconsin Alumni Research Foundation)), and a National Science Foundation (NSF) Graduate Research Fellowship (DGE-1256259). The NMR experiments were conducted at the National Magnetic Resonance Facility at Madison, which is supported by the National Institutes of Health (NIH; P41 GM103399, P41 GM66326, RR02781, and RR08438) and the NSF (DMB-8415048, OIA-9977486, and BIR-9214394). MS instrumentation at UW – Madison was supported by the NIH (1S10 OD020022-1) and NSF (CHE-9974839).

3.8 References

1. Vuong, C., and Otto, M. (2002) *Staphylococcus epidermidis* infections, *Microb. Infect. 4*, 481-489.

2. von Eiff, C., Peters, G., and Heilmann, C. (2002) Pathogenesis of infections due to coagulase-negative staphylococci, *Lancet Infect. Dis. 2*, 677-685.

3. Otto, M. (2009) *Staphylococcus epidermidis*--the 'accidental' pathogen, *Nat. Rev. Microbiol. 7*, 555-567.

4. Mack, D., Davies, A. P., Harris, L. G., Rohde, H., Horstkotte, M. A., and Knobloch, J. K. (2007) Microbial interactions in *Staphylococcus epidermidis* biofilms, *Anal. Bioanal. Chem. 387*, 399-408.

5. McCann, M. T., Gilmore, B. F., and Gorman, S. P. (2008) *Staphylococcus epidermidis* device-related infections: pathogenesis and clinical management, *J. Pharm. Pharmacol. 60*, 1551-1571.

6. Rogers, K. L., Fey, P. D., and Rupp, M. E. (2009) Coagulase-negative staphylococcal infections, *Infect. Dis. Clin. North Am. 23*, 73-98.

7. Mertens, A., and Ghebremedhin, B. (2013) Genetic determinants and biofilm formation of clinical *Staphylococcus epidermidis* isolates from blood cultures and indwelling devises, *Eur. J. Microbiol. Immunol. (Bp) 3*, 111-119.

8. Harris, L. G., Dudley, E., Rohde, H., Frommelt, L., Siemssen, N., Wilkinson, T. S., and Mack, D. (2017) Limitations in the use of PSMgamma, agr, RNAIII, and biofilm formation as biomarkers to define invasive *Staphylococcus epidermidis* from chronic biomedical device-associated infections, *Int. J. Med. Microbiol. 307*, 382-387.

9. Costerton, J. W., Stewart, P. S., and Greenberg, E. P. (1999) Bacterial biofilms: a common cause of persistent infections, *Science 284*, 1318-1322.

10. Claessens, J., Roriz, M., Merckx, R., Baatsen, P., Van Mellaert, L., and Van Eldere, J. (2015) Inefficacy of vancomycin and teicoplanin in eradicating and killing *Staphylococcus epidermidis* biofilms in vitro, *Int. J. Antimicrob. Agents 45*, 368-375.

11. Sabate Bresco, M., Harris, L. G., Thompson, K., Stanic, B., Morgenstern, M., O'Mahony, L., Richards, R. G., and Moriarty, T. F. (2017) Pathogenic Mechanisms and Host Interactions in *Staphylococcus epidermidis* Device-Related Infection, *Front. Microbiol. 8*, 1401.

12. Vuong, C., Durr, M., Carmody, A. B., Peschel, A., Klebanoff, S. J., and Otto, M. (2004) Regulated expression of pathogen-associated molecular pattern molecules in *Staphylococcus epidermidis*: quorum-sensing determines pro-inflammatory capacity and production of phenol-soluble modulins, *Cell. Microbiol. 6*, 753-759.

13. Kong, K. F., Vuong, C., and Otto, M. (2006) Staphylococcus quorum sensing in biofilm formation and infection, *Int. J. Med. Microbiol. 296*, 133-139.

14. Yao, Y., Vuong, C., Kocianova, S., Villaruz, A. E., Lai, Y., Sturdevant, D. E., and Otto, M. (2006) Characterization of the *Staphylococcus epidermidis* accessory-gene regulator response: quorum-sensing regulation of resistance to human innate host defense, *J. Infect. Dis. 193*, 841-848.

15. Wang, C., Li, M., Dong, D., Wang, J., Ren, J., Otto, M., and Gao, Q. (2007) Role of ClpP in biofilm formation and virulence of *Staphylococcus epidermidis*, *Microb. Infect. 9*, 1376-1383.

16. Cheung, G. Y., Joo, H. S., Chatterjee, S. S., and Otto, M. (2014) Phenol-soluble modulins - critical determinants of staphylococcal virulence, *FEMS Microbiol. Rev. 38*, 698-719.

17. Otto, M. (2014) Phenol-soluble modulins, *Int. J. Med. Microbiol. 304*, 164-169.

18. Camilli, A., and Bassler, B. L. (2006) Bacterial small-molecule signaling pathways, *Science 311*, 1113-1116.

19. Rutherford, S. T., and Bassler, B. L. (2012) Bacterial quorum sensing: its role in virulence and possibilities for its control, *Cold Spring Harb. Perspect. Med. 2*.

20. Lyon, G. J., and Novick, R. P. (2004) Peptide signaling in *Staphylococcus aureus* and other Gram-positive bacteria, *Peptides 25*, 1389-1403.

21. George, E. A., and Muir, T. W. (2007) Molecular mechanisms of agr quorum sensing in virulent staphylococci, *ChemBioChem 8*, 847-855.

22. Novick, R. P., and Geisinger, E. (2008) Quorum sensing in staphylococci, *Annu. Rev. Genet. 42*, 541-564.

23. Thoendel, M., Kavanaugh, J. S., Flack, C. E., and Horswill, A. R. (2011) Peptide signaling in the staphylococci, *Chem. Rev. 111*, 117-151.

24. Otto, M. (2004) Virulence factors of the coagulase-negative staphylococci, *Front. Biosci. 9*, 841-863.

25. Wang, R., Khan, B. A., Cheung, G. Y., Bach, T. H., Jameson-Lee, M., Kong, K. F., Queck, S. Y., and Otto, M. (2011) *Staphylococcus epidermidis* surfactant peptides promote biofilm maturation and dissemination of biofilm-associated infection in mice, *J. Clin. Invest. 121*, 238-248.

26. Otto, M. (2013) Staphylococcal infections: mechanisms of biofilm maturation and detachment as critical determinants of pathogenicity, *Annu. Rev. Med. 64*, 175-188.

27. Le, K. Y., Dastgheyb, S., Ho, T. V., and Otto, M. (2014) Molecular determinants of staphylococcal biofilm dispersal and structuring, *Front. Cell. Infect. Microbiol. 4*, 167.

28. Cheung, G. Y., Rigby, K., Wang, R., Queck, S. Y., Braughton, K. R., Whitney, A. R., Teintze, M., DeLeo, F. R., and Otto, M. (2010) *Staphylococcus epidermidis* strategies to avoid killing by human neutrophils, *PLoS Pathog. 6*, e1001133.

29. Boles, B. R., and Horswill, A. R. (2008) Agr-mediated dispersal of *Staphylococcus aureus biofilms*, *PLoS Pathog. 4*, e1000052.

30. Olson, M. E., Todd, D. A., Schaeffer, C. R., Paharik, A. E., Van Dyke, M. J., Buttner, H., Dunman, P. M., Rohde, H., Cech, N. B., Fey, P. D., and Horswill, A. R. (2014) *Staphylococcus epidermidis* agr quorum-sensing system: signal identification, cross talk, and importance in colonization, *J. Bacteriol. 196*, 3482-3493.

31. Qin, L., Da, F., Fisher, E. L., Tan, D. C., Nguyen, T. H., Fu, C. L., Tan, V. Y., McCausland, J. W., Sturdevant, D. E., Joo, H. S., Queck, S. Y., Cheung, G. Y., and Otto, M. (2017) Toxin Mediates Sepsis Caused by Methicillin-Resistant *Staphylococcus epidermidis*, *PLoS Pathog. 13*, e1006153.

32. Le, K. Y., and Otto, M. (2015) Quorum-sensing regulation in staphylococci-an overview, *Front. Microbiol*. *6*, 1174.

33. Mayville, P., Ji, G., Beavis, R., Yang, H., Goger, M., Novick, R. P., and Muir, T. W. (1999) Structure-activity analysis of synthetic autoinducing thiolactone peptides from *Staphylococcus aureus* responsible for virulence, *Proc. Natl. Acad. Sci. USA 96*, 1218-1223.

34. Lyon, G. J., Mayville, P., Muir, T. W., and Novick, R. P. (2000) Rational design of a global inhibitor of the virulence response in *Staphylococcus aureus*, based in part on localization of the site of inhibition to the receptor-histidine kinase, AgrC, *Proc. Natl. Acad. Sci. USA 97*, 13330-13335.

35. P, M., Affas, Z., Reynolds, C., Holden, M. T., Wood, S. J., Saint, S., Cockayne, A., Hill, P. J., Dodd, C. E., Bycroft, B. W., Chan, W. C., and Williams, P. (2001) Structure, activity and evolution of the group I thiolactone peptide quorum-sensing system of *Staphylococcus aureus*, *Mol. Microbiol. 41*, 503-512.

36. Lyon, G. J., Wright, J. S., Muir, T. W., and Novick, R. P. (2002) Key determinants of receptor activation in the agr autoinducing peptides of *Staphylococcus aureus*, *Biochemistry 41*, 10095-10104.

37. Scott, R. J., Lian, L. Y., Muharram, S. H., Cockayne, A., Wood, S. J., Bycroft, B. W., Williams, P., and Chan, W. C. (2003) Side-chain-to-tail thiolactone peptide inhibitors of the staphylococcal quorum-sensing system, *Bioorg. Med. Chem. Lett. 13*, 2449-2453.

38. Fowler, S. A., Stacy, D. M., and Blackwell, H. E. (2008) Design and synthesis of macrocyclic peptomers as mimics of a quorum sensing signal from *Staphylococcus aureus*, *Org. Lett. 10*, 2329-2332.

39. George, E. A., Novick, R. P., and Muir, T. W. (2008) Cyclic peptide inhibitors of staphylococcal virulence prepared by Fmoc-based thiolactone peptide synthesis, *J. Am. Chem. Soc. 130*, 4914-4924.

40. Tal-Gan, Y., Stacy, D. M., Foegen, M. K., Koenig, D. W., and Blackwell, H. E. (2013) Highly potent inhibitors of quorum sensing in *Staphylococcus aureus* revealed through a systematic synthetic study of the group-III autoinducing peptide, *J. Am. Chem. Soc. 135*, 7869-7882.

41. Tal-Gan, Y., Stacy, D. M., and Blackwell, H. E. (2014) N-Methyl and peptoid scans of an autoinducing peptide reveal new structural features required for inhibition and activation of AgrC quorum sensing receptors in *Staphylococcus aureus*, *Chem. Commun. (Camb.) 50*, 3000-3003.

42. Johnson, J. G., Wang, B., Debelouchina, G. T., Novick, R. P., and Muir, T. W. (2015) Increasing AIP Macrocycle Size Reveals Key Features of agr Activation in *Staphylococcus aureus*, *ChemBioChem 16*, 1093-1100.

43. Vasquez, J. K., Tal-Gan, Y., Cornilescu, G., Tyler, K. A., and Blackwell, H. E. (2017) Simplified AIP-II Peptidomimetics Are Potent Inhibitors of *Staphylococcus aureus* AgrC Quorum Sensing Receptors, *ChemBioChem 18*, 413-423.

44. Kirchdoerfer, R. N., Garner, A. L., Flack, C. E., Mee, J. M., Horswill, A. R., Janda, K. D., Kaufmann, G. F., and Wilson, I. A. (2011) Structural basis for ligand recognition and discrimination of a quorum-quenching antibody, *J. Biol. Chem. 286*, 17351-17358.

45. Nielsen, A., Mansson, M., Bojer, M. S., Gram, L., Larsen, T. O., Novick, R. P., Frees, D., Frokiaer, H., and Ingmer, H. (2014) Solonamide B inhibits quorum sensing and reduces *Staphylococcus aureus* mediated killing of human neutrophils, *PLoS One 9*, e84992.

46. Sully, E. K., Malachowa, N., Elmore, B. O., Alexander, S. M., Femling, J. K., Gray, B. M., DeLeo, F. R., Otto, M., Cheung, A. L., Edwards, B. S., Sklar, L. A., Horswill, A. R., Hall, P. R., and Gresham, H. D. (2014) Selective chemical inhibition of agr quorum sensing in *Staphylococcus aureus* promotes host defense with minimal impact on resistance, *PLoS Pathog. 10*, e1004174.

47. Tal-Gan, Y., Ivancic, M., Cornilescu, G., Yang, T., and Blackwell, H. E. (2016) Highly Stable, Amide-Bridged Autoinducing Peptide Analogues that Strongly Inhibit the AgrC Quorum Sensing Receptor in *Staphylococcus aureus*, *Angew. Chem. Int. Ed. Engl. 55*, 8913-8917.

48. Yang, T., Tal-Gan, Y., Paharik, A. E., Horswill, A. R., and Blackwell, H. E. (2016) Structure-Function Analyses of a *Staphylococcus epidermidis* Autoinducing Peptide Reveals Motifs Critical for AgrC-type Receptor Modulation, *ACS Chem. Biol. 11*, 1982-1991.

49. Tal-Gan, Y., Ivancic, M., Cornilescu, G., and Blackwell, H. E. (2016) Characterization of structural elements in native autoinducing peptides and non-native analogues that permit the differential modulation of AgrC-type quorum sensing receptors in S*taphylococcus aureus*, *Org. Biomol. Chem. 14*, 113-121.

50. Tal-Gan, Y., Ivancic, M., Cornilescu, G., Cornilescu, C. C., and Blackwell, H. E. (2013) Structural characterization of native autoinducing peptides and abiotic analogues reveals key features essential for activation and inhibition of an AgrC quorum sensing receptor in *Staphylococcus aureus*, *J. Am. Chem. Soc. 135*, 18436-18444.

51. Khan, B. A., Yeh, A. J., Cheung, G. Y., and Otto, M. (2015) Investigational therapies targeting quorum-sensing for the treatment of *Staphylococcus aureus* infections, *Expert Opin. Investig. Drugs 24*, 689-704.

52. Carmody, A. B., and Otto, M. (2004) Specificity grouping of the accessory gene regulator quorum-sensing system of *Staphylococcus epidermidis* is linked to infection, *Arch. Microbiol. 181*, 250-253.

CHAPTER 4:

Development of Synthetic Pan-Group Agonists of the Quorum Sensing Receptor AgrC in *Staphylococcus epidermidis*

Contribution: T. Yang designed the experiments, performed the fluorescence reporter assays, and prepared the manuscript. K. H. J. West assisted with peptide synthesis, reporter assays, and writing. W. Shen carried out peptide synthesis. S. R. Ruderman assisted with peptide synthesis. H. E. Blackwell guided the project and assited with manuscript preparation.

*This chapter is being prepared as a manuscript intended for publication under the same title.

4.1 Abstract

Staphylococcus epidermidis is a common nosocomial pathogen, particularly in device-associated infections, due to its ability to form robust biofilms. The accessory gene regulator (*agr*) quorum sensing (QS) system plays an important role in the pathogenesis of *S. epidermidis*, and the intentional activation of the *agr* system using exogenous autoinducing peptide (AIP), the signal molecule for the system, has been shown to reduce biofilm accumulation. To date, three different AIPs (AIP-I–III) have been identified in *S. epidermidis*, resulting in the categorization of three *agr* specificity groups, and these AIPs can exhibit cross-group inhibitory activities. The development of synthetic agonists capable of activating the receptors from all three *agr* groups would allow for the study of *agr* activation as a strategy to promote *S. epidermidis* biofilm dispersion. Such pan-group agonists are yet to be identified, in part due to the lack of information on structure-activity relationships (SARs) for the native AIPs, AIP-II and AIP-III. Herein, we report the first systematic SAR characterization of *S. epidermidis* AIP-II and AIP-III, and the application of these new SAR data and those reported for AIP-I for the identification of a first set of pan-group agonists for the *agr* systems in *S. epidermidis*. These AIP analogs, along with additional SARs uncovered in our study, provide scaffolds for additional structural characterization and further optimization to yield more efficacious pan-group agonists. These pan-group agonists represent new tools for assessing the impact of targeting QS in limiting *S. epidermidis* infectivity.

4.2 Introduction

Bacteria can monitor their local population density and coordinate their collective behaviors using a chemical-based intercellular communication process called quorum sensing (QS) *(1-3)*. For many pathogens, these behaviors include the formation of surface-attached colonies called biofilms and the production of virulence factors *(4-7)*. Consequently, QS is an attractive target for the development of non-antibiotic, or "anti-virulence", approaches to limit the infectivity of pathogens *(3, 8, 9)*. One such pathogen is the gram-positive bacterium *Staphylococcus epidermidis*, a member of the human microbiota that normally colonizes the skin and the mucosal tissues *(10)*. Recently, *S. epidermidis* has been identified to be a leading causative agent in nosocomial device-associated infections, in part due to its ability to form robust biofilm on abiotic surfaces *(11-15)*. The barrier provided by the biofilm, combined with the emergence of antibiotic resistances, makes *S. epidermidis* infection difficult to treat by traditional antimicrobials and, thereby, a public health burden *(10, 11, 14, 16-20)*. Anti-virulence approaches to control *S. epidermidis* infection and biofilm growth could address these treatment challenges.

The primary QS circuit in *S. epidermidis* is the accessory gene (*agr*) regulator system (Figure 4.1A) *(21-23)*. The *agr* system consists of four components named AgrA-D and is regulated by a signaling molecule called the autoinducing peptide (or AIP) *(21-25)*. The primary structure for the AIP is contained in the propeptide AgrD, which is processed and secreted into the extracellular milieu as the mature signal by AgrB *(26, 27)*. Once a threshold local concentration is reached, the AIP signal can bind effectively to its cognate receptor AgrC, a transmembrane histidine kinase *(28)*. AgrC then activates the response regulator AgrA through phosphorelay, and the phosphorylated AgrA upregulates gene expression from the P2 and P3 promoters *(29)*. The P2 promoter induces the expression of the entire *agr* operon, thus forming an auto-induction circuit typical of a QS system *(30)*, whereas the P3 promoter drives the expression of RNAIII, the main effector molecule of the *agr* system that modulates downstream

gene expression *(31)*. Phosphorylated AgrA also directly upregulates the expression of a group of small amphipathic peptides known as phenol-soluble modulins (PSMs), which, along with RNAIII, play important roles in the biofilm life cycle and virulence of *S. epidermidis (32-34)*.

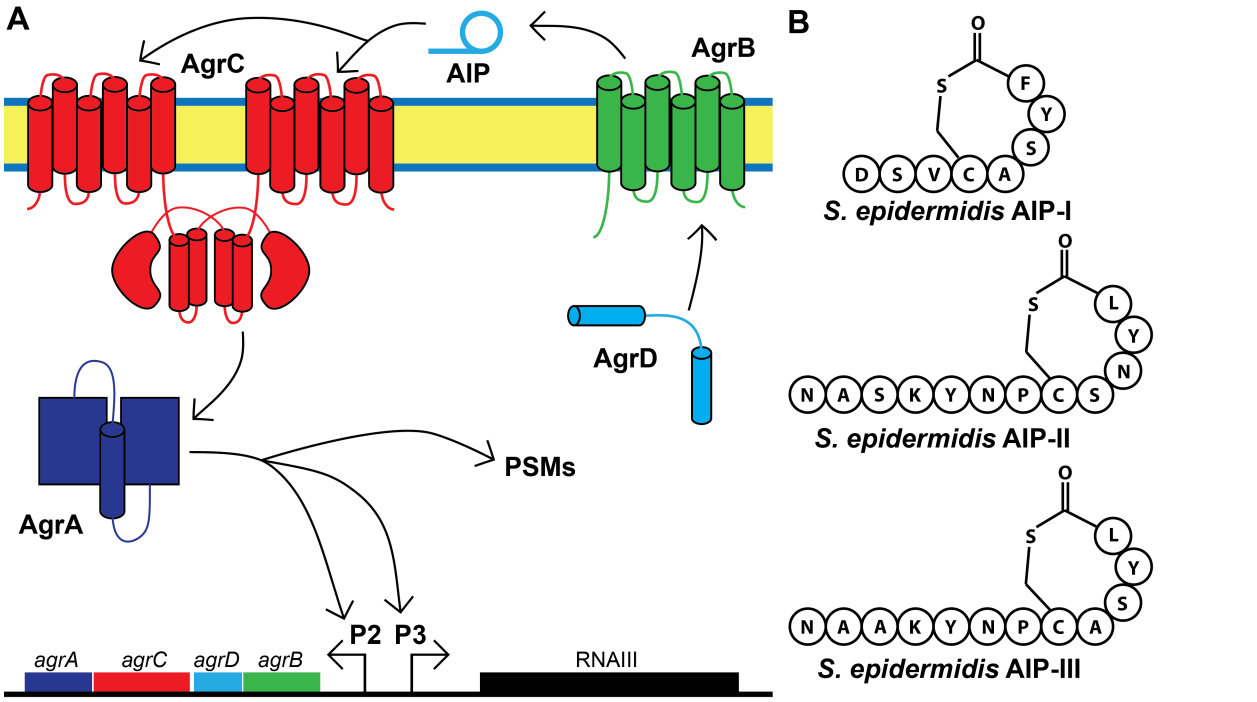


Figure 4.1: The *agr* system and the associated AIP signals of *S. epidermidis*. (A) Simplified diagram of the *agr* system. AgrD, which contains the sequence for the mature signal, is processed and secreted by AgrB to yield the autoinducing peptide signal (or AIP). Upon reaching a threshold extracellular concentration, AIP can effectively bind the dimer of the transmembrane receptor AgrC. The AIP-bound AgrC dimer activates AgrA through phosphorelay, and phosphorelated AgrA then drives gene expression from the P2, P3, and psm promoters. P2 encodes the entire *agr* system, while P3 turns on the expression of RNAIII, the main effector molecule of the *agr* system. (B) The primary structures of the known AIPs (AIP-I–III) belonging to the three *agr* specificity groups (Groups I–III) of *S. epidermidis*.

A number of studies investigating the impact of the *agr* system on *S. epidermidis* pathogenesis have shown that activation of the *agr* system is important for optimal skin colonization *(35)*, protection against the defense mechanisms of the innate immune system *(4, 36)*, and bacterial dissemination and tissue infiltration *(36-39)*. Consequently, inhibition of the *agr* system could attenuate virulence and limit infectivity *(25, 35, 37, 40)*. However, the established roles of the *agr* system in *S. epidermidis* biofilm formation *(4, 41, 42)*, the primary

mechanism by which *S. epidermidis* causes device-associated infection *(10, 19, 34)*, suggests that intentional *activation* of the *agr* system actually may be more beneficial. Specifically, in strains that form polysaccharide intercellular adhesin dependent biofilm, the *agr* system suppresses the expression of surface-attached AtlE protein *(43)*, an important adhesion factor for initial attachment. Furthermore, PSMs and proteases are found to facilitate bacterial detachment from biofilm, and both are upregulated by the *agr* system *(32, 37, 39)*. Artificial activation of the *agr* system, therefore, could limit *S. epidermidis* infection by reducing biofilm growth on surfaces and rendering the dispersed bacteria more susceptible to antimicrobials *(13, 44)*. Indeed, previous studies with *S. epidermidis* and the closely related human pathogen, *Staphylococcus aureus*, have demonstrated the reduction of biofilm accumulation via the activation of the *agr* system by both native and non-native agonists *(45, 46)*.

While the artificial activation of the *agr* system could be readily achieved by the administration of the native peptide signal, the broad application of this approach to reduce biofilm accumulation of *S. epidermidis* is complicated by the presence of three *agr* specificity groups of *S. epidermidis* (Group I–III), where each group is defined by the unique sequence of its AIP (Figure 4.1B) *(35, 47)*. Driving the complexity is that the different AIPs (AIP-I–III) exhibit cross-group inhibitory behaviors, such that AIP-I significantly inhibits the *agr* systems in Group II and Group III, while AIP-II and AIP-III are strong inhibitors of the *agr* system in Group I *(35)*. As a result, applying the native agonist to reduce biofilm accumulation requires the identification of the *agr* specificity group of the target *S. epidermidis* strain and is only effective against one specificity group at a time *(7)*. Biofilm formed by an unidentified strain or mixed groups would thus render the strategy ineffective.

This challenge could be overcome with an agonist, or a cocktail of agonists, capable of targeting all three groups of *S. epidermidis* without any inhibitory activities *(7)*. However, to date, no such pan-group agonist has been identified. We recently reported the first systematic structure-activity relationship (SAR) study of the *S. epidermidis* AIP-I, and although we identified

non-native agonists with enhanced potency against AgrC-I as well as potent pan-group antagonists targeting all three AgrC receptors, we did not uncover any AIP analogs with agonistic activities in all three groups *(46)*. Similar SAR studies in *S. aureus* have also yielded non-native pan-group antagonists against all *S. aureus agr* specificity groups but no pan-group agonists *(48-58)*. Interestingly, one analog of a *S. aureus* native AIP has been reported to activate the AgrC receptor from a different *S. aureus agr* group, despite the parent AIP being an inhibitor of that receptor *(51)*. This finding suggests that a cross-group inhibitor can be converted into an activator. In addition, our NMR structural study of *S. epidermidis* AIP-I and its analogs (as reported in Chapter 3) suggests that the structural motif for AgrC-I activation is highly modular and could be introduced into a different AIP scaffold to turn that AIP scaffold into an agonist against AgrC-I. Lastly, *S. epidermidis* AIP-II and AIP-III are very similar in sequence, and they do not exhibit cross-group inhibition against each other *(35)*. Taken together, we hypothesize that a pan-group agonist, or a cocktail of agonists without cross-group inhibitory activities, could be designed for the *agr* systems in *S. epidermidis* by combining chemical features important for receptor activation for each native AIP. However, such features have only been identified for AIP-I *(46)*, little is known about the SARs of signal:receptor interactions for AIP-II and AIP-III.

Herein, we report the first systematic SAR characterization of *S. epidermidis* AIP-II and AIP-III, and the application of these new SAR data and those reported for AIP-I for the identification of a first set of pan-group agonists for the *agr* systems in *S. epidermidis*. These pan-group agonists represent powerful new tools to assess the effectiveness of targeting the *agr* system for biofilm dispersion, and they serve as exciting new scaffolds for additional structural studies and probe design to improve our understanding of receptor activation of the *agr* system in *S. epidermidis*.

4.3 Results and Discussion

4.3.1 Preliminary SARs of AIP-II and AIP-III.

In order to identify the chemical features important for activation of AgrC-II and AgrC-III of *S. epidermidis*, we characterized the SARs for AIP-II and AIP-III by systematically replacing each amino acid with either alanine or the corresponding D-amino acid to explore the roles of the side chains and the stereocenters in the signal:receptor interaction (note, Cys8 was not mutated to Ala due to its essentiality for forming the macrocycle, and the Ala residues that are part of the native sequence did not need alanine substitutions). In addition, a series of analogs removing residues from the exocyclic tail of the native AIPs were designed to understand the impact of exocyclic tail length on the signal:receptor interaction. The set of AIP-II and AIP-III analogs (listed in Tables 4.1 and 4.2) were synthesized using solid-phase peptide chemistry and purified by HPLC using modified procedures based on our established protocols (see Methods section for details) *(46, 58, 59)*.

Each analog was then tested for its effect on the cognate AgrC receptors using wild-type *S. epidermidis* Group II and III fluorescence reporter strains (see Methods), which contain a reporter plasmid encoding a *gfp* gene under the control of the P3 promoter *(35)*. Under high cell-density conditions, these strains generate sufficient amount of native AIPs to activate the *agr* system, which upregulates the expression from the P3 promoter and leads to the production of GFP. Therefore, the level of GFP fluorescence correlates with the extent of AgrC activation, and a decrease in GFP fluorescence indicates receptor antagonism. To observe receptor agonism, we used a known inhibitor of AgrC-II and AgrC-III to block receptor activation by the endogenously produced AIPs and measured the extent by which AIP-II and AIP-III analogs can outcompete the inhibitor and turn on the *agr* system *(46)*. We also evaluated the activities of the native *S. epidermidis* AIPs (AIP-I–III) as a control for the fluorescence reporter assay, as their effects on AgrC-II and AgrC-III have been described previously *(35)*. The results of the fluorescence reporter assay are summarized in Tables 4.1 and 4.2. Compound potency, as measured by the IC_{50} and EC_{50} values derived from dose-response analyses, is only reported

for Group III due to the inconsistencies associated with the Group II reporter strain. Specifically, the parent strain (*S. epidermidis* 1457) for the Group II reporter strain is a prolific biofilm forming strain. Since biofilm formation is typically associated with lower *agr* activity, the reporter strain is inconsistent in the activation of its *agr* system for reliable fluorescence readout. Nevertheless, the overall activity, or efficacy, profiles of the peptides assayed with the Group II reporter strain are reproducible, which allowed us to identify the AIP side chains and stereocenters important for AgrC-II binding and activation.

Table 4.1: Activities for the alanine and D-amino acid scan analogs of *S. epidermidis* AIP-II against AgrC-II as determined using a fluorescence reporter strain.[a,b]

Peptide Name	Sequence	Receptor Activity
AIP-II N1A	A-A-S-K-Y-N-P-(C-S-N-Y-L)	Agonist
AIP-II S3A	N-A-A-K-Y-N-P-(C-S-N-Y-L)	Agonist
AIP-II K4A	N-A-S-A-Y-N-P-(C-S-N-Y-L)	Agonist
AIP-II Y5A	N-A-S-K-A-N-P-(C-S-N-Y-L)	Antagonist
AIP-II N6A	N-A-S-K-Y-A-P-(C-S-N-Y-L)	Antagonist
AIP-II P7A	N-A-S-K-Y-N-A-(C-S-N-Y-L)	Antagonist
AIP-II S9A	N-A-S-K-Y-N-P-(C-A-N-Y-L)	Agonist
AIP-II N10A	N-A-S-K-Y-N-P-(C-S-A-Y-L)	Agonist
AIP-II Y11A	N-A-S-K-Y-N-P-(C-S-N-A-L)	Inactive[c]
AIP-II L12A	N-A-S-K-Y-N-P-(C-S-N-Y-A)	Inactive[c]
AIP-II D-N1	DN-A-S-K-Y-N-P-(C-S-N-Y-L)	Agonist
AIP-II D-A2	N-DA-S-K-Y-N-P-(C-S-N-Y-L)	N/A[d]
AIP-II D-S3	N-A-DS-K-Y-N-P-(C-S-N-Y-L)	Agonist
AIP-II D-K4	N-A-S-DK-Y-N-P-(C-S-N-Y-L)	Agonist
AIP-II D-Y5	N-A-S-K-DY-N-P-(C-S-N-Y-L)	Antagonist
AIP-II D-N6	N-A-S-K-Y-DN-P-(C-S-N-Y-L)	Antagonist
AIP-II D-P7	N-A-S-K-Y-N-DP-(C-S-N-Y-L)	Antagonist
AIP-II D-C8	N-A-S-K-Y-N-P-(DC-S-N-Y-L)	Inactive[c]
AIP-II D-S9	N-A-S-K-Y-N-P-(C-DS-N-Y-L)	Agonist
AIP-II D-N10	N-A-S-K-Y-N-P-(C-S-DN-Y-L)	Agonist
AIP-II D-Y11	N-A-S-K-Y-N-P-(C-S-N-DY-L)	Inactive[c]
AIP-II D-L12	N-A-S-K-Y-N-P-(C-S-N-Y-DL)	Agonist
AIP-II 11aa	A-S-K-Y-N-P-(C-S-N-Y-L)	Agonist
AIP-II 10aa	S-K-Y-N-P-(C-S-N-Y-L)	Agonist
AIP-II 9aa	K-Y-N-P-(C-S-N-Y-L)	Agonist[e]
AIP-II 8aa	Y-N-P-(C-S-N-Y-L)	Antagonist[e]
AIP-I	D-S-V-(C-A-S-Y-F)	Antagonist
AIP-II	N-A-S-K-Y-N-P-(C-S-N-Y-L)	Agonist
AIP-III	N-A-A-K-Y-N-P-(C-A-S-Y-L)	Agonist

[a] See Methods for details regarding the reporter strain and assay procedures. MS and HPLC characterization data and dose-response curves are in the Supplementary Information. [b] Agonism assay performed in the presence of a known inhibitor against AgrC-II to block receptor activation by endogenously produced AIP-II. [c] Dose-response curves revealed neither agonism nor antagonism activities over the concentration range tested. [d] Compound not assayed due to challenges associated with the synthesis. [e] Activities first shown in ref. 46. Red indicates receptor inhibition; green indicates receptor activation.

Table 4.2: IC_{50} and EC_{50} values for alanine and D-amino acid scan analogs of *S. epidermidis* AIP-III against AgrC-III as determined using the fluorescence reporter strain.[a]

Peptide Name	Sequence	IC_{50} [nM]	EC_{50}[b] [nM]
AIP-III N1A	A-A-A-K-Y-N-P-(C-A-S-Y-L)	-	71.6
AIP-III K4A	N-A-A-A-Y-N-P-(C-A-S-Y-L)	-	1320
AIP-III Y5A	N-A-A-K-A-N-P-(C-A-S-Y-L)	120	-
AIP-III N6A	N-A-A-K-Y-A-P-(C-A-S-Y-L)	124	-
AIP-III P7A	N-A-A-K-Y-N-A-(C-A-S-Y-L)	157	-
AIP-III S10A	N-A-A-K-Y-N-P-(C-A-A-Y-L)	-	N.D.[c]
AIP-III Y11A	N-A-A-K-Y-N-P-(C-A-S-A-L)	Inactive[d]	
AIP-III L12A	N-A-A-K-Y-N-P-(C-A-S-Y-A)	Inactive[d]	
AIP-III D-N1	DN-A-A-K-Y-N-P-(C-A-S-Y-L)	-	74.0
AIP-III D-A2	N-DA-A-K-Y-N-P-(C-A-S-Y-L)	-	88.9
AIP-III D-A3	N-A-DA-K-Y-N-P-(C-A-S-Y-L)	-	702
AIP-III D-K4	N-A-A-DK-Y-N-P-(C-A-S-Y-L)	28.6	-
AIP-III D-Y5	N-A-A-K-DY-N-P-(C-A-S-Y-L)	49.8	-
AIP-III D-N6	N-A-A-K-Y-DN-P-(C-A-S-Y-L)	1310	-
AIP-III D-P7	N-A-A-K-Y-N-DP-(C-A-S-Y-L)	1160	-
AIP-III D-C8	N-A-A-K-Y-N-P-(DC-A-S-Y-L)	N/A[e]	
AIP-III D-A9	N-A-A-K-Y-N-P-(C-DA-S-Y-L)	Inactive[d]	
AIP-III D-S10	N-A-A-K-Y-N-P-(C-A-DS-Y-L)	-	99.5
AIP-III D-Y11	N-A-A-K-Y-N-P-(C-A-S-DY-L)	Inactive[d]	
AIP-III D-L12	N-A-A-K-Y-N-P-(C-A-S-Y-DL)	-	>2000
AIP-III 11aa	A-A-K-Y-N-P-(C-A-S-Y-L)	-	55.1
AIP-III 10aa	A-K-Y-N-P-(C-A-S-Y-L)	-	29.0
AIP-III 9aa	K-Y-N-P-(C-A-S-Y-L)	-	31.9
AIP-III 8aa	Y-N-P-(C-A-S-Y-L)	19.6	-
AIP-I	D-S-V-(C-A-S-Y-F)	2.02	-
AIP-II	N-A-S-K-Y-N-P-(C-S-N-Y-L)	-	>2000
AIP-III	N-A-A-K-Y-N-P-(C-A-S-Y-L)	-	65.7

[a] See Methods for details regarding the reporter strain and assay procedures. MS and HPLC characterization data, dose-response curves, and 95% confidence intervals (CI) for IC_{50} and EC_{50} values are available in the Supplementary Information. [b] Agonism assay performed in the presence of an inhibitor against AgrC-III (25nM AIP-I D1AS6AV3A) to block receptor activation by endogenously produced AIP-III. [c] The agonist dose-response curve showed downturn at higher concentration (see text). [d] Dose-response curves revealed neither agonism nor antagonism activities over the concentration range tested. [e] Compound not assayed due to complications with purification.

Though the activity of the native AIP-I against AgrC-II and AgrC-III was in agreement with a previous report, the activity of AIP-II towards Group III and the activity of AIP-III towards Group II differed *(35)*. Instead of showing no cross-group activities, cross-group activation was

observed, albeit only weakly so for AIP-II. This difference is most likely the result of variances in assay protocol, particularly the use of AgrC antagonists in our protocol to block the activation of the *agr* system by endogenous AIPs.

Given their structural similarities, the observed trends in SARs for AIP-II and AIP-III unsurprisingly were also quite comparable. Both AIPs require the bulky, hydrophobic residues (Tyr11 and Leu12) within the macrocycle to be present for receptor binding and activation, as replacement with alanine resulted in complete loss of activity. Residue Tyr11 in both AIPs is also intolerant to change in stereochemistry, as the substitution with the corresponding D-amino acid caused a complete loss of activity as well. On the other hand, substitution of Leu12 with the corresponding D-amino acid only reduced the potency of, but did not abolish, the agonistic activity. We note that the impact of stereochemistry at these two residues in AIP-II and AIP-III on the AIP:AgrC interaction is the same as that of the equivalent residues in AIP-I *(46)*, implying that the hydrophobic residues in all three AIPs likely adopt similar orientations. We also identified three residues (Tyr5, Asn6, and Pro7) in the exocyclic tail portion of both AIP-II and AIP-III to be important for receptor activation, as mutations to either alanine or the corresponding D-amino acid converted the resulting peptide from an agonist to an antagonist. While the potency of the AIP-II analogs was not determined, the varying efficacies of the AIP-III analogs containing D-amino acid substitutions at these three positions imply that each residue contribute differently to the interactions between AIP and the cognate AgrC receptor. Assaying additional analogs and structural studies will provide more insights into the roles of these residues. Overall, the aforementioned SAR trends for AIP-II and AIP-III are in agreement with the current model for activation of AgrC by its cognate AIP in *S. epidermidis* and *S. aureus (46, 51, 57, 60, 61)*, where the hydrophobic residues of the AIP macrocycle interact with a proposed hydrophobic patch on the AgrC receptor for signal binding while the residues on the exocyclic tail of the AIP form contacts with the receptor to induce activation.

More surprisingly, the first three residues from the N-terminus (Asn1, Ala2, and Ser3/Ala3) in both AIP-II and AIP-III were found to have little to no impact on receptor binding or activation. Most of the alanine and D-amino acid replacements at these positions had little effect on the activity of the resulting peptides when compared to the native AIPs. AIP-III D-A3 is the only analog to show a reduction in potency, but it remained as an effective agonist towards the cognate receptor AgrC-III. Moreover, AIP analogs with these three residues removed from the N-terminus (AIP-II/III 11aa, AIP-II/III 10aa, AIP-II/III 9aa) remained agonists with the same, if not better, potency against the cognate AgrC receptors, suggesting that these residues do engage in any meaningful contacts with the receptor and are likely solvent exposed. Removal of the fourth residue, Lys4, from the N-terminus of both AIPs resulted in an analog (AIP-II/III 8aa) with inhibitory activity towards the cognate receptors, indicating that this residue is required for receptor activation. However, the side chain of Lys4 appears to be non-essential for receptor activation, as the alanine substitution in both AIPs maintained the agonistic activity towards the cognate receptors, though with reduced potency compared to the native AIPs. For AIP-II, a similar effect was also observed for the D-amino acid substitution at Lys4, while for AIP-III, D-amino acid substitution at Lys4 resulted in an antagonist, implying that the role of Lys4 for in AIP:AgrC-II and AIP:AgrC-III interactions is likely different. A more focused SAR study is needed to delineate the exact nature of the role of Lys4, and is ongoing.

Lastly, we turn to Cys8 and the two endocyclic residues that follow. Prior SAR studies in *S. aureus* and *S. epidermidis* have established the thioester linkage to be crucial for receptor binding, and ring-opened versions of the native AIPs were inactive towards their cognate receptors *(48, 62)*. We assumed that the importance of thioester linkage is preserved for AIP-II and AIP-III as well, and did not make the Cys to Ala substitutions for our SAR study. We did investigate the importance of the stereochemistry of the residue, and while the AIP-III D-Cys8 was not assayed due to difficulties with peptide purification, the D-amino acid replacement of Cys8 in AIP-II caused a significant loss of activity, which is in agreement with our prior SAR

characterization of *S. epidermidis* AIP-I. This loss of activity could be attributed to either the stringent requirement for the local stereochemistry at the Cys residue or a global change in conformation of the macrocycle that prevented proper recognitions of the hydrophobic residues by the AgrC receptor. The first two endocyclic residues that follow Cys8, Ser9/Asn10 for AIP-II and Ala9/Ser10 for AIP-III, are two of the three residues that differ between AIP-II and AIP-III, with the third residue being Ser3 for AIP-II and Ala3 for AIP-III. Since residue Ser3 and Ala3 appear to play little to no role in receptor binding and activation for AIP-II and AIP-III, respectively, as discussed above, the differences at the first two endocyclic residues between AIP-II and AIP-III most likely dictate the receptor specificity of the native AIPs. For AIP-III, the role of the Ala9 side chain of was not explored in this study, as the residue is already an alanine, but the replacement with the corresponding D-amino acid resulted in a complete loss of activity. A similar effect was observed upon inversion of stereochemistry at this residue in AIP-II D-S9, with only very weak agonistic activity retained. The alanine substitution at AIP-II Ser9, however, was better tolerated, as the loss of agonistic potency was much smaller. For both AIP-II and AIP-III, alanine and D-amino acid mutations at residue 10 (Asn10 for AIP-II and Ser10 for AIP-III) caused a significant loss of potency, but did not change the agonistic profile of the peptides. Unexpectedly, while AIP-III S10A maintained an agonistic activity profile overall, the dose-response of the peptide at the higher concentrations showed a decrease in AgrC-III activation. This downward turn of the dose-response curve is not well understood at this time. Taken together, while residue 9 and 10 of AIP-II and AIP-III clearly make significant contributions to signal:receptor interactions that are likely responsible for the receptor specificity of the two AIPs, both residues are tolerant, to an extent, to alterations without converting from an agonist to an antagonist.

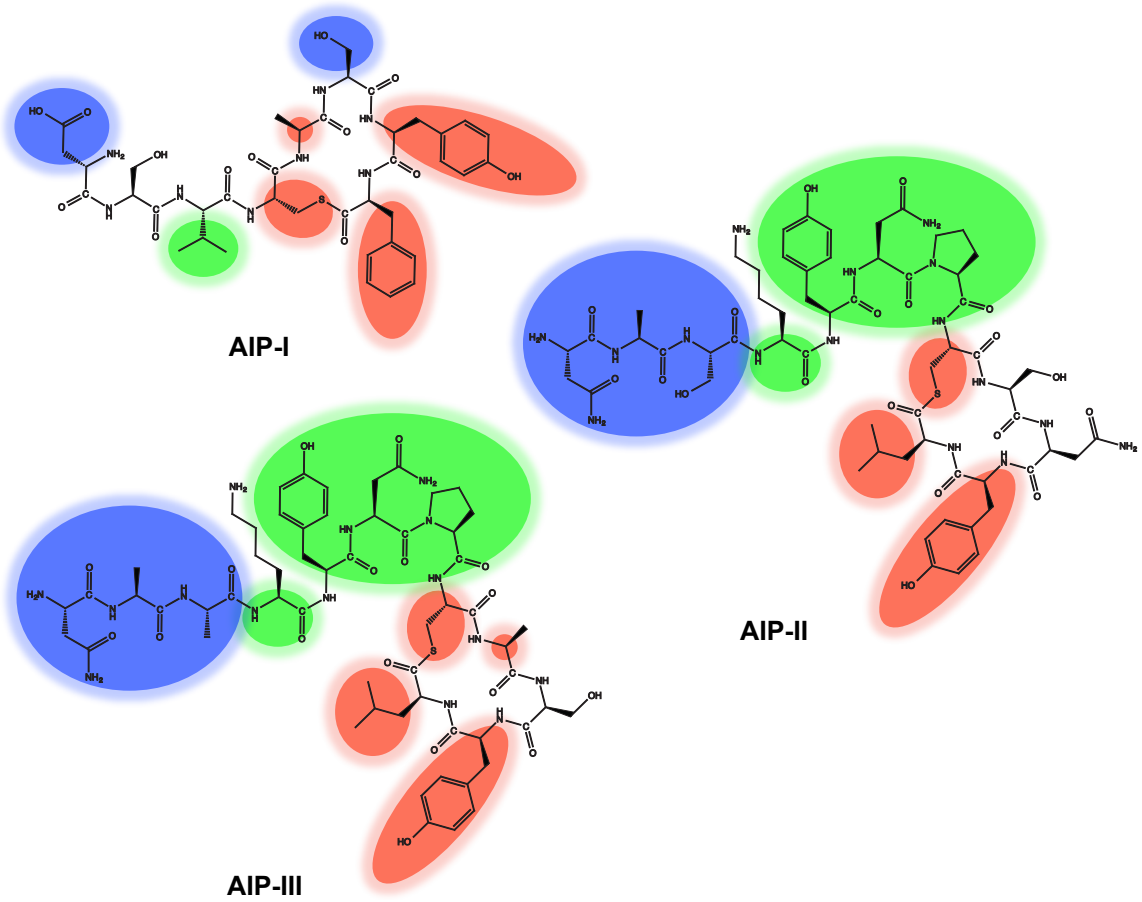


Figure 4.2: Summary of the known SAR trends for the activation of the three AgrC receptors by their cognate AIPs. SAR for AIP-I was reproduced from ref 46. Red: essential for receptor binding. Green: crucial for receptor activation. Blue: either inconsequential or detrimental to receptor binding and activation. Remaining residues contribute to receptor activation, but are tolerant to changes.

4.3.2 Incorporation of AgrC-I activating motifs into AIP-II scaffold.

Our preliminary SAR characterization of AIP-II and AIP-III has revealed key residues and features important for AgrC-II and AgrC-III activation (Figure 4.2). In particular, we propose that: 1) the macrocyclic hydrophobic residues of all three native *S. epidermidis* AIPs likely adopt a similar orientation that is important for receptor binding; 2) AIP-II and AIP-III can be shortened from 12-mers to 9-mers by removing the first three N-terminal residues and still maintain the potency of the native signal; 3) the remaining exocyclic tail residues of AIP-II and AIP-III are important for receptor activation; and 4) the first two endocyclic residues of AIP-II and AIP-III are likely responsible for the receptor specificity and can be altered without causing a conversion to

an antagonist. Our prior study of AIP-I has identified the branched hydrophobic side chain of a valine residue (Val3) to be important for AgrC-I activation *(46)*, and this structural motif must be properly oriented relative to the macrocycle.

Based on the existing SAR for all three native AIPs of *S. epidermidis*, we made our first attempt of designing a pan-group agonist by introducing the branched hydrophobic motif important for AgrC-I activation to the AIP-II 9aa scaffold (primary structure: K-Y-N-P-(C-S-N-Y-L)). We chose AIP-II 9aa due to our previous observation of it being a highly potent antagonist against AgrC-I *(46)*, which indicates strong receptor affinity. We also examined the tail/macrocycle hybrids of AIP-I and AIP-II 9aa, as well as AIP-I and AIP-III 9aa. These AIP analogs were screened against fluorescence reporter strains of all three groups for agonism and antagonisms as described above, with a minor modification made for Group II. Specifically, a small amount of AgrC-II agonist was added to the overnight culture of Group II prior to the fluorescence reporter assay in order to keep the reporter activity of Group II strain consistent throughout the assays (see Methods for details). The activities of this set of analogs are summarized in Table 4.3, with activity of the native AIPs included for reference.

Table 4.3: IC_{50} (shown in red) and EC_{50} (shown in green) values for potential pan-group agonist analogs of *S. epidermidis* AIP against the known AgrC receptors (AgrC-I–III) as determined using fluorescence reporter strains.[a]

	AgrC-I		AgrC-II		AgrC-III	
Peptide	IC_{50}/EC_{50}[b] (CI) [nM]	Max Act.[c] (S.D.) [%]	IC_{50}/EC_{50}[b] (CI) [nM]	Max Act.[c] (S.D.) [%]	IC_{50}/EC_{50}[b] (CI) [nM]	Max Act.[c] (S.D.) [%]
AIP-I	160 (102 – 250)	147 (± 33.5)	14.7 (10.5 – 20.6)	28.4 (± 7.53)	2.02 (1.33 – 3.05)	8.17 (± 1.00)
AIP-II	9.64[d] (7.99 – 11.6)	3.47[d] (± 0.69)	1070 (741 – 1530)	360 (± 45.6)	>2000	39.1 (± 13.9)
AIP-III	34.3[d] (31.4 – 37.4)	5.68[d] (± 1.22)	613 (309 – 1220)	173 (± 38.3)	65.7 (48.7 – 88.5)	220 (± 26.7)
AIPII9aaN3L	11.2 (8.85 – 14.1)	6.46 (± 1.32)	223 (65.6 – 757)	21.6 (± 3.53)	>2000	63.5 (± 4.88)
AIPII9aaN3V	8.36 (7.13 – 9.79)	6.14 (± 1.25)	367 (220 – 613)	26.2 (± 6.11)	Inactive[e]	
AIPII9aaP4V	74.9 (53.6 – 105)	13.2 (± 2.04)	1260 (659 – 2400)	290 (± 41.9)	>2000	43.3 (± 5.87)
AIPIIaaP4L	6.44 (5.58 – 7.44)	8.54 (± 0.41)	522 (292 – 932)	72.6 (± 14.7)	104 (86.3 – 125)	15.4 (± 6.79)
AIPII9aaP4Vtail AIPIring	70.6 (43.5 – 115)	148 (± 25.9)	0.56 (0.03 – 11.1)	22.4 (± 6.93)	36.8 (15.5 – 87.4)	46.8 (± 4.00)
AIPItail AIPIIring	215 (175 – 265)	35.4 (± 1.39)	>2000	57.39 (± 2.31)	>2000	67.7 (± 5.01)
AIPItail AIPIIIring	1870 (947 – 3680)	129 (± 14.9)	50.2 (23.1 – 109)	10.6 (± 7.94)	31.5 (22.9 – 43.2)	6.81 (± 0.38)
AIPII9aatail AIPIring	>2000	51.1 (± 6.63)	58.4 (31.4 – 109)	58.3 (± 4.76)	0.92 (0.69 – 1.22)	223 (± 31.9)

[a] See footnote in **Table 4.1**. [b] Agonism assay performed in the presence of 25nM AIP-I D1AS6AV3A (a previously identified pan-group antagonist *(46)*) to block receptor activation by endogenously produced AIPs. [c] Maximal Activity (Max Act.) is defined as the highest reporter activity (for agonism assay) or the lowest reporter activity (for antagonism assay) the peptide could achieve over the concentration range tested. [d] Values are from ref. 46. [e] Maximum inhibition did not exceed 30%. CI = 95% confidence intervals. S.D. = standard deviation of peptide's maximum activity determined from at least 2 biological replicates

To introduce the branched hydrophobic feature into AIP-II 9aa, we replaced either Asn3 or Pro4 with valine or a leucine. At the outset, we chose to replace Pro4 due to its position relative to the macrocycle, which is the same as that of Val3 in AIP-I. In case that the structural rigidity of the proline residue is crucial to signal:receptor interactions for AIP-II and AIP-III, we also chose to mutate the nearby residue Asn3. Although none of the resulting analogs showed agonistic activity towards more than one AgrC receptor, we were intrigued by the activity of the analog AIPII9aaP4V. Based on our structural study of AIP-I and its analogs, we expected that the placement of a valine residue immediately next to the macrocycle would allow the resulting

AIP analogs to gain the capability of activating AgrC-I. However, AIPII9aaP4V is an antagonist against AgrC-I, but remains as an agonist against AgrC-II, suggesting that the side chain structure of the proline is not essential for receptor activation of AgrC-II. One possible explanation for the lack of AgrC-I agonism is the improper orientation of the valine residue relative to the macrocycle due to the difference in macrocycle sequence between AIP-I and AIP-II, which is an important structural feature revealed by the prior study. To test this hypothesis, we synthesized and assayed the chimeric analog AIPII9aaP4Vtail AIPIring, which replaces the macrocycle of AIPII9aaP4V with that of AIP-I. Supporting our proposed explanation, AIPII9aaP4Vtail AIPIring is an agonist against AgrC-I, with potency and efficacy similar to that of native AIP-I despite the significant differences in the exocyclic tail, but behaves as an antagonist against AgrC-II. Interestingly, this analog also possesses agonistic activity against AgrC-III, albeit with lower efficacy. Given the similarity between the macrocycle of AIP-I and AIP-III, the primary structure of AIPII9aaP4Vtail AIPIring (K-Y-N-V-C-A-S-Y-F) closely resembles that of AIP-III 9aa (K-Y-N-P-C-A-S-Y-L), a potent agonist of AgrC-III, which could explain the analog's agonistic activity against AgrC-III. The reduction in efficacy is likely a result of the mutation of Pro4 to Val4, as our preliminary SAR characterization of AIP-II and AIP-III identified the proline to be important for receptor activation. Nevertheless, AIPII9aaP4Vtail AIPIring represents the second case where a cross-group inhibitor of the *agr* system in Staphylococci is converted to an agonist *(51)*. Furthermore, since the difference in macrocycle sequences is responsible for the receptor agonism specificity of AIPII9aaP4Vtail AIPIring and AIPII9aaP4V, we hypothesize that alterations in the macrocycle could lead to a peptide with agonistic activity toward all three receptors.

We also evaluated the exocyclic tail and macrocycle hybrids of the native AIP sequences. While we do not expect any of such hybrids to be capable of activating all three AgrC receptors, as the native sequences of the exocyclic tail do not contain all of the residues known to be important for receptor activation in all three groups (AIP-I does not contain the K-Y-N-P portion,

whereas AIP-II and AIP-III do not have the valine residue immediately next to the macrocycle), these hybrids will allow us to examine whether the macrocycles are interchangeable among the native AIPs without altering the mode of action. The activities of both AIPItail AIPIIring hybrid and AIPItail AIPIIIring hybrid are as expected. Specifically, the lack of key activating residues for AgrC-II and AgrC-III in the AIP-I exocyclic tail prevented the hybrids from activating AgrC-II and AgrC-III. Differences, or the lack thereof, in the macrocycle structures, as discussed above, cause AIPItail AIPIIIring to be capable of activating AgrC-I but not AIPItail AIPIIring, suggesting that the macrocycles are not completely interchangeable and the macrocyclic residues likely play a role in forming correct contacts with the receptor for activation. Unexpectedly, the combination of the exocyclic tail of AIP-II/AIP-III 9aa with the macrocycle of AIP-I resulted in an AIP analog with agonistic activity toward all three AgrC receptors. Specifically, even though the potency and the efficacy are both poor, we did not expect this hybrid AIP analog to be an agonist of any capacity in AgrC-I, since the valine residue, which is present in all known AgrC-I agonists, is absent in this analog. One likely explanation may be that the proline residue provides sufficient hydrophobic bulk that can partially replace the hydrophobic interactions initiated by the valine residue. A more in-depth study is needed to explain the observation. Nonetheless, despite the relatively poor activity in Group I and Group II, AIPII9aatail AIPIring represents the first known pan-group agonist for the *agr* systems in *S. epidermidis*, which encouraged us in our design process.

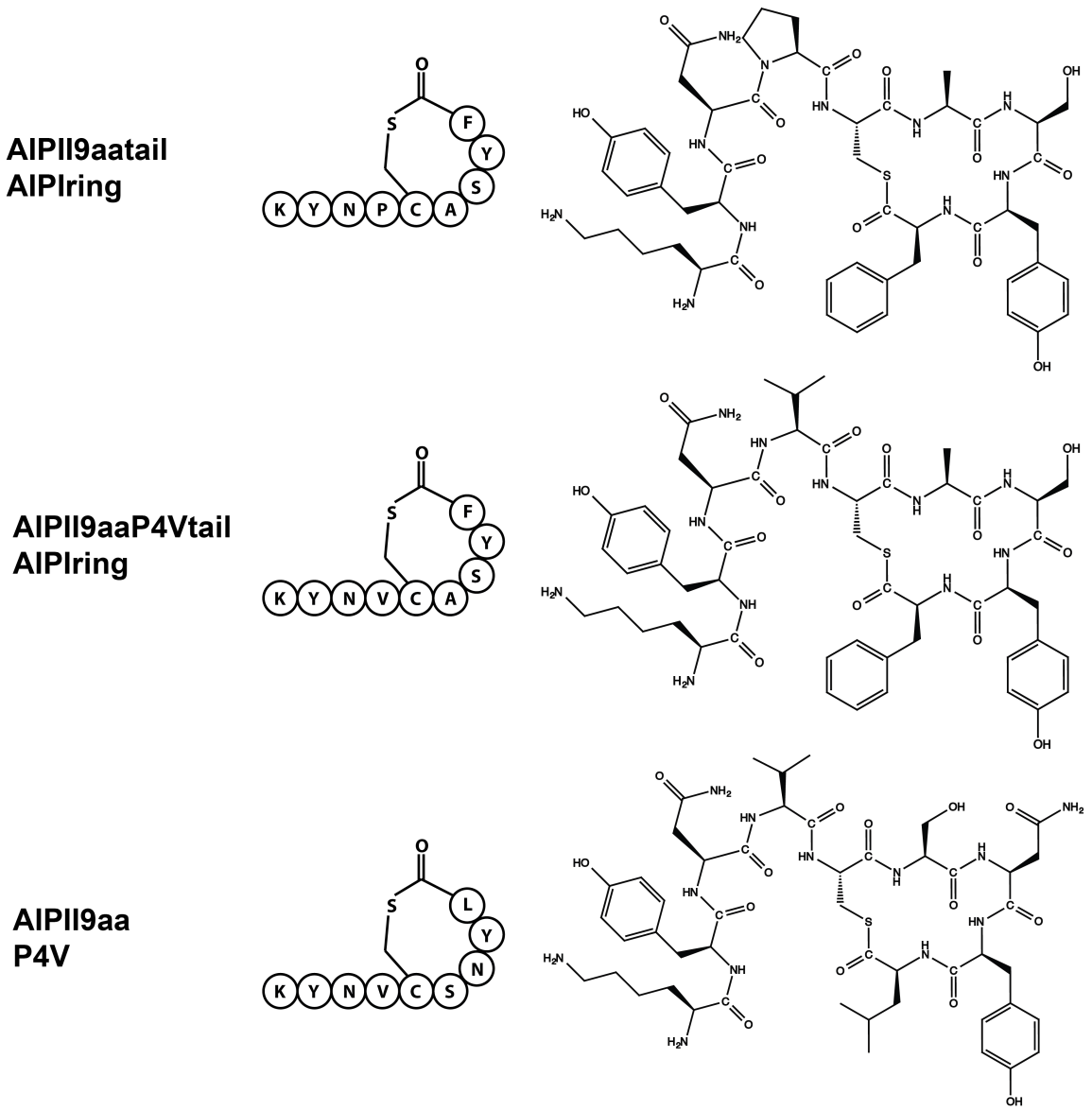


Figure 4.3: Scaffolds of interest identified from the first attempt of designing pan-group agonists for the *agr* system of *S. epidermidis*. Each scaffold is shown with the name, the single-letter abbreviations, and the full structure.

4.3.3 Activities of AIPII9aaP4Vtail AIPIring analogs.

From our first attempt of designing *S. epidermidis* pan-group agonists, we identified three scaffolds of interest that deserved further investigation (Figure 4.3). We first focused on AIPII9aaP4Vtail AIPIring, which is an agonist in both AgrC-I and AgrC-III. To broaden the receptor agonism specificity to include AgrC-II, we designed five analogs where the macrocycle

structure was changed to be more like the native AIP-II. The activities of these analogs were assessed using the fluorescence reporter assay described above, and the assay data are summarized in Table 4.4.

Table 4.4: IC_{50} (shown in red) and EC_{50} (shown in green) values for analogs of the AIPII9aaP4Vtail AIPIring scaffold against the known AgrC receptors (AgrC-I–III) as determined using fluorescence reporter strains.[a] Parent compound (in italic) included for reference.

	AgrC-I		AgrC-II		AgrC-III	
Peptide	IC_{50}/EC_{50}[b] (CI) [nM]	Max Act.[c] (S.D.) [%]	IC_{50}/EC_{50}[b] (CI) [nM]	Max Act.[c] (S.D.) [%]	IC_{50}/EC_{50}[b] (CI) [nM]	Max Act.[c] (S.D.) [%]
AIPII9aaP4Vtail AIPIring	*70.6 (43.5 – 115)*	*148 (± 25.9)*	*0.56 (0.03 – 11.1)*	*22.4 (± 6.93)*	*36.8 (15.5 – 87.4)*	*46.8 (± 4.00)*
AIPII9aaP4Vtail AIPIringA6S	822 (495 – 1360)	116 (± 13.7)	3.87 (2.20 – 6.79)	11.8 (± 2.70)	0.74 (0.54 – 1.02)	11.4 (± 1.58)
AIPII9aaP4Vtail AIPIringA6SS7A	169 (124 – 229)	92.6 (± 6.40)	0.82 (0.07 – 9.10)	13.4 (± 3.95)	0.49 (0.34 – 0.72)	11.9 (± 0.87)
AIPII9aaP4Vtail AIPIringS7N	662 (335 – 1310)	156 (± 17.9)	121 (85.6 – 170)	19.0 (± 2.71)	81.4 (74.7 – 88.7)	31.5 (± 3.54)
AIPII9aaP4Vtail AIPIringS7A	12.0 (8.51 – 16.9)	157 (± 25.7)	0.61 (0.15 – 2.50)	24.4 (± 7.92)	N.D.[d]	40.8 (± 7.75)
AIPII9aaP4Vtail AIPIringF9L	1010 (709 – 1430)	140 (± 19.6)	0.86 (0.07 – 9.85)	13.4 (± 3.23)	>2000	54.1 (± 7.35)

[a,b,c] See footnotes in **Table 4.3**. [d] Data could not be fitted to a sigmoidal curve for EC_{50} calculation. CI = 95% confidence intervals. S.D. = standard deviation of peptide's maximum activity determined from 3 biological replicates.

Despite the changes made to the residues in the macrocycle, none of the analogs was able to activate AgrC-II to any extent. We note, however, that none of the analogs has Ser and Asn at residue 6 and residue 7, which are the amino acids found at those positions in the macrocycle of AIP-II. The low activity of these analogs is in agreement with our preliminary SAR of AIP-II, which highlighted these two residues to be important for receptor activation specificity. The activities of these analogs against AgrC-III are also in agreement with our SAR of AIP-III, as the analogs lose AgrC-III agonism activity when the macrocycle is less AIP-III-like. Interestingly, all analogs remained as agonists in AgrC-I, with one analog, AIPII9aaP4Vtail AIPIringS7A, being more than 10 times more potent than the native AIP-I. The tolerance of AgrC-I towards changes made in the macrocycle further supports the model of AgrC-I activation proposed in

our prior study (ref). We also note that the Phe to Leu mutation appears to significantly reduce compound potency, and, in addition to the analogs presented in this section, this effect was also observed when comparing the activity of the hybrid analog AIPItail AIPIIIring (D-S-V-C-A-S-Y-L) to that of AIP-I (D-S-V-C-A-S-Y-F) (Table 4.3). Thus, while both a Leu and a Phe residue provide sufficient hydrophobic interactions for receptor binding, Phe may be preferred by *S. epidermidis* AgrC receptors. This observation is particularly fascinating, since our recent study on designing simplified peptidomimetics for inhibiting *S. aureus* AgrC receptors uncovered three potent *S. aureus* AgrC inhibitors that all containing phenylalanines in the macrocycle *(58)*. The rationale for the preference of Phe by AgrC receptors in both *S. epidermidis* and *S. aureus* is not clear at this time, and efforts to better understand this observation are underway.

4.3.4 Activities of AIPII9aaP4V analogs.

As a complement to the analog design based on the AIPII9aaP4Vtail AIPIring scaffold, we next synthesized five analogs based on the AIPII9aaP4V scaffold, where changes were made to the macrocycle such that the macrocycle is more AIP-I/AIP-III like. The analogs were assessed in the same fluorescence reporter assay, and the data are presented in Table 4.5.

Table 4.5: IC_{50} (shown in red) and EC_{50} (shown in green) values for analogs of the AIPII9aaP4V scaffold against the known AgrC receptors (AgrC-I–III) as determined using fluorescence reporter strains.[a] Parent compound (in italic) included for reference.

	AgrC-I		AgrC-II		AgrC-III	
Peptide	IC_{50}/EC_{50}[b] (CI) [nM]	Max Act.[c] (S.D.) [%]	IC_{50}/EC_{50}[b] (CI) [nM]	Max Act.[c] (S.D.) [%]	IC_{50}/EC_{50}[b] (CI) [nM]	Max Act.[c] (S.D.) [%]
AIPII9aaP4V	*74.9 (53.6 – 105)*	*13.2 (± 2.04)*	*1260 (659 – 2400)*	*290 (± 41.9)*	*>2000*	*43.3 (± 5.87)*
AIPII9aaP4VS6A	Inactive[d]		>2000	63.3 (± 7.71)	>2000	41.6 (± 8.90)
AIPII9aaP4VN7A	>2000	66.2 (± 7.31)	137 (14.6 – 1290)	52.6 (± 7.60)	11.6 (7.33 – 18.2)	10.5 (± 2.91)
AIPII9aaP4VN7S	>2000	73.4 (± 8.64)	12.3 (9.65 – 15.7)	37.9 (± 11.0)	18.0 (9.91 – 32.8)	11.6 (± 3.62)
AIPII9aaP4VS6AN7A	130 (97.1 – 175)	133 (± 11.3)	152 (28.1 – 824)	52.2 (± 6.29)	1240 (639 – 2390)	43.3 (± 4.47)
AIPII9aaP4VL9F	2.16 (0.63 – 7.37)	21.2 (± 1.53)	169 (54.3 – 523)	211 (± 26.2)	36.2 (16.9 – 77.4)	13.0 (± 5.23)

[a,b,c] See footnotes in **Table 4.3**. [d] Dose-response curves revealed neither agonism nor antagonism activities over the concentration range tested. CI = 95% confidence intervals. S.D. = standard deviation of peptide's maximum activity determined from at least 2 biological replicates.

In agreement with our model for AgrC-I activation, three out of the five analogs tested were capable of activating AgrC-I. The overall low potency of these compounds could be attributed to the presence of the Leu residue in the macrocycle, as we discussed above. In contrast, AIPII9aaP4VL9F gained potency compared to the parent compound as both an agonist and an antagonist, further strengthening our assertion that Phe may be preferred for receptor binding. We were surprised to find, however, that a majority of the analogs remained agonists in AgrC-II, the reduced activity notwithstanding. In particular, AIPII9aaP4VS6A, AIPII9aaP4VN7A, and AIPII9aaP4VS6AN7A have counterparts derived from the AIPII9aaP4Vtail AIPIring scaffold, and those counterparts are antagonists against AgrC-II (Table 4.4). The only difference between the two sets of analogs is the C-terminal residue, which is Leu for the AgrC-II agonists and Phe for the AgrC-II antagonists. How the Phe to Leu substitution switched an antagonist to an agonist in AgrC-II is not clear. Nevertheless, we were excited to identify a second analog in this focused study, AIPII9aaP4VS6AN7A, that was capable pan-group agonism in the *agr* systems in *S. epidermidis*. Inspired by the success of uncovering a pan-group agonist from the AIPII9aaP4V

scaffold, we designed an additional set of analogs, focusing on mutating the first two endocyclic amino acids following the cysteine residue. However, almost all of the peptides showed antagonistic activity against all three receptors, with a majority of them having poor potency (Table 4.11). Accordingly, AIPII9aaP4VS6AN7A remains the only pan-group agonist identified from the AIPII9aaP4V scaffold. Interestingly, one of the most potent pan-group antagonists against the AgrC receptors in *S. epidermidis* reported in our recent study also has two Ala residues at the first two endocyclic positions, suggesting that these residues may facilitate AIP recognition by all three receptors.

4.3.5 Optimization of the AIPII9aatail AIPIring scaffold.

Finally, we turned to the AIPII9aatail AIPIring scaffold, the first pan-group agonist uncovered in this study. While an excellent agonist for AgrC-III, AIPII9aatail AIPIring has relatively weak activities in AgrC-I and AgrC-II. Aiming to improve activity towards AgrC-I and II, we synthesized five more analogs with substitutions made in the macrocycle. The fluorescence reporter assay results for these analogs are shown in Table 4.6.

Table 4.6: IC_{50} (shown in red) and EC_{50} (shown in green) values for analogs of the AIPII9aatail AIPIring scaffold against the known AgrC receptors (AgrC-I–III) as determined using fluorescence reporter strains.[a] Parent compound (in italic) included for reference.

	AgrC-I		AgrC-II		AgrC-III	
Peptide	IC_{50}/EC_{50}[b] (CI) [nM]	Max Act.[c] (S.D.) [%]	IC_{50}/EC_{50}[b] (CI) [nM]	Max Act.[c] (S.D.) [%]	IC_{50}/EC_{50}[b] (CI) [nM]	Max Act.[c] (S.D.) [%]
AIPII9aatail AIPIring	*>2000*	*51.1 (± 6.63)*	*58.4 (31.4 – 109)*	*58.3 (± 4.76)*	*0.92 (0.69 – 1.22)*	*223 (± 31.9)*
AIPII9aatail AIPIringA6S	0.99 (0.87 – 1.13)	7.23 (± 0.60)	587 (234 – 1470)	86.8 (± 19.8)	9.60 (6.47 – 14.3)	201 (± 22.6)
AIPII9aatail AIPIringA6SS7A	0.31 (0.27 – 0.36)	6.90 (± 0.97)	278 (122 – 632)	185 (± 42.6)	9.51 (6.34 – 14.3)	215 (± 25.1)
AIPII9aatail AIPIringS7N	15.4 (12.7 – 18.8)	9.52 (± 0.47)	>2000	378 (± 64.2)	>2000	484 (± 29.2)
AIPII9aatail AIPIringS7A	865 (693 – 1080)	38.4 (± 1.35)	64.6 (34.4 – 122)	133 (± 23.5)	1.45 (1.00 – 2.12)	386 (± 70.4)
AIPII9aatail AIPIringA6SS7N	0.48 (0.44 – 0.52)	6.29 (± 0.66)	208 (129 -335)	889 (± 157)	>2000	469 (± 26.0)

[a,b,c] See footnotes in **Table 4.3**. CI = 95% confidence intervals. S.D. = standard deviation of peptide's maximum activity determined from 3 biological replicates.

With the key activating residues for AgrC-II and AgrC-III all present (the four amino acids in the exocyclic tail), all analogs derived from the AIPII9aatail AIPIring scaffold remained as agonists against both AgrC-II and AgrC-III. As the macrocycle became more AIP-II-like, the activity for AgrC-II improved as expected. Interestingly, while all analogs exhibited comparable efficacy as agonists in AgrC-III, the potency of Asn-containing analogs was reduced drastically, indicating that the Asn residue in the macrocycle is preventing optimal interactions with AgrC-III and results in decreased receptor affinity. Although this series of analogs did lead to peptides with improved activity towards AgrC-II when compared to the parent compound, we were not able to improve the activity int AgrC-I. In fact, only one of the five analogs retained the pan-group agonist behavior (AIPII9aatail AIPIringS7A), and though this analog had a better efficacy in AgrC-II than the parent compound, the activity in AgrC-I actually worsened. Given that this set of peptides, including the parent compound, all lack a valine residue near the macrocycle, which is present in all of the potent agonists targeting AgrC-I, we hypothesize that analogs containing different substitutions at the proline position may yield ligands capable of satisfying the necessary interactions needed for activation of all three AgrC receptors. The synthesis and evaluation of such AIP analogs are currently underway.

4.4 Summary

S. epidermidis is an important nosocomial pathogen, particularly for device-associated infections, and its ability to form robust biofilm is a primary mechanism by which the infections are established *(10, 13, 19)*. The QS circuit in *S. epidermidis*, the *agr* system, plays an important role in the biofilm life cycle and virulence of the pathogen, making the *agr* system an attractive target for limiting infectivity *(25, 35, 37-39)*. In particular, intentional activation of the *agr* system could lead to reduced biofilm accumulation and render the dispersed bacteria more susceptible to antimicrobials *(13, 44)*. However, the cross-group inhibitory activities observed for

the native AIPs of the different *agr* specificity groups in *S. epidermidis* prevent the use of native AIPs for activating the *agr* system in all groups of *S. epidermidis (7, 35)*. A pan-group agonist, or a cocktail of agonists that each lack any inhibitory activities, is needed to make targeting the *agr* system for biofilm dispersion more practical *(7)*. In this study, we report the design and identification of the first set of AIP analogs with agonistic activities towards all three AgrC receptors in *S. epidermidis*.

Our prior study characterizing the SARs of AIP-I:AgrC-I interactions provided us with key features critical for AgrC-I activation *(46)*. Herein, we extended the SAR study to examine AIP-II and AIP-III, and our preliminary examination has now revealed residues important for AgrC-II and AgrC-III activation. Based on our findings from the SAR experiments, we designed a series of AIP analogs containing the known features important for AgrC activation in all three groups of *S. epidermidis,* and we were excited to uncover three AIP analogs with agonistic activities against all three AgrC receptors, without confounding antagonistic activities against any of the receptors. Though the efficacy of these peptides needs improvement, they represent to our knowledge the first reported pan-group agonists of the *agr* systems in a Staphylococcal species. Characterization of the 3-dimensional structures of these agonists will provide us further insights into the structural motifs that enabled agonism towards all three AgrC receptors. Efforts towards this goal are underway.

This study also provided an improved understanding of signal:receptor interactions for the *S. epidermidis agr* systems. Beyond the SARs gained from the systematic alanine and D-amino acid scans of AIP-II and AIP-III, we also observed that having a Phe at the C-terminal position improved the potency of the AIP analogs in all three AgrC receptors. In fact, the introduction of Phe residues resulted in a number of AIP analogs that are much more potent agonists against AgrC-II and AgrC-III when compared to the native AIPs (between 5 to 50-fold). More importantly, we identified a position in the AIP analogs that deserves more in-depth characterization in order to improve agonist efficacy towards all three AgrC receptors.

Specifically, the structure of the exocyclic residue nearest to the macrocycle appears to dictate which receptors are better activated by the AIP analogs. The present study only examined two amino acids (Val and Pro) at that position extensively, and the effect of introducing other natural and unnatural amino acids (such as the unnatural amino acid 3-methyl proline, which adds a branched hydrophobic feature to the proline residue) at the position needs to be evaluated. Building on the pan-group agonist scaffolds uncovered in this study, even more effective pan-group agonists could be developed. Such compounds, along with the new agonists reported herein and our previously reported pan-group antagonists, serve as new tools for better assessing the effects of targeting QS as an approach towards limiting the infectivity of *S. epidermidis*.

4.5 Methods

4.5.1 Biological reagents, strains, and general methods

Reagents were purchased from commercial sources and used according to company's instructions. The *S. epidermidis* fluorescence reporter strains AH3408 (Group I), AH3567 (Group II), and AH3409 (Group III) were grown in Tryptic Soy Broth (TSB, from Sigma) supplemented with 10 μg/mL of erythromycin *(35)*, and all cultures were incubated at 37 °C with shaking at 200 rpm unless noted otherwise. A Biotek Synergy 2 microplate reader operating Gen5 software was used to record absorbance and fluorescence measurements. IC_{50}/EC_{50} values and the corresponding 95% confidence intervals were determined from sigmoidal curve fits using GraphPad Prism software (v. 6.0).

4.5.2 Chemical reagents and instrumentation

Reagents and solvents were purchased from commercial sources (Sigma-Aldrich or Chem-Impex International) and used as received, except for dichloromethane (CH_2Cl_2), which was dried and kept dry over molecular sieves. Resins for solid-phase peptide synthesis was

purchased from NovaBiochem. Water (18 MΩ) was purified using a Barnstead Nanopure system (Thermo Scientific).

Reverse-phase high performance liquid chromatography (RP-HPLC) was carried out on a Shimadzu system equipped with a SLC-10Avp controller, a LC-10AT pump, a FCV-ALvp solvent mixer, and a SPC-10MAvp UV/Vis diode array detector. Peptide purification was performed on a semi-preparative Kromasil Eternity C_{18} column (10 mm x 250 mm, 5 µm particle size with 100 Å pore size) with a 5 mL/min flow rate, and analytical samples were run on an analytical Kromasil Eternity C_{18} column (4.6 mm x 250 mm, 5 µm particle size with 100 Å pore size) with a 1 mL/min flow rate. Solvent A = 18 MΩ water + 0.1% trifluoroacetic acid (TFA); solvent B = acetonitrile + 0.1% TFA. Linear peptides were purified over a linear gradient of 20% → 50% solvent B over 30 min, and cyclic peptides were purified over a linear gradient of 20% → 35% solvent B over 27 min. Peptide purity was determined using a linear gradient of 10% → 95% solvent B over 27 min, with integration of peaks detected at 220 nm.

MALDI-TOF mass spectrometry (MS) data were obtained using a Bruker microflex LRF spectrometer equipped with a 337 nm laser and a reflectron. Exact mass (EM) data were obtained using a Thermo Q Exactive Plus ESI-Q-IT (orbitrap) mass spectrometer.

4.5.3 Peptide synthesis

Linear version of the *S. epidermidis* AIP analogs were synthesized using a modified protocol of the Fmoc/tBu based solid-phase peptide synthesis approach developed by Blanco-Canosa and Dawson *(58, 59)*. All reactions were mixed by agitation on a shaker. Briefly, Dawson 3-(Fmoc-amino)-4-aminobenzoyl (Dbz) AM resin (100-200 mesh) was swelled in CH_2Cl_2 for 40 min, and the solvent was exchanged for dimethylformamide (DMF). The Fmoc-group deprotections were achieved using piperidine solution (20% in DMF, 2 mL, 5 min x 3). For each amino acid coupling, except for the final coupling, Fmoc-protected amino acid (4 mole equivalent relative to the resins), *N*-[(dimethylamino)-1*H*-1,2,3-triazolo-[4,5-*b*]pyridin-1-

ylmethylene]-*N*-methylmethanaminium hexafluorophosphate *N*-oxide (HATU, 4 mole equivalent), and diisopropylethylamine (DIPEA, 8 mole equivalent) were dissolved in 2 mL of DMF, preactivated for 1 min, and added to the resin for 30 min. For the final coupling, Boc-protected amino acids were used instead. Following the final amino acid coupling, the Dbz group was activated by the addition of 4-nitrophenylchloroformate in CH_2Cl_2 (4 mole equivalent, 30 min x 2), and then treated with DIPEA (0.5 M in DMF) for 10 min three times. The resin was washed with DMF, CH_2Cl_2, and diethyl ether, dried under N_2, and reduced for 18 hr under vacuum. To cleave the linear peptide, the resin was resuspended in a cleavage cocktail of TFA/CH_2Cl_2/H_2O/triisopropyl silane (90:5:2.5:2.5) for 2 hr. The resulting mixture was syringe-filtered, rinsed with the cleavage cocktail once, and precipitated in diethyl ether at -20 °C for at least 1 hr. The precipitate was dissolved in acetonitrile/H_2O (1:1) and lyophilized.

The linear AIP analog was purified by semi-preparative RP-HPLC as described above, and the fractions with the desired product, as confirmed by MADLI-MS, were collected, lyophilized, and then cyclized according our previously established protocol *(46)*. The cyclic peptide product was purified by RP-HPLC, and its identity and purity were confirmed by EM measurement and analytical RP-HPLC, respectively. Purified AIP analog was lyophilized, weighed, and stored as 1 mM stock solutions in DMSO at 4 °C. EM and analytical HPLC data are available in the Supplementary Information. The native *S. epidermidis* AIPs, as well as AIP-II 11aa, 10aa, 9aa, and 8aa, were all previously prepared in our laboratory, and therefore were not re-synthesized for the present study.

4.5.4 Fluorescence reporter assay

Agonism and antagonism assays for all three AgrC receptors were performed using our previously established protocol with two modifications *(46)*. To block AgrC activation by endogenously produced AIP, AIP-I D1AS6AV3A, a pan-group antagonist uncovered in our prior study *(46)*, at a final concentration of 25 nM (> 5 x IC_{50} for all three receptors) was used for the

agonism assay. For the assessment of potential pan-group agonists, Group II overnight cultures were also augmented with 500 nM of AIP-II 9aa, an agonist against AgrC-II, to ensure consistent activation of the *agr* system (AIP-II 9aa was used over AIP-II due to compound availability).

4.6 Supplementary Information

4.6.1 MS and HPLC data

Table 4.7: MS and HPLC data for the *S. epidermidis* AIP-II analogs synthesized in this study. EM = exact mass. Rt = retention time.

Peptide Name	Sequence	Calc. EM	Obs. EM	Rt (min)	Purity (%)
AIP-II N1A	A-A-S-K-Y-N-P-(C-S-N-Y-L)	1312.5991	1312.6010	18.5	>99
AIP-II S3A	N-A-A-K-Y-N-P-(C-S-N-Y-L)	1339.6100	1339.6121	16.0	>99
AIP-II K4A	N-A-S-A-Y-N-P-(C-S-N-Y-L)	1298.5471	1298.5459	16.7	>99
AIP-II Y5A	N-A-S-K-A-N-P-(C-S-N-Y-L)	1263.5787	1263.5764	17.1	>97
AIP-II N6A	N-A-S-K-Y-A-P-(C-S-N-Y-L)	1312.5991	1312.6021	17.6	>99
AIP-II P7A	N-A-S-K-Y-N-A-(C-S-N-Y-L)	1329.5893	1329.5895	17.3	>99
AIP-II S9A	N-A-S-K-Y-N-P-(C-A-N-Y-L)	1339.1600	1339.1606	17.3	>99
AIP-II N10A	N-A-S-K-Y-N-P-(C-S-A-Y-L)	1312.5991	1312.6014	17.7	>99
AIP-II Y11A	N-A-S-K-Y-N-P-(C-S-N-A-L)	1263.5787	1263.5811	16.3	>99
AIP-II L12A	N-A-S-K-Y-N-P-(C-S-N-Y-A)	1313.5580	1313.5575	15.3	>99
AIP-II D-N1	DN-A-S-K-Y-N-P-(C-S-N-Y-L)	678.3056 $[M+2H]^{2+}$	678.3054 $[M+2H]^{2+}$	16.0	>97
AIP-II D-S3	N-A-DS-K-Y-N-P-(C-S-N-Y-L)	678.3056 $[M+2H]^{2+}$	678.3051 $[M+2H]^{2+}$	15.9	>97
AIP-II D-K4	N-A-S-DK-Y-N-P-(C-S-N-Y-L)	678.3056 $[M+2H]^{2+}$	678.3063 $[M+2H]^{2+}$	16.0	>96
AIP-II D-Y5	N-A-S-K-DY-N-P-(C-S-N-Y-L)	678.3056 $[M+2H]^{2+}$	678.3061 $[M+2H]^{2+}$	16.1	>95
AIP-II D-N6	N-A-S-K-Y-DN-P-(C-S-N-Y-L)	678.3056 $[M+2H]^{2+}$	678.3049 $[M+2H]^{2+}$	15.9	>94
AIP-II D-P7	N-A-S-K-Y-N-DP-(C-S-N-Y-L)	678.3056 $[M+2H]^{2+}$	678.3065 $[M+2H]^{2+}$	16.0	>97
AIP-II D-C8	N-A-S-K-Y-N-P-(DC-S-N-Y-L)	678.3056 $[M+2H]^{2+}$	678.3066 $[M+2H]^{2+}$	16.8	>97
AIP-II D-S9	N-A-S-K-Y-N-P-(C-DS-N-Y-L)	678.3056 $[M+2H]^{2+}$	678.3041 $[M+2H]^{2+}$	16.2	>97
AIP-II D-N10	N-A-S-K-Y-N-P-(C-S-DN-Y-L)	678.3056 $[M+2H]^{2+}$	678.3040 $[M+2H]^{2+}$	15.8	>98
AIP-II D-Y11	N-A-S-K-Y-N-P-(C-S-N-DY-L)	678.3056 $[M+2H]^{2+}$	678.3044 $[M+2H]^{2+}$	15.5	>95
AIP-II D-L12	N-A-S-K-Y-N-P-(C-S-N-Y-DL)	678.3056 $[M+2H]^{2+}$	678.3047 $[M+2H]^{2+}$	15.6	>99

Table 4.8: MS and HPLC data for the *S. epidermidis* AIP-III analogs synthesized in this study. EM = exact mass. Rt = retention time.

Peptide Name	Sequence	Calc. EM	Obs. EM	Rt (min)	Purity (%)
AIP-III N1A	A-A-A-K-Y-N-P-(C-A-S-Y-L)	627.3028 $[M+2H]^{2+}$	627.3029 $[M+2H]^{2+}$	18.4	>96
AIP-III K4A	N-A-A-A-Y-N-P-(C-A-S-Y-L)	620.2768 $[M+2H]^{2+}$	620.2776 $[M+2H]^{2+}$	18.8	>99
AIP-III Y5A	N-A-A-K-A-N-P-(C-A-S-Y-L)	602.7926 $[M+2H]^{2+}$	602.7935 $[M+2H]^{2+}$	17.8	>97
AIP-III N6A	N-A-A-K-Y-A-P-(C-A-S-Y-L)	627.3028 $[M+2H]^{2+}$	627.3038 $[M+2H]^{2+}$	18.4	>99
AIP-III P7A	N-A-A-K-Y-N-A-(C-A-S-Y-L)	635.7979 $[M+2H]^{2+}$	635.7994 $[M+2H]^{2+}$	18.1	>99
AIP-III S10A	N-A-A-K-Y-N-P-(C-A-A-Y-L)	640.8082 $[M+2H]^{2+}$	640.8109 $[M+2H]^{2+}$	19.4	>99
AIP-III Y11A	N-A-A-K-Y-N-P-(C-A-S-A-L)	602.7926 $[M+2H]^{2+}$	602.7922 $[M+2H]^{2+}$	17.7	>96
AIP-III L12A	N-A-A-K-Y-N-P-(C-A-S-Y-A)	627.7822 $[M+2H]^{2+}$	627.7824 $[M+2H]^{2+}$	16.8	>97
AIP-III D-N1	DN-A-A-K-Y-N-P-(C-A-S-Y-L)	648.8057 $[M+2H]^{2+}$	648.8054 $[M+2H]^{2+}$	16.7	>99
AIP-III D-A2	N-DA-A-K-Y-N-P-(C-A-S-Y-L)	648.8057 $[M+2H]^{2+}$	648.8050 $[M+2H]^{2+}$	16.8	>99
AIP-III D-A3	N-A-DA-K-Y-N-P-(C-A-S-Y-L)	648.8057 $[M+2H]^{2+}$	648.8056 $[M+2H]^{2+}$	16.7	>99
AIP-III D-K4	N-A-A-DK-Y-N-P-(C-A-S-Y-L)	648.8057 $[M+2H]^{2+}$	648.8052 $[M+2H]^{2+}$	16.7	>98
AIP-III D-Y5	N-A-A-K-DY-N-P-(C-A-S-Y-L)	648.8057 $[M+2H]^{2+}$	648.8055 $[M+2H]^{2+}$	16.7	>99
AIP-III D-N6	N-A-A-K-Y-DN-P-(C-A-S-Y-L)	648.8057 $[M+2H]^{2+}$	648.8052 $[M+2H]^{2+}$	16.5	>99
AIP-III D-P7	N-A-A-K-Y-N-DP-(C-A-S-Y-L)	648.8057 $[M+2H]^{2+}$	648.8061 $[M+2H]^{2+}$	16.6	>99
AIP-III D-A9	N-A-A-K-Y-N-P-(C-DA-S-Y-L)	648.8057 $[M+2H]^{2+}$	648.8063 $[M+2H]^{2+}$	16.9	>99
AIP-III D-S10	N-A-A-K-Y-N-P-(C-A-DS-Y-L)	648.8057 $[M+2H]^{2+}$	648.8063 $[M+2H]^{2+}$	16.5	>97
AIP-III D-Y11	N-A-A-K-Y-N-P-(C-A-S-DY-L)	648.8057 $[M+2H]^{2+}$	648.8062 $[M+2H]^{2+}$	15.9	>99
AIP-III D-L12	N-A-A-K-Y-N-P-(C-A-S-Y-DL)	648.8057 $[M+2H]^{2+}$	648.8060 $[M+2H]^{2+}$	16.2	>99
AIP-III 11aa	A-A-K-Y-N-P-(C-A-S-Y-L)	1182.5612	1182.5618	17.9	>98
AIP-III 10aa	A-K-Y-N-P-(C-A-S-Y-L)	1111.5241	1111.5226	18.0	>96
AIP-III 9aa	K-Y-N-P-(C-A-S-Y-L)	1040.4870	1040.4851	18.0	>97
AIP-III 8aa	Y-N-P-(C-A-S-Y-L)	912.3920	912.3917	19.4	>97

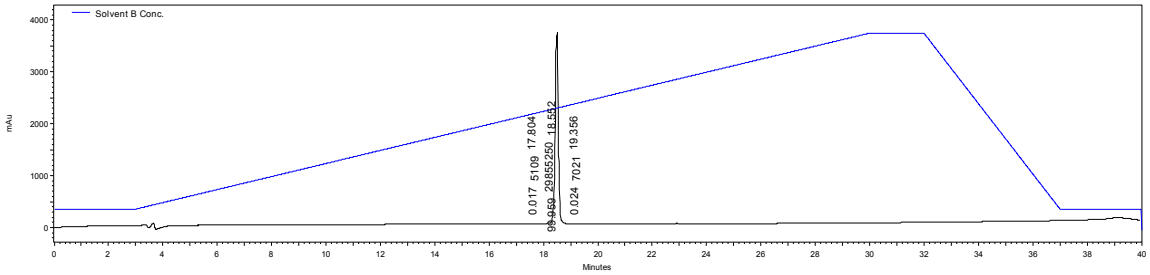
Table 4.9: MS and HPLC data for the *S. epidermidis* AIP analogs synthesized for pan-group agonist evaluation. EM = exact mass. Rt = retention time. α = L-2-Aminobutyric acid

Peptide Name	Sequence	Calc. EM	Obs. EM	Rt (min)	Purity (%)
AIPII9aaN3L	K-Y-L-P-(C-S-N-Y-L)	541.7706 $[M+2H]^{2+}$	541.7706 $[M+2H]^{2+}$	17.7	>92
AIPII9aaN3V	K-Y-V-P-(C-S-N-Y-L)	534.7628 $[M+2H]^{2+}$	534.7624 $[M+2H]^{2+}$	17.0	>97
AIPII9aaP4V	K-Y-N-V-(C-S-N-Y-L)	543.2579 $[M+2H]^{2+}$	543.2575 $[M+2H]^{2+}$	17.0	>95
AIPII9aaP4L	K-Y-N-L-(C-S-N-Y-L)	1099.5241	1099.5240	17.7	>97
AIPII9aaP4Vtail AIPIring	K-Y-N-V-(C-A-S-Y-F)	538.7471 $[M+2H]^{2+}$	538.7466 $[M+2H]^{2+}$	17.8	>96
AIPItail AIPIIring	D-S-V-(C-S-N-Y-L)	882.3662	882.3660	17.0	>94
AIPItail AIPIIIring	D-S-V-(C-A-S-Y-L)	839.3604	839.3613	18.8	>96
AIPII9aatail AIPIring	K-Y-N-P-(C-A-S-Y-F)	1074.4713	1074.4710	17.6	>95
AIPII9aaP4Vtail AIPIringA6S	K-Y-N-V-(C-S-S-Y-F)	1092.4819	1092.4828	18.1	>92
AIPII9aaP4Vtail AIPIringA6SS7A	K-Y-N-V-(C-S-A-Y-F)	1076.4870	1076.4878	19.0	>91
AIPII9aaP4Vtail AIPIringS7N	K-Y-N-V-(C-A-N-Y-F)	1103.4979	1103.4988	18.4	>98
AIPII9aaP4Vtail AIPIringS7A	K-Y-N-V-(C-A-A-Y-F)	1060.4921	1060.4928	19.4	>93
AIPII9aaP4Vtail AIPIringF9L	K-Y-N-V-(C-A-S-Y-L)	1042.5026	1042.5037	17.9	>97
AIPII9aaP4VS6A	K-Y-N-V-(C-A-N-Y-L)	535.2604 $[M+2H]^{2+}$	535.2603 $[M+2H]^{2+}$	17.6	>98
AIPII9aaP4VN7A	K-Y-N-V-(C-S-A-Y-L)	521.7550 $[M+2H]^{2+}$	521.7549 $[M+2H]^{2+}$	18.0	>97
AIPII9aaP4VN7S	K-Y-N-V-(C-S-S-Y-L)	1058.4975	1058.4988	17.7	>95
AIPII9aaP4VS6AN7A	K-Y-N-V-(C-A-A-Y-L)	513.7575 $[M+2H]^{2+}$	513.7578 $[M+2H]^{2+}$	18.6	>94
AIPII9aaP4VL9F	K-Y-N-V-(C-S-N-Y-F)	560.2500 $[M+2H]^{2+}$	560.2503 $[M+2H]^{2+}$	17.8	>99
AIPII9aaP4VN7α	K-Y-N-V-(C-S-α-Y-L)	528.7623 $[M+2H]^{2+}$	528.7626 $[M+2H]^{2+}$	19.4	>97
AIPII9aaP4VS6α	K-Y-N-V-(C-α-N-Y-L)	542.2682 $[M+2H]^{2+}$	542.2680 $[M+2H]^{2+}$	18.5	>96
AIPII9aaP4VS6G	K-Y-N-V-(C-G-N-Y-L)	1055.4979	1055.4988	17.9	>95
AIPII9aaP4VS6T	K-Y-N-V-(C-T-N-Y-L)	1099.5241	1099.5251	18.3	>93
AIPII9aaP4VN7L	K-Y-N-V-(C-S-L-Y-L)	1084.5496	1084.5497	19.9	>96
AIPII9aaP4VN7T	K-Y-N-V-(C-S-T-Y-L)	1072.5132	1072.5137	18.7	>95
AIPII9aaP4VN7G	K-Y-N-V-(C-S-G-Y-L)	1028.4870	1028.4875	18.0	>96
AIPII9aaP4VN7V	K-Y-N-V-(C-S-V-Y-L)	535.7706 $[M+2H]^{2+}$	535.7705 $[M+2H]^{2+}$	19.8	>93
AIPII9aaP4VN7Q	K-Y-N-V-(C-S-Q-Y-L)	550.2657 $[M+2H]^{2+}$	550.2654 $[M+2H]^{2+}$	18.5	>96
AIPII9aaP4VN7D	K-Y-N-V-(C-S-D-Y-L)	1086.4925	1086.4920	18.2	>93

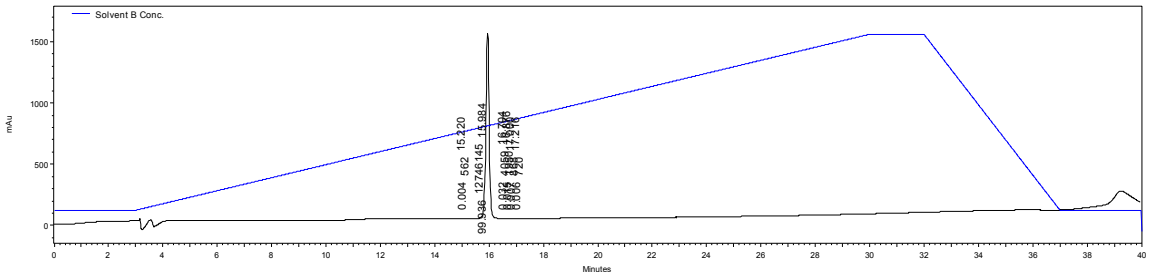
AIPII9aatail AIPIringA6S	K-Y-N-P-(C-S-S-Y-F)	1090.4662	1090.4663	19.1	>97
AIPII9aatail AIPIringA6SS7A	K-Y-N-P-(C-S-A-Y-F)	1074.4713	1074.4692	19.5	>95
AIPII9aatail AIPIringS7N	K-Y-N-P-(C-A-N-Y-F)	1101.4822	1101.4825	16.9	>98
AIPII9aatail AIPIringS7A	K-Y-N-P-(C-A-A-Y-F)	1058.4764	1058.4752	17.9	>97
AIPII9aatail AIPIringA6SS7N	K-Y-N-P-(C-S-N-Y-F)	1117.4771	1117.4780	16.8	>98

4.6.2 HPLC traces for S. epidermidis AIP analogs

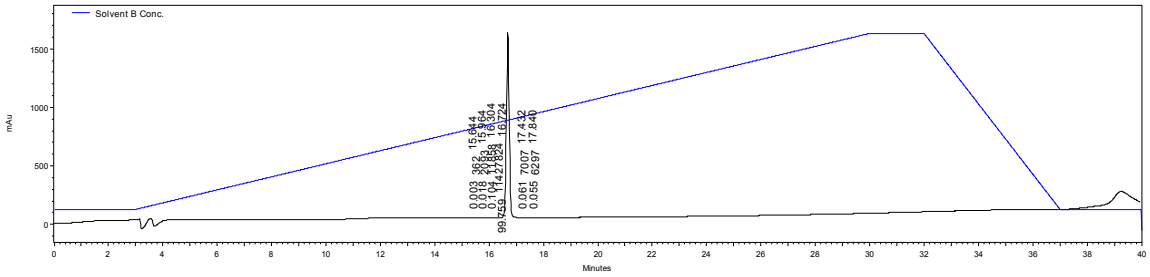
AIP-II N1A



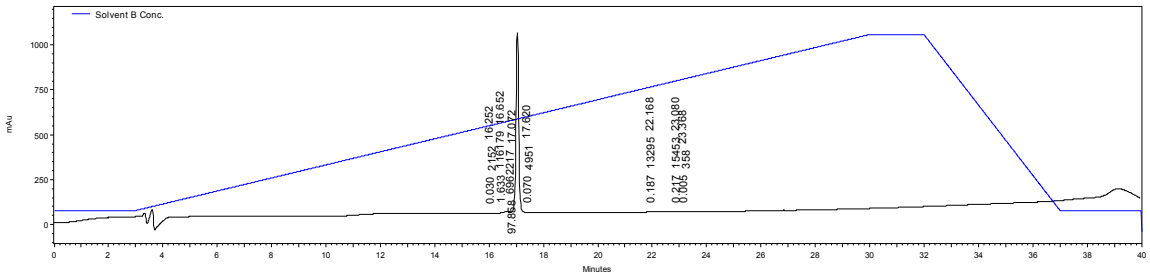
AIP-II S3A



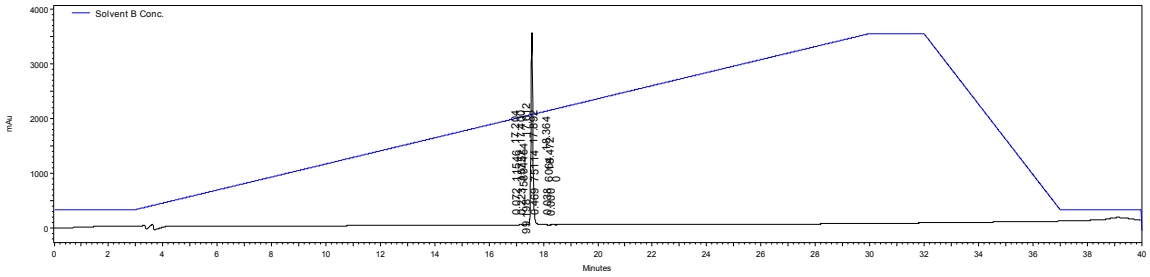
AIP-II K4A



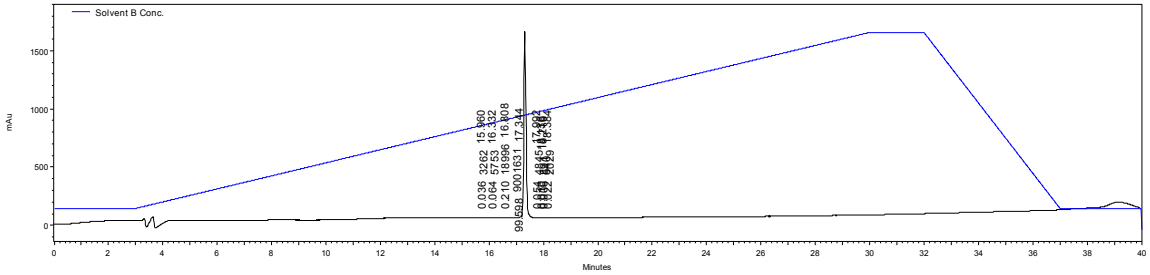
AIP-II Y5A



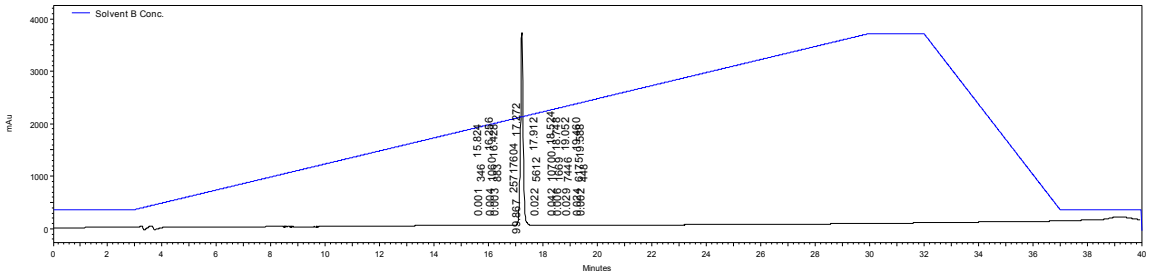
AIP-II N6A



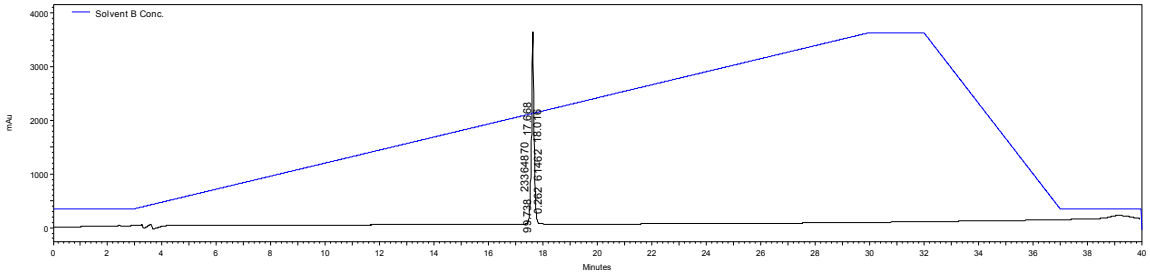
AIP-II P7A



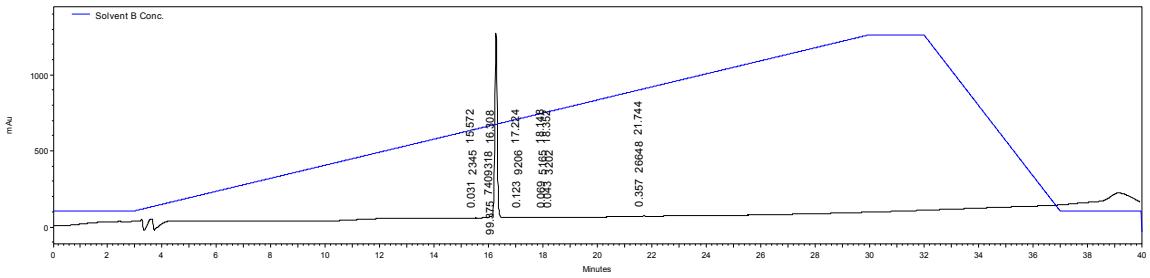
AIP-II S9A



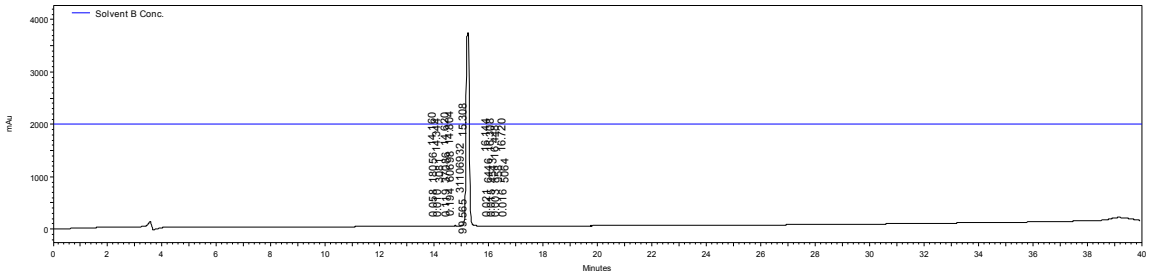
AIP-II N10A



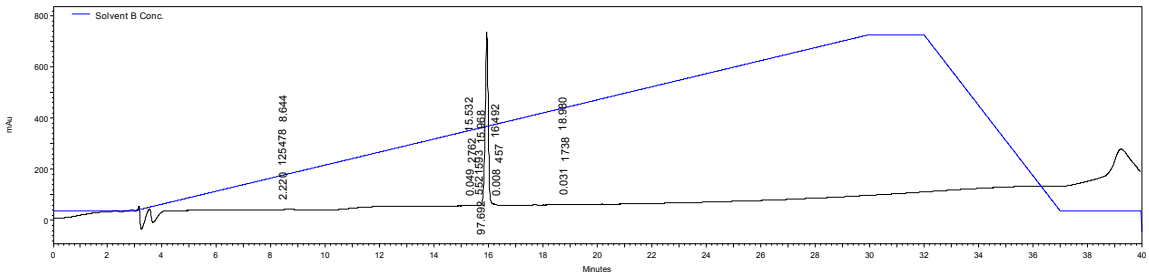
AIP-II Y11A



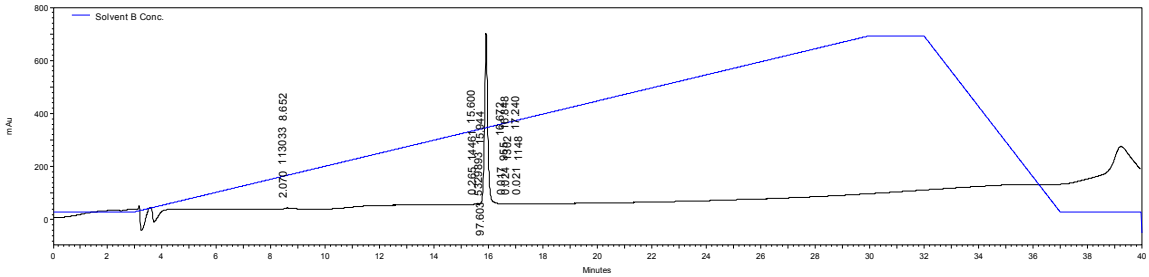
AIP-II L12A



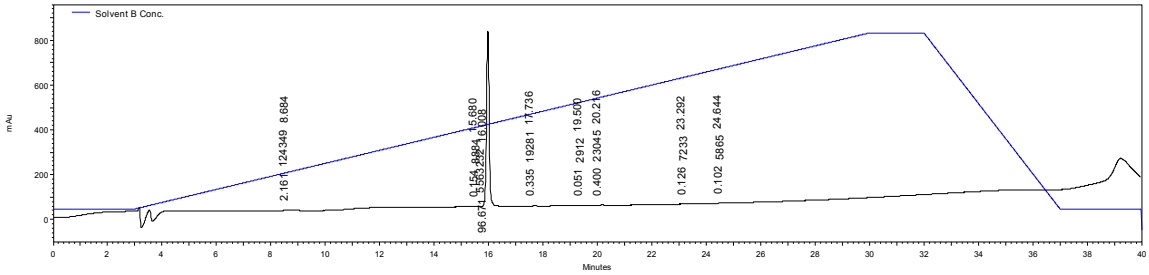
AIP-II D-N1



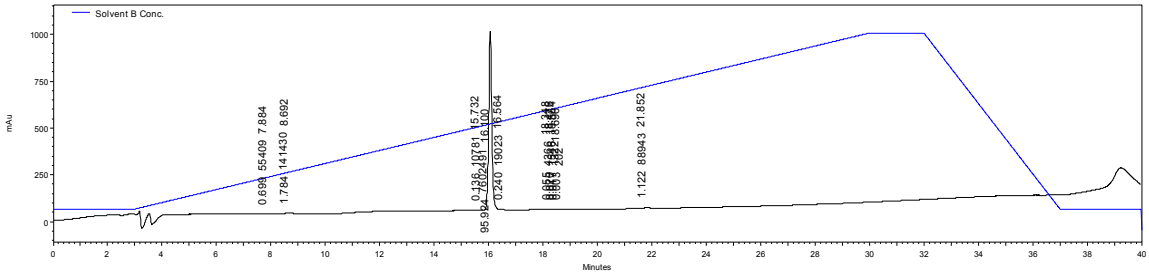
AIP-II D-S3



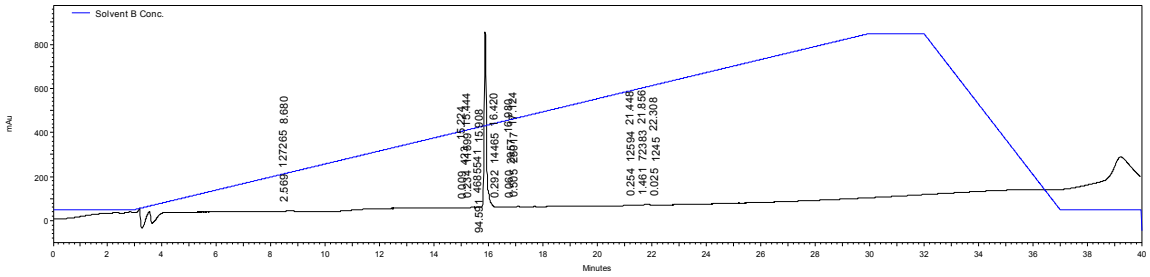
AIP-II D-K4



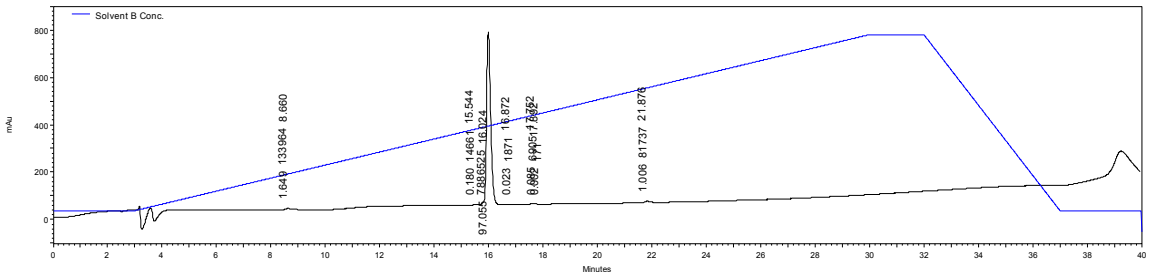
AIP-II D-Y5



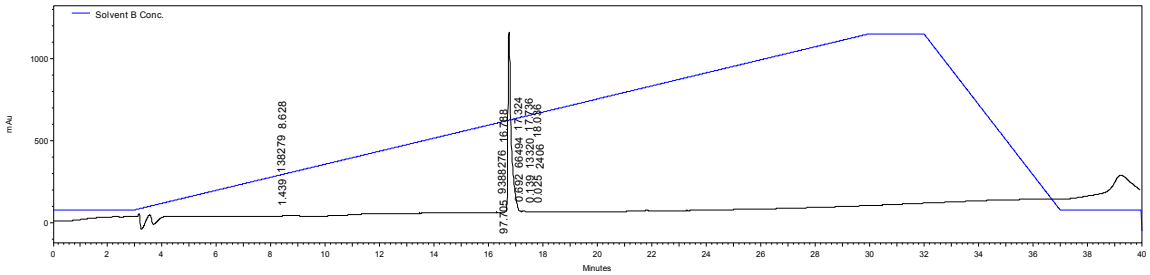
AIP-II D-N6



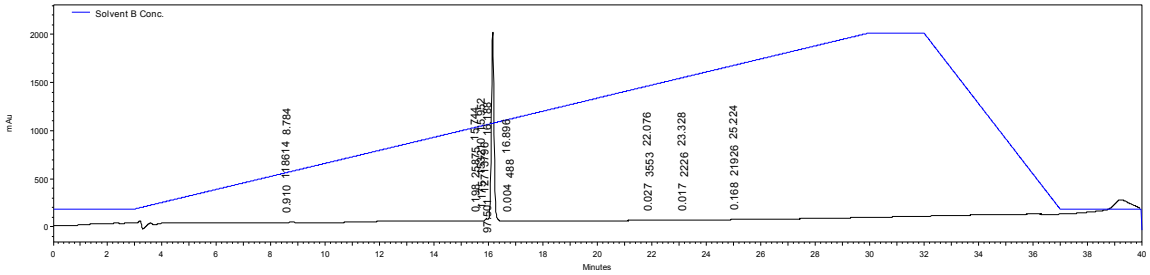
AIP-II D-P7



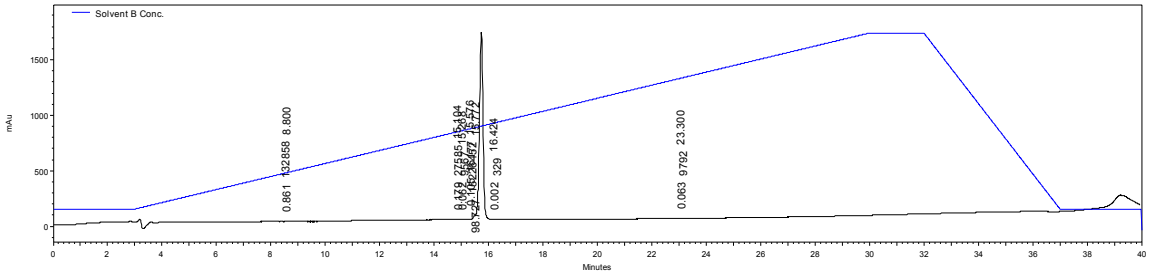
AIP-II D-C8



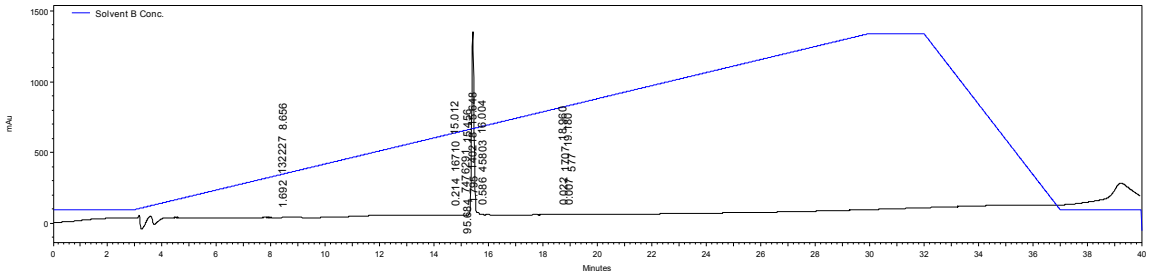
AIP-II D-S9



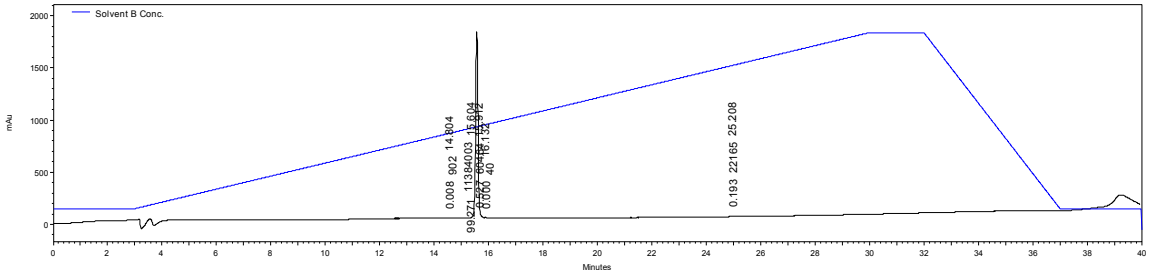
AIP-II D-N10



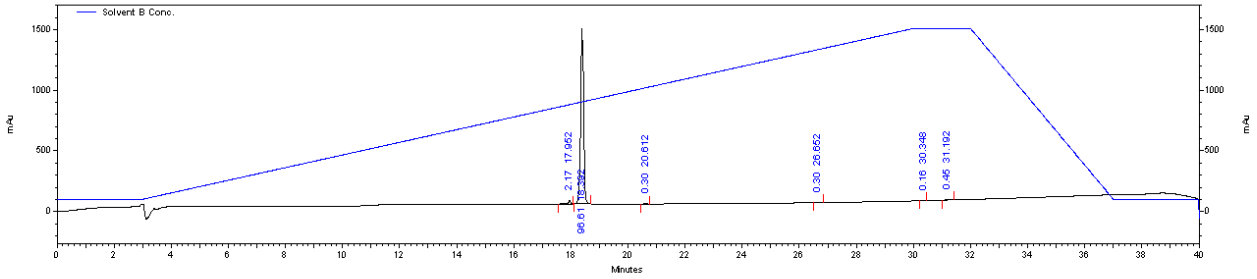
AIP-II D-Y11



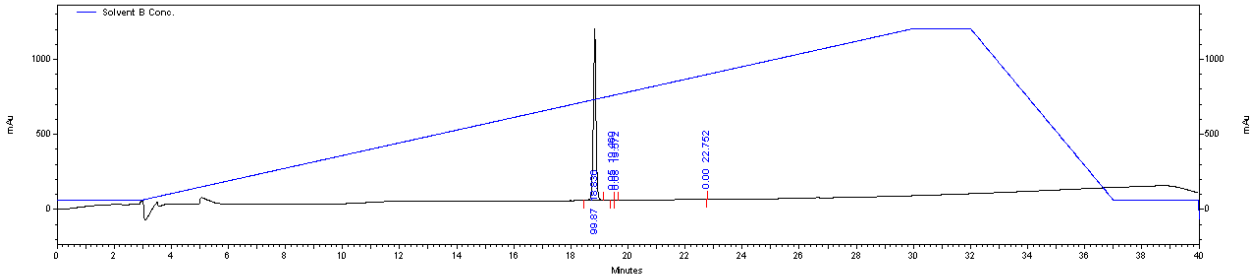
AIP-II D-L12



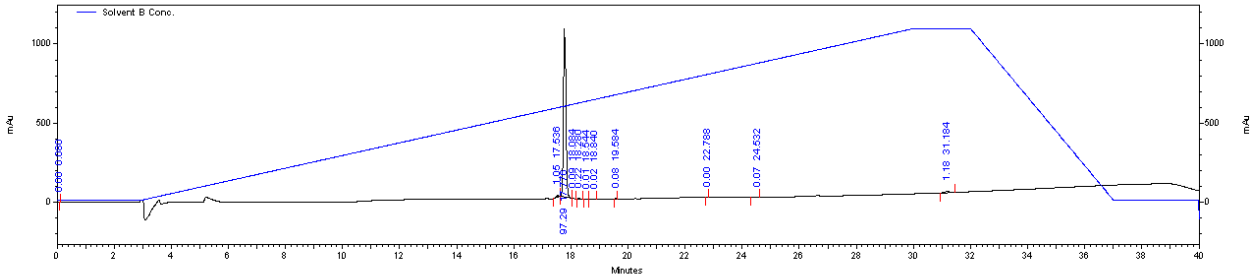
AIP-III N1A



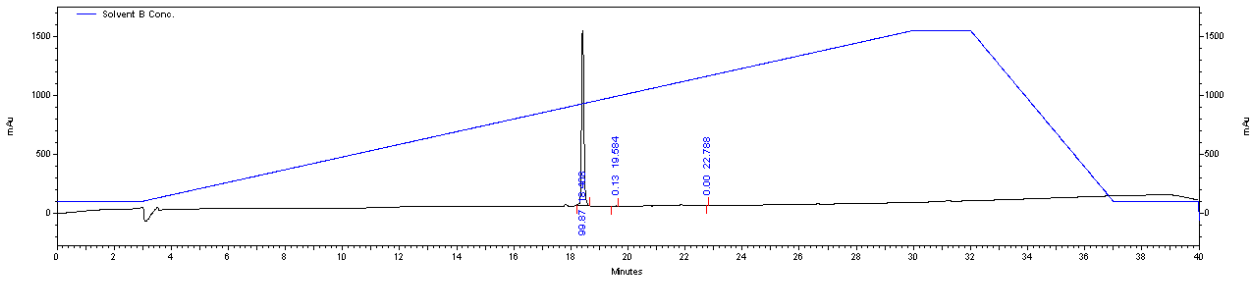
AIP-III K4A



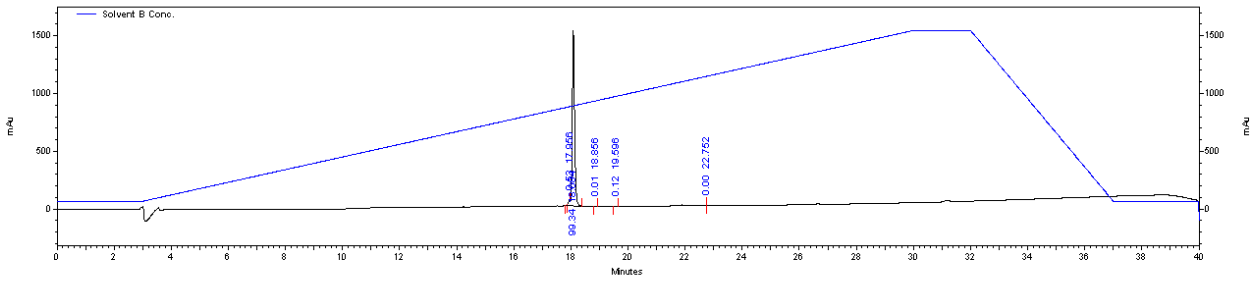
AIP-III Y5A



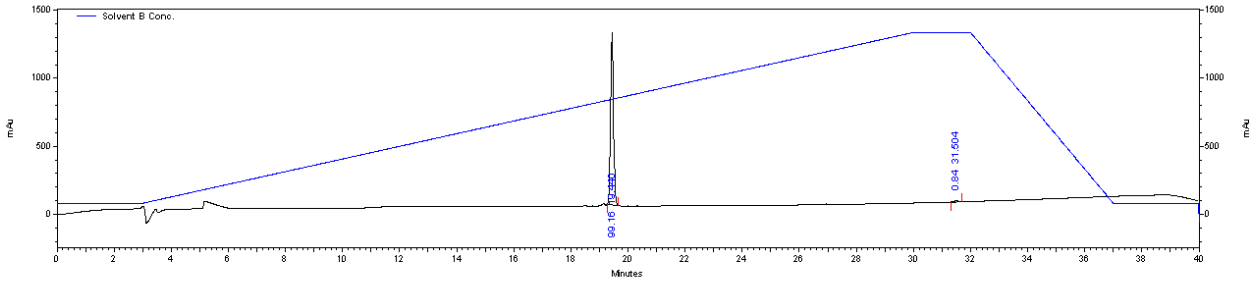
AIP-III N6A



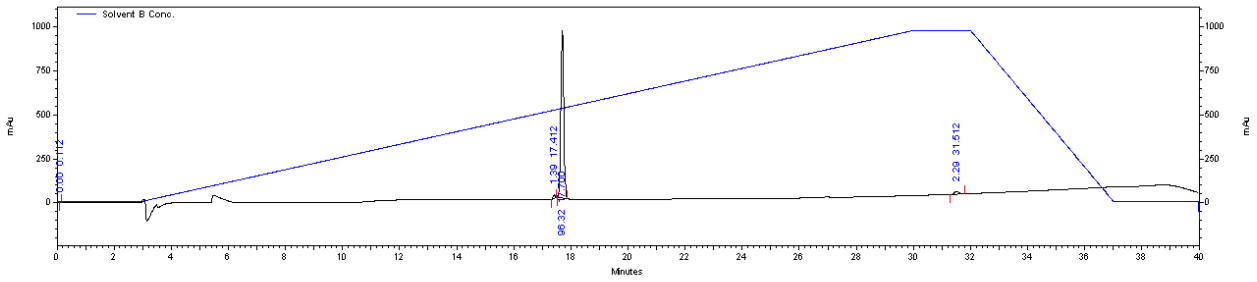
AIP-III P7A



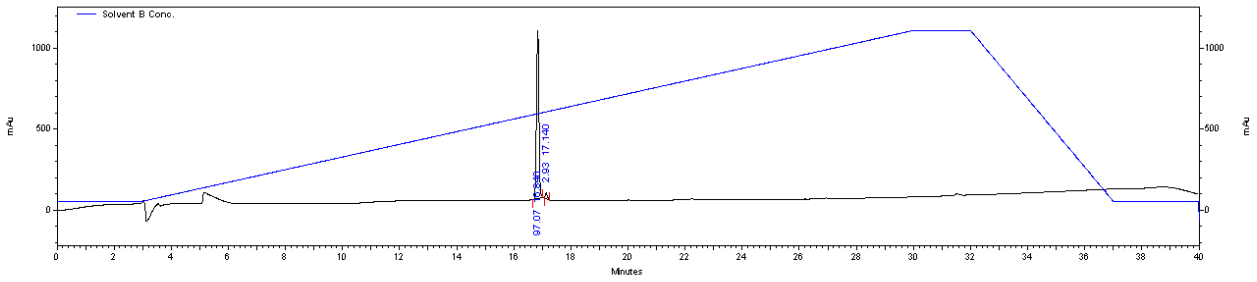
AIP-III S10A



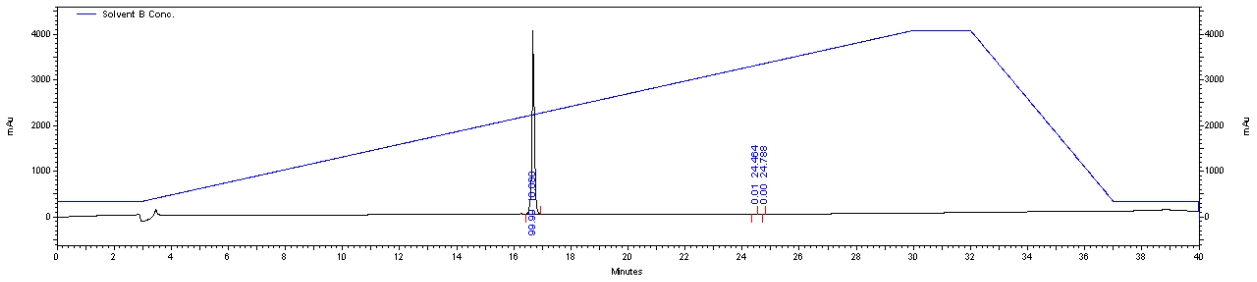
AIP-III Y11A



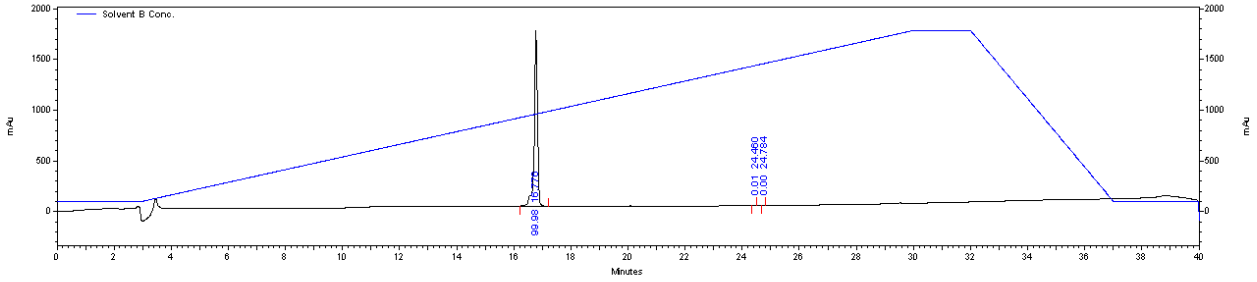
AIP-III L12A



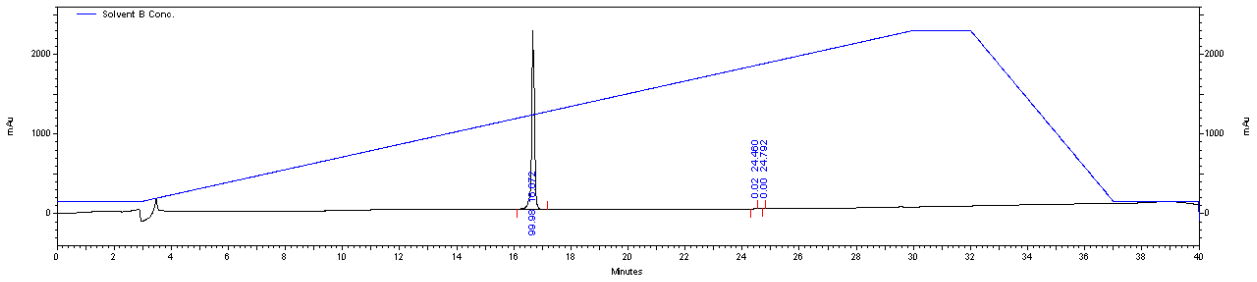
AIP-III D-N1



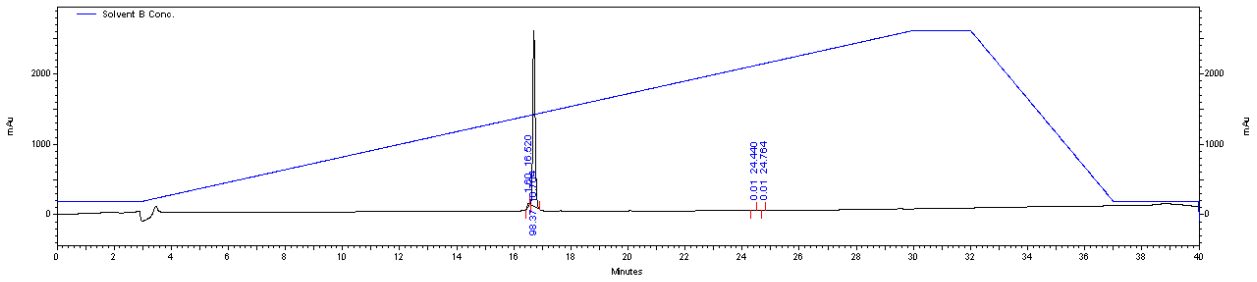
AIP-III D-A2



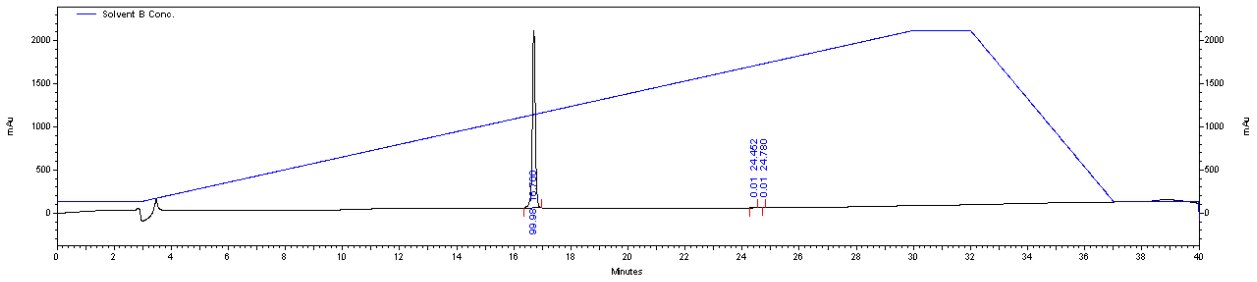
AIP-III D-A3



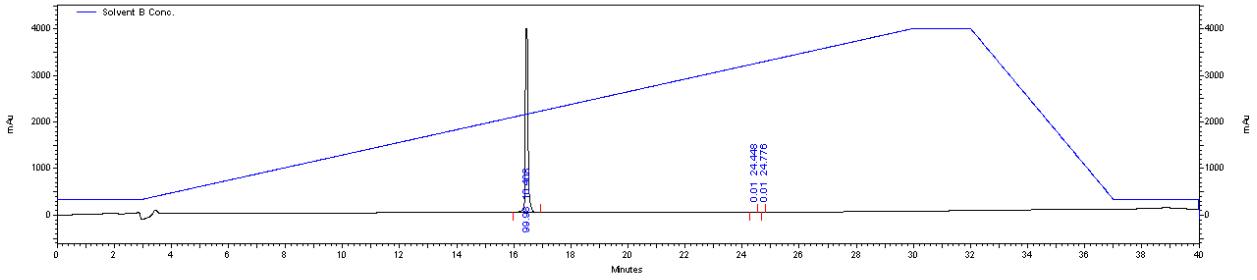
AIP-III D-K4



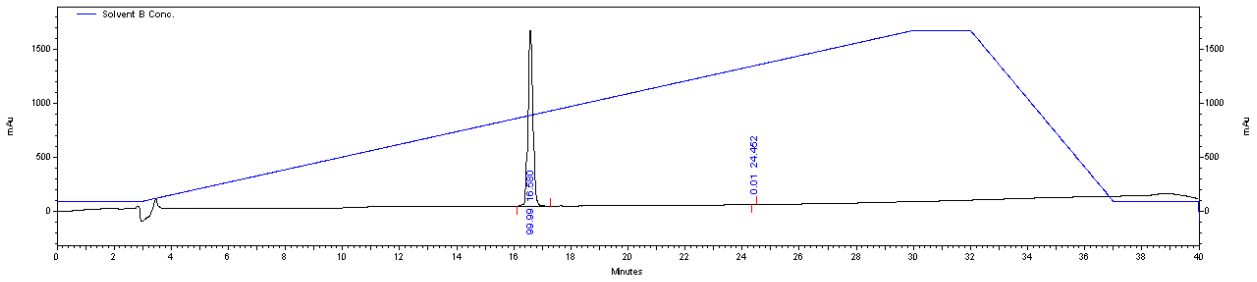
AIP-III D-Y5



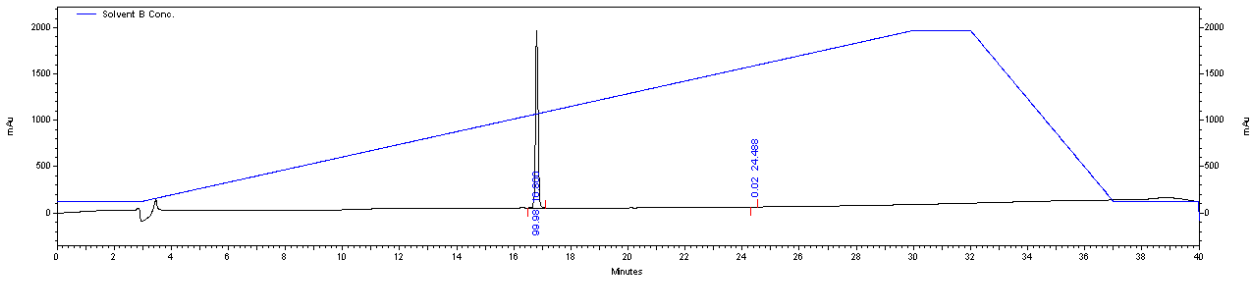
AIP-III D-N6



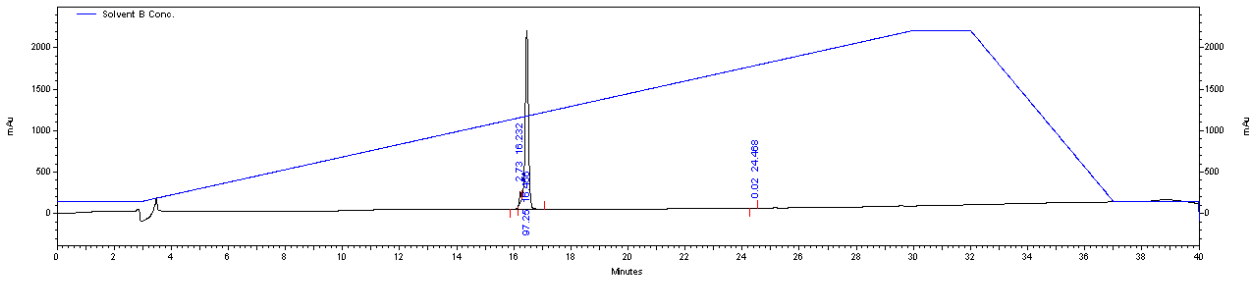
AIP-III D-P7



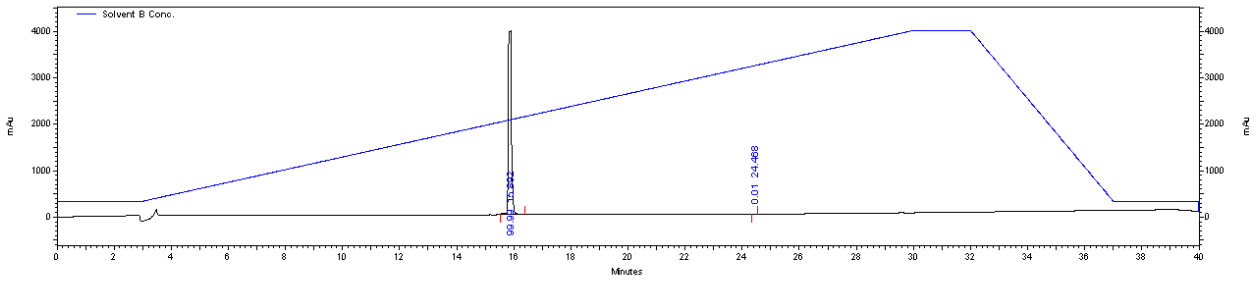
AIP-III D-A9



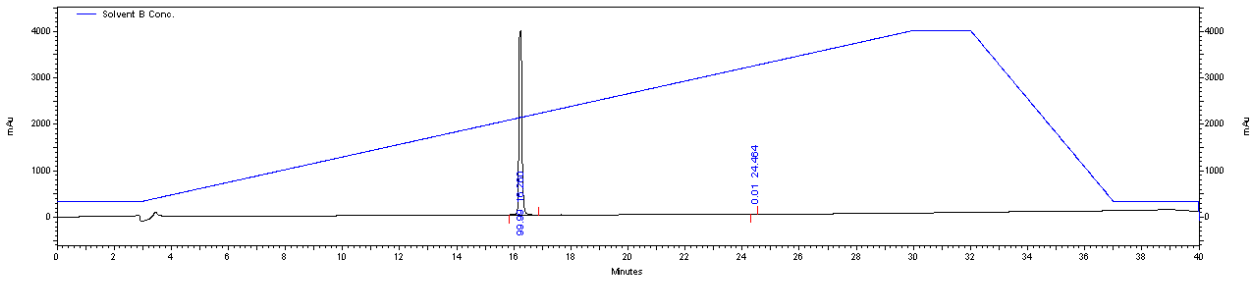
AIP-III D-S10



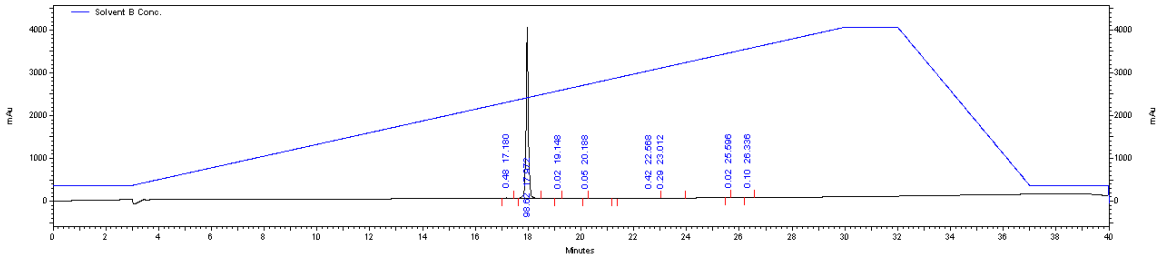
AIP-III D-Y11



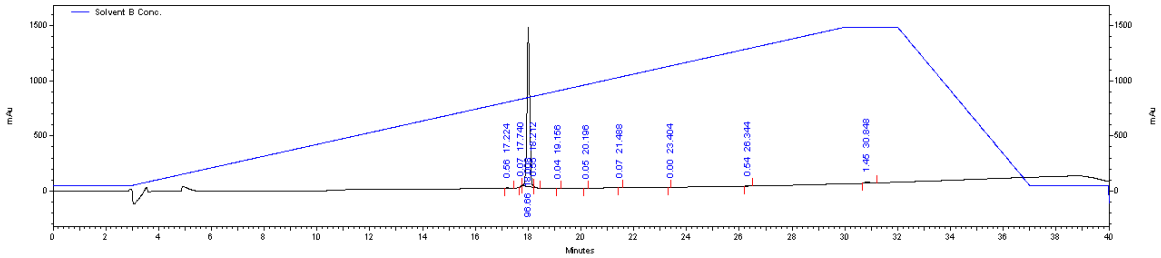
AIP-III D-L12



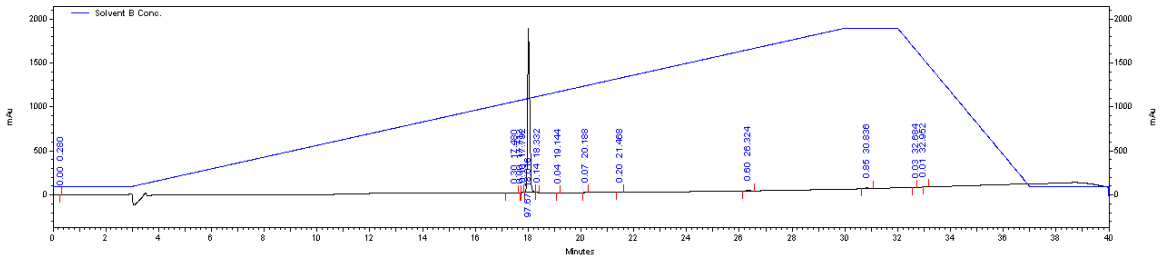
AIP-III 11aa



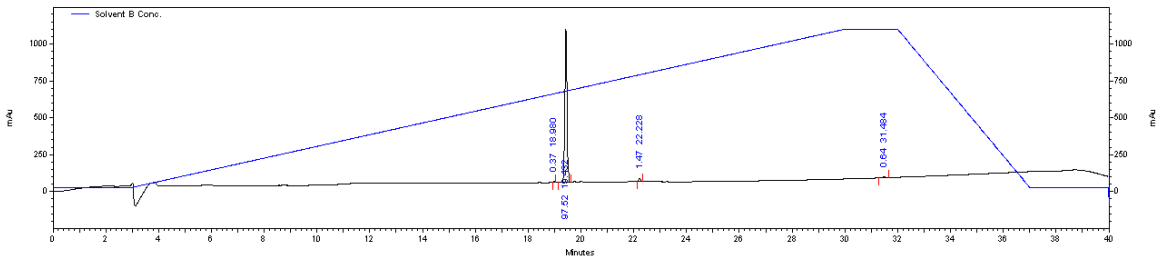
AIP-III 10aa



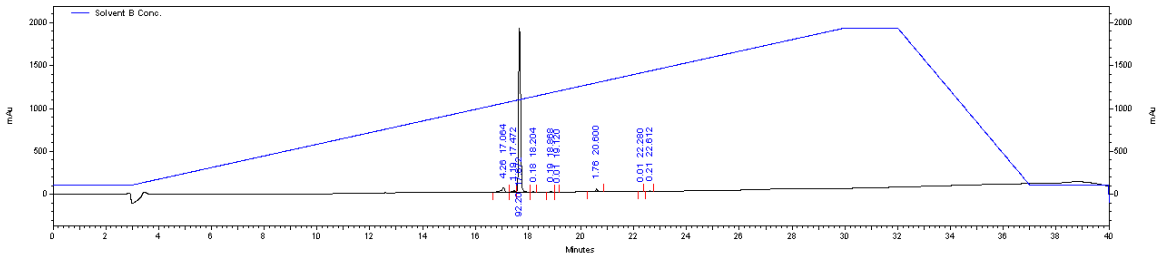
AIP-III 9aa



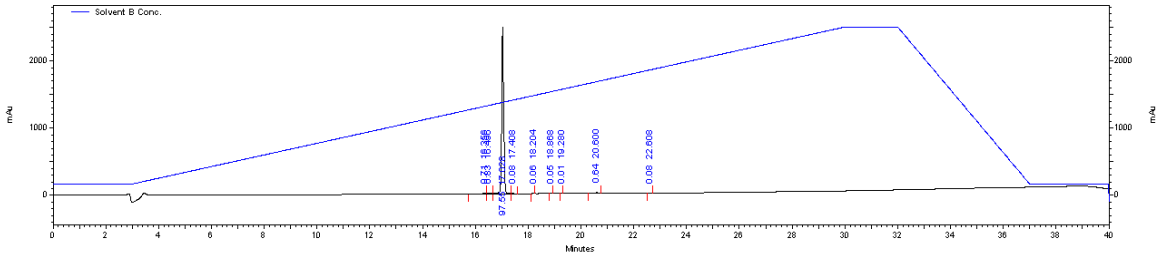
AIP-III 8aa



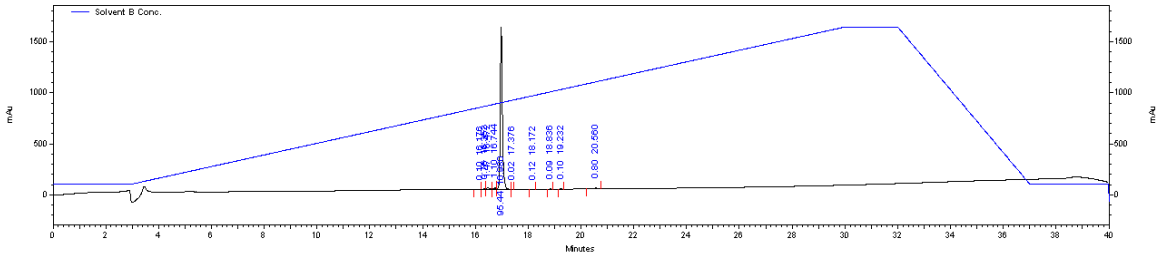
AIPII9aaN3L



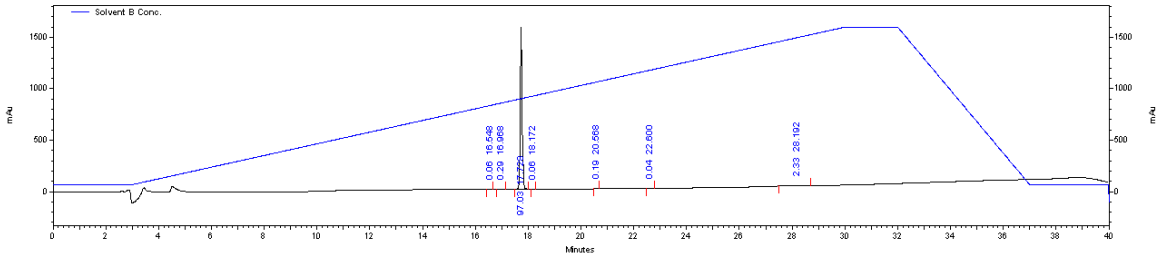
AIPII9aaN3V



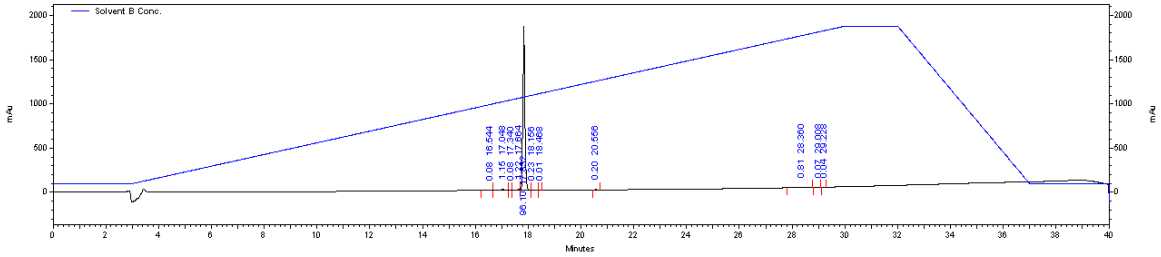
AIPII9aaP4V



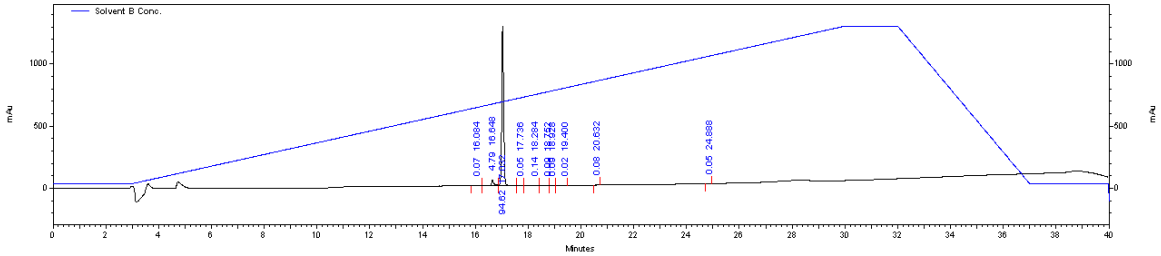
AIPII9aaP4L



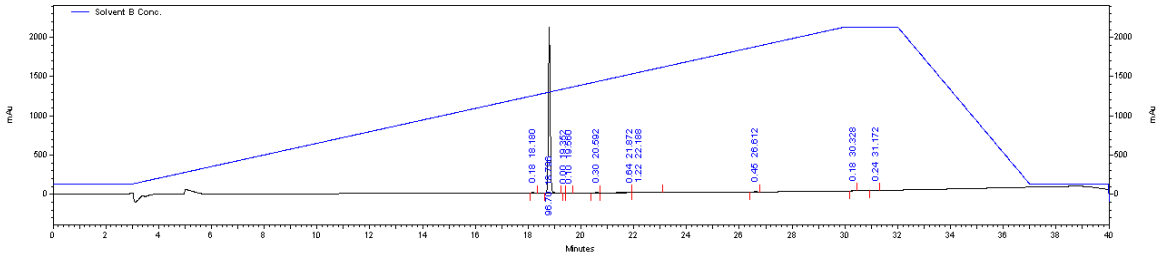
AIPII9aaP4Vtail AIPIring



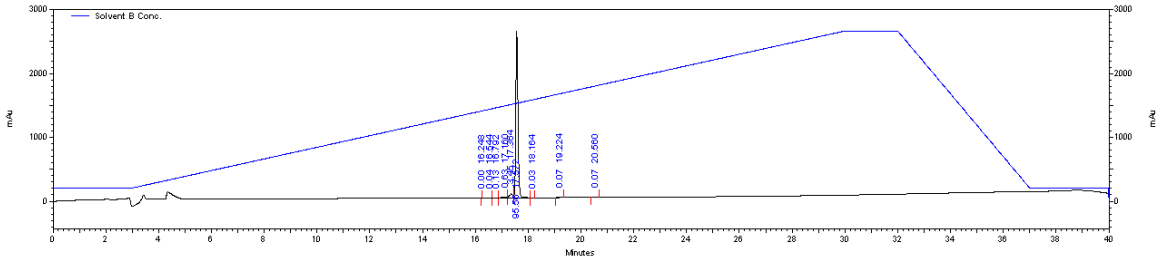
AIPItail AIPIIring



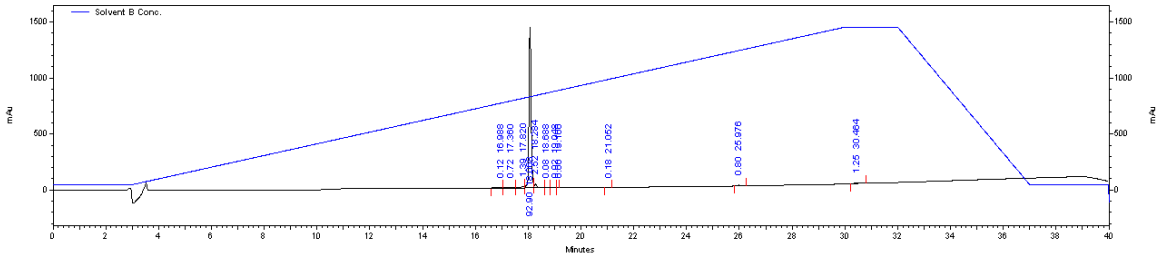
AIPItail AIPIIIring



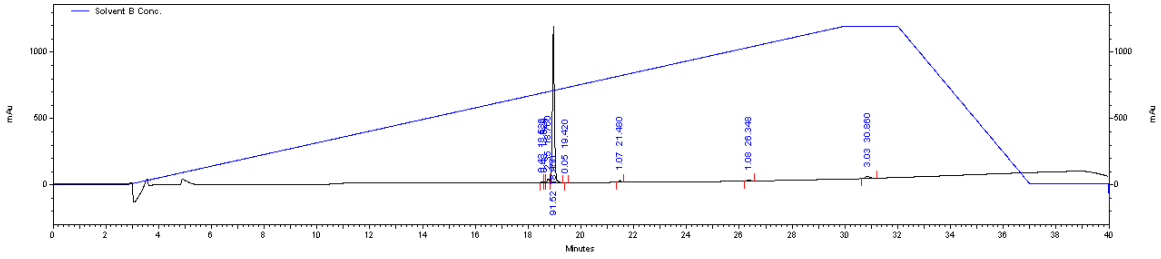
AIPII9aatail AIPIring



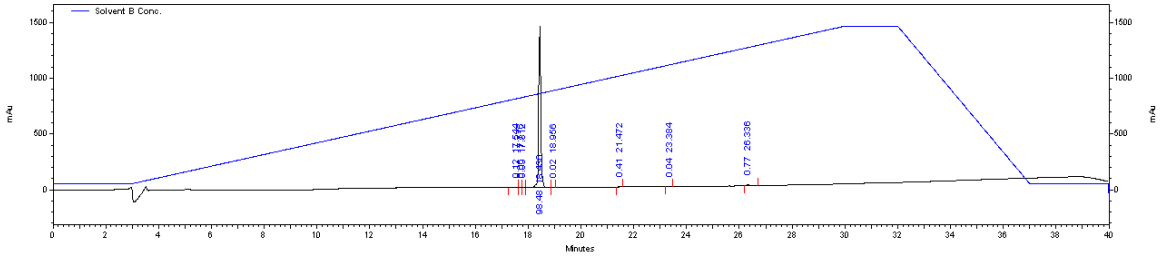
AIPII9aaP4Vtail AIPIringA6S



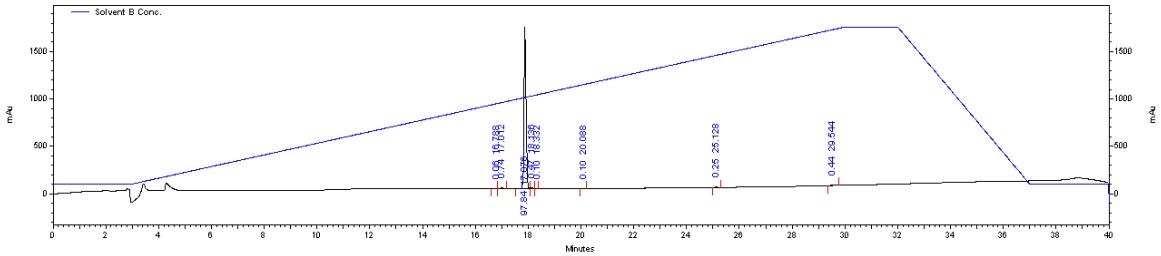
AIPII9aaP4Vtail AIPIringA6SS7A



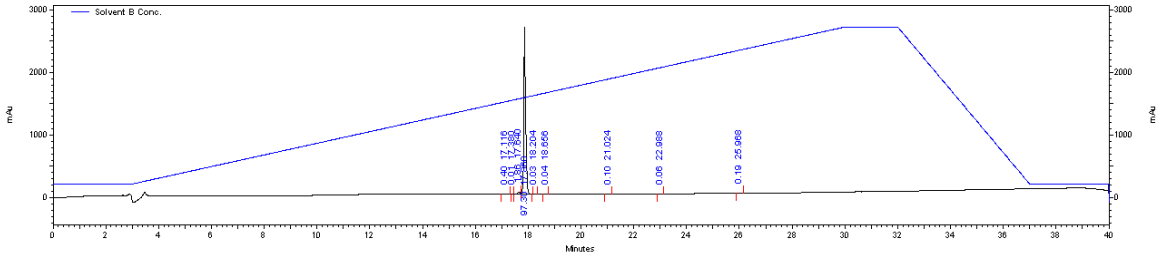
AIPII9aaP4Vtail AIPIringS7N



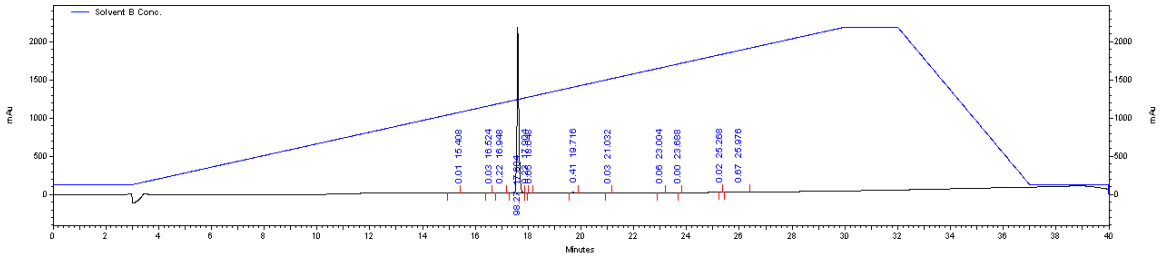
AIPII9aaP4Vtail AIPIringS7A



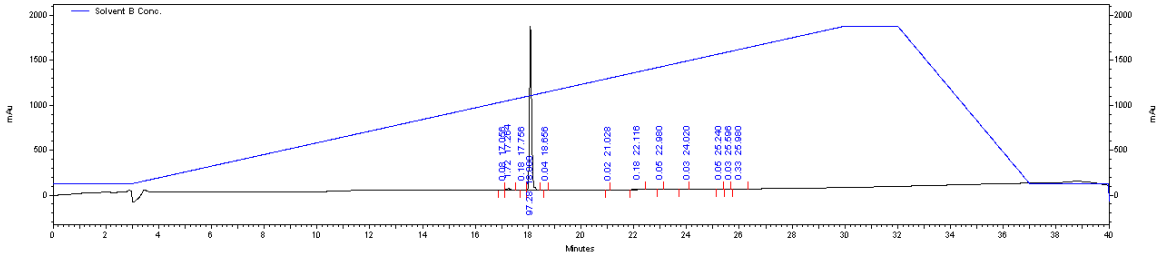
AIPII9aaP4Vtail AIPIringF9L



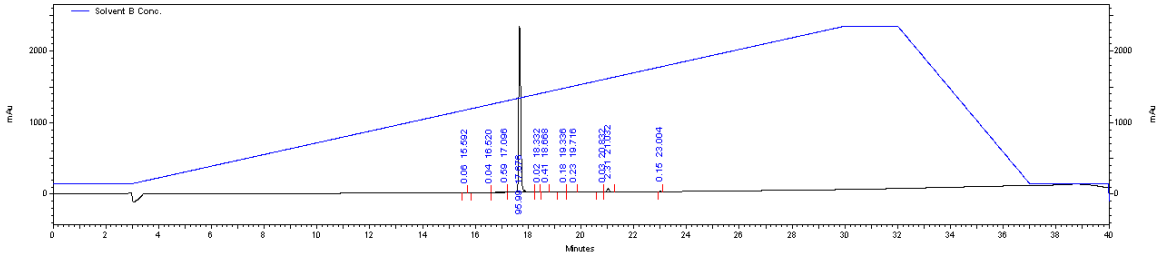
AIPII9aaP4VS6A



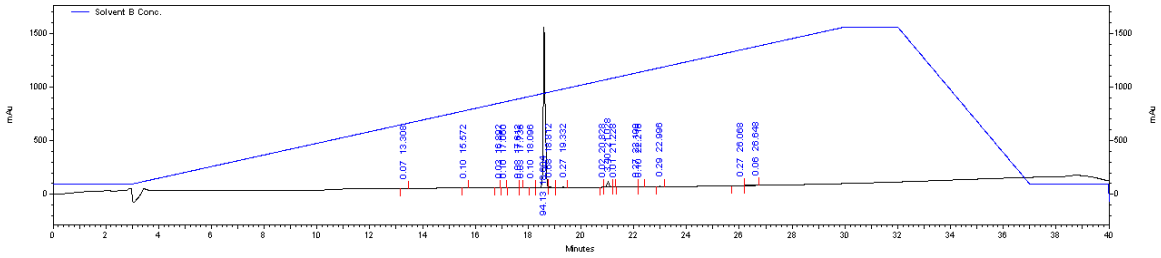
AIPII9aaP4VN7A



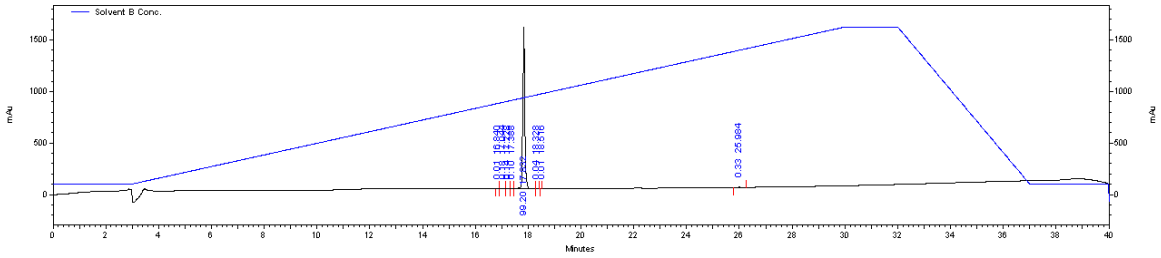
AIPII9aaP4VN7S



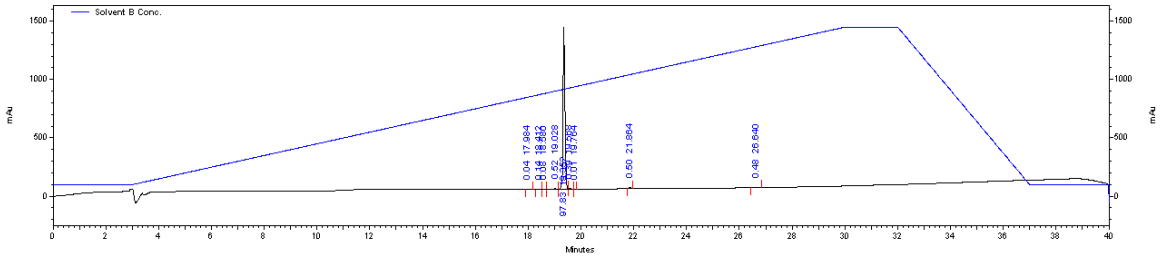
AlPII9aaP4VS6AN7A



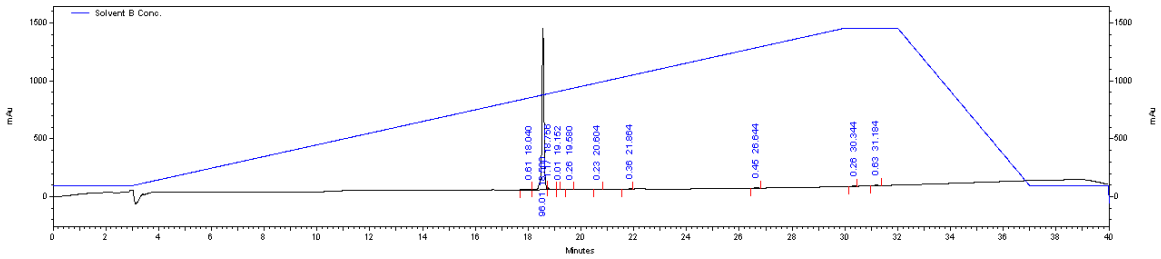
AlPII9aaP4VL9F



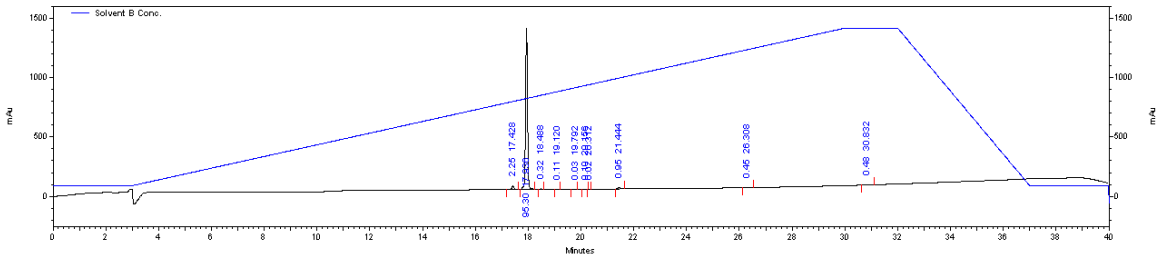
AlPII9aaP4VN7α



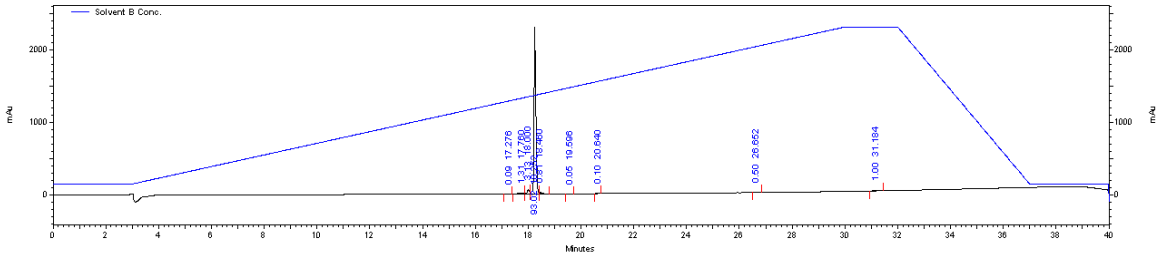
AlPII9aaP4VS6α



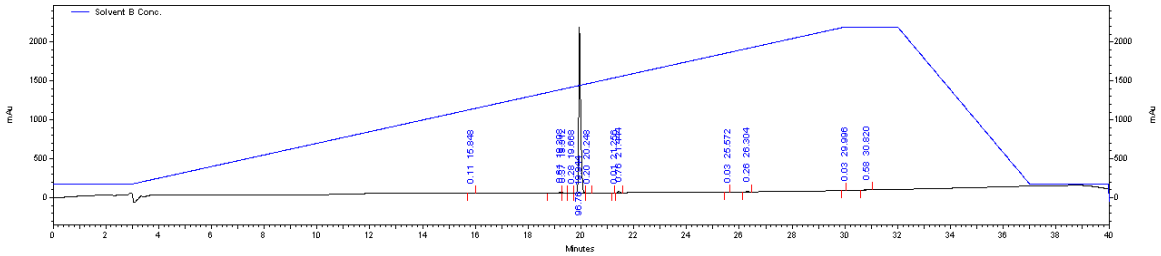
AlPII9aaP4VS6G



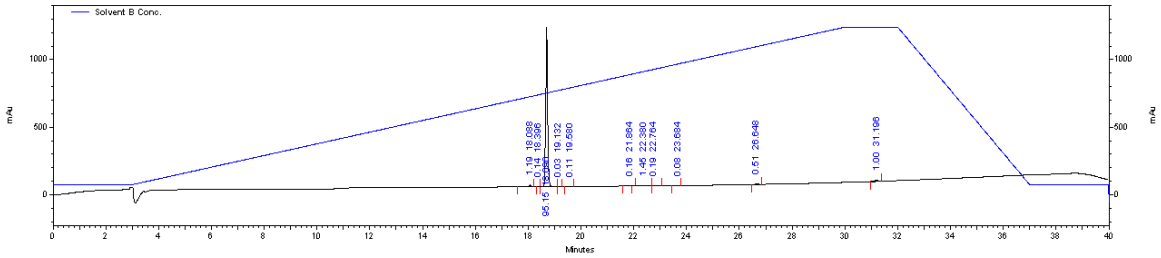
AIPII9aaP4VS6T



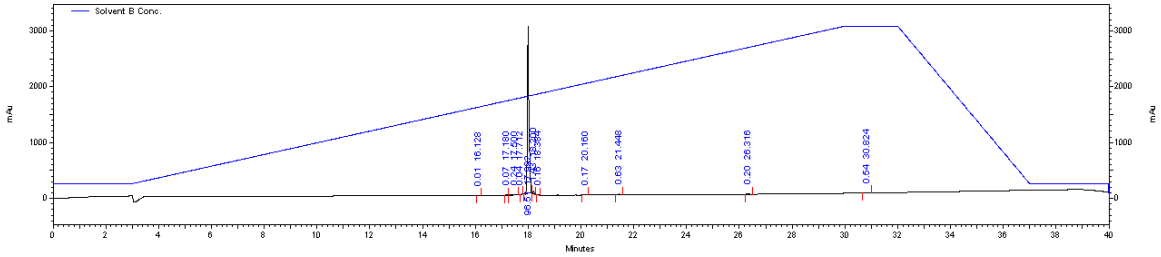
AIPII9aaP4VN7L



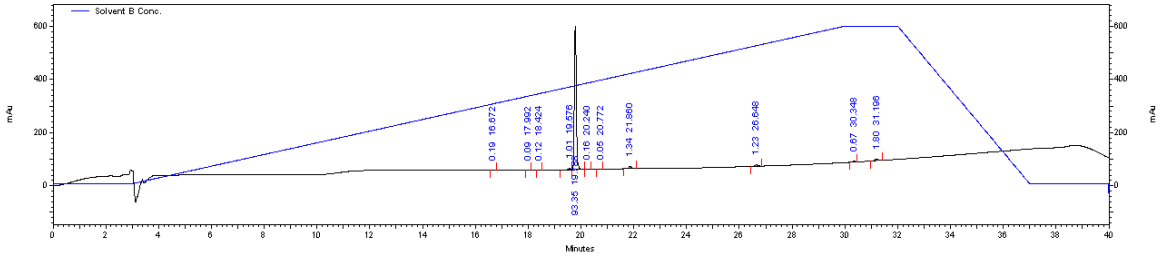
AIPII9aaP4VN7T



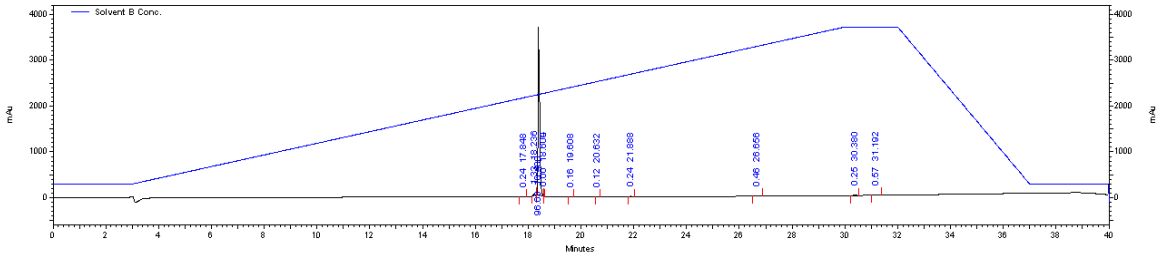
AIPII9aaP4VN7G



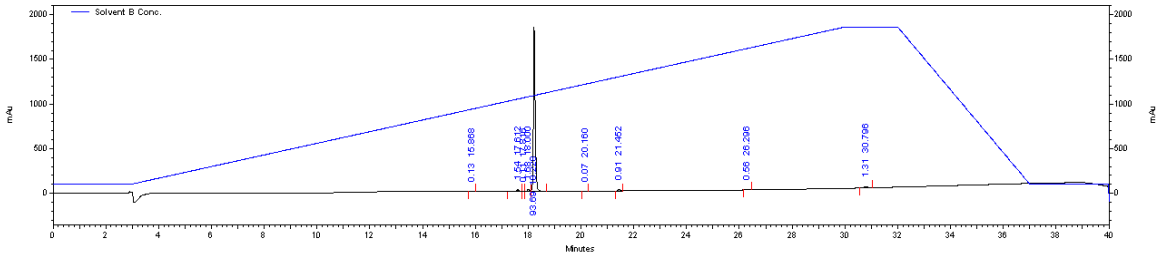
AIPII9aaP4VN7V



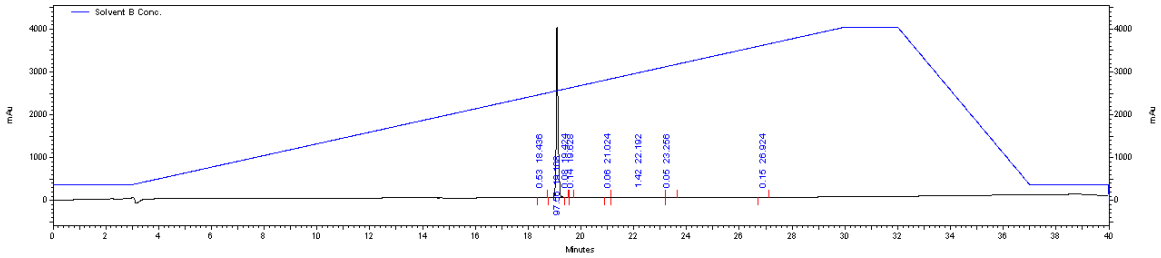
AIPII9aaP4VN7Q



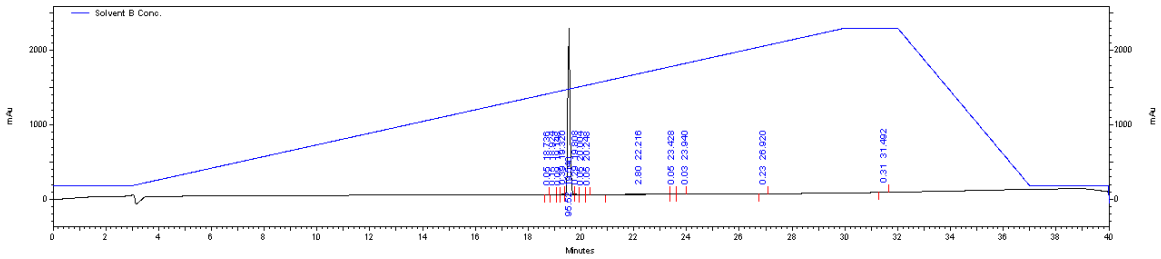
AIPII9aaP4VN7D



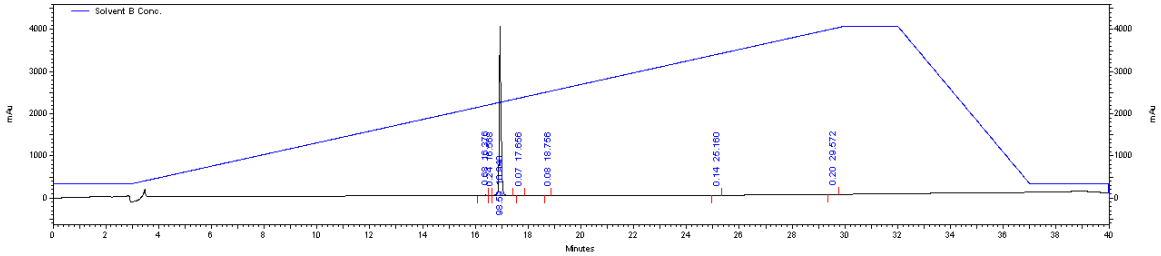
AIPII9aatail AIPIringA6S



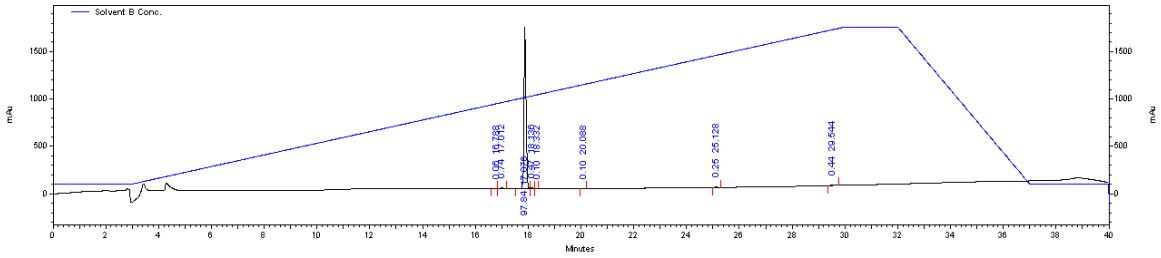
AIPII9aatail AIPIringA6SS7A



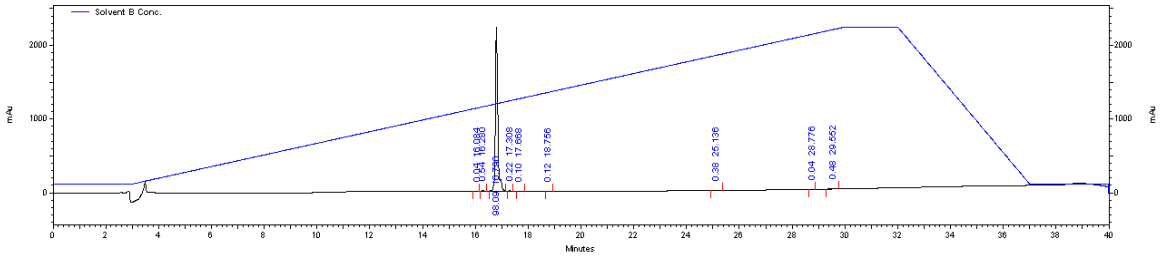
AIPII9aatail AIPIringS7N



AIPII9aatail AIPIringS7A



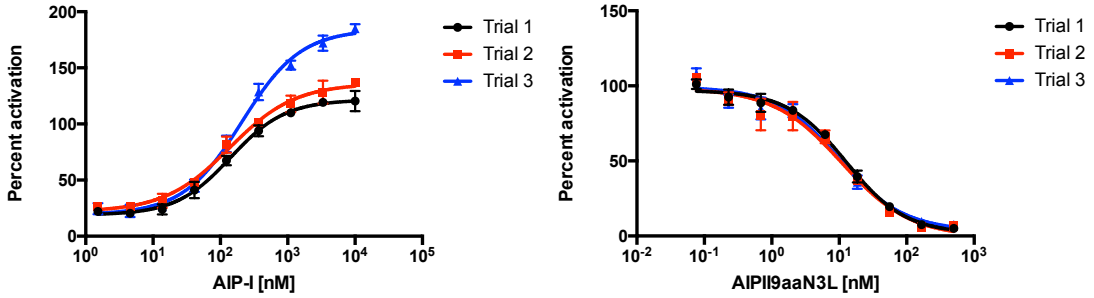
AIPII9aatail AIPIringA6SS7N

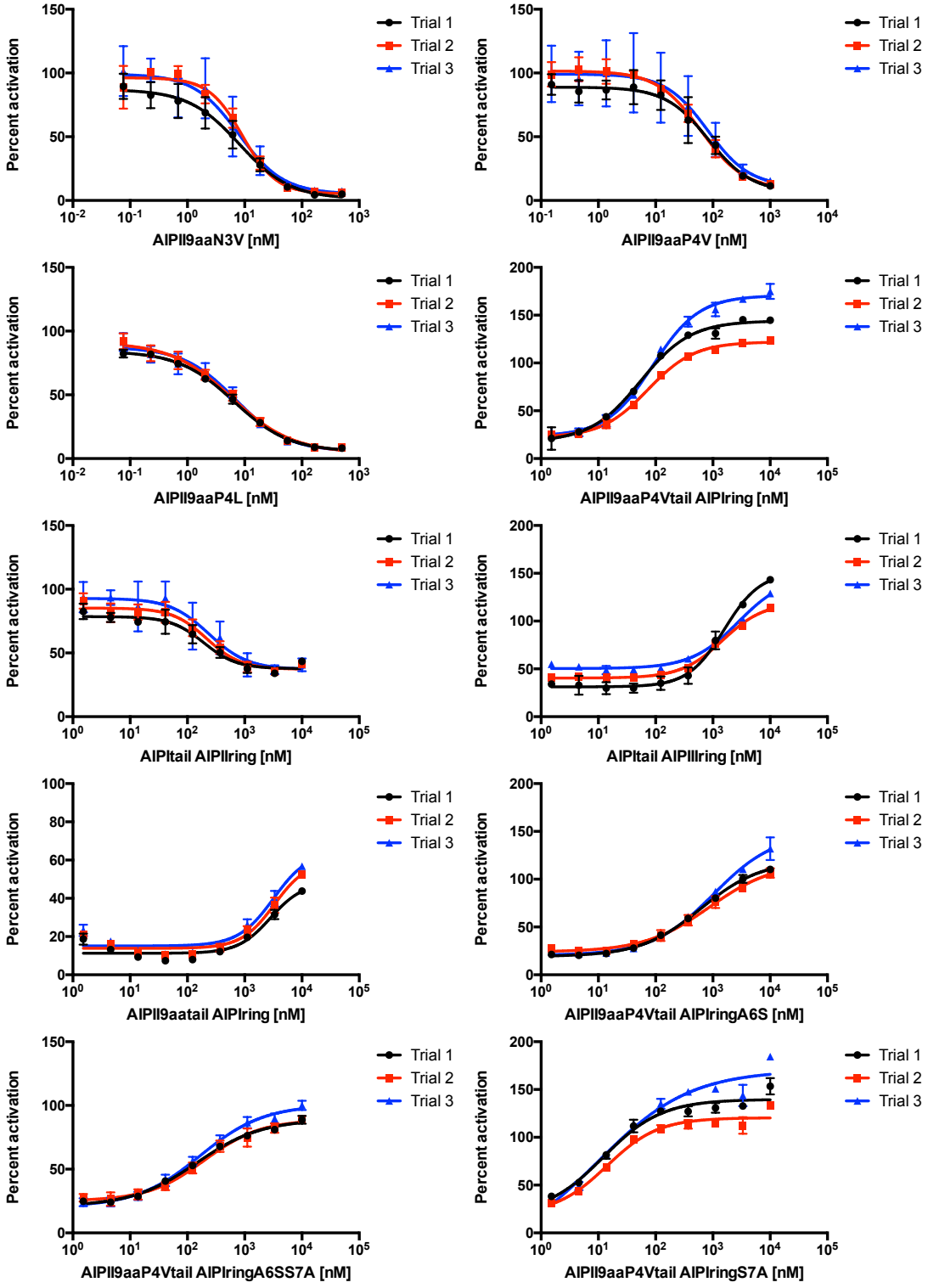


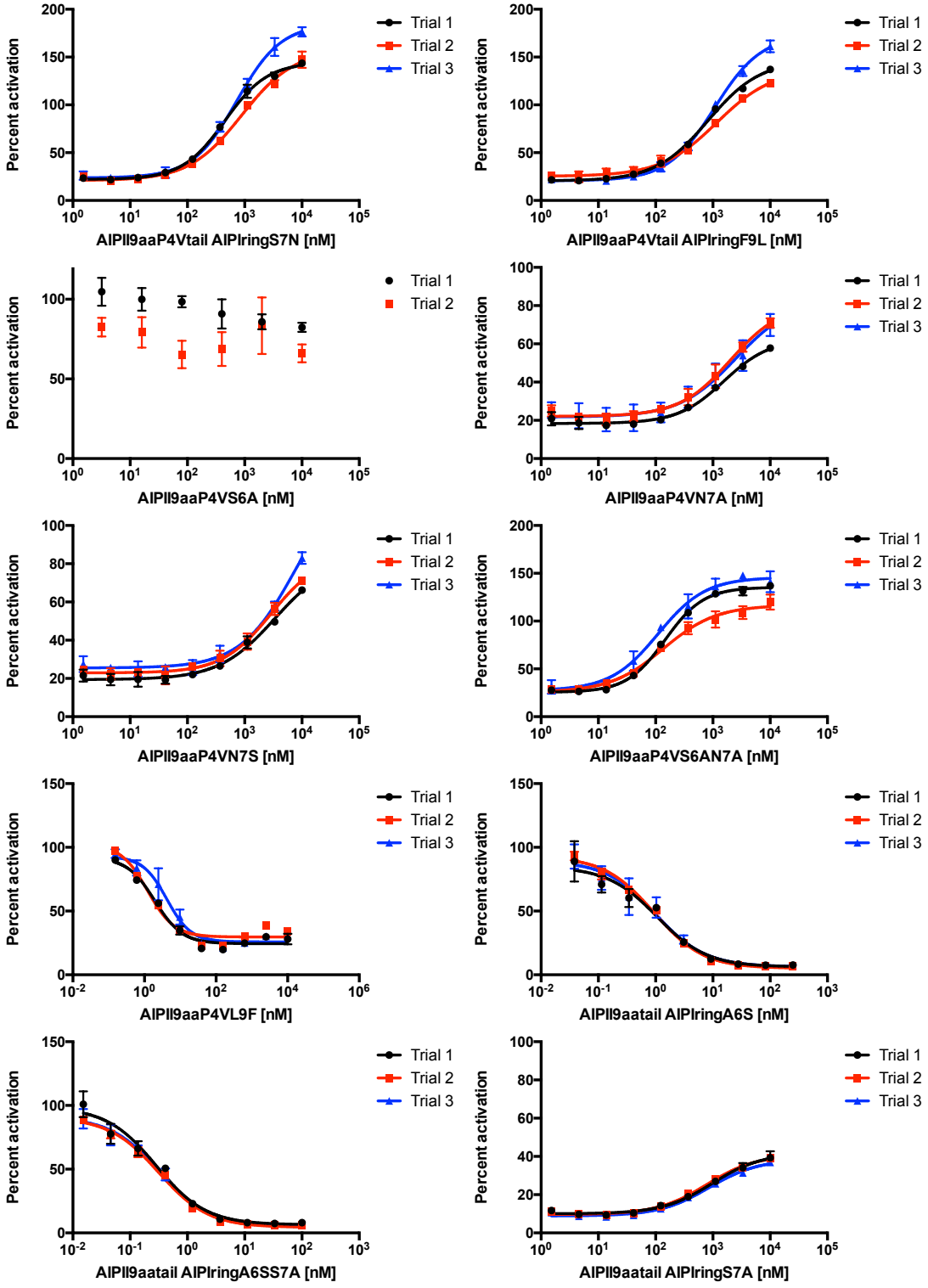
4.6.3 S. epidermidis AgrC fluorescence dose-response curves

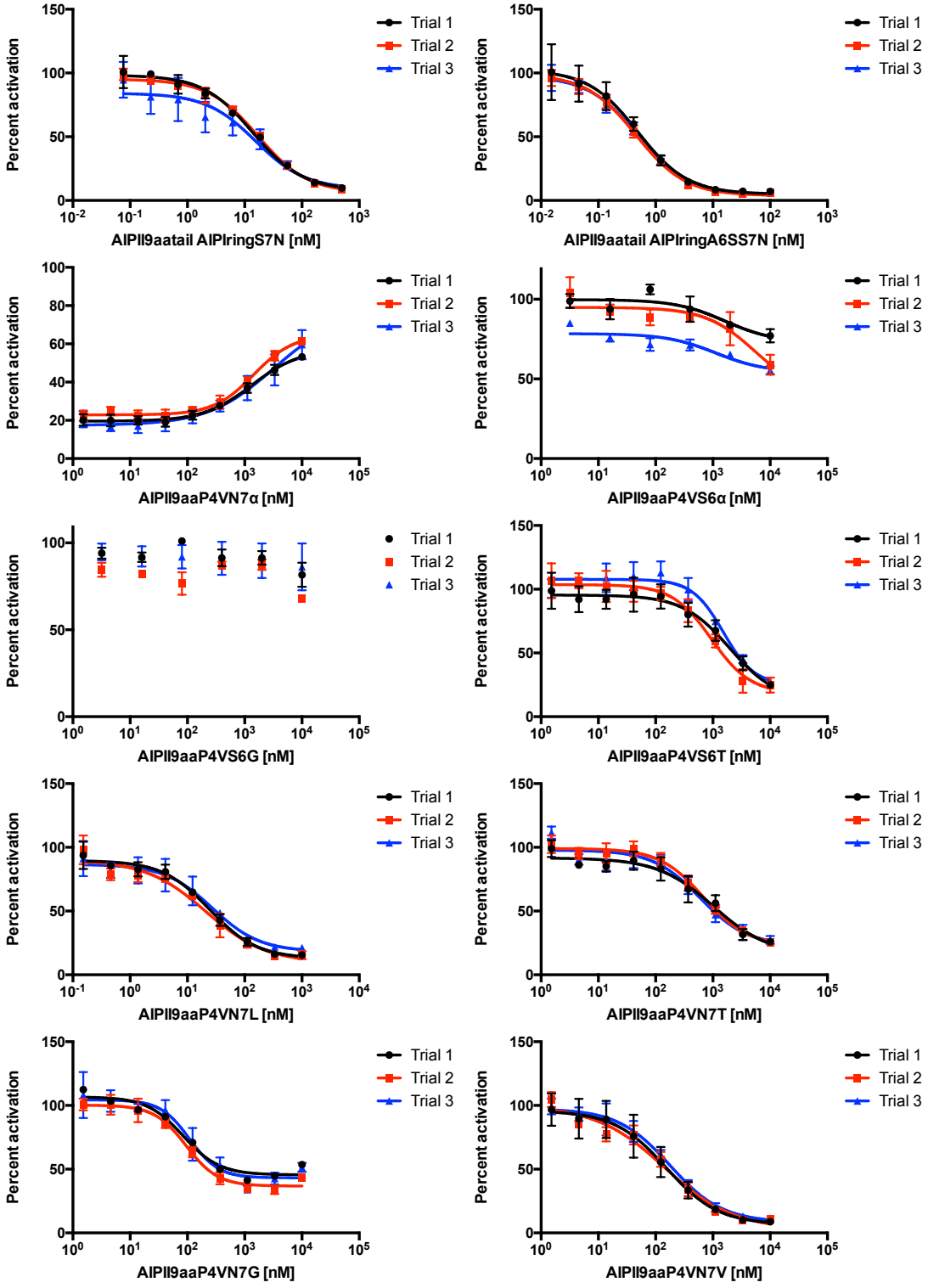
The analogs were assayed over increasing concentrations in the S. epidermidis fluorescence reporter strains for AgrC receptor agonism and antagonism (see main text for details). Agonism dose-response curves were obtained with the addition known inhibitor against the receptor of interest to block receptor activation by endogenous AIPs. Three biological replicates were shown; error bars represent standard deviation of three technical replicates within each biological replicate. Percent activation was normalized to a DMSO control.

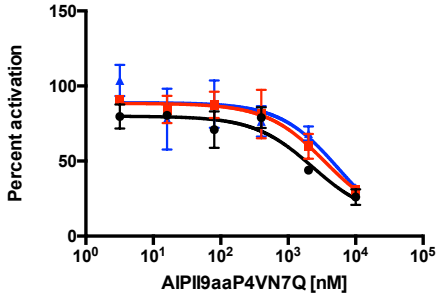
S. epidermidis AH3408 (Group I)

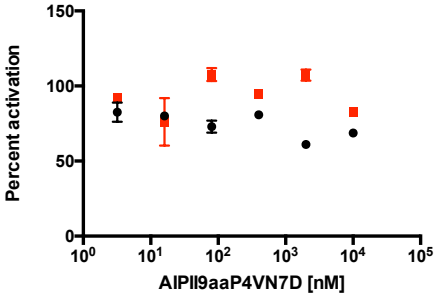



Percent activation
Trial 1
Trial 2
Trial 3
AlPII9aaN3V [nM]
AlPII9aaP4V [nM]
AlPII9aaP4L [nM]
AlPII9aaP4Vtail AlPIring [nM]
AlPItail AlPIIring [nM]
AlPItail AlPIIIring [nM]
AlPII9aatail AlPIring [nM]
AlPII9aaP4Vtail AlPIringA6S [nM]
AlPII9aaP4Vtail AlPIringA6SS7A [nM]
AlPII9aaP4Vtail AlPIringS7A [nM]

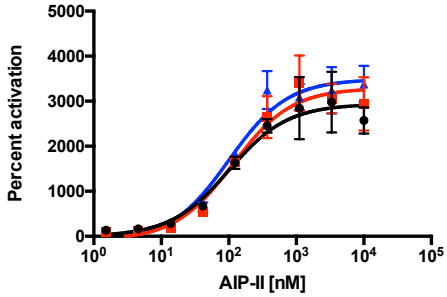

Percent activation
AIPII9aaP4Vtail AIPIringS7N [nM]
AIPII9aaP4Vtail AIPIringF9L [nM]
AIPII9aaP4VS6A [nM]
AIPII9aaP4VN7A [nM]
AIPII9aaP4VN7S [nM]
AIPII9aaP4VS6AN7A [nM]
AIPII9aaP4VL9F [nM]
AIPII9aatail AIPIringA6S [nM]
AIPII9aatail AIPIringA6SS7A [nM]
AIPII9aatail AIPIringS7A [nM]
Trial 1
Trial 2
Trial 3

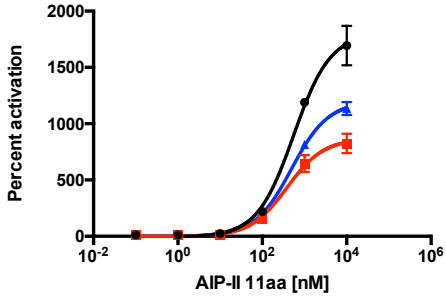

Percent activation
Trial 1
Trial 2
Trial 3
AIPII9aatail AIPIringS7N [nM]
AIPII9aatail AIPIringA6SS7N [nM]
AIPII9aaP4VN7α [nM]
AIPII9aaP4VS6α [nM]
AIPII9aaP4VS6G [nM]
AIPII9aaP4VS6T [nM]
AIPII9aaP4VN7L [nM]
AIPII9aaP4VN7T [nM]
AIPII9aaP4VN7G [nM]
AIPII9aaP4VN7V [nM]

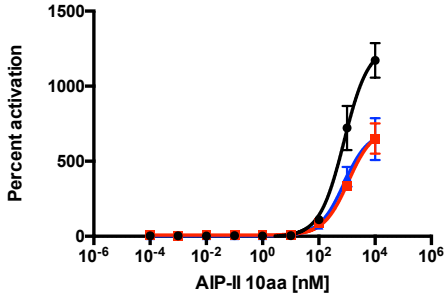


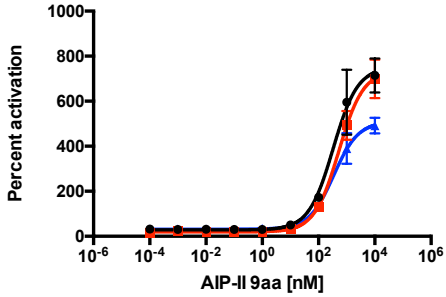


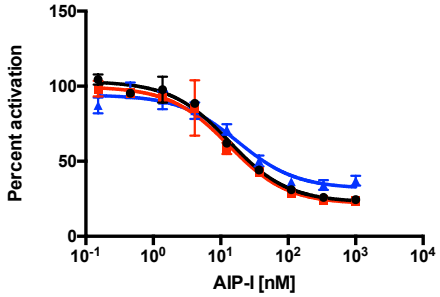
S. epidermidis AH3567 (Group II)

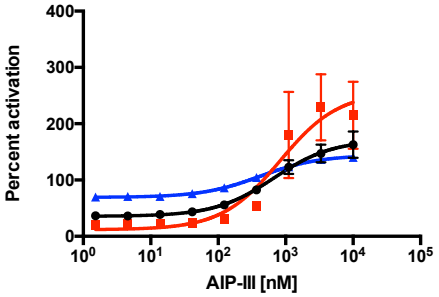


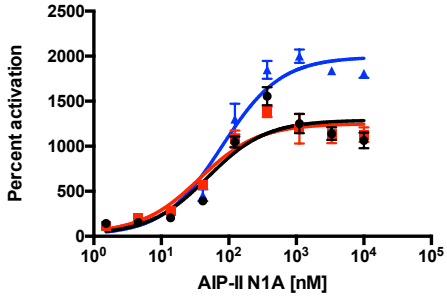


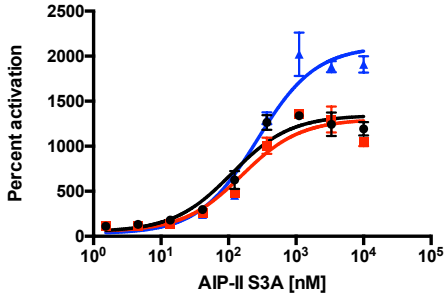


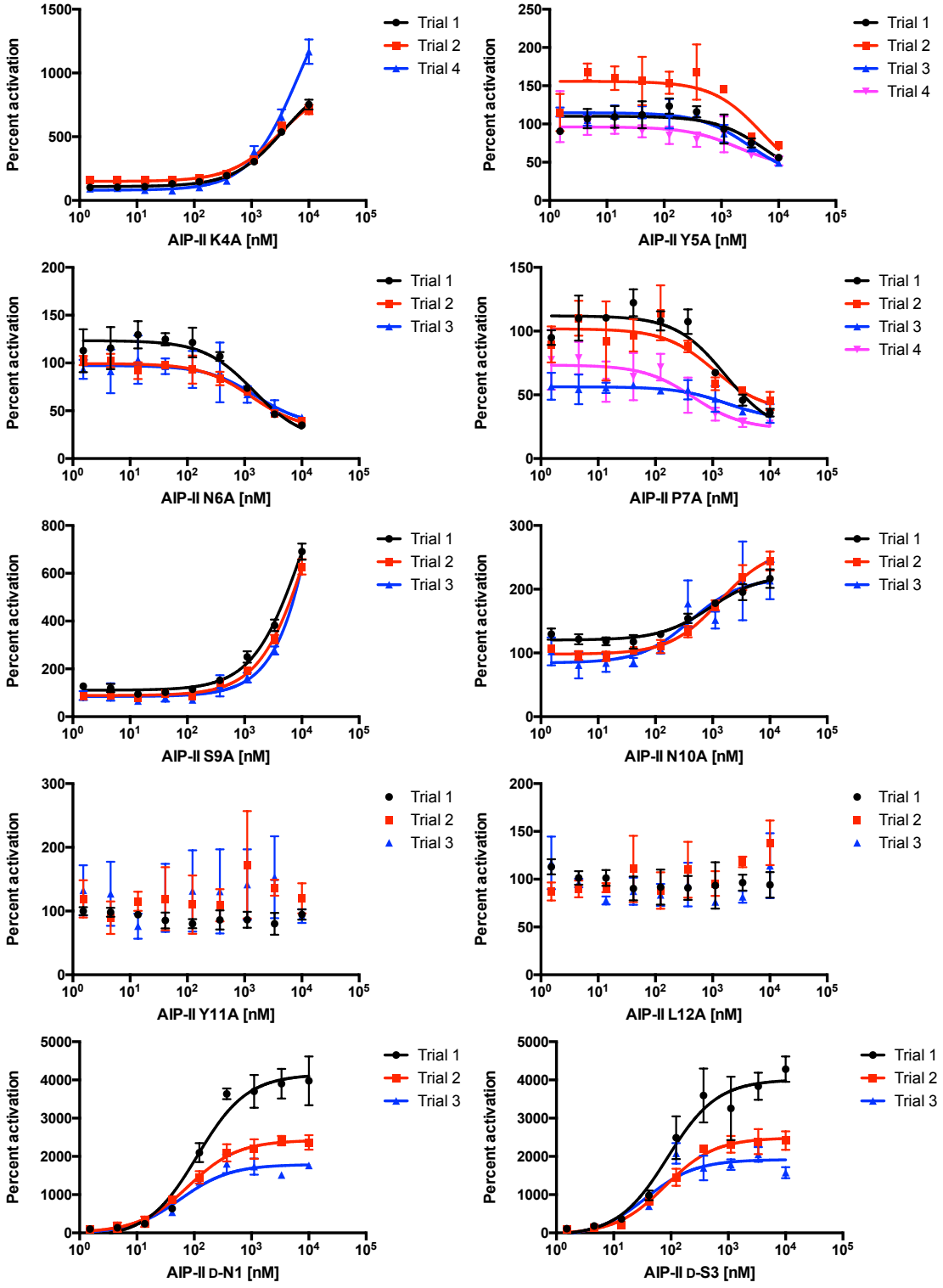


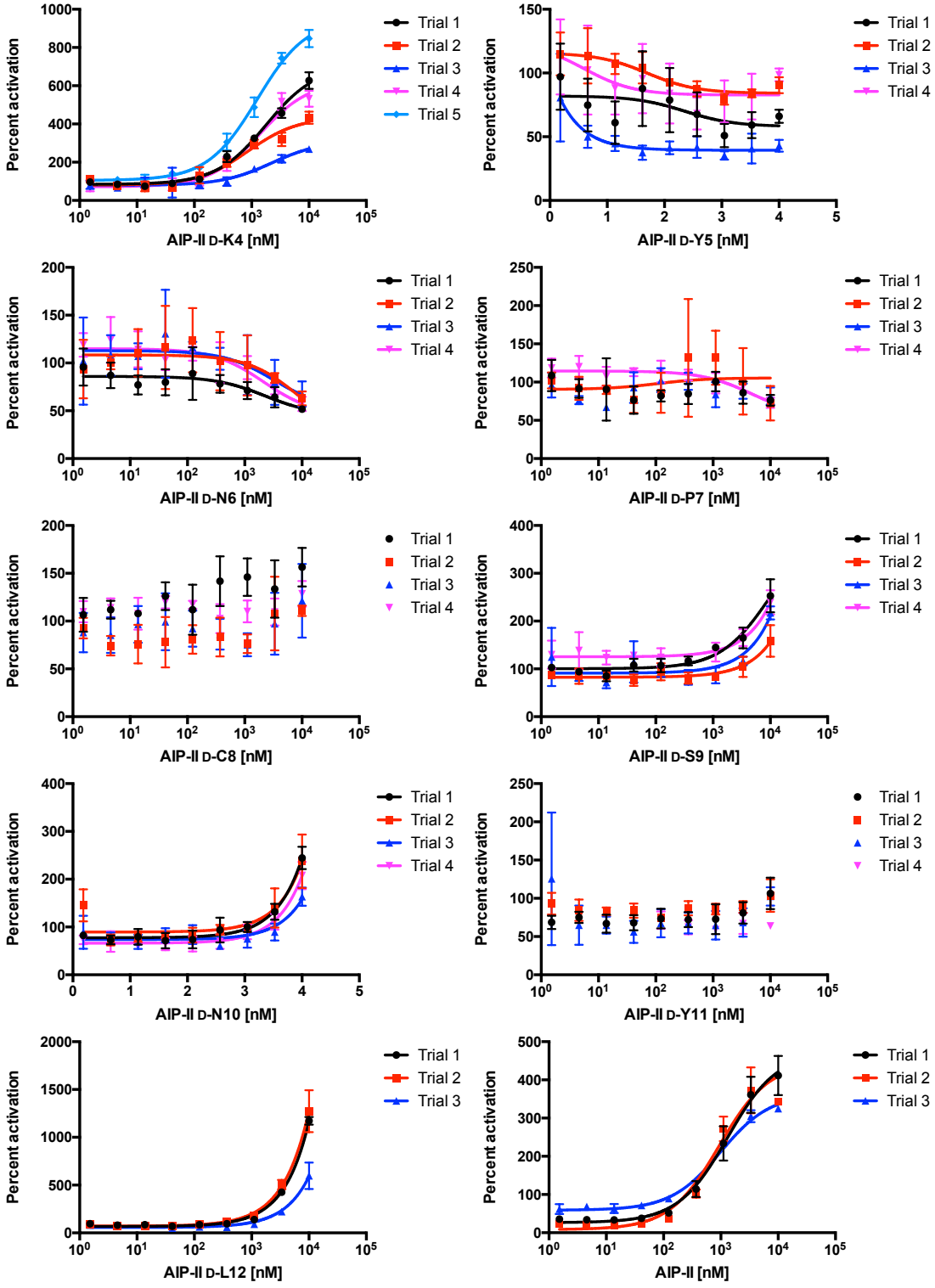


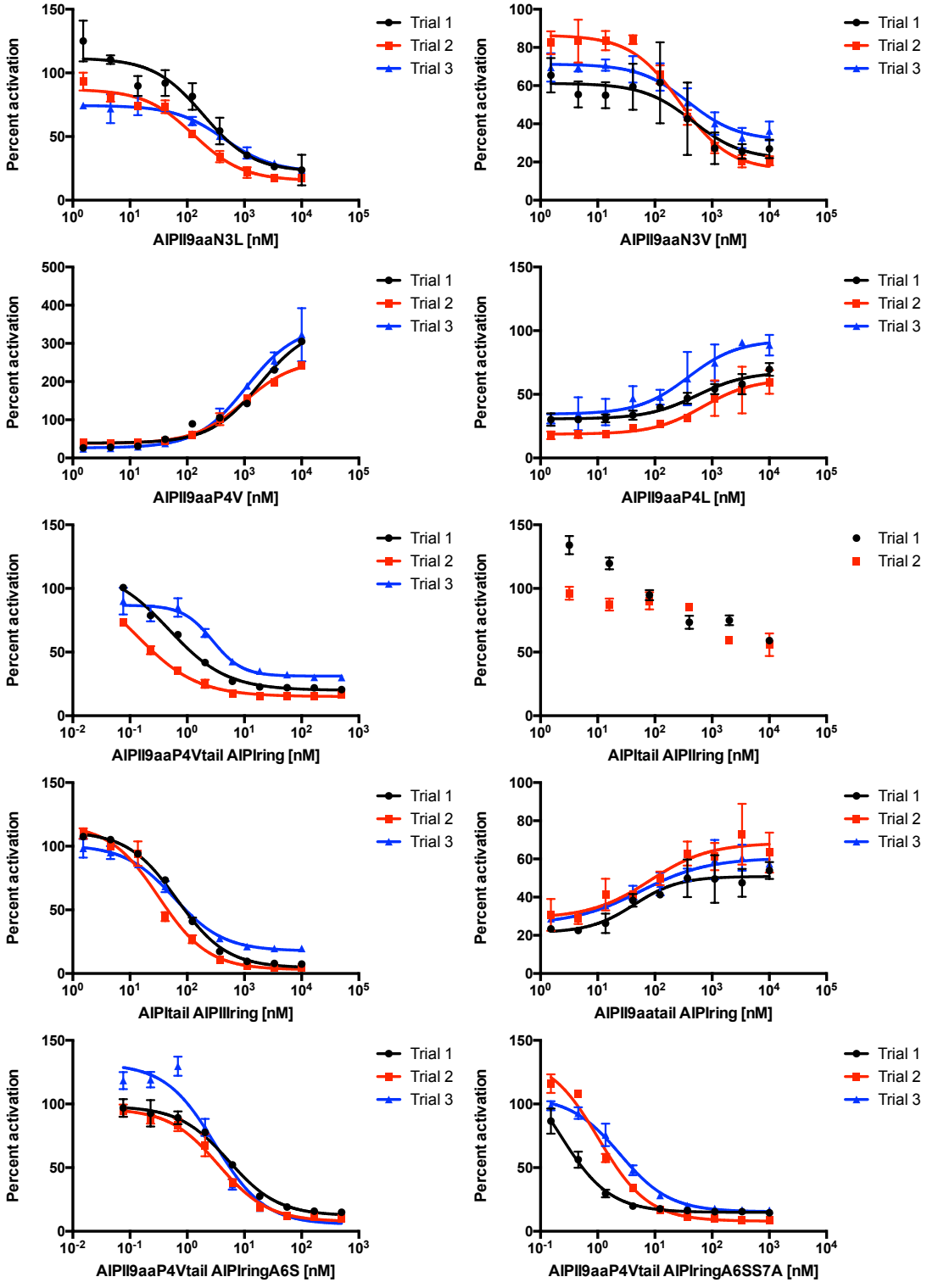


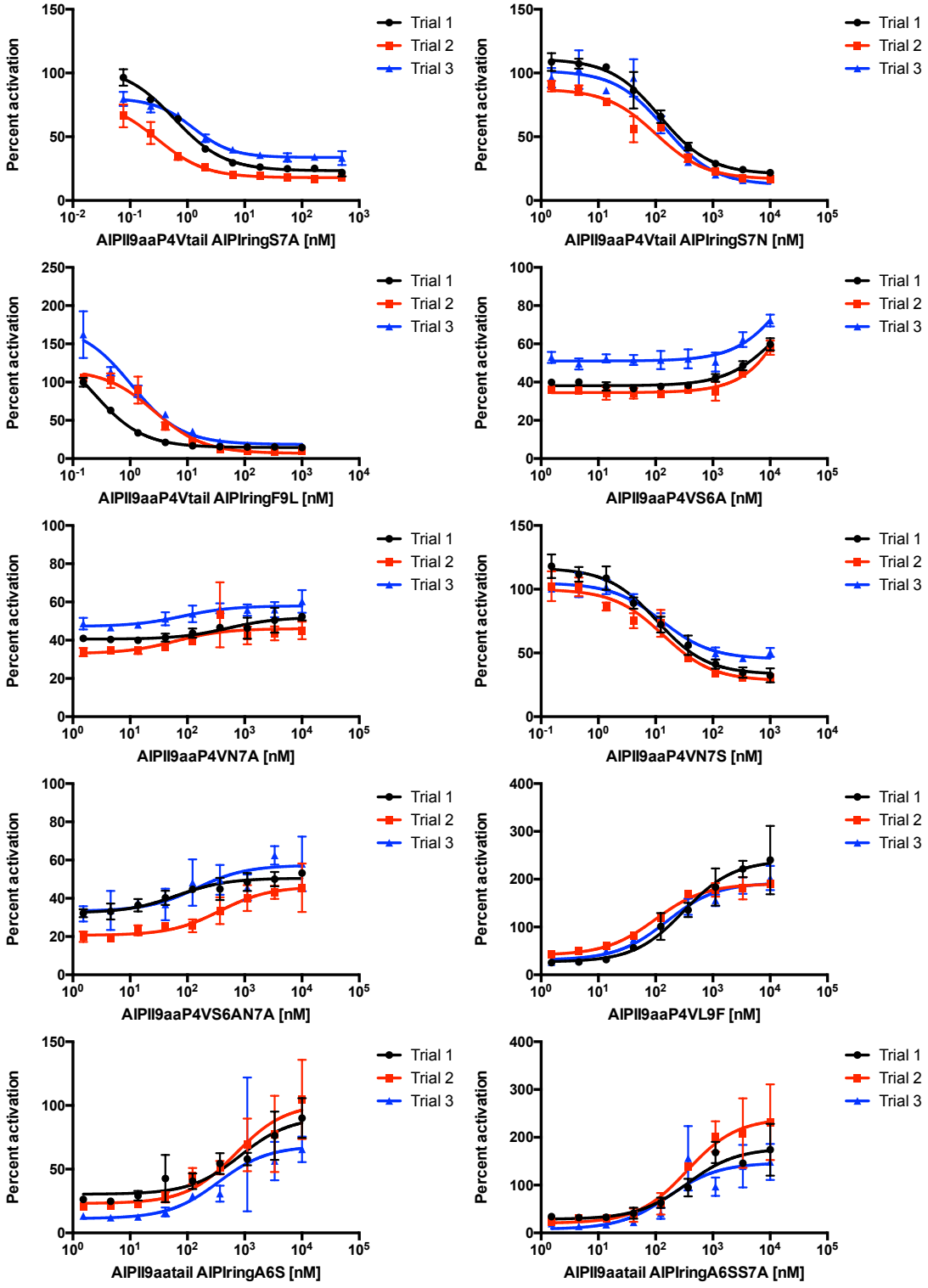


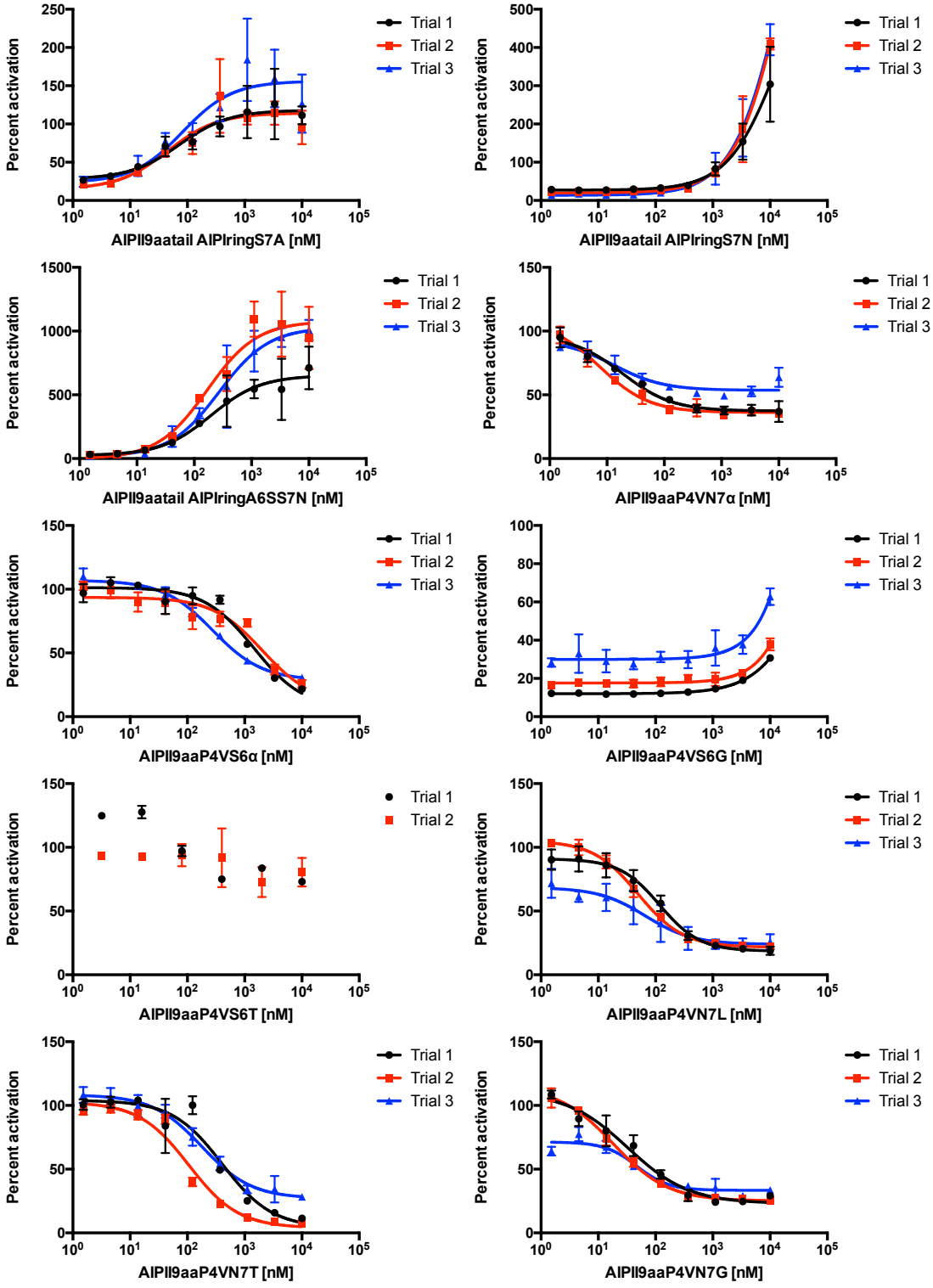


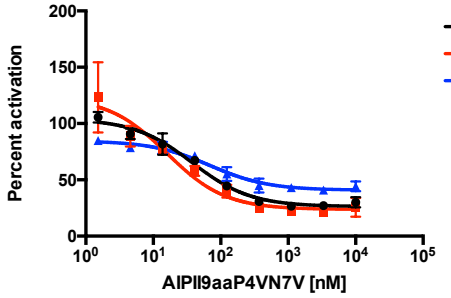

Percent activation
AIP-II K4A [nM]
AIP-II Y5A [nM]
AIP-II N6A [nM]
AIP-II P7A [nM]
AIP-II S9A [nM]
AIP-II N10A [nM]
AIP-II Y11A [nM]
AIP-II L12A [nM]
AIP-II D-N1 [nM]
AIP-II D-S3 [nM]
Trial 1
Trial 2
Trial 3
Trial 4

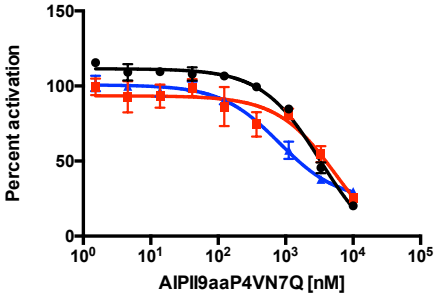

Percent activation
AIP-II D-K4 [nM]
Trial 1
Trial 2
Trial 3
Trial 4
Trial 5
AIP-II D-Y5 [nM]
AIP-II D-N6 [nM]
AIP-II D-P7 [nM]
AIP-II D-C8 [nM]
AIP-II D-S9 [nM]
AIP-II D-N10 [nM]
AIP-II D-Y11 [nM]
AIP-II D-L12 [nM]
AIP-II [nM]

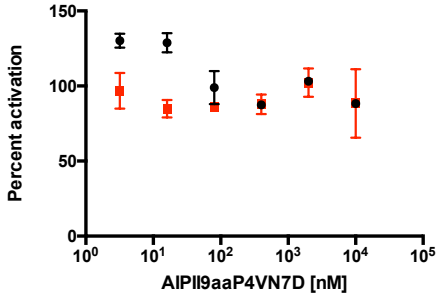

Percent activation
Trial 1
Trial 2
Trial 3
AIPII9aaN3L [nM]
AIPII9aaN3V [nM]
AIPII9aaP4V [nM]
AIPII9aaP4L [nM]
AIPII9aaP4Vtail AIPIring [nM]
AIPItail AIPIIring [nM]
AIPII9aatail AIPIring [nM]
AIPII9aaP4Vtail AIPIringA6S [nM]
AIPII9aaP4Vtail AIPIringA6SS7A [nM]


Percent activation
Trial 1
Trial 2
Trial 3
AIPII9aaP4Vtail AIPIringS7A [nM]
AIPII9aaP4Vtail AIPIringS7N [nM]
AIPII9aaP4Vtail AIPIringF9L [nM]
AIPII9aaP4VS6A [nM]
AIPII9aaP4VN7A [nM]
AIPII9aaP4VN7S [nM]
AIPII9aaP4VS6AN7A [nM]
AIPII9aaP4VL9F [nM]
AIPII9aatail AIPIringA6S [nM]
AIPII9aatail AIPIringA6SS7A [nM]

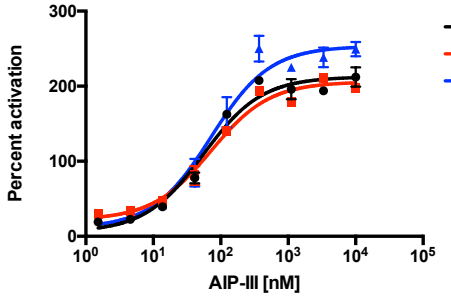

Percent activation
AlPII9aatail AlPIringS7A [nM]
AlPII9aatail AlPIringS7N [nM]
AlPII9aatail AlPIringA6SS7N [nM]
AlPII9aaP4VN7α [nM]
AlPII9aaP4VS6α [nM]
AlPII9aaP4VS6G [nM]
AlPII9aaP4VS6T [nM]
AlPII9aaP4VN7L [nM]
AlPII9aaP4VN7T [nM]
AlPII9aaP4VN7G [nM]
Trial 1
Trial 2
Trial 3

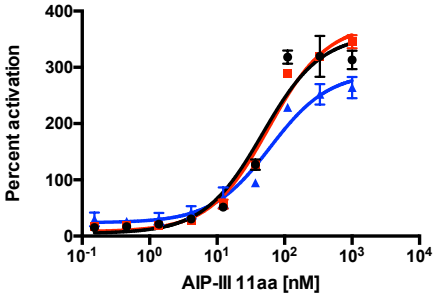


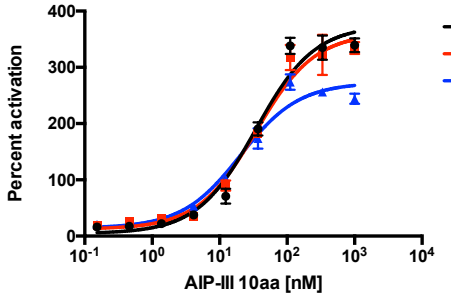


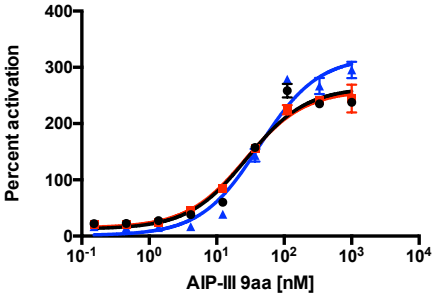


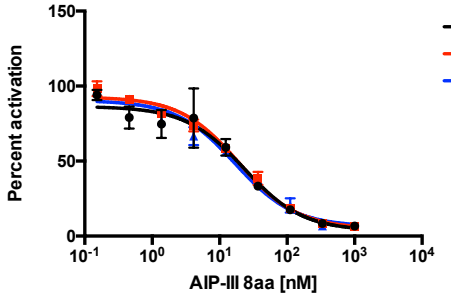
S. epidermidis AH3409 (Group III)

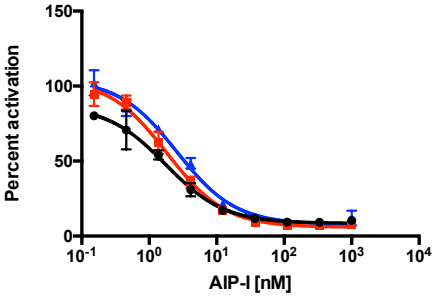


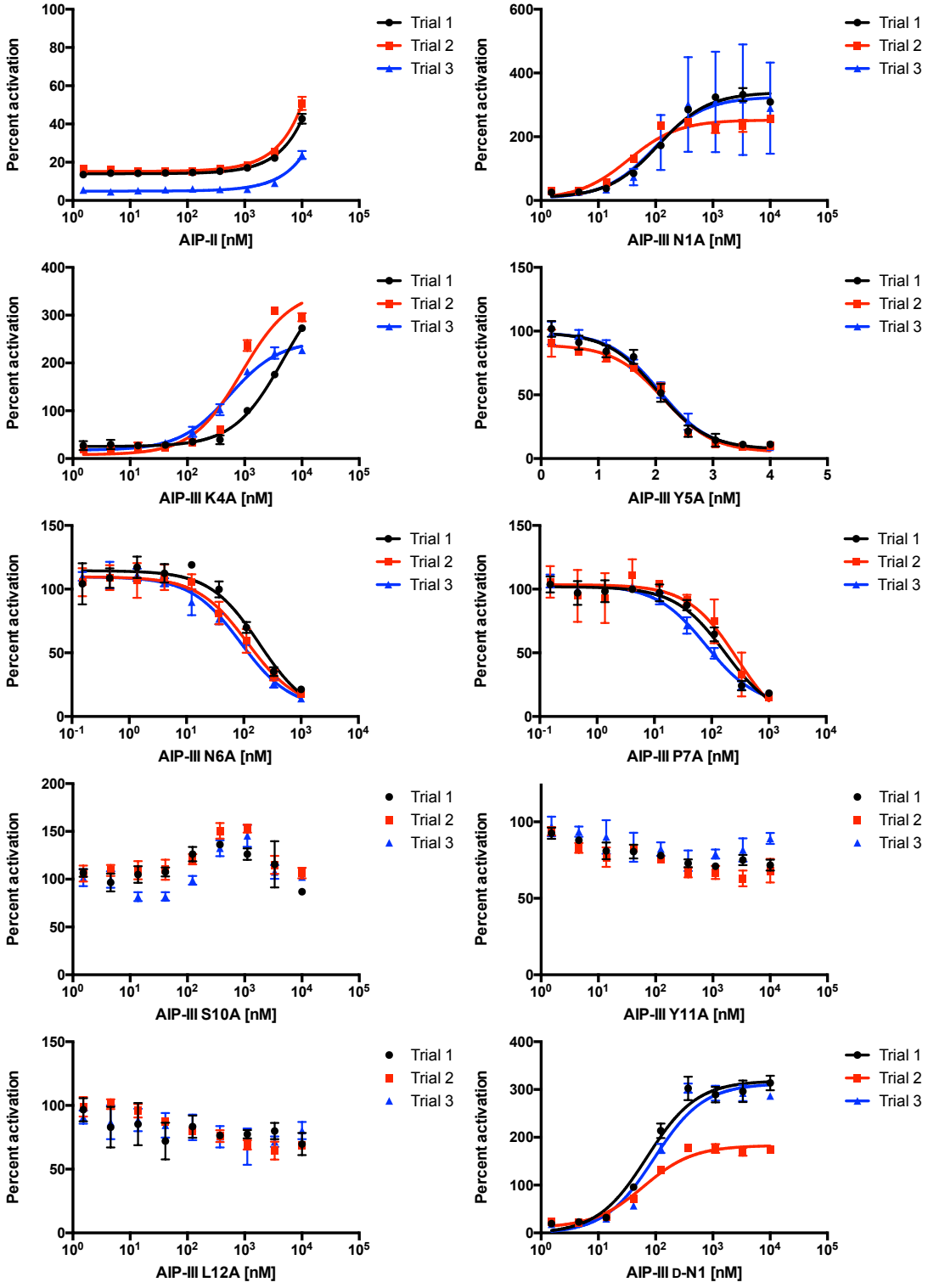


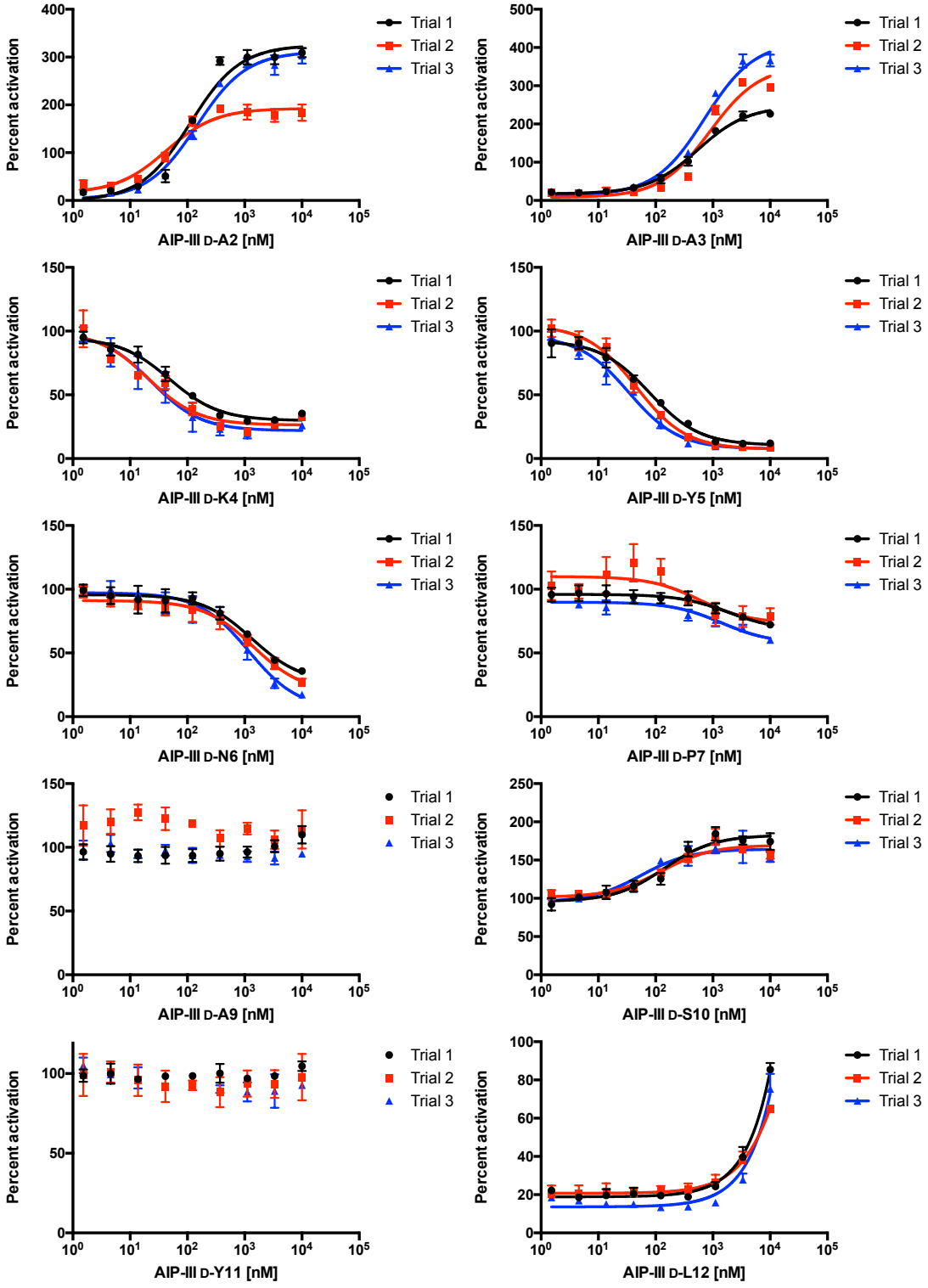


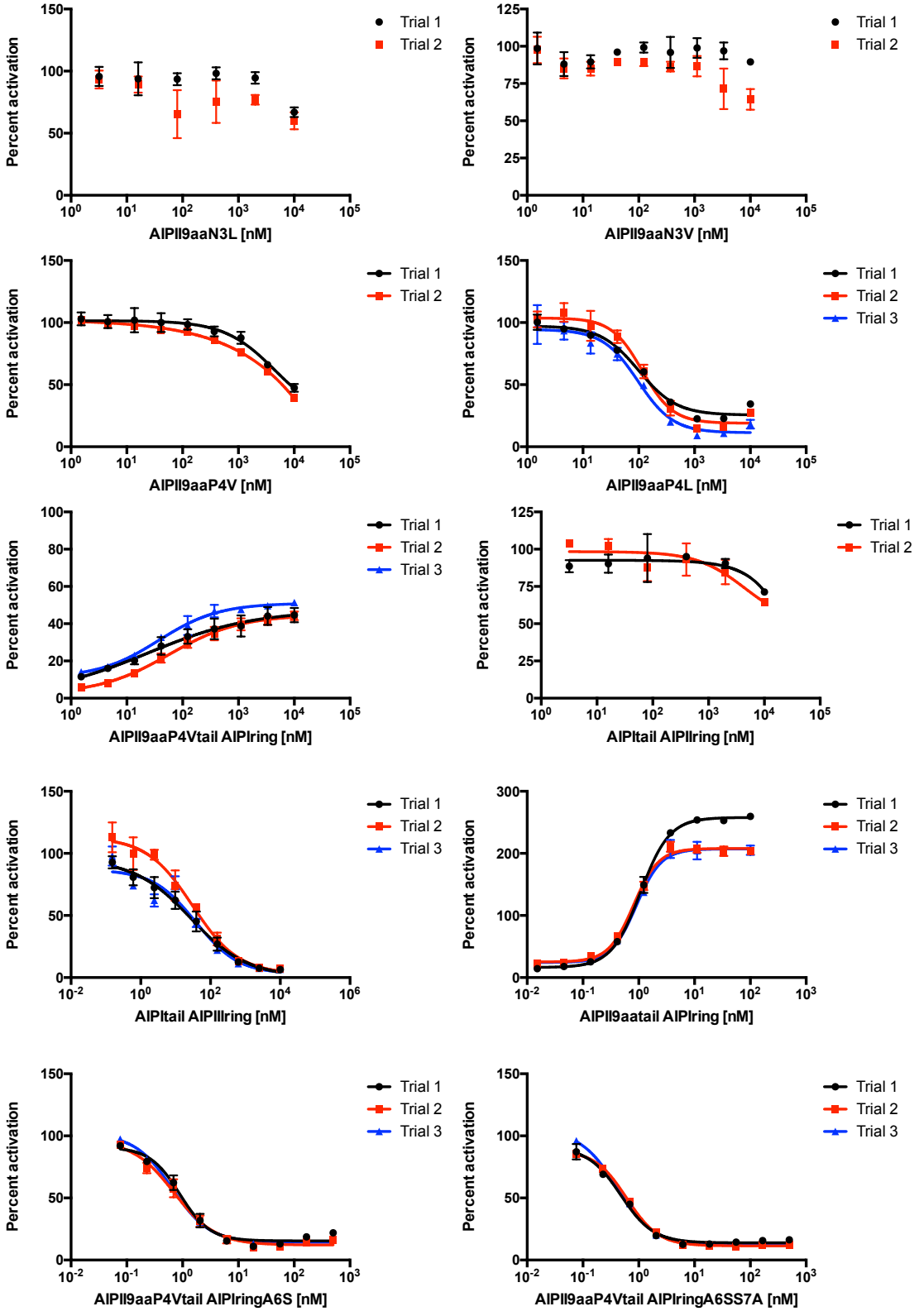


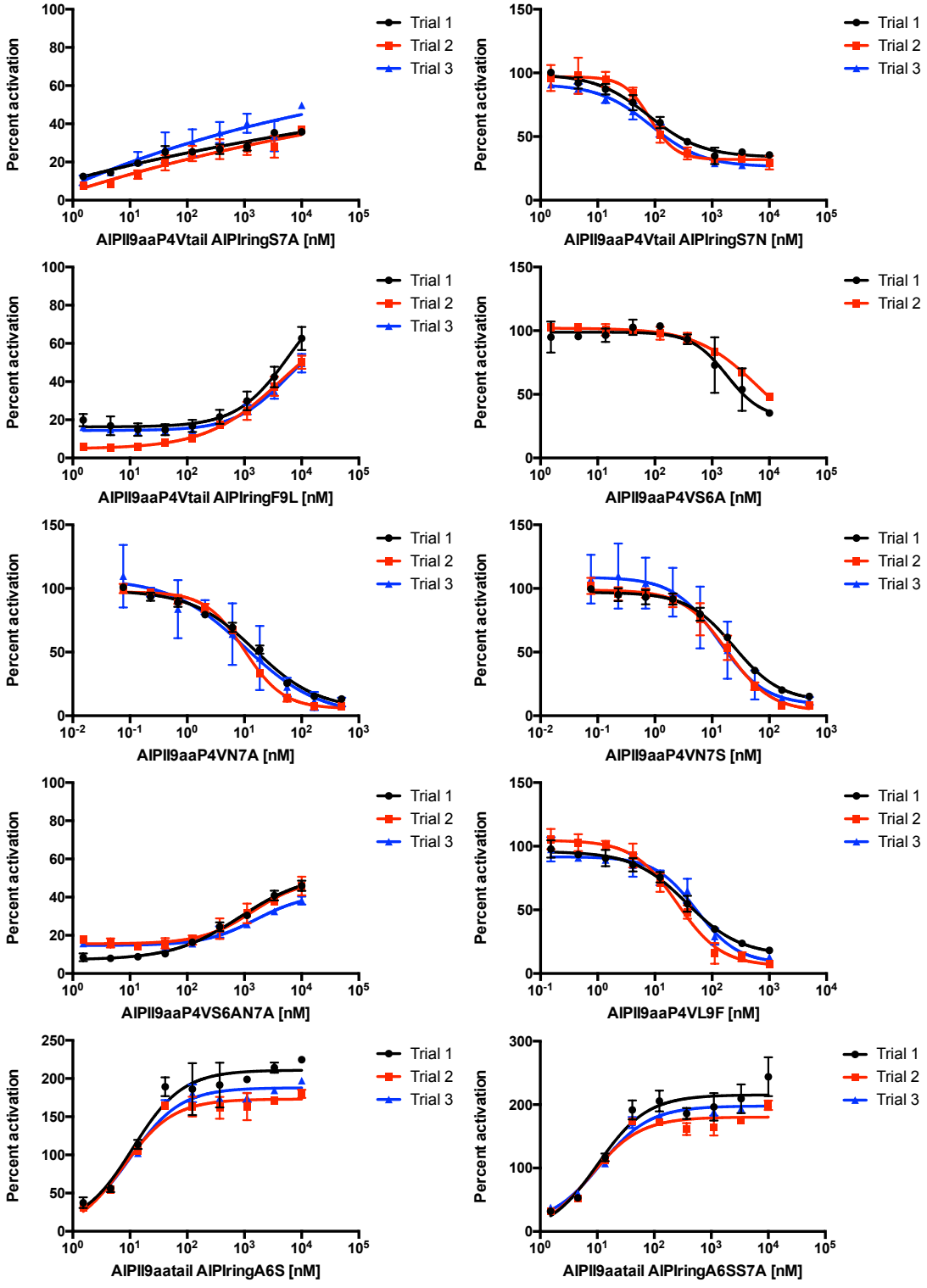


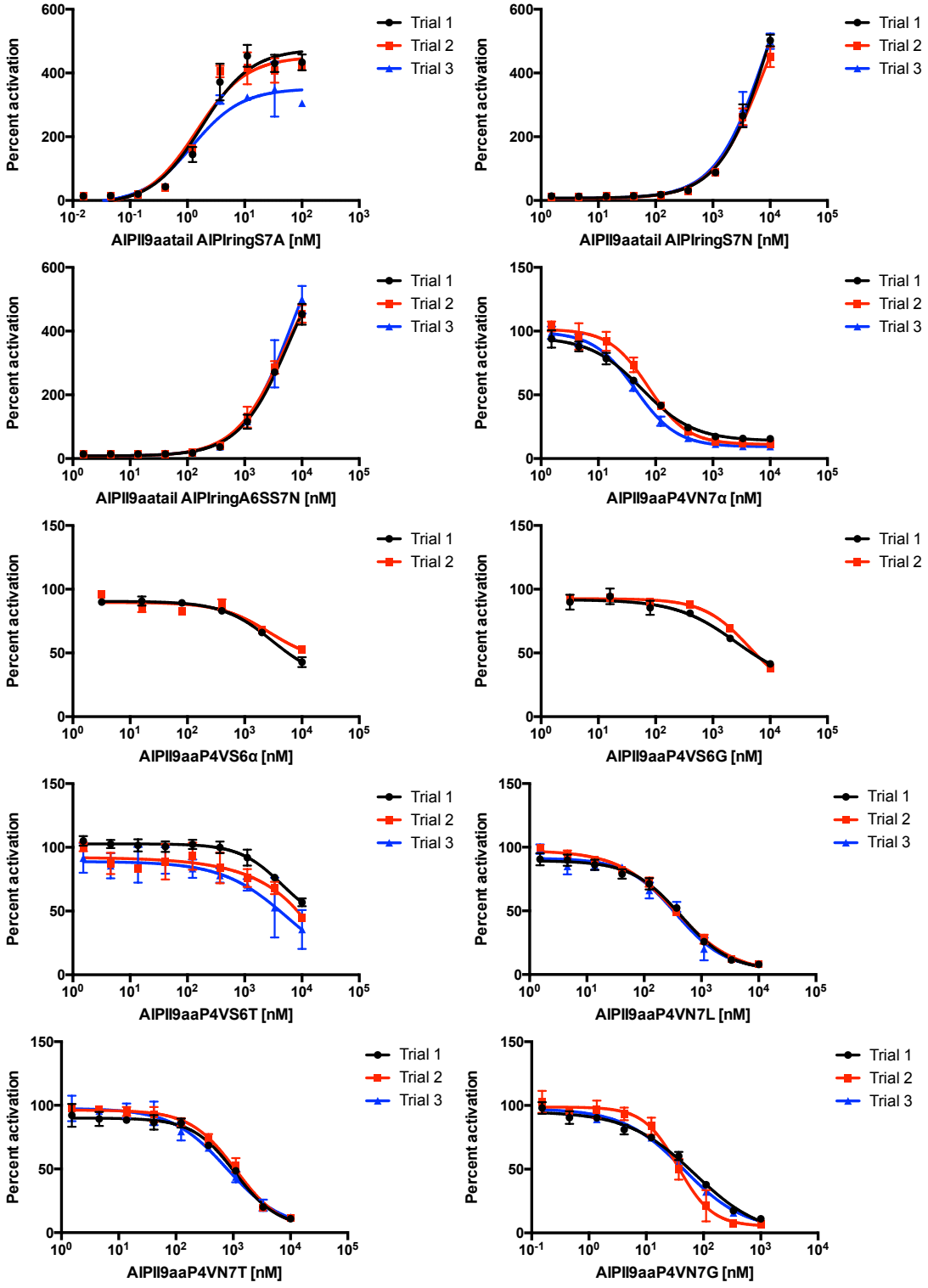



Percent activation
AIP-II [nM]
AIP-III N1A [nM]
AIP-III K4A [nM]
AIP-III Y5A [nM]
AIP-III N6A [nM]
AIP-III P7A [nM]
AIP-III S10A [nM]
AIP-III Y11A [nM]
AIP-III L12A [nM]
AIP-III D-N1 [nM]
Trial 1
Trial 2
Trial 3


Percent activation
AIP-III D-A2 [nM]
AIP-III D-A3 [nM]
AIP-III D-K4 [nM]
AIP-III D-Y5 [nM]
AIP-III D-N6 [nM]
AIP-III D-P7 [nM]
AIP-III D-A9 [nM]
AIP-III D-S10 [nM]
AIP-III D-Y11 [nM]
AIP-III D-L12 [nM]
Trial 1
Trial 2
Trial 3


Percent activation
AIPII9aaN3L [nM]
Trial 1
Trial 2
Percent activation
AIPII9aaN3V [nM]
Trial 1
Trial 2
Percent activation
AIPII9aaP4V [nM]
Trial 1
Trial 2
Percent activation
AIPII9aaP4L [nM]
Trial 1
Trial 2
Trial 3
Percent activation
AIPII9aaP4Vtail AIPIring [nM]
Trial 1
Trial 2
Trial 3
Percent activation
AIPItail AIPIIring [nM]
Trial 1
Trial 2
Percent activation
AIPIItail AIPIIIring [nM]
Trial 1
Trial 2
Trial 3
Percent activation
AIPII9aatail AIPIring [nM]
Trial 1
Trial 2
Trial 3
Percent activation
AIPII9aaP4Vtail AIPIringA6S [nM]
Trial 1
Trial 2
Trial 3
Percent activation
AIPII9aaP4Vtail AIPIringA6SS7A [nM]
Trial 1
Trial 2
Trial 3


Percent activation
Trial 1
Trial 2
Trial 3
AlPII9aaP4Vtail AlPIringS7A [nM]
AlPII9aaP4Vtail AlPIringS7N [nM]
AlPII9aaP4Vtail AlPIringF9L [nM]
AlPII9aaP4VS6A [nM]
AlPII9aaP4VN7A [nM]
AlPII9aaP4VN7S [nM]
AlPII9aaP4VS6AN7A [nM]
AlPII9aaP4VL9F [nM]
AlPII9aatail AlPIringA6S [nM]
AlPII9aatail AlPIringA6SS7A [nM]


Percent activation
AIPII9aatail AIPIringS7A [nM]
AIPII9aatail AIPIringS7N [nM]
AIPII9aatail AIPIringA6SS7N [nM]
AIPII9aaP4VN7α [nM]
AIPII9aaP4VS6α [nM]
AIPII9aaP4VS6G [nM]
AIPII9aaP4VS6T [nM]
AIPII9aaP4VN7L [nM]
AIPII9aaP4VN7T [nM]
AIPII9aaP4VN7G [nM]
Trial 1
Trial 2
Trial 3

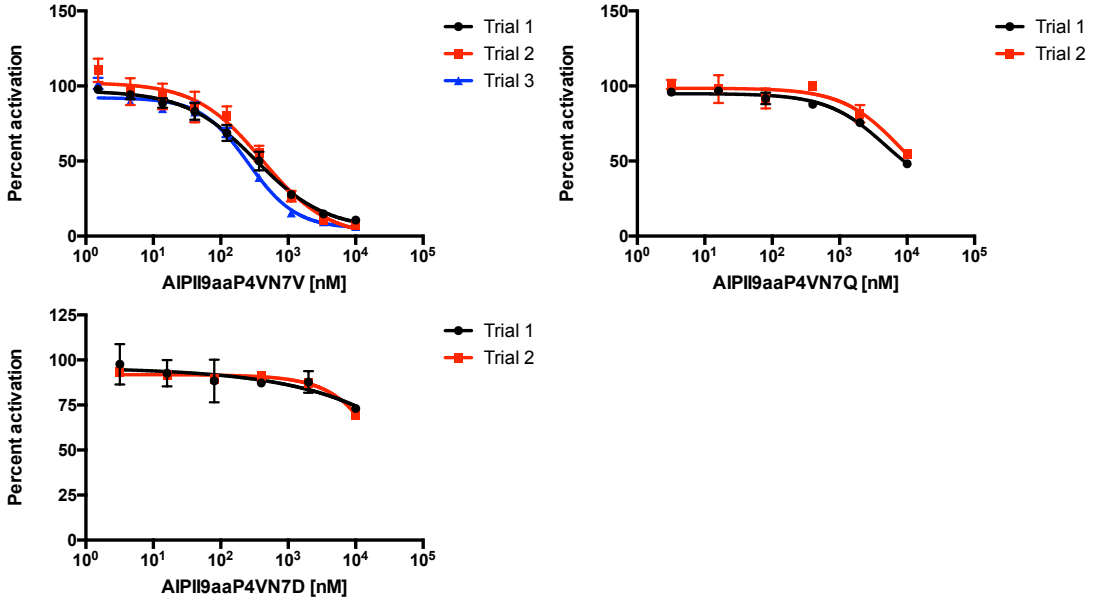

Percent activation
150
100
50
0
10^0 10^1 10^2 10^3 10^4 10^5
AlPll9aaP4VN7V [nM]
Trial 1
Trial 2
Trial 3
Percent activation
150
100
50
0
10^0 10^1 10^2 10^3 10^4 10^5
AlPll9aaP4VN7Q [nM]
Trial 1
Trial 2
Percent activation
125
100
75
50
25
0
10^0 10^1 10^2 10^3 10^4 10^5
AlPll9aaP4VN7D [nM]
Trial 1
Trial 2

Table 4.10: IC_{50} values, EC_{50} values, and 95% confident intervals for the active analogs assayed for AIP-III SAR characterization, as determined using the fluorescence reporter strain for Group III.[a]

Peptide Name	Sequence	IC_{50} [nM] (CI)	EC_{50}[b] [nM] (CI)
AIP-III N1A	A-A-A-K-Y-N-P-(C-A-S-Y-L)	-	71.6 (20.0 – 257)
AIP-III K4A	N-A-A-A-Y-N-P-(C-A-S-Y-L)	-	1320 (141 - 12300)
AIP-III Y5A	N-A-A-K-A-N-P-(C-A-S-Y-L)	120 (95.0 – 152)	-
AIP-III N6A	N-A-A-K-Y-A-P-(C-A-S-Y-L)	124 (58.8 – 261)	-
AIP-III P7A	N-A-A-K-Y-N-A-(C-A-S-Y-L)	157 (44.7 – 551)	-
AIP-III D-N1	DN-A-A-K-Y-N-P-(C-A-S-Y-L)	-	74.0 (48.4 – 113)
AIP-III D-A2	N-DA-A-K-Y-N-P-(C-A-S-Y-L)	-	88.9 (24.7 – 320)
AIP-III D-A3	N-A-DA-K-Y-N-P-(C-A-S-Y-L)	-	702 (431 – 1140)
AIP-III D-K4	N-A-A-DK-Y-N-P-(C-A-S-Y-L)	28.6 (11.4 – 71.8)	-
AIP-III D-Y5	N-A-A-K-DY-N-P-(C-A-S-Y-L)	49.8 (21.6 – 115)	-
AIP-III D-N6	N-A-A-K-Y-DN-P-(C-A-S-Y-L)	1310 (1090 – 1570)	-
AIP-III D-P7	N-A-A-K-Y-N-DP-(C-A-S-Y-L)	1160 (347 – 3900)	-
AIP-III D-S10	N-A-A-K-Y-N-P-(C-A-DS-Y-L)	-	99.5 (36.1 – 275)
AIP-III D-L12	N-A-A-K-Y-N-P-(C-A-S-Y-DL)	-	>2000
AIP-III 11aa	A-A-K-Y-N-P-(C-A-S-Y-L)	-	55.1 (41.9 – 72.5)
AIP-III 10aa	A-K-Y-N-P-(C-A-S-Y-L)	-	29.0 (15.9 – 53.0)
AIP-III 9aa	K-Y-N-P-(C-A-S-Y-L)	-	31.9 (19.4 – 52.7)
AIP-III 8aa	Y-N-P-(C-A-S-Y-L)	19.6 (14.4 – 26.7)	-
AIP-I	D-S-V-(C-A-S-Y-F)	2.02 (1.33 – 3.05)	-
AIP-II	N-A-S-K-Y-N-P-(C-S-N-Y-L)	-	>2000
AIP-III	N-A-A-K-Y-N-P-(C-A-S-Y-L)	-	65.7 (48.7 – 88.5)

[a] See main text for details on the fluorescence reporter strain and assay procedure. See above for MS and HPLC data and dose-response curves for the analogs. Each IC_{50}/EC_{50} value is obtained from 3 biological replicates. [b] Agonism assay was carried out in the presence of 25nM AIP-I D1AS6AV3A, a previously reported antagonist against AgrC-III, to block receptor activation by endogenously produced AIP-III.

Table 4.11: IC_{50} (shown in red) and EC_{50} (shown in green) values for the additional analogs synthesized based on the AIPII9aaP4V scaffold against the known AgrC receptors (AgrC-I–III) as determined using the fluorescence reporter strains. [a]

	AgrC-I		AgrC-II		AgrC-III	
Peptide	IC_{50}/EC_{50} [b] (CI) [nM]	Max Act. [c] (S.D.) [%]	IC_{50}/EC_{50} [b] (CI) [nM]	Max Act. [c] (S.D.) [%]	IC_{50}/EC_{50} [b] (CI) [nM]	Max Act. [c] (S.D.) [%]
AIPII9aaP4VN7α	1830 (694 – 4800)	58.1 (± 4.31)	12.3 (4.92 – 30.5)	40.4 (± 7.85)	57.3 (34.5 – 95.2)	12.1 (± 3.17)
AIPII9aaP4VS6α	>2000	63.8 (± 11.6)	933 (115 – 7560)	26.1 (± 4.55)	>2000	47.8 (± 7.05)
AIPII9aaP4VS6G	Inactive [d]		>2000	43.8 (± 16.9)	>2000	39.9 (± 2.21)
AIPII9aaP4VS6T	1410 (681 – 2930)	25.8 (± 1.57)	Inactive [d]		>2000	45.8 (± 10.7)
AIPII9aaP4VN7L	24.0 (18.4 – 31.4)	17.4 (± 3.37)	73.0 (30.7 – 173)	22.3 (± 3.57)	386 (306 – 487)	8.27 (± 0.33)
AIPII9aaP4VN7T	749 (427 – 1310)	26.3 (± 0.92)	198 (52.2 – 747)	15.8 (± 11.0)	980 (658 – 1460)	11.6 (± 0.67)
AIPII9aaP4VN7G	95.4 (74.3 – 123)	36.6 (± 4.03)	30.6 (12.1 – 77.6)	26.9 (± 2.25)	48.6 (24.6 – 96.1)	9.45 (± 2.60)
AIPII9aaP4VN7V	158 (127 – 197)	10.3 (± 1.36)	34.7 (8.14 – 148)	29.8 (± 10.1)	326 (207 – 514)	8.18 (± 2.24)
AIPII9aaP4VN7Q	>2000	29.7 (± 3.24)	>2000	25.2 (± 4.73)	>2000	51.33 (± 4.52)
AIPII9aaP4VN7D	Inactive [d]		Inactive [d]		Inactive [d]	

[a] See main text for details on the fluorescence reporter strains and assay procedures. See above for MS and HPLC data and dose-response curves for the analogs. [b] Agonism assay was performed in the presence of 25nM AIP-I D1AS6AV3A (a previously identified pan-group antagonist) to block receptor activation by endogenously produced AIPs. [c] Max Activity (Max Act.) is defined as the highest reporter activity (for agonism assay) or the lowest reporter activity (for antagonism assay) the peptide could achieve over the concentration range tested. [d] Maximum inhibition did not exceed 30%. CI = 95% confidence intervals. S.D. = standard deviation of peptide's maximum activity determined from at least 2 biological replicates.

4.7 Acknowledgments

This work was supported by the Office of Naval Research (N00014-14-1-0791), the Burroughs Wellcome Fund, and the UW2020: WARF Discovery Institute award. T.Y. was supported in part by the UW – Madison NIH Biotechnology Training Program (T32 GM08349). K.H.J.W was supported in part by the UW – Madison NIH Chemistry-Biology Interface Training Program (T32 GM008505 and the UW – Madison Office of the Vice Chancellor for Research and Graduate Education (with funding from the Wisconsin Alumni Research Foundation)). W.S. was supported in part by the chemistry department research scholarship, the biochemistry department research scholarship, and the Hilldale Undergraduate Scholarship. S.R. was

supported in part by the Research Experience for Undergraduates program in Chemistry and Chemical and Biological Engineering. MS instrumentation at UW – Madison is supported by the NIH (1S10 OD020022-1) and a generous gift from Paul J. Bender. We thank Professor Alexander Horswill for generously providing the *S. epidermidis* reporter strains.

4.8 References

1. Fuqua, C., and Greenberg, E. P. (2002) Listening in on bacteria: acyl-homoserine lactone signalling, *Nat. Rev. Mol. Cell Biol. 3*, 685-695.

2. Camilli, A., and Bassler, B. L. (2006) Bacterial small-molecule signaling pathways, *Science 311*, 1113-1116.

3. Rutherford, S. T., and Bassler, B. L. (2012) Bacterial quorum sensing: its role in virulence and possibilities for its control, *Cold Spring Harb. Perspect. Med. 2*.

4. Kong, K. F., Vuong, C., and Otto, M. (2006) Staphylococcus quorum sensing in biofilm formation and infection, *Int. J. Med. Microbiol. 296*, 133-139.

5. Wang, B., and Muir, T. W. (2016) Regulation of Virulence in *Staphylococcus aureus*: Molecular Mechanisms and Remaining Puzzles, *Cell Chem. Biol. 23*, 214-224.

6. Yan, J., Sharo, A. G., Stone, H. A., Wingreen, N. S., and Bassler, B. L. (2016) *Vibrio cholerae* biofilm growth program and architecture revealed by single-cell live imaging, *Proc. Natl. Acad. Sci. USA 113*, E5337-5343.

7. Kim, M. K., Zhao, A., Wang, A., Brown, Z. Z., Muir, T. W., Stone, H. A., and Bassler, B. L. (2017) Surface-attached molecules control *Staphylococcus aureus* quorum sensing and biofilm development, *Nat. Microbiol. 2*, 17080.

8. Waters, C. M., and Bassler, B. L. (2005) Quorum sensing: cell-to-cell communication in bacteria, *Annu. Rev. Cell Dev. Biol. 21*, 319-346.

9. Parker, C. T., and Sperandio, V. (2009) Cell-to-cell signalling during pathogenesis, *Cell. Microbiol. 11*, 363-369.

10. Otto, M. (2009) *Staphylococcus epidermidis*--the 'accidental' pathogen, *Nat. Rev. Microbiol. 7*, 555-567.

11. von Eiff, C., Peters, G., and Heilmann, C. (2002) Pathogenesis of infections due to coagulase-negative staphylococci, *Lancet Infect. Dis. 2*, 677-685.

12. Vuong, C., and Otto, M. (2002) *Staphylococcus epidermidis* infections, *Microb. Infect. 4*, 481-489.

13. McCann, M. T., Gilmore, B. F., and Gorman, S. P. (2008) *Staphylococcus epidermidis* device-related infections: pathogenesis and clinical management, *J. Pharm. Pharmacol. 60*, 1551-1571.

14. Rogers, K. L., Fey, P. D., and Rupp, M. E. (2009) Coagulase-negative staphylococcal infections, *Infect. Dis. Clin. North Am. 23*, 73-98.

15. Mertens, A., and Ghebremedhin, B. (2013) Genetic determinants and biofilm formation of clinical *Staphylococcus epidermidis* isolates from blood cultures and indwelling devises, *Eur. J. Microbiol. Immunol. (Bp) 3*, 111-119.

16. Costerton, J. W., Stewart, P. S., and Greenberg, E. P. (1999) Bacterial biofilms: a common cause of persistent infections, *Science 284*, 1318-1322.

17. Schommer, N. N., Christner, M., Hentschke, M., Ruckdeschel, K., Aepfelbacher, M., and Rohde, H. (2011) *Staphylococcus epidermidis* uses distinct mechanisms of biofilm formation to interfere with phagocytosis and activation of mouse macrophage-like cells 774A.1, *Infect. Immun. 79*, 2267-2276.

18. Claessens, J., Roriz, M., Merckx, R., Baatsen, P., Van Mellaert, L., and Van Eldere, J. (2015) Inefficacy of vancomycin and teicoplanin in eradicating and killing *Staphylococcus epidermidis* biofilms in vitro, *Int. J. Antimicrob. Agents 45*, 368-375.

19. Sabate Bresco, M., Harris, L. G., Thompson, K., Stanic, B., Morgenstern, M., O'Mahony, L., Richards, R. G., and Moriarty, T. F. (2017) Pathogenic Mechanisms and Host Interactions in *Staphylococcus epidermidis* Device-Related Infection, *Front. Microbiol. 8*, 1401.

20. Hoiby, N., Ciofu, O., Johansen, H. K., Song, Z. J., Moser, C., Jensen, P. O., Molin, S., Givskov, M., Tolker-Nielsen, T., and Bjarnsholt, T. (2011) The clinical impact of bacterial biofilms, *Int. J. Oral. Sci. 3*, 55-65.

21. Lyon, G. J., and Novick, R. P. (2004) Peptide signaling in *Staphylococcus aureus* and other Gram-positive bacteria, *Peptides 25*, 1389-1403.

22. Novick, R. P., and Geisinger, E. (2008) Quorum sensing in staphylococci, *Annu. Rev. Genet. 42*, 541-564.

23. Thoendel, M., Kavanaugh, J. S., Flack, C. E., and Horswill, A. R. (2011) Peptide signaling in the staphylococci, *Chem. Rev. 111*, 117-151.

24. George, E. A., and Muir, T. W. (2007) Molecular mechanisms of agr quorum sensing in virulent staphylococci, *ChemBioChem 8*, 847-855.

25. Le, K. Y., and Otto, M. (2015) Quorum-sensing regulation in staphylococci-an overview, *Front. Microbiol. 6*, 1174.

26. Ji, G., Beavis, R. C., and Novick, R. P. (1995) Cell density control of staphylococcal virulence mediated by an octapeptide pheromone, *Proc. Natl. Acad. Sci. USA 92*, 12055-12059.

27. Kavanaugh, J. S., Thoendel, M., and Horswill, A. R. (2007) A role for type I signal peptidase in *Staphylococcus aureus* quorum sensing, *Mol. Microbiol. 65*, 780-798.

28. Ji, G., Beavis, R., and Novick, R. P. (1997) Bacterial interference caused by autoinducing peptide variants, *Science 276*, 2027-2030.

29. Wang, B., Zhao, A., Novick, R. P., and Muir, T. W. (2014) Activation and inhibition of the receptor histidine kinase AgrC occurs through opposite helical transduction motions, *Mol. Cell 53*, 929-940.

30. Queck, S. Y., Jameson-Lee, M., Villaruz, A. E., Bach, T. H., Khan, B. A., Sturdevant, D. E., Ricklefs, S. M., Li, M., and Otto, M. (2008) RNAIII-independent target gene control by the agr quorum-sensing system: insight into the evolution of virulence regulation in *Staphylococcus aureus*, *Mol. Cell 32*, 150-158.

31. Novick, R. P., Ross, H. F., Projan, S. J., Kornblum, J., Kreiswirth, B., and Moghazeh, S. (1993) Synthesis of staphylococcal virulence factors is controlled by a regulatory RNA molecule, *EMBO J. 12*, 3967-3975.

32. Vuong, C., Durr, M., Carmody, A. B., Peschel, A., Klebanoff, S. J., and Otto, M. (2004) Regulated expression of pathogen-associated molecular pattern molecules in *Staphylococcus epidermidis*: quorum-sensing determines pro-inflammatory capacity and production of phenol-soluble modulins, *Cell. Microbiol. 6*, 753-759.

33. Otto, M. (2014) Phenol-soluble modulins, *Int. J. Med. Microbiol. 304*, 164-169.

34. Harris, L. G., Dudley, E., Rohde, H., Frommelt, L., Siemssen, N., Wilkinson, T. S., and Mack, D. (2017) Limitations in the use of PSMgamma, agr, RNAIII, and biofilm formation as biomarkers to define invasive *Staphylococcus epidermidis* from chronic biomedical device-associated infections, *Int. J. Med. Microbiol. 307*, 382-387.

35. Olson, M. E., Todd, D. A., Schaeffer, C. R., Paharik, A. E., Van Dyke, M. J., Buttner, H., Dunman, P. M., Rohde, H., Cech, N. B., Fey, P. D., and Horswill, A. R. (2014) *Staphylococcus epidermidis* agr quorum-sensing system: signal identification, cross talk, and importance in colonization, *J. Bacteriol. 196*, 3482-3493.

36. Yao, Y., Vuong, C., Kocianova, S., Villaruz, A. E., Lai, Y., Sturdevant, D. E., and Otto, M. (2006) Characterization of the *Staphylococcus epidermidis* accessory-gene regulator response: quorum-sensing regulation of resistance to human innate host defense, *J. Infect. Dis. 193*, 841-848.

37. Wang, R., Khan, B. A., Cheung, G. Y., Bach, T. H., Jameson-Lee, M., Kong, K. F., Queck, S. Y., and Otto, M. (2011) *Staphylococcus epidermidis* surfactant peptides promote biofilm maturation and dissemination of biofilm-associated infection in mice, *J. Clin. Invest. 121*, 238-248.

38. Otto, M. (2013) Staphylococcal infections: mechanisms of biofilm maturation and detachment as critical determinants of pathogenicity, *Annu. Rev. Med. 64*, 175-188.

39. Le, K. Y., Dastgheyb, S., Ho, T. V., and Otto, M. (2014) Molecular determinants of staphylococcal biofilm dispersal and structuring, *Front. Cell. Infect. Microbiol. 4*, 167.

40. Qin, L., Da, F., Fisher, E. L., Tan, D. C., Nguyen, T. H., Fu, C. L., Tan, V. Y., McCausland, J. W., Sturdevant, D. E., Joo, H. S., Queck, S. Y., Cheung, G. Y., and Otto, M. (2017) Toxin Mediates Sepsis Caused by Methicillin-Resistant *Staphylococcus epidermidis*, *PLoS Pathog. 13*, e1006153.

41. Otto, M. (2004) Virulence factors of the coagulase-negative staphylococci, *Front. Biosci. 9*, 841-863.

42. Mack, D., Davies, A. P., Harris, L. G., Rohde, H., Horstkotte, M. A., and Knobloch, J. K. (2007) Microbial interactions in *Staphylococcus epidermidis* biofilms, *Anal. Bioanal. Chem. 387*, 399-408.

43. Vuong, C., Gerke, C., Somerville, G. A., Fischer, E. R., and Otto, M. (2003) Quorum-sensing control of biofilm factors in *Staphylococcus epidermidis*, *J. Infect. Dis. 188*, 706-718.

44. Davies, D. (2003) Understanding biofilm resistance to antibacterial agents, *Nat. Rev. Drug Discov. 2*, 114-122.

45. Boles, B. R., and Horswill, A. R. (2008) Agr-mediated dispersal of *Staphylococcus aureus* biofilms, *PLoS Pathog. 4*, e1000052.

46. Yang, T., Tal-Gan, Y., Paharik, A. E., Horswill, A. R., and Blackwell, H. E. (2016) Structure-Function Analyses of a *Staphylococcus epidermidis* Autoinducing Peptide Reveals Motifs Critical for AgrC-type Receptor Modulation, *ACS Chem. Biol. 11*, 1982-1991.

47. Carmody, A. B., and Otto, M. (2004) Specificity grouping of the accessory gene regulator quorum-sensing system of *Staphylococcus epidermidis* is linked to infection, *Arch. Microbiol. 181*, 250-253.

48. Mayville, P., Ji, G., Beavis, R., Yang, H., Goger, M., Novick, R. P., and Muir, T. W. (1999) Structure-activity analysis of synthetic autoinducing thiolactone peptides from *Staphylococcus aureus* responsible for virulence, *Proc. Natl. Acad. Sci. USA 96*, 1218-1223.

49. Lyon, G. J., Mayville, P., Muir, T. W., and Novick, R. P. (2000) Rational design of a global inhibitor of the virulence response in *Staphylococcus aureus*, based in part on localization of the site of inhibition to the receptor-histidine kinase, AgrC, *Proc. Natl. Acad. Sci. USA 97*, 13330-13335.

50. McDowell, P., Affas, Z., Reynolds, C., Holden, M. T., Wood, S. J., Saint, S., Cockayne, A., Hill, P. J., Dodd, C. E., Bycroft, B. W., Chan, W. C., and Williams, P. (2001) Structure, activity and evolution of the group I thiolactone peptide quorum-sensing system of *Staphylococcus aureus*, *Mol. Microbiol. 41*, 503-512.

51. Lyon, G. J., Wright, J. S., Muir, T. W., and Novick, R. P. (2002) Key determinants of receptor activation in the agr autoinducing peptides of *Staphylococcus aureus*, *Biochemistry 41*, 10095-10104.

52. Scott, R. J., Lian, L. Y., Muharram, S. H., Cockayne, A., Wood, S. J., Bycroft, B. W., Williams, P., and Chan, W. C. (2003) Side-chain-to-tail thiolactone peptide inhibitors of the staphylococcal quorum-sensing system, *Bioorg. Med. Chem. Lett. 13*, 2449-2453.

53. Fowler, S. A., Stacy, D. M., and Blackwell, H. E. (2008) Design and synthesis of macrocyclic peptomers as mimics of a quorum sensing signal from *Staphylococcus aureus*, *Org. Lett. 10*, 2329-2332.

54. George, E. A., Novick, R. P., and Muir, T. W. (2008) Cyclic peptide inhibitors of staphylococcal virulence prepared by Fmoc-based thiolactone peptide synthesis, *J. Am. Chem. Soc. 130*, 4914-4924.

55. Tal-Gan, Y., Stacy, D. M., Foegen, M. K., Koenig, D. W., and Blackwell, H. E. (2013) Highly potent inhibitors of quorum sensing in *Staphylococcus aureus* revealed through a systematic synthetic study of the group-III autoinducing peptide, *J. Am. Chem. Soc. 135*, 7869-7882.

56. Tal-Gan, Y., Stacy, D. M., and Blackwell, H. E. (2014) N-Methyl and peptoid scans of an autoinducing peptide reveal new structural features required for inhibition and activation of AgrC quorum sensing receptors in *Staphylococcus aureus*, *Chem. Commun. (Camb.) 50*, 3000-3003.

57. Johnson, J. G., Wang, B., Debelouchina, G. T., Novick, R. P., and Muir, T. W. (2015) Increasing AIP Macrocycle Size Reveals Key Features of agr Activation in *Staphylococcus aureus*, *ChemBioChem 16*, 1093-1100.

58. Vasquez, J. K., Tal-Gan, Y., Cornilescu, G., Tyler, K. A., and Blackwell, H. E. (2017) Simplified AIP-II Peptidomimetics Are Potent Inhibitors of *Staphylococcus aureus* AgrC Quorum Sensing Receptors, *ChemBioChem 18*, 413-423.

59. Blanco-Canosa, J. B., and Dawson, P. E. (2008) An efficient Fmoc-SPPS approach for the generation of thioester peptide precursors for use in native chemical ligation, *Angew. Chem. Int. Ed. Engl. 47*, 6851-6855.

60. Tal-Gan, Y., Ivancic, M., Cornilescu, G., Cornilescu, C. C., and Blackwell, H. E. (2013) Structural characterization of native autoinducing peptides and abiotic analogues reveals key features essential for activation and inhibition of an AgrC quorum sensing receptor in *Staphylococcus aureus*, *J. Am. Chem. Soc. 135*, 18436-18444.

61. Khan, B. A., Yeh, A. J., Cheung, G. Y., and Otto, M. (2015) Investigational therapies targeting quorum-sensing for the treatment of *Staphylococcus aureus* infections, *Expert Opin. Investig. Drugs 24*, 689-704.

62. Otto, M., Sussmuth, R., Jung, G., and Gotz, F. (1998) Structure of the pheromone peptide of the *Staphylococcus epidermidis* agr system, *FEBS Lett. 424*, 89-94.

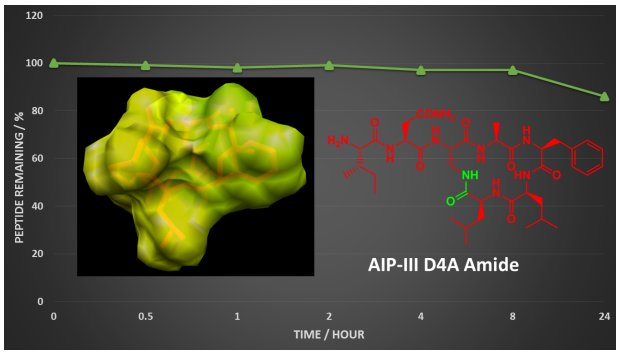
CHAPTER 5:

Highly Stable, Amide-Bridged Autoinducing Peptide Analogues that Strongly Inhibit the AgrC Quorum Sensing Receptor in *Staphylococcus aureus*

Contribution: Y. Tal-Gan designed the experiments, synthesized the peptides, analyzed the NMR data, performed fluorescence reporter strain assays, the peptide stability analysis, and wrote the manuscript. M. Ivancic carried out the NMR experiments and assisted with manuscript writing. G. Cornilescu assisted with NMR analyses. T. Yang assisted with stability analysis and assisted with manuscript writing. H. E. Blackwell guided the project and assisted with manuscript preparation.

*This chapter is published under the same title; *Angew. Chem. Int. Ed. Engl.* **2016,** *55*, 8913 – 8917. Copyright 2016 WILEY-VCH Verlag GmbH & Co.

5.1 Abstract



The common pathogen *Staphylococcus aureus* uses quorum sensing (QS) to coordinate the production of virulence factors and establish infections at high cell density. Blocking QS pathways has attracted considerable interest as an approach to suppress virulence in *S. aureus*. Toward this goal, we recently developed analogues of a native autoinducing peptide (AIP-III) signal that can inhibit AgrC-type QS receptors and attenuate virulence phenotypes. Application of these compounds is limited, however, as they contain hydrolytically unstable thioester linkages and have only low aqueous solubilities. Herein, we report amide-linked AIP analogs with greatly enhanced hydrolytic stabilities and solubilities relative to our prior analogs, whilst maintaining strong potencies as AgrC receptor inhibitors in all four groups of *S. aureus*. These compounds represent powerful new tools for the study of QS in this bacterium.

5.2 Introduction

Quorum sensing (QS) is a cell-cell signaling mechanism that is intimately connected to virulence in many common pathogens *(1, 2)*, including *Staphylococcus aureus (3, 4)*. QS enables bacteria to assess their population density and synchronize group behaviors at high cell number, allowing pathogens to effectively overwhelm their host *(2)*. Bacteria with non-functional QS systems have been shown to be less virulent in numerous infection models *(5-8)*. Accordingly, inhibition of QS in bacterial pathogens has gained attention over the past ~15 years as a potential target to combat infection *(2, 9, 10)*, and substantial recent effort has been focused on QS in *S. aureus (4, 6, 7, 9)*.

QS in bacteria, at the most basic level, is regulated by small molecule or peptide signals and their cognate receptors *(1, 2)*. Signal concentration in a given environment increases with cell density, and once a threshold concentration is reached, productive signal:receptor binding alters gene expression levels to permit the initiation of group behaviors, such as toxin production, motility, or biofilm formation *(1, 2)*. *S. aureus*, like other staphylococcal species, uses an accessory gene regulator (*agr*) system for QS that is centered around the interaction between the autoinducing peptide (AIP) signal and its target transmembrane receptor, AgrC *(3, 4)*. To date, four distinct AIP:AgrC pairs have been characterized in *S. aureus* strains, forming four QS specificity groups (I–IV). The *S. aureus* AIP signals, along with the AIPs from most other staphylococcal species, share two main structural features: (i) a macrocyclic thioester linked via a conserved cysteine and the C-terminus, and (ii) an N-terminal exocyclic tail (Figure 5.1) *(4)*.

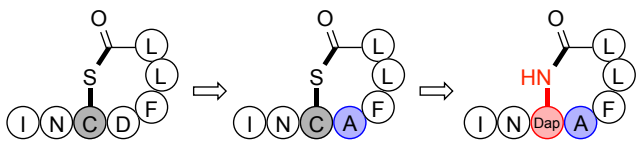


Figure 5.1: Structures of a native AIP (AIP-III), an inhibitor derived therefrom (AIP-III D4A), and a representative scaffold studied herein (AIP-III D4A Amide). Single letter codes used for amino acids; Dap = diamino propionic acid.

To date, most efforts to block QS in *S. aureus* have focused on the AIP ligand, either with the intent to competitively inhibit AIP:AgrC binding *(11)* or, to a lesser extent, sequester the AIP ligand away from its target receptor *(9)*. Blocking downstream transcriptional activation by AgrC (via AgrA) has also been accomplished *(6)*. These chemical strategies provide means to modulate the *agr* system with both temporal and spatial control, gain insights into its role in *S. aureus* infections, and probe its viability as a therapeutic target. Our laboratory has focused primarily on blocking AIP:AgrC binding, and we recently reported analogues of AIP-III (Figure 5.1) that inhibit AgrC receptors and associated toxin production in *S. aureus (12-14)*. Despite their high potencies, these compounds (and many other reported AIP analogs) *(11)* have significant limitations, most notably the instability of the native thioester bridge and their relatively low solubilities in aqueous media. Herein, we report an approach toward addressing these shortcomings through the development of new AIP-III analogs containing non-native amide bridges that are highly potent, stable, and soluble pan-group inhibitors of *agr*-type QS in *S. aureus*.

5.3 Results and Discussion

We evaluated AIP-III in our initial studies to further expand the known AIP SAR trends *(13)*, and discovered AIP-III to provide a superior peptidic scaffold for the design of pan-group AgrC inhibitors. A seemingly simple modification to the native AIP-III structure, replacing Asp4 with Ala, converted the peptide into an extremely potent inhibitor, AIP-III D4A (Figure 5.1). Subsequent NMR studies revealed that this replacement drastically altered the structure of AIP-III *(12)*. While AIP-III displayed a distinctive hydrophobic, triangular “knob” composed of three endocyclic side chains (Phe5, Leu6, and Leu7) and a separately positioned N-terminal tail domain presenting an “anchor point” necessary for activation, the D4A modification caused the peptide to fold up on itself into a compact, amphipathic spheroid where the hydrophobic knob

effectively sequestered the N-terminal tail *(12)*. We propose that this compact knob structure allows AIP-III D4A to compete with the native ligand for AgrC receptors and, in the absence of a correctly positioned N-terminal tail, inhibit their function. The limited hydrolytic stability and aqueous solubility, however, of AIP-III D4A and related analogs have significantly slowed their further application *(15)*.

In the current study, we sought to leverage our past results and redesign AIP-III D4A to increase its versatility as a probe to study QS in *S. aureus*. We reasoned that replacement of the thioester with an amide linkage (Figure 5.1) would increase its hydrolytic stability, and potentially its solubility, in aqueous media. Surprisingly, very few non-thioester AIP analogs have been studied to date *(11)*. We previously examined an AIP-I peptoid-peptide analog with a lactam bridge *(16)*, but this compound was of limited activity. Muir *(5, 17)*, Williams *(18)*, and Otto *(19)* have previously examined lactam replacements in the native *S. aureus* AIP-I and AIP-II signals and the *S. epidermidis* AIP-I signal, and identified peptides capable of moderate non-cognate AgrC receptor inhibition and very weak cognate (i.e., self) receptor activation. No other lactam-derived AIP analogs have been reported, to our knowledge. As AIP-III D4A can strongly inhibit all four AgrC receptors (I–IV), we were also interested to learn if this pan-group activity profile would be maintained in its lactam analog.

Table 5.1: Peptides evaluated in this study.[a] Dap = diamino propionic acid.

Peptide name	Sequence
AIP-III Amide	Ile-Asn-(Dap-Asp-Phe-Leu-Leu)
AIP-III D4A Amide	Ile-Asn-(Dap-Ala-Phe-Leu-Leu)
tAIP-III D2A Amide	Ac-(Dap-Ala-Phe-Leu-Leu)
AIP-III[b]	Ile-Asn-(Cys-Asp-Phe-Leu-Leu)
AIP-III D4A[b]	Ile-Asn-(Cys-Ala-Phe-Leu-Leu)
tAIP-III D2A[b]	Ac-(Cys-Ala-Phe-Leu-Leu)

[a] See Table 5.4 in the SI for MS and HPLC characterization data. [b] Control peptides; reported in ref. 13.

To initiate our investigations, we developed a solid-phase synthetic route to amide-bridged AIP analogues (see SI) in which the conserved Cys was replaced with diamino propionic acid (Dap). We applied this route for the construction of three new AIP-III analogues (listed in Table 5.1): the amide version of native AIP-III; and the amide versions of our two most potent AgrC inhibitors, AIP-III D4A and its truncated analogue, tAIP-III D2A (lacking the N-terminal tail) *(13)*. Simple logP calculations on these peptides (in octanol/water; see SI) indicated that the lactam engendered reduced hydrophobicity relative to their thioester precursors, suggestive that they could have enhanced solubilities in aqueous media.

We evaluated the amide-bridged peptides for their abilities to modulate AgrC receptor activity in all four *S. aureus* groups using reporter gene assays. For AgrC activation, we used a set of *S. aureus agr*-null strains each harbouring two plasmids, i.e., a P3-blaZ reporter and *agr*CA from groups-I, -II, -III, or -IV *(20)*. QS activation was quantified by measuring β-lactamase activity. For AgrC inhibition, we used *S. aureus* strains (groups-I–IV) with functional *agr* circuits and P3-*gfp* reporter plasmids *(21)*. In these strains, QS inhibition caused by exogenous peptide can be quantified by measuring GFP fluorescence.

None of the amide-bridged AIPs were capable of AgrC activation in any of the groups (at concentrations up to 40 μM). This result for AIP-III Amide is congruent with previous studies of the AIP-I and AIP-II lactams, both of which are only very weak cognate receptor agonists *(17, 18)*. Turning to the inhibition data (Table 5.2), AIP-III Amide was found to be a very weak to moderate inhibitor of the four AgrC receptors; interestingly, it was most potent against AgrC-III, which contrasts with the lack of self-inhibition observed previously for the AIP-I and AIP-II lactams *(5, 17, 18)*. These results, when compared to the relatively potent non-cognate receptor antagonism displayed by the native AIP-III signal (Table 5.2), underscore the importance of the thioester linkage for strong non-cognate AgrC receptor inhibition by the native AIP-III scaffold.

Table 5.2: IC_{50} values of the amide-bridged AIP analogs against AgrCs I–IV determined using *S. aureus* fluorescence reporter strains.[a]

Peptide name	Inhibition (IC_{50} nM)[b]			
	AgrC-I	AgrC-II	AgrC-III	AgrC-IV
AIP-III Amide	>1000	>1000	75.2	299
AIP-III D4A Amide	1.20	2.19	0.0551	0.192
tAIP-III D2A Amide	1.50	13.9	0.216	0.189
AIP-III[c]	5.05	5.63	-[d]	8.53
AIP-III D4A[c]	0.485	0.429	0.0506	0.0349
tAIP-III D2A[c]	0.257	0.900	0.329	0.0957

[a] See SI for details of reporter strains and methods, and plots of antagonism dose response curves. All assays performed in triplicate. [b] IC_{50} values determined by testing AIPs over a range of concentrations (200 fM – 10 μM). See SI for 95% confidence ranges. [c] Control peptides, data from ref. 13. [d] Receptor agonist.

Gratifyingly, and in contrast to AIP-III Amide, the amide-bridged analogues of our lead inhibitor, AIP-III D4A, had largely comparable inhibitory activities as their parent thioester counterparts (Table 5.2). With the exception of tAIP-III D2A Amide against AgrC-II (15-fold reduction in activity compared to tAIP-III D2A), the activity differences between the amide-bridged analogues and their thioester counterparts did not exceed a 5-fold reduction, and, in most cases, the activity differences were within error. These results suggest that the AIP-III D4A and tAIP- III D2A scaffolds are more tolerant to linkage modifications relative to the native AIP-III signal.

We next examined the 3D structures of the new lactam AIP-III analogues to gain insights into the origins of their biological activities. Specifically, we were interested to determine if the consensus structural features that we previously identified as critical for AgrC-III inhibition and activation (see above) applied to these amide-bridged analogues as well *(12, 14)*. We used NMR spectroscopy to elucidate the 3D solution structures of the new peptides, utilizing conditions analogous to those in our past report (see SI) *(12)*. Starting with AIP-III Amide, as this analogue was incapable of AgrC-III activation and instead moderately inhibited AgrC-III, we

expected it to possess a hydrophobic knob motif to enable the interaction with AgrC-III, but to lack an appropriate fourth anchor point in the correct orientation. The NMR data revealed that this analogue did possess a triangular knob motif analogous to AIP-III (Figure 5.2A); however, unlike AIP-III where the exocyclic tail projects from the top of the triangular knob to presumably correctly orient the activating anchor (Figure 5.2B), the exocyclic tail in AIP-III Amide projects from the left side of the triangular knob (Figure 5.9A) and the Ile1 side chain is located in close proximity to the Leu7 side chain (Figure 5.10A). We propose that this alternate tail orientation for AIP-III Amide hinders AgrC-III activation; it may also present a steric blockade that prevents the knob portion from productively binding to AgrC receptors in general, thus providing an explanation for the relatively low activity of this peptide overall in any of the *S. aureus* groups.

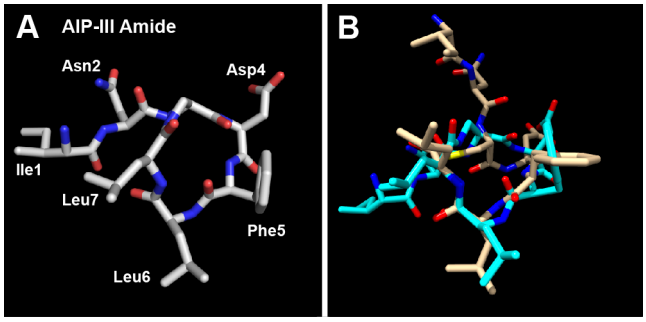


Figure 5.2: A) Heavy atom lowest energy structure of AIP-III Amide. B) Overlay of AIP-III Amide (cyan) and AIP-III (tan) structures. AIP-III structure from ref. 12.

As AIP-III D4A Amide exhibited activities comparable to those of its parent thioester (AIP-III D4A) in the reporter assays, we expected this analogue to possess a largely similar structure in solution (i.e., a knob motif that lacks an activation anchor point in the correct orientation). We observed just this. Although the conformation of the AIP-III D4A Amide macrocycle was somewhat different than that of its thioester analogue, the overall structure of AIP-III D4A Amide revealed an endocyclic knob motif, with the tail residing behind the macrocycle and projecting to the left side (Figures 5.3, 5.9B, and 5.11), and the Ile1 side chain distanced from Leu7 (relative to AIP-III Amide; Figure 5.10B). We reason that this orientation of the AIP-III D4A Amide tail

disallows activation, but does not restrict competitive AgrC binding (and thereby the observed strong inhibition), in contrast to the AIP-III Amide tail (see Figure 5.10A vs. 5.10B).

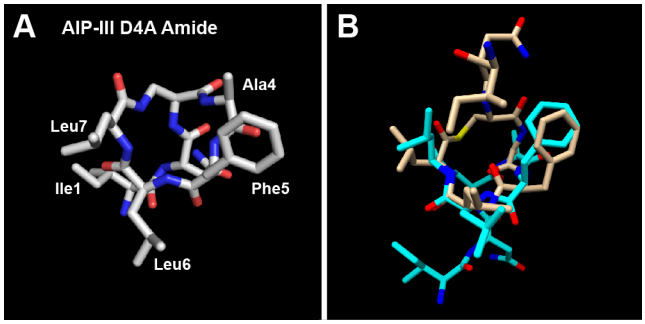


Figure 5.3: A) Heavy atom lowest energy structure of AIP-III D4A Amide. B) Overlay of AIP-III D4A Amide (cyan) and AIP-III D4A (tan) structures. AIP-III D4A structure from ref. 12.

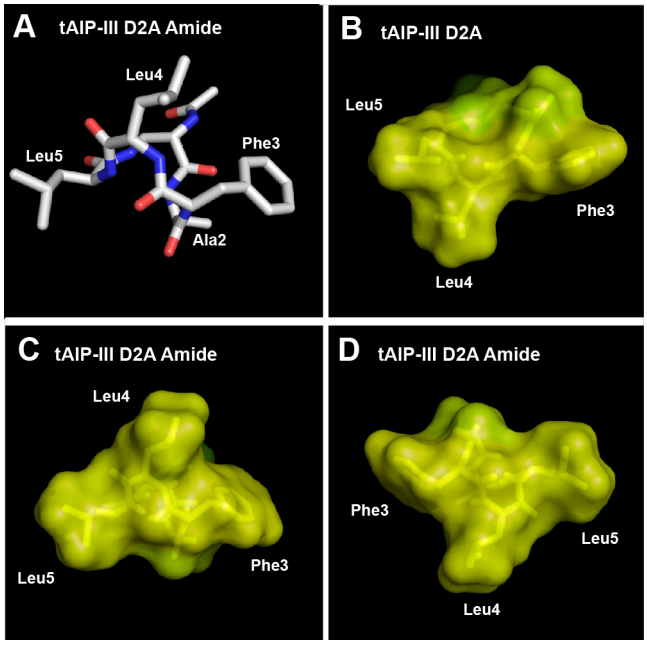


Figure 5.4: A) Heavy atom lowest energy structure of tAIP-III D2A Amide. Space-filling models of B) tAIP-III D2A, C) tAIP-III D2A Amide and D) tAIP-III D2A Amide (showing the alternate triangular knob) displaying hydrophobic (yellow) and hydrophilic (green) surfaces. tAIP-III D2A structure from ref. 12.

Turning to tAIP-III D2A Amide, this peptide had similar inhibitory activities as its thioester counterpart (tAIP-III D2A) against AgrC-III and -IV, and was only slightly less potent against AgrC-I and -II. We thus expected to observe a triangular knob motif for this analogue as well, similar to that we had previously observed for tAIP-III D2A *(12)*. The NMR analyses of tAIP-III

D2A Amide revealed a very structured conformation (Figures 5.4A and 5.9C; backbone atoms RMSD of 0.01 Å for the 10-structure ensemble, and heavy atom RMSD more than 2-fold lower than its thioester counterpart). Interestingly, this analogue displayed a “reversed” triangular knob motif when compared to tAIP-III D2A (see space-filling representations in Figure 5.4); namely, when viewed with the Phe3 and Leu5 residues to the right and left, respectively, the Leu4 side chain in tAIP-III D2A Amide is positioned higher than those for Phe3 and Leu5 (Figure 5.4C), as opposed to being lower as in tAIP-III D2A (Figure 5.4B). It is tempting to speculate that tAIP-III D2A Amide binds AgrC receptors in an opposite way relative to other AIP-III derivatives; that is, the Phe3 residue interacts with the AgrC binding pocket usually occupied by Leu5, and Leu5 interacts with the binding pocket usually occupied by Phe3 (see Figures 5.4C vs. 5.4D). In our prior study, we previously hypothesized that the roles of the hydrophobic side chains of AIP-III (as part of the knob or as the anchor) may be interchangeable *(12)*. Additional studies are needed to fully explore this possibility for tAIP-III D2A Amide. Nevertheless, the 3D structures of the three amide-bridged analogues—AIP-III Amide, AIP-III D4A Amide and tAIP-III D2A Amide—when coupled with their biological activity profiles in the AgrC reporter assays, support the general structural trends that we have previously identified for AgrC inhibition and activation.

As the last aim of this study, we sought to determine whether the replacement of the labile thioester with an amide linkage confers increased overall stability to the peptides. We had observed empirically that all three lactam-bridged AIPs were more soluble in aqueous media relative to the parent thioesters, congruent with the logP calculations. To probe stability, we initially chose to compare the stability of AIP-III D4A to its amide analogue, AIP-III D4A Amide. However, AIP-III D4A could not be solubilized at the concentrations necessary for the stability studies, further underscoring the solubility limitations of this compound. We thus chose to compare the stability of the native AIP-III to AIP-III D4A Amide instead.

To monitor hydrolytic stability, solutions of the two peptides (0.33 mM) were prepared in different buffers (PBS, pH 7.4 and ammonium carbonate, pH 8.0) and incubated at 37° C. To

monitor proteolytic stability, a mixture of Trypsin and Chymotrypsin was added to the peptides in ammonium carbonate prior to incubation. HPLC was used to quantitate the amount of intact peptide over time (Figure 5.5). In PBS, 30% of the AIP-III thioester was degraded after 72 h, while AIP-III D4A Amide remained intact (Figure 5.5A). In the more alkaline ammonium carbonate solution, the stability of the thioester-linked peptide dramatically decreased, and AIP-III was fully degraded in ~8 h. In contrast, AIP-III D4A Amide was found to be relatively stable at pH 8.0, with >90% and >60% of intact peptide remaining after 24 h and 72 h, respectively *(22)*. Treatment of the peptides with Trypsin/Chymotrypsin in ammonium carbonate yielded similar results as in the buffer alone (Figure 5.5B). This result is not unexpected, as cyclization is a common method to confer proteolytic stability to linear peptides *(23, 24)*. Nonetheless, the replacement of the thioester with an amide linkage markedly increased the overall hydrolytic stabilities of the peptides. Further, the amide replacement increased the aqueous solubilities of the peptides and significantly facilitated their purification and overall handling *(25)*. As such, the amide-bridged AIP analogues reported herein constitute valuable new tools to study the role of *agr*-type QS in *S. aureus* virulence, especially in biologically relevant environments. We are currently working to better delineate the mechanisms by which these peptides inhibit AgrC type receptors, along with minimizing their chemical scaffold to improve synthetic access to this class of probes on scale. These studies will be reported in due course.

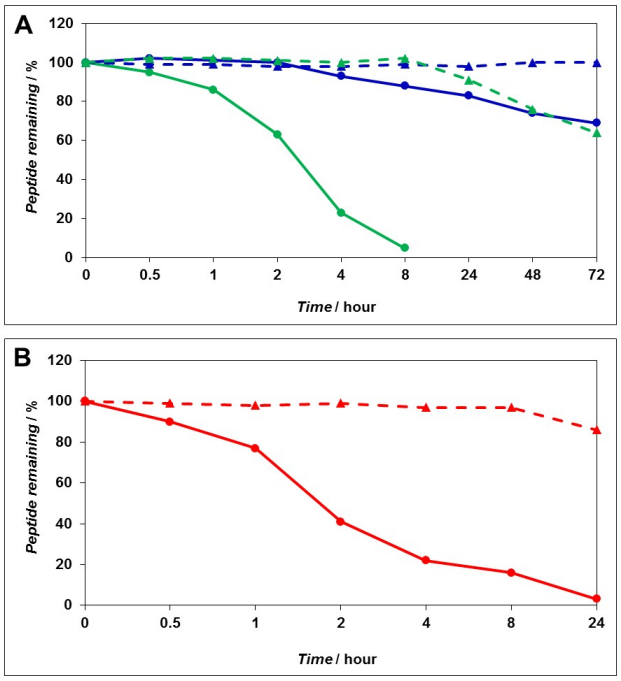


Figure 5.5: Peptide stability studies as monitored by HPLC. AIP-III and AIP-III D4A Amide data are shown as circles with solid lines or triangles with dashed lines, respectively. A) Stability in aqueous solutions (blue is PBS, pH 7.4; green is ammonium carbonate, pH 8.0). B) Stability towards enzymatic degradation by Trypsin/Chymotrypsin (red).

5.4 Methods

5.4.1 Chemical reagents and instrumentation

All standard chemical reagents were purchased from commercial sources (Alfa-Aesar, Sigma-Aldrich, or Acros) and used without further purification. Solvents were purchased from commercial sources (Sigma-Aldrich or J.T. Baker) and used as obtained. Water (18 MΩ) was purified using a Millipore Analyzer Feed System. Solid-phase resin was purchased from Chem-Impex.

Reversed-phase high performance liquid chromatography (RP-HPLC) was performed using a Shimadzu system equipped with an SCL-10Avp controller, an LC-10AT pump, an FCV-10ALvp solvent mixer, and an SPD-10MAvp UV/vis diode array detector. An analytical Phenomenex Gemini C18 column (5 μm, 4.6 mm × 250 mm, 110 Å) was used for analytical RP-HPLC work. A semi-preparative Phenomenex Gemini C18 column (5 μm, 10 mm × 250 mm,

110 Å) was used for preparative RP-HPLC work. Standard RP-HPLC conditions were as follows: flow rates = 1 mL min-1 for analytical separations and 5 mL min-1 for semi-preparative separations; mobile phase A = 18 MΩ water + 0.1% trifluoroacetic acid (TFA); mobile phase B = acetonitrile (ACN) + 0.1% TFA. Purities were determined by integration of peaks with UV detection at 220 nm. Cyclic peptides were purified using a linear gradient (75% → 55% A over 30 min). Overall sample purity was determined using a linear gradient (90% → 5% A over 27 min).

MALDI-TOF mass spectrometry (MS) data were obtained on a Bruker RELEX II spectrometer equipped with a 337 nm laser and a reflectron. In positive ion mode, the acceleration voltage was 25 kV. To confirm peptide identity following synthesis, exact mass (EM) data were obtained on a Waters (Micromass) LCT ESI-TOF mass spectrometer, and the samples were sprayed with a sample cone voltage of 20 V to minimize in-source fragmentation. To assess peptide stability, EM data were obtained on a Thermo Q Exactive PlusTM ESI-Q-IT (orbitrap) mass spectrometer. Tandem MS (MS/MS) measurements were made with a Bruker ULTRAFLEX III (MALDI-TOF/TOF) mass spectrometer equipped with a SmartBeam laser and a LIFT cell.

5.4.2 Peptide synthesis and purification

The amide-bridged AIP-III analogues were synthesized on L-Leu preloaded 2-chlorotrityl resin (0.9 mmol/g) using standard Fmoc/tBu SPPS procedures (see Scheme S-1 below). Cys residues were replaced with diamino propionic acid (Dap). For the full-length AIP analogues, the final residue added was Boc-Ile-OH. The truncated AIP analogue was capped with an acetyl group prior to cleavage. The peptidyl-resin was treated with 2 mL of 2% trifluoroacetic acid (TFA) in CH2Cl2 (5 x 2 min) to effect cleavage, followed by extensive washes with CH2Cl2 (3 x 5 mL). The washes were combined, and the solvent was removed under reduced pressure to

afford a yellow oil. The oil was dissolved in H2O:Acetonitrile (10 mL; 1:1 solution) and lyophilized.

To effect macrolactamization, the crude solid (10 mg) was dissolved in CH2Cl2 (5 mL), benzotriazol-1-yl-oxytripyrrolidinophosphonium hexafluorophosphate (PyBOP, 2 equiv.) and N,N-Diisopropylethylamine (DIPEA, 4 equiv.) were added, and the solution was stirred overnight. The solvent was removed under reduced pressure. To effect deprotection, a 5 mL solution of TFA:CH2Cl2:H2O:triisopropylsilane (TIPS) (90:5:2.5:2.5) was added, and the solution was allowed to stir for 2 h. A cooled solution of diethyl ether:hexane (1:1 40 mL, 0 °C) was added, and the peptide was allowed to precipitate in a freezer at -20 °C overnight. The precipitated peptide solution was centrifuged, and the supernatant was removed to yield a white solid. The solid was dissolved in H2O:Acetonitrile (1:1 solution), lyophilized, dissolved in H2O:Acetonitrile (7:3 solution), and purified by semi-preparative RP-HPLC (25–30% isolated yields).

The purified peptides were characterized by analytical RP-HPLC, HRMS, and MS/MS (for full-length peptides to confirm correct lactam formation). See SI for full characterization data.

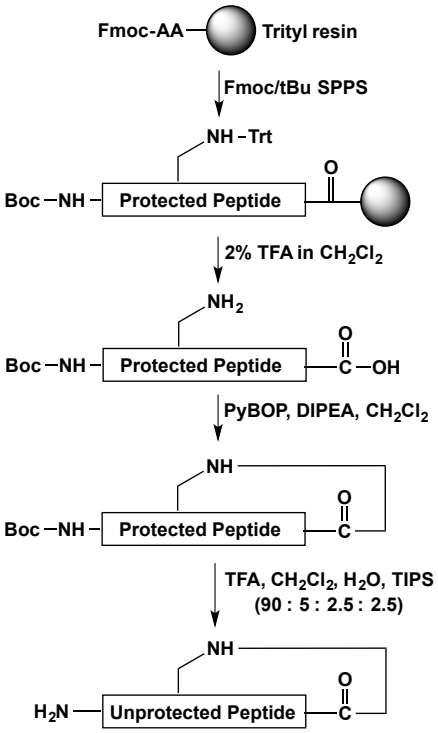


Figure 5.6: Solid-phase synthetic route to amide-bridged AIP-III analogues.

5.4.3 Biological reagents and strain information

All standard biological reagents were purchased from Sigma-Aldrich and used according to enclosed instructions. Brain heart infusion (BHI) was prepared as instructed with pH = 7.35.

The bacterial strains used in this study are listed in Table 5.3. Bacterial cultures were grown in a standard laboratory incubator at 37 °C with shaking (200 rpm) unless noted otherwise. The bacterial dilutions and incubation periods were chosen in each assay to provide the greatest dynamic range between positive and negative controls for each bacterial strain. Absorbance and fluorescence measurements were obtained using a Biotek Synergy 2 microplate reader using Gen5 data analysis software. All biological assays were performed in triplicate. IC50 values were calculated using GraphPad Prism software (v. 4.0) using a sigmoidal curve fit.

Table 5.3: *S. aureus* strains used in this study listed according to group.

Assay-type	Strain	Reference
Fluorescence		
Group-I	AH1677	*(21)*
Group-II	AH430	*(21)*
Group-III	AH1747	*(21)*
Group-IV	AH1872	*(21)*
b-Lactamase		
Group-I	RN9222	*(20)*
Group-II	RN9372	*(20)*
Group-III	RN9532	*(20)*
Group-IV	RN9371	*(20)*

5.4.4 Compound handling protocol

Stock solutions of AIPs and AIP analogues (1 mM) were prepared in DMSO and stored at 4 °C in sealed vials. The amount of DMSO used in bacteriological assays did not exceed 4% (v/v). Black or clear polystyrene 96-well microtiter plates (Costar) were used for bacteriological assays.

5.4.5 Fluorescence assay protocol

Peptide stock solutions were diluted with DMSO in serial dilutions (either 1:3 or 1:5), and 2 µL of the diluted solution was added to each of the wells in a black 96-well microtiter plate. An overnight culture of *S. aureus* GFP strain (Table 5.3) was diluted 1:50 with fresh BHI (pH 7.35). A 198-µL portion of diluted culture was added to each well of the microtiter plate containing peptide. Plates were incubated at 37 °C for 24 h. Fluorescence (EX 500 nm / EM 540 nm) and OD600 of each well were then recorded using a plate reader, and IC_{50} values were calculated.

5.4.6 β-lactamase assay protocol

We utilized a β-lactamase/nitrocefin assay protocol analogous to that of Novick and co-workers *(26)*, except that β-lactamase activity was monitored at a single time point (i.e., 20 min) as opposed to determining a rate profile for enzyme activity (the single time point reading gave comparable data trends). In brief, peptide stock solutions were diluted with DMSO in serial dilutions, and 2 μL aliquots of the diluted solutions were added to each of the wells of a clear 96-well microtiter plate. An overnight culture of *S. aureus* β-lactamase strain (Table 5.3) was diluted 1:50 with fresh BHI, and the bacteria were incubated until reaching early exponential phase (OD600 = 0.16). A 50-μL portion of culture was added to each well of the microtiter plate containing peptide. Plates were incubated for 1 h. The OD_{600} of each well was recorded using a plate reader, followed by the addition of sodium azide (5 μL of a 50 mM solution) and nitrocefin solution (the β-lactamase substrate; 50 μL of a 132 μg/mL solution in 0.1 M sodium phosphate buffer, pH 5.8). The plate was incubated in the dark for 20 min, and the absorbance (at 495 nm) of each well was recorded. No EC_{50} values were calculated in this study, as no compounds showed appreciable agonistic activity at concentrations up to 40 mM.

5.4.7 Peptide stability assay

To monitor hydrolytic stability, the peptides (~0.3 mg) were dissolved in 1 mL of either PBS (pH 7.4) or aqueous Ammonium Carbonate (200 mM, pH 8.0) to yield ~0.33 mM solutions. The peptide solutions were incubated with shaking at 37 °C. Samples (100 μL) were taken at 0, 0.5, 1, 2, 4, 8, 24, 48, and 72 h, and evaluated immediately for peptide degradation using analytical RP-HPLC (see above for details of instrumentation and method).

To monitor enzymatic stability, the peptides (0.3 mg) were dissolved in 1 mL aqueous Ammonium Carbonate (200 mM, pH 8.0), and a 10-μL aliquot of 25 μg/mL Trypsin and Chymotrypsin solution (diluted from a 2.5 mg/mL Trypsin solution; Sigma) in aqueous Ammonium Carbonate (200 mM) was added prior to incubation with shaking at 37 °C. Sample stability over time was analysed using RP-HPLC (analogous to hydrolysis studies above). The

total amount of Trypsin and Chymotrypsin (0.25 μg/mL) is comparable to the natural concentration in serum *(27, 28)*.

5.4.8 General NMR methods

All NMR spectra were recorded on a Varian Inova 600 MHz spectrometer at 298 K, using 1.0–1.5 mM solutions of the peptides in 70% H2O/30% CD3CN, pH 3.65 (conditions analogous to our prior study) *(12)*. Spectra were processed using the Vnmr software package (v. 6.1C; Varian) and NMRPipe software *(29)*. Chemical shifts were referenced to CD3CN at 1.94 ppm. Two-dimensional (2-D) homonuclear experiments gcosy, wgtocsy (tocsy *(30)* using DIPSI spinlock and the 3-9-19 water suppression sequence) and wgroesy (rotating frame NOE experiment with pulsed T-Roesy *(32)* spin lock and the 3-9-19 water suppression sequence) were acquired. The gcosy experiments were collected with 1754 and 512 real data points in the direct and indirect dimensions, respectively, with 16 scans per data point. For the wgtocsy experiments, 1536 and 256 real data points were collected in the direct and indirect dimensions, respectively, with 16 scans per data point. A relaxation delay of 2 sec was used for both the gcosy and wgtocsy experiments, with a mixing time of 80 ms for the wgtocsy. For the wgroesy experiments, 3080 real data points were used in the direct dimension, with 300 data points in the indirect dimension, and the 64 scans per data point. A relaxation delay of 3 sec and a mixing time of 300 ms were used. Presaturation water suppression was used in the 32 scan 1H 1-D experiments with 30272 real data points.

All spectra were analyzed using SPARKY software *(33)*. Assignment of resonances for each peptide (listed in Tables 5.6–5.8) was achieved using standard sequential assignment methodology *(34)*. The number of ROEs observed for each peptide are listed in Table 5.9. The volumes of the ROE peaks were calculated by SPARKY and converted into a continuous distribution of interproton distance restraints, with a uniform 20% distance error applied to take into account spin diffusion. Three-dimensional (3-D) structure calculations and refinements

made use of the torsion angle molecular dynamics and the internal variable dynamics modules *(35)* of Xplor-NIH (v. 2.31) *(36)*, with patches for the amide bridge and ring closure. The target function minimized was comprised of the experimental NMR restraints (ROE-derived interproton distances and torsion angles), a repulsive van der Waals potential for the non-bonded contacts *(37)*, a torsion angle database potential of mean force *(38)*, and a gyration volume potential *(39)*. The RMSD values for each peptide structure are listed in Table 5.9. PyMOL *(40)* and Chimera *(41)* were used for visual analysis and presentation of the peptide structures.

The pdb files for AIP-III Amide, AIP-III D4A Amide, and tAIP-III D2A Amide are included as additional Supporting Information.

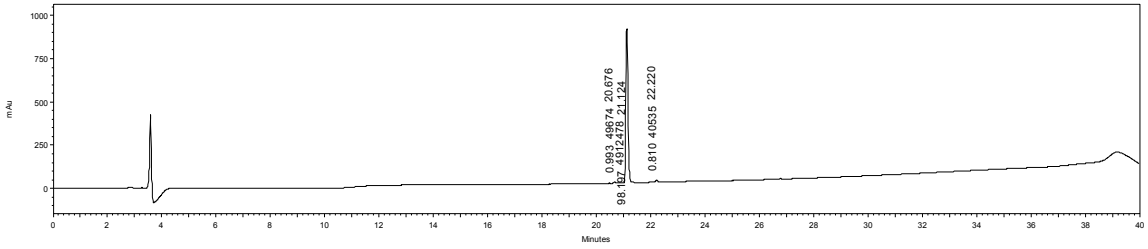
5.5 Supplementary Information

Table 5.4: MS and HPLC data for AIP-III analogues in this study. EM = Exact Mass.

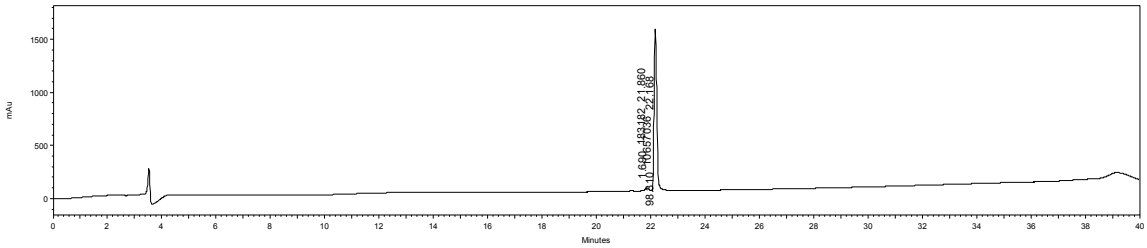
Compound name	Structure	Calc. EM	Obs. EM	Purity (%)
AIP-IIII Amide	Ile-Asn-(Dap-Asp-Phe-Leu-Leu)	802.4458	802.4447	>98
AIP-III D4A Amide	Ile-Asn-(Dap-Ala-Phe-Leu-Leu)	758.4560	758.4554	>98
tAIP-III D2A Amide	Ac-(Dap-Ala-Phe-Leu-Leu)	573.3396	573.3395	>99

5.5.1 HPLC traces for AIP-III analogues

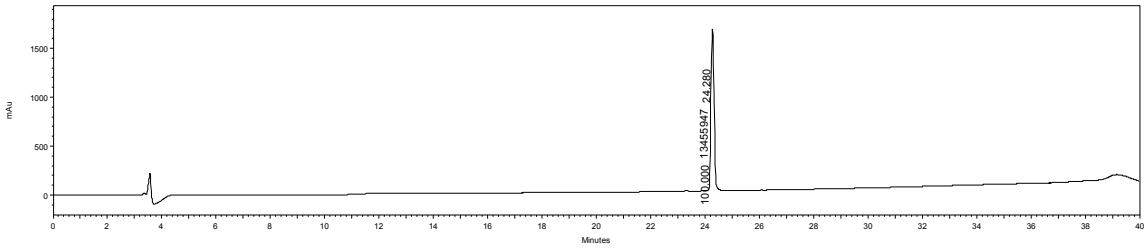
AIP-III Amide



AIP-III D4A Amide



tAIP-III D2A Amide



5.5.2 MS/MS analysis of select AIP-III analogues

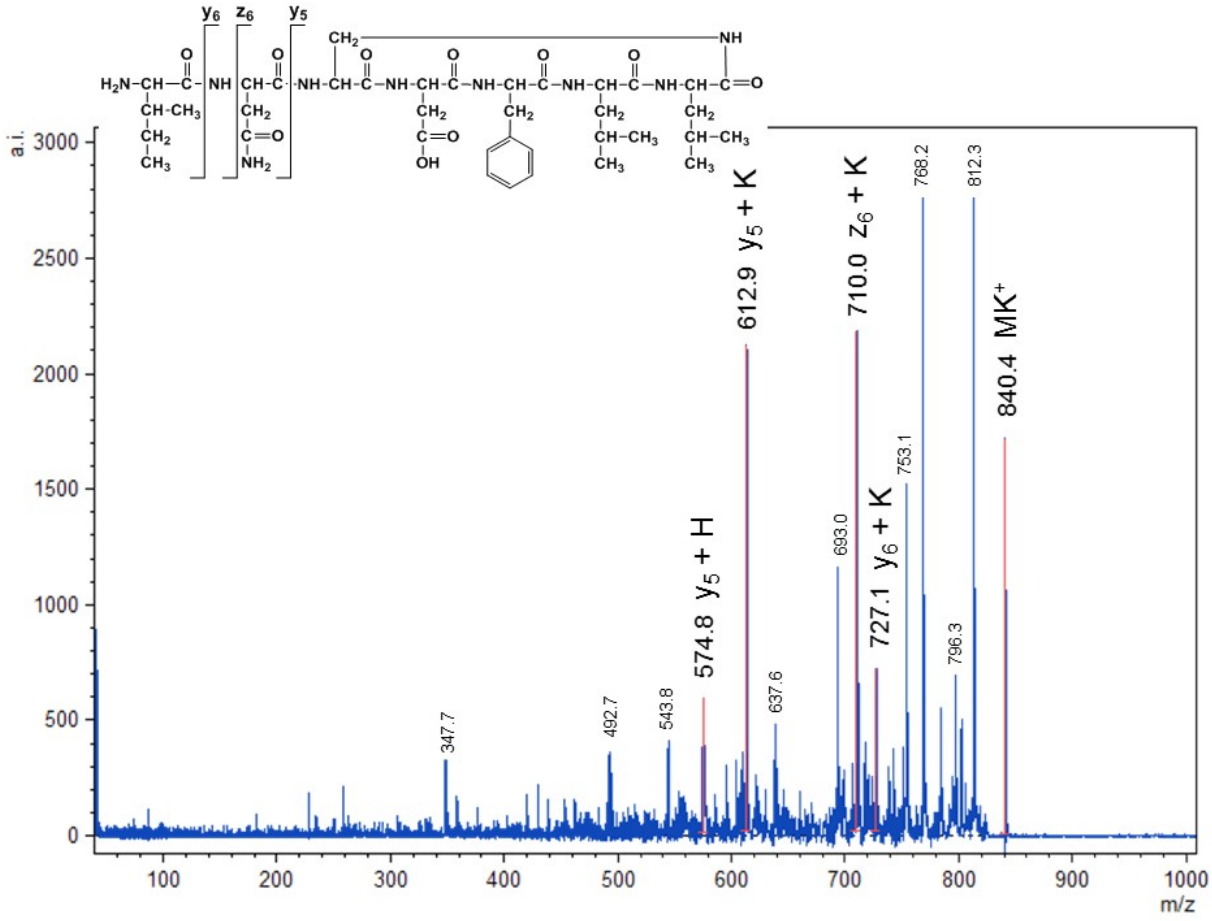


Figure 5.7: Positive ion MS/MS analysis of AIP-III Amide. The absence of fragments smaller than y_5 supports macrocyclization between the carboxy terminus and the side chain of the Dap residue.

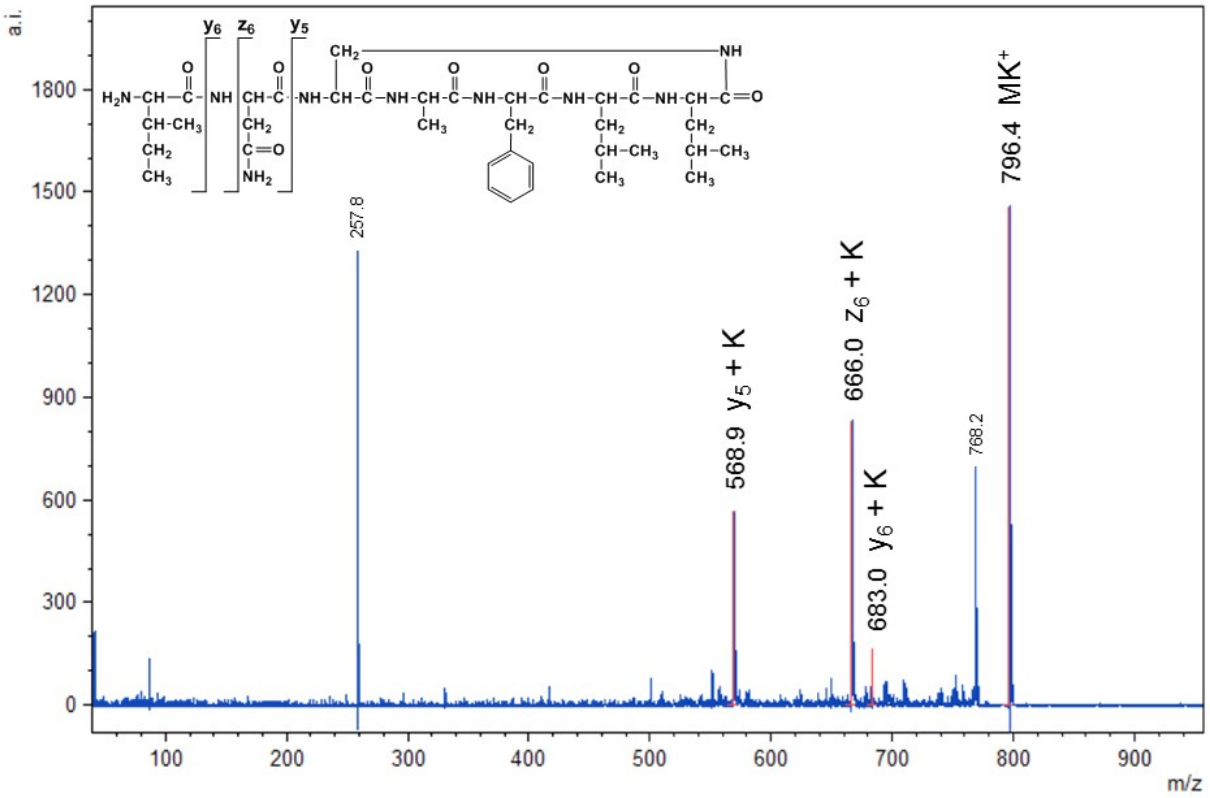


Figure 5.8: Positive ion MS/MS analysis of AIP-III D4A Amide. The absence of fragments smaller than y_5 supports macrocyclization between the carboxy terminus and the side chain of the Dap residue.

5.5.3 Calculated log P values for representative peptides

Log P values (for octanol/water) for AIP-III D4A and AIP-III D4A Amide were calculated using four common online programs. These values and associated websites are provided below. Lower values indicate a compound is more hydrophilic/polar.

http://www.molinspiration.com/

AIP-III D4A: 1.30

AIP-III D4A Amide: 0.01

http://www.organic-chemistry.org/prog/peo/

AIP-III D4A: -1.18

AIP-III D4A Amide: -1.62

http://vcclab.org/web/alogps/

AIP-III D4A: 1.06

AIP-III D4A Amide: 0.67

https://ilab.acdlabs.com/iLab2/index.php

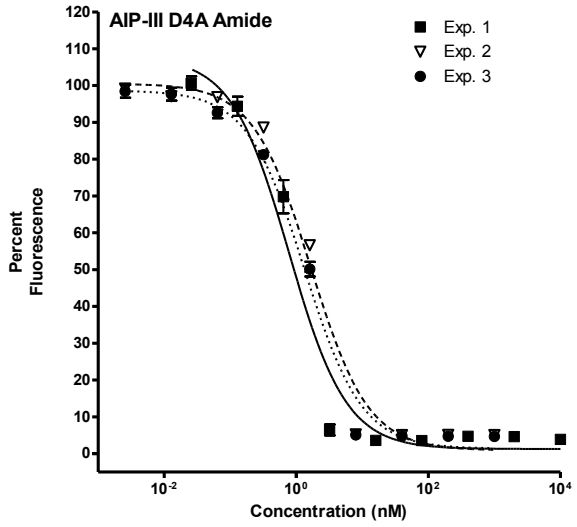
AIP-III D4A: -0.13

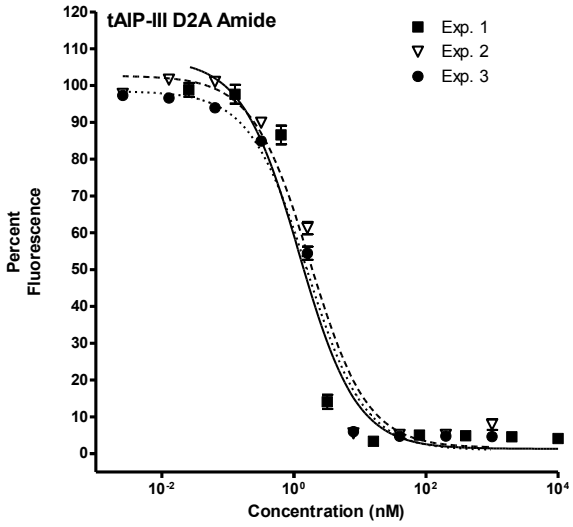
AIP-III D4A Amide: -0.85

5.5.4 Fluorescence antagonism dose response curves

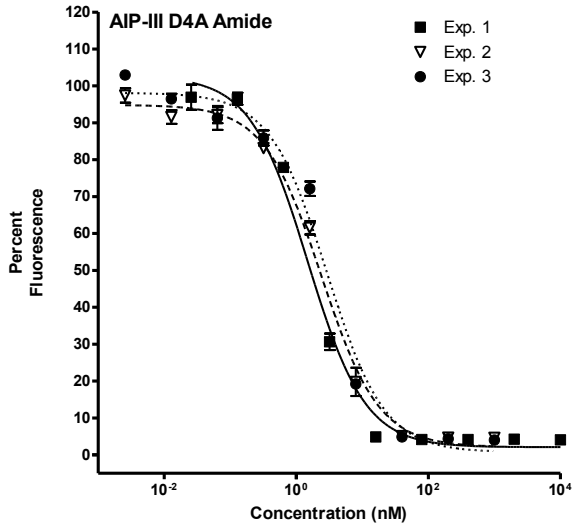
Peptides were screened over varying concentrations in the four *S. aureus* GFP reporter strains (Table 5.3). The peptide tested in each plot below is indicted in bold at top left. Each dose response experiment was performed in triplicate on three separate occasions [i.e., experiments (Exp.) #1–3; shown for each peptide below]. Error bars indicate standard error of the mean of triplicate values. See section above for details of assay and strains.

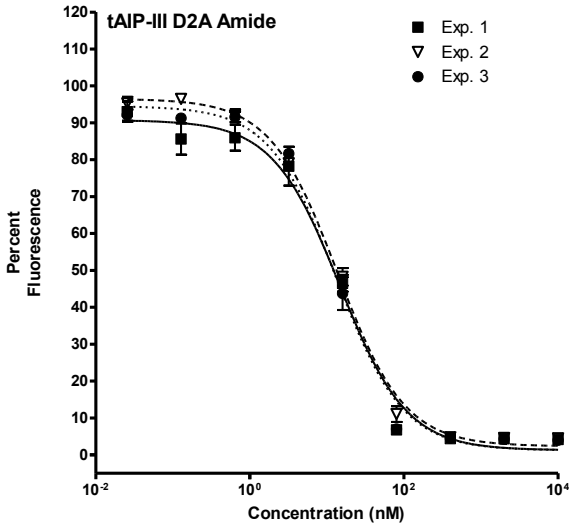
S. aureus AH1677 (Group-I)



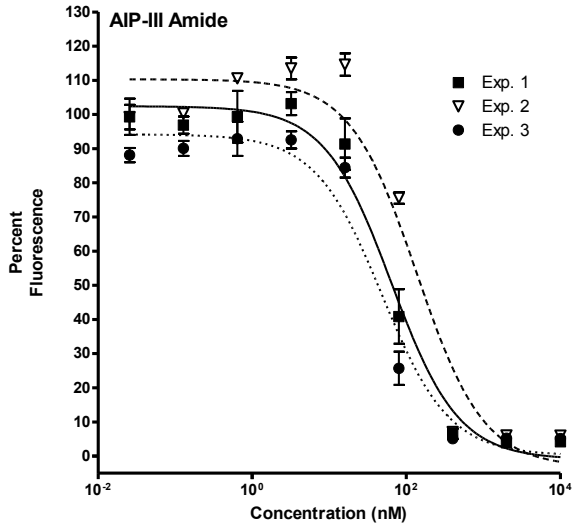


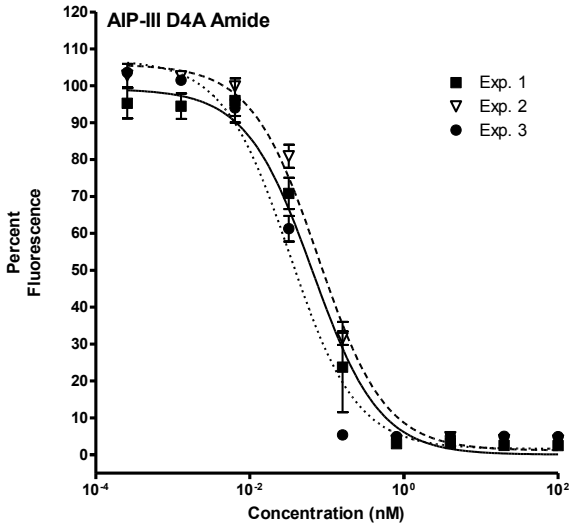
S. aureus AH430 (Group-II)

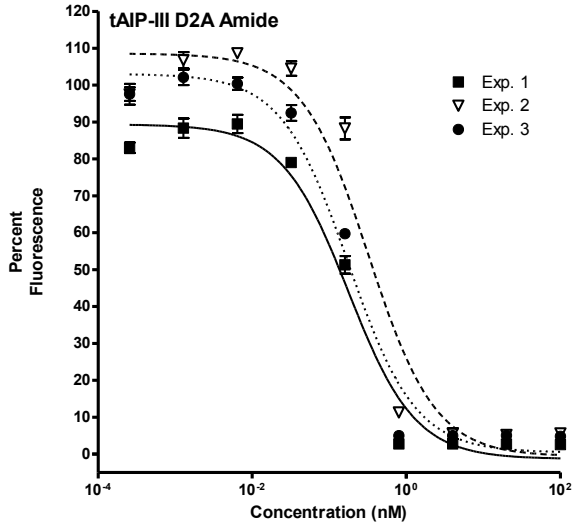




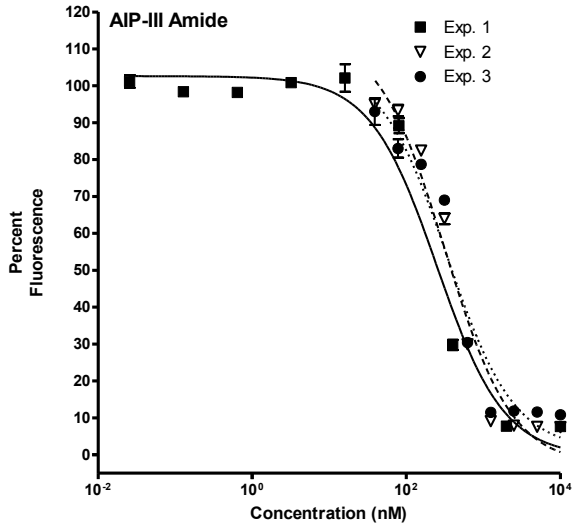
S. aureus AH1747 (Group-III)

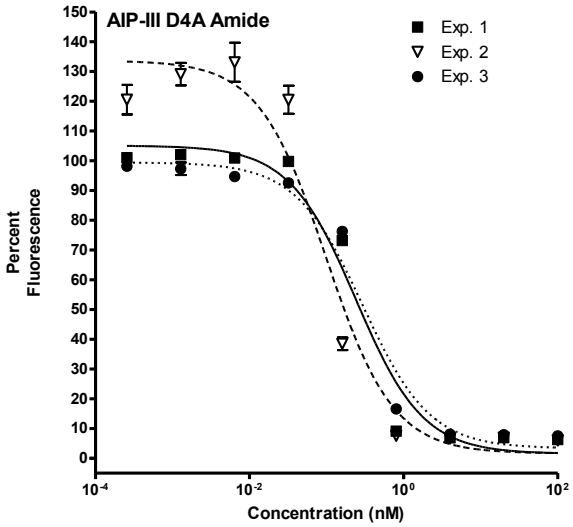






S. aureus AH1872 (Group-IV)





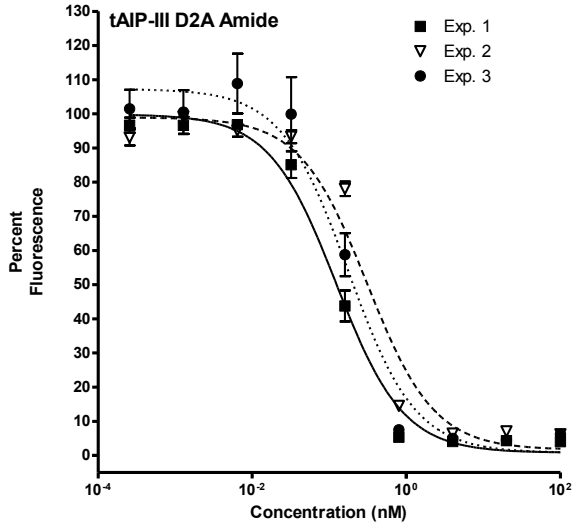


Table 5.5: Complete set of IC_{50} values and 95% confidence ranges for the amide-bridged AIP analogues and control AIPs against AgrC I–IV as determined using the *S. aureus* fluorescence reporter strains.[a]

Peptide name	Sequence	Inhibition (IC_{50} nM)[b]			
		AgrC-I	AgrC-II	AgrC-III	AgrC-IV
AIP-III Amide	Ile-Asn-(Dap-Asp-Phe-Leu-Leu)	>1000	>1000	75.2 (26.3–215)	299 (220–408)
AIP-III D4A Amide	Ile-Asn-(Dap-Ala-Phe-Leu-Leu)	1.20 (0.558–2.59)	2.19 (1.12–4.31)	0.0551 (0.0227–0.134)	0.192 (0.0608–0.603)
tAIP-III D2A Amide	Ac-(Dap-Ala-Phe-Leu-Leu)	1.50 (1.02–2.20)	13.9 (12.6–15.3)	0.216 (0.110–0.426)	0.189 (0.0756–0.472)
AIP-III[c]	Ile-Asn-(Cys-Asp-Phe-Leu-Leu)	5.05 (2.46–10.4)	5.63 (1.89–16.7)	–[d]	8.53 (4.15–17.5)
AIP-III D4A[c]	Ile-Asn-(Cys-Ala-Phe-Leu-Leu)	0.485 (0.289–0.813)	0.429 (0.208–0.886)	0.0506 (0.0227–0.113)	0.0349 (0.0123–0.0990)
tAIP-III D2A[c]	Ac-(Cys-Ala-Phe-Leu-Leu)	0.257 (0.102–0.646)	0.900 (0.842–0.963)	0.329 (0.215–0.502)	0.0957 (0.0375–0.245)

[a] See above for details of reporter strains, experimental procedures, and plots of antagonism dose response curves. All assays performed in triplicate. [b] IC_{50} values determined by testing peptides over a range of concentrations (200 fM – 10 μM). Range indicates 95% confidence interval of triplicate experiments. [c] Control peptides, data reproduced from reference 13. [d] Receptor agonist.

5.5.5 Peptide stability studies

We observed ~10% and ~40% degradation of AIP-III D4A Amide in 200 mM ammonium carbonate at pH 8 over 24 h and 72 h, respectively. We were initially surprised by this result, but after further study, we hypothesized that deamidation of the Asparagine side chain (Asn2) was responsible for the degradation product in ammonium carbonate. Nonenzymatic deamidation of Asn has been shown to occur in proteins and peptides, and ammonia and carbonate are proposed to catalyze such reaction *(22)*. To test our hypothesis, we incubated AIP-III D4A Amide in 200 mM ammonium carbonate solution at pH 8 for 72 h and separated the starting material from the degradation product using semi-preparative RP-HPLC (see Methods section above; linear gradient 62% → 52% A over 27 min). The two compounds isolated were submitted for exact mass (EM) measurements. Based on the exact masses determined, we were able to confirm that the major compound in the solution after 72 h was the starting material

AIP-III D4A Amide (Calculated EM [M+H]+: 758.4559; Experimental EM [M+H]+: 758.4559), and the exact mass of the minor degradation product only differed from the theoretical mass of the deamidation product by 4 ppm (Calculated EM [M+H]+: 759.4400; Experimental EM 759.4397), strongly supporting our hypothesis. We suspect that this minor product is an artifact of working in ammonium carbonate and would not be observed in a significant amount in other common buffers (e.g., phosphate-buffered saline (PBS)).

We performed similar HPLC and MS experiments with AIP-III to demonstrate the susceptibility of the thioester linkage to hydrolysis under alkaline conditions. Unexpectedly, we did not observe a simple hydrolysis product in the fractions isolated using semi-preparative RP-HPLC (linear gradient 70% → 55% A over 27 min). Instead, the EM data showed one major product with a mass close to that of an oxidation product resulting from the addition of a single oxygen atom to AIP-III (Calculated EM [M+H]+: 835.4024; Experimental EM [M+H]+: 835.4258) and two minor products (Experimental EM [M+H]+: 846.4163 and 854.3994). Since we could not match the mass of any proposed degradation product to the masses obtained experimentally, we suspect that the presence of ammonium carbonate and the reactive groups in AIP-III combined to produce a more complex set of degradation products. In support of our hypothesis, when we incubated AIP-III in phosphate-buffered saline (PBS) buffer at pH 8 instead of ammonium carbonate for 72 h, our preliminary MS data suggest that the main degradation product is derived from thioester hydrolysis (Calc. EM [M+Na]+: 859.4000; Experimental MALDI [M+Na]+: 860.5). Additional experiments are in progress to confirm the identification of this product and to better delineate the reactions taking place with AIP-III in the ammonium carbonate buffer.

5.5.6 NMR chemical shift assignments, numbers of assigned ROEs, and RMSD values

Table 5.6: Chemical shift assignments for AIP-III Amide.

Residue	HN (ppm)	Hα (ppm)	Hβ (ppm)	Others (ppm)
Ile1		3.76		Hγ 1.40, 1.11, 0.89; Hδ 0.82
Asn2	8.58	4.51	2.72, 2.66	Hδ 7.40, 6.69
Dap3	8.26	4.34	3.70, 3.34	Hγ 7.46
Asp4	8.42	4.26	2.62	
Phe5	7.58	4.56	2.94, 2.88	Hδ 7.14; Hε 7.27; Hζ 7.23
Leu6	8.74	3.80	1.50	Hγ 1.13; Hδ 0.78, 0.71
Leu7	7.94	4.24	1.56	Hγ 1.52; Hδ 0.81, 0.74

Table 5.7: Chemical shift assignments for AIP-III D4A Amide.

Residue	HN (ppm)	Hα (ppm)	Hβ (ppm)	Others (ppm)
Ile1		3.74	1.84	Hγ 1.38, 1.09, 0.87; Hδ 0.82
Asn2	8.51	4.58	2.69, 2.59	Hδ 7.40, 6.70
Dap3	7.92	4.30	3.53, 3.27	Hγ 7.14
Ala4	8.20	4.08	1.14	
Phe5	8.33	4.06	3.12	Hδ 7.14; Hε 7.29
Leu6	7.89	3.95	1.82, 1.52	Hγ 1.39; Hδ 0.82, 0.77
Leu7	7.84	4.21	1.74	Hγ 1.61; Hδ 0.89, 0.80

Table 5.8: Chemical shift assignments for tAIP-III D2A Amide.

Residue	HN (ppm)	Hα (ppm)	Hβ (ppm)	Others (ppm)
Ac0		1.87		
Dap1	7.85	4.29	3.54, 3.23	Hγ 7.11
Ala2	8.16	4.11	1.15	
Phe3	8.34	4.06	3.13	Hδ 7.14; Hε 7.29; Hζ 7.23
Leu4	7.86	3.97	1.81, 1.53	Hγ 1.39; Hδ 0.82, 0.77
Leu5	7.84	4.23	1.75	Hγ 1.63; Hδ 0.90, 0.80

Table 5.9: Number of assigned ROEs and RMSD values for each peptide.

Peptide name	Total ROEs	Intra-residue ROEs	Inter-residue ROEs			Backbone RMSD (Å)[a]	Heavy atom RMSD (Å)[a]
			i - i+1	*i - i+2*	other		
AIP-III[b]						0.25	0.84
AIP-III D4A[b]						0.42	0.84
tAIP-III D2A[b]						0.22	0.79
AIP-III Amide	105	66	29	5	5	0.13	0.64
AIP-III D4A Amide	112	70	27	6	9	0.43	0.85
tAIP-III D2A Amide	85	53	21	3	8	0.01	0.32

[a] RMSD values calculated for the 10-structure ensemble of each peptide. [b] Control compound. Data reproduced from reference 12.

5.5.7 Additional images of calculated peptide structures

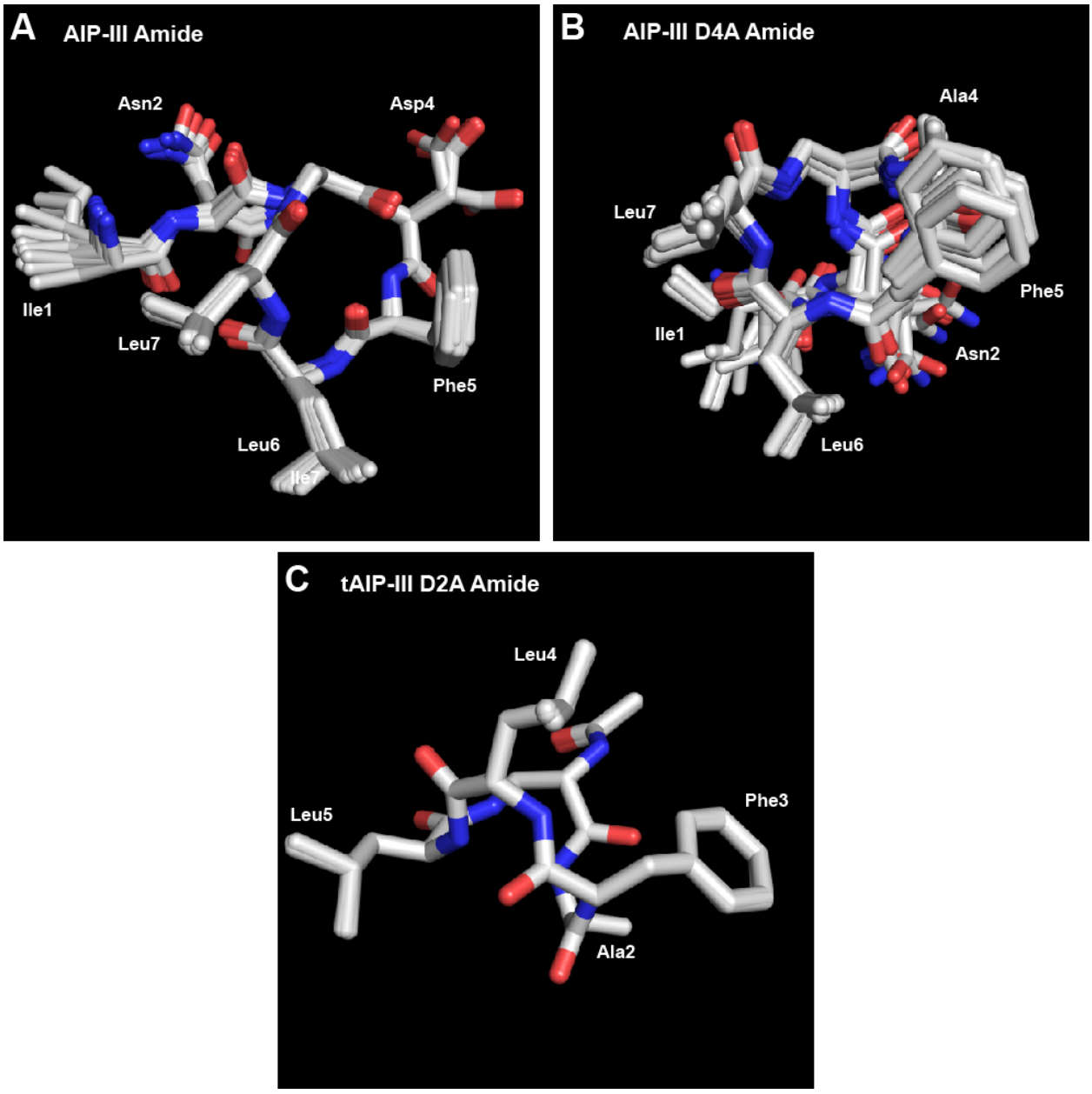


Figure 5.9: Images of the heavy atom 10-structure ensembles for A) AIP-III Amide; B) AIP-III D4A Amide; and C) tAIP-III D2A Amide. For all structures, carbon is silver, oxygen is red, and nitrogen is blue.

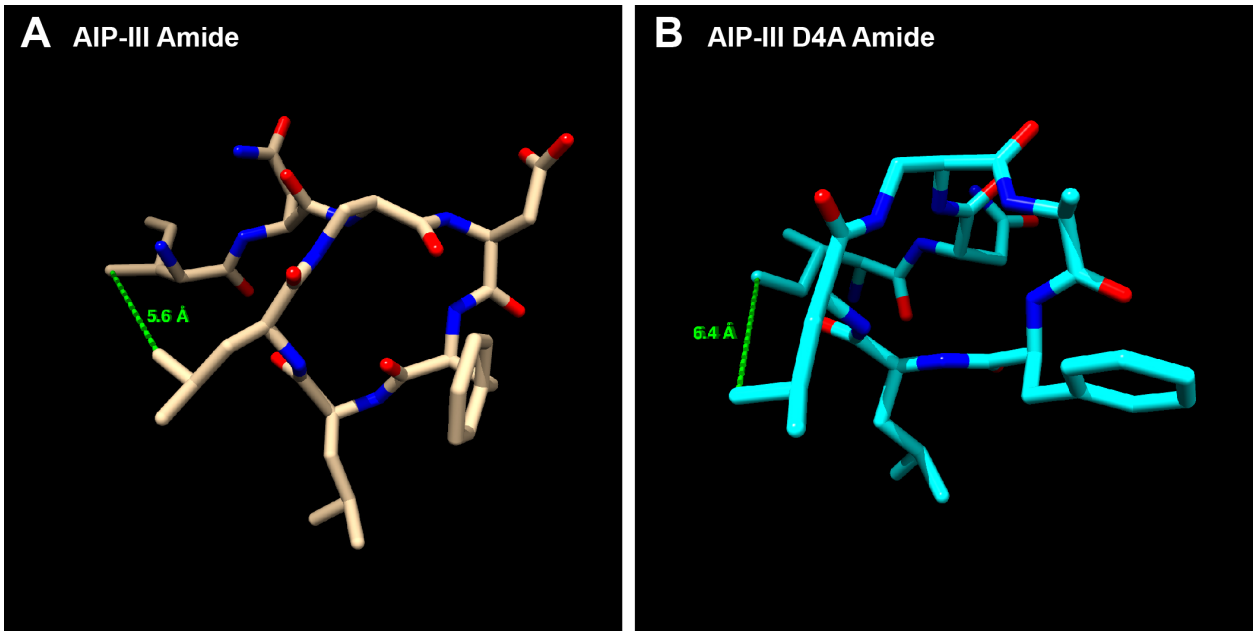


Figure 5.10: Images of the heavy atom lowest energy structures for A) AIP-III Amide; and B) AIP-III D4A Amide showing the distance between Leu7 and Ile1. The Ile1 side chain in AIP-III Amide is almost 1 Å closer to the triangular knob than the same side chain in AIP-III D4A Amide. The difference in the activity profile of these two analogs could result in part from the proximity differences between the exocyclic IleI side chain and the endocyclic knob motif. See main text.

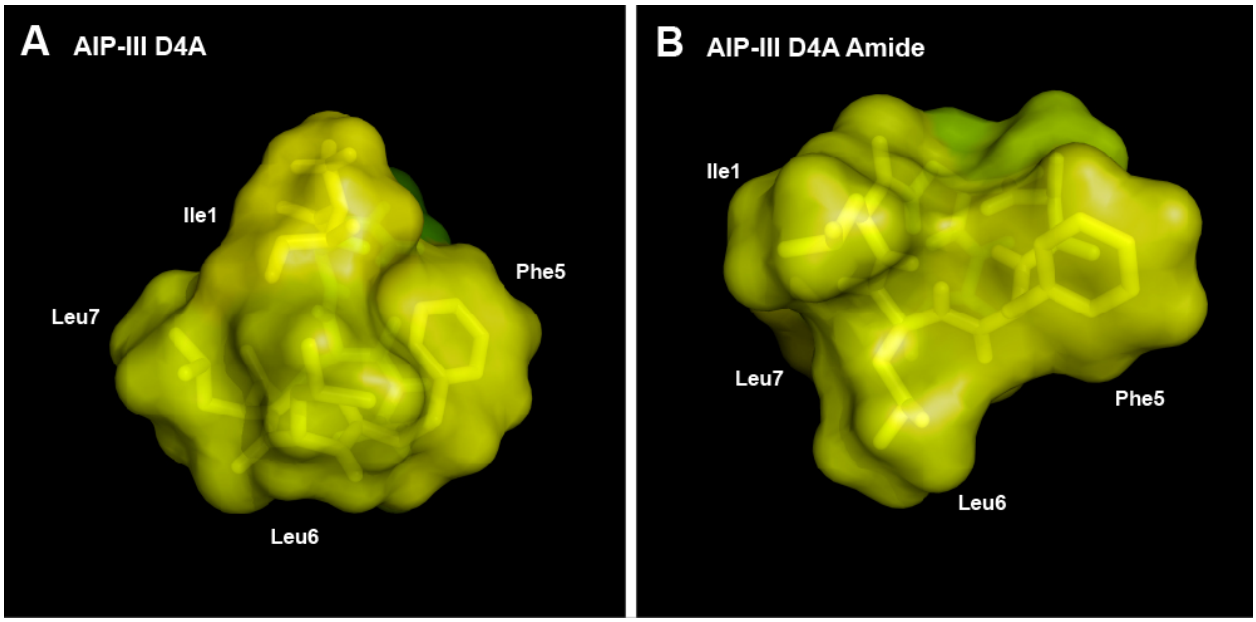


Figure 5.11: Space-filling models of A) AIP-III D4A and B) AIP-III D4A Amide displaying hydrophobic (yellow) and hydrophilic (green) surfaces. These models are positioned to showcase the endocyclic hydrophobic knob motif.

5.6 Acknowledgements

This research was supported by the Office of Naval Research (N00014-14-1-0791), Kimberly-Clark Corporation, and Burroughs Welcome Fund. T. Y. was supported in part by the UW–Madison NIH Biotechnology Training Program (T32 GM08349). The National Magnetic Resonance Facility at Madison is supported by the NIH (P41 GM103399). NMR facilities in the Department of Chemistry are supported in part by the NIH (1 S10 RR13866-01). We thank Prof. Richard Novick and Prof. Alexander Horswill for generously providing *S. aureus* strains, and Joseph Vasquez for technical assistance.

5.7 References

1. Fuqua, C., and Greenberg, E. P. (2002) Listening in on bacteria: acyl-homoserine lactone signalling, *Nat. Rev. Mol. Cell Biol. 3*, 685-695.

2. Rutherford, S. T., and Bassler, B. L. (2012) Bacterial quorum sensing: its role in virulence and possibilities for its control, *Cold Spring Harb. Perspect. Med. 2*.

3. Novick, R. P., and Geisinger, E. (2008) Quorum sensing in staphylococci, *Annu. Rev. Genet. 42*, 541-564.

4. Thoendel, M., Kavanaugh, J. S., Flack, C. E., and Horswill, A. R. (2011) Peptide signaling in the staphylococci, *Chem. Rev. 111*, 117-151.

5. Mayville, P., Ji, G., Beavis, R., Yang, H., Goger, M., Novick, R. P., and Muir, T. W. (1999) Structure-activity analysis of synthetic autoinducing thiolactone peptides from *Staphylococcus aureus* responsible for virulence, *Proc. Natl. Acad. Sci. USA 96*, 1218-1223.

6. Sully, E. K., Malachowa, N., Elmore, B. O., Alexander, S. M., Femling, J. K., Gray, B. M., DeLeo, F. R., Otto, M., Cheung, A. L., Edwards, B. S., Sklar, L. A., Horswill, A. R., Hall, P. R., and Gresham, H. D. (2014) Selective chemical inhibition of agr quorum sensing in *Staphylococcus aureus* promotes host defense with minimal impact on resistance, *PLoS Pathog. 10*, e1004174.

7. Khan, B. A., Yeh, A. J., Cheung, G. Y., and Otto, M. (2015) Investigational therapies targeting quorum-sensing for the treatment of *Staphylococcus aureus* infections, *Expert Opin. Investig. Drugs 24*, 689-704.

8. O'Loughlin, C. T., Miller, L. C., Siryaporn, A., Drescher, K., Semmelhack, M. F., and Bassler, B. L. (2013) A quorum-sensing inhibitor blocks *Pseudomonas aeruginosa* virulence and biofilm formation, *Proc. Natl. Acad. Sci. USA 110*, 17981-17986.

9. Amara, N., Krom, B. P., Kaufmann, G. F., and Meijler, M. M. (2011) Macromolecular inhibition of quorum sensing: enzymes, antibodies, and beyond, *Chem. Rev. 111*, 195-208.

10. Galloway, W. R., Hodgkinson, J. T., Bowden, S. D., Welch, M., and Spring, D. R. (2011) Quorum sensing in Gram-negative bacteria: small-molecule modulation of AHL and AI-2 quorum sensing pathways, *Chem. Rev. 111*, 28-67.

11. Gordon, C. P., Williams, P., and Chan, W. C. (2013) Attenuating *Staphylococcus aureus* virulence gene regulation: a medicinal chemistry perspective, *J. Med. Chem. 56*, 1389-1404.

12. Tal-Gan, Y., Ivancic, M., Cornilescu, G., Cornilescu, C. C., and Blackwell, H. E. (2013) Structural characterization of native autoinducing peptides and abiotic analogues reveals key features essential for activation and inhibition of an AgrC quorum sensing receptor in *Staphylococcus aureus*, *J. Am. Chem. Soc. 135*, 18436-18444.

13. Tal-Gan, Y., Stacy, D. M., Foegen, M. K., Koenig, D. W., and Blackwell, H. E. (2013) Highly potent inhibitors of quorum sensing in *Staphylococcus aureus* revealed through a systematic synthetic study of the group-III autoinducing peptide, *J. Am. Chem. Soc. 135*, 7869-7882.

14. Tal-Gan, Y., Stacy, D. M., and Blackwell, H. E. (2014) N-Methyl and peptoid scans of an autoinducing peptide reveal new structural features required for inhibition and activation of AgrC quorum sensing receptors in *Staphylococcus aureus*, *Chem. Commun. (Camb.) 50*, 3000-3003.

15. Kratochvil, M. J., Tal-Gan, Y., Yang, T., Blackwell, H. E., and Lynn, D. M. (2015) Nanoporous Superhydrophobic Coatings that Promote the Extended Release of Water-Labile Quorum Sensing Inhibitors and Enable Long-Term Modulation of Quorum Sensing in *Staphylococcus aureus*, *ACS Biomater. Sci. Eng. 1*, 1039-1049.

16. Fowler, S. A., Stacy, D. M., and Blackwell, H. E. (2008) Design and synthesis of macrocyclic peptomers as mimics of a quorum sensing signal from *Staphylococcus aureus*, *Org. Lett. 10*, 2329-2332.

17. Lyon, G. J., Wright, J. S., Christopoulos, A., Novick, R. P., and Muir, T. W. (2002) Reversible and specific extracellular antagonism of receptor-histidine kinase signaling, *J. Biol. Chem. 277*, 6247-6253.

18. McDowell, P., Affas, Z., Reynolds, C., Holden, M. T., Wood, S. J., Saint, S., Cockayne, A., Hill, P. J., Dodd, C. E., Bycroft, B. W., Chan, W. C., and Williams, P. (2001) Structure, activity and evolution of the group I thiolactone peptide quorum-sensing system of *Staphylococcus aureus*, *Mol. Microbiol. 41*, 503-512.

19. Otto, M., Echner, H., Voelter, W., and Gotz, F. (2001) Pheromone cross-inhibition between Staphylococcus aureus and *Staphylococcus epidermidis*, *Infect. Immun. 69*, 1957-1960.

20. Lyon, G. J., Wright, J. S., Muir, T. W., and Novick, R. P. (2002) Key determinants of receptor activation in the agr autoinducing peptides of *Staphylococcus aureus*, *Biochemistry 41*, 10095-10104.

21. Kirchdoerfer, R. N., Garner, A. L., Flack, C. E., Mee, J. M., Horswill, A. R., Janda, K. D., Kaufmann, G. F., and Wilson, I. A. (2011) Structural basis for ligand recognition and discrimination of a quorum-quenching antibody, *J. Biol. Chem. 286*, 17351-17358.

22. Tyler-Cross, R., and Schirch, V. (1991) Effects of amino acid sequence, buffers, and ionic strength on the rate and mechanism of deamidation of asparagine residues in small peptides, *J. Biol. Chem. 266*, 22549-22556.

23. Young, T. S., Young, D. D., Ahmad, I., Louis, J. M., Benkovic, S. J., and Schultz, P. G. (2011) Evolution of cyclic peptide protease inhibitors, *Proc. Natl. Acad. Sci. USA 108*, 11052-11056.

24. Lawson, K. V., Rose, T. E., and Harran, P. G. (2013) Template-constrained macrocyclic peptides prepared from native, unprotected precursors, *Proc. Natl. Acad. Sci. USA 110*, E3753-3760.

25. Manifold-Wheeler, B. C., Elmore, B. O., Triplett, K. D., Castleman, M. J., Otto, M., and Hall, P. R. (2016) Serum Lipoproteins Are Critical for Pulmonary Innate Defense against *Staphylococcus aureus* Quorum Sensing, *J. Immunol. 196*, 328-335.

26. Ji, G., Beavis, R. C., and Novick, R. P. (1995) Cell density control of staphylococcal virulence mediated by an octapeptide pheromone, *Proc. Natl. Acad. Sci. USA 92*, 12055-12059.

27. Ruddell, W. S., Mitchell, C. J., Hamilton, I., Leek, J. P., and Kelleher, J. (1981) Clinical value of serum immunoreactive trypsin concentration, *Br. Med. J. (Clin. Res. Ed.) 283*, 1429-1432.

28. Artigas, J. M., Garcia, M. E., Faure, M. R., and Gimeno, A. M. (1981) Serum trypsin levels in acute pancreatic and non-pancreatic abdominal conditions, *Postgrad. Med. J. 57*, 219-222.

29. Delaglio, F., Grzesiek, S., Vuister, G. W., Zhu, G., Pfeifer, J., and Bax, A. (1995) NMRPipe: a multidimensional spectral processing system based on UNIX pipes, *J. Biomol. NMR 6*, 277-293.

30. Bax, A. and Davis, D. G. (1985) MLEV-17-Based Two-Dimensional Homonuclear Magnetization Transfer Spectroscopy, *J. Magn. Reson. Ser. A 65, 355-360.*

31. Levitt, M. H., Freeman, R., and Frenkiel, T. (1982) Broadband heteronuclear decoupling, *J. Magn. Reson. 47,* 328-330.

32. Hwang, T. L. and Shaka, A. J. (1992) Cross relaxation without TOCSY: transverse rotating-fram Overhauser effect spectroscopy, *J. Am. Chem. Soc. 114,* 3157-3159

33. Goddard, T D. and Kneller, D. G. (2007) pp. SPARKY, v. 3.114, University of California: San Francisco

34. Wüthrich, K. (1986) *NMR of Proteins and Nucleic Acids,* John Wiley & Sons, New York.

35. Schwieters, C. D. and Clore, G. M. (2001) Internal coordinates for molecular dynamics and minimization in structure determination and refinement, *J. Magn. Reson. 152*, 288-302.

36. Schwieters, C. D., Kuszewski, J. J., Tjandra, N., and Clore, G. M. (2003) The Xplor-NIH NMR molecular structure determination package, *J. Magn. Reson. 160*, 65-73.

37. Nilges, M., Clore, G. M., and Gronenborn, A. M. (1988) Determination of three-dimensional structures of proteins from interproton distance data by hybrid distance geometry-dynamical simulated annealing calculations, *FEBS Lett. 229*, 317-324.

38. Clore, G. M., and Kuszewski, J. (2002) Chi(1) rotamer populations and angles of mobile surface side chains are accurately predicted by a torsion angle database potential of mean force, *J. Am. Chem. Soc. 124*, 2866-2867.

39. Schwieters, C. D., and Clore, G. M. (2008) A pseudopotential for improving the packing of ellipsoidal protein structures determined from NMR data, *J. Phys. Chem. B 112*, 6070-

6073.

40. Xu, P., Lin, W., and Zou, X. (2002) Synthesis of a Peptidomimetic HCMV Protease Inhibitor Library, *Synthesis 8*, 1017-1026.

41. Pettersen, E. F., Goddard, T. D., Huang, C. C., Couch, G. S., Greenblatt, D. M., Meng, E. C., and Ferrin, T. E. (2004) UCSF Chimera--a visualization system for exploratory research and analysis, *J. Comput. Chem. 25*, 1605-1612.

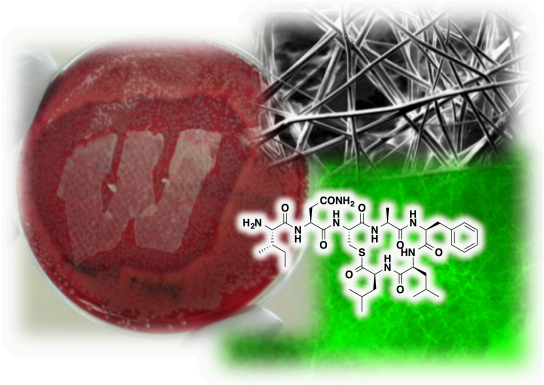
CHAPTER 6:

Non-Woven Polymer Nanofiber Coatings that Inhibit Quorum Sensing in *Staphylococcus aureus*: Toward New Non-Bactericidal Approaches to Infection Control

Contributions: M. J. Kratochvil designed and performed experiments for constructing inhibitor embedded nanofiber coatings, characterized the coatings, and wrote the manuscript. T. Yang designed and performed the biological assays and assisted with manuscript preparation. H. E. Blackwell and D. M. Lynn guided the project and assisted with manuscript writing.

*This chapter is published under the same title; *ACS. Infect. Dis.* **2017,** *3,* 271-280. Copyright 2017 American Chemical Society.

6.1 Abstract



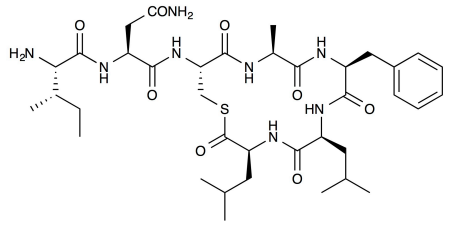
We report the fabrication and biological evaluation of non-woven polymer nanofiber coatings that inhibit quorum sensing (QS) and virulence in the human pathogen *Staphylococcus aureus*. Our results demonstrate that macrocyclic peptide **1**, a potent synthetic non-bactericidal quorum sensing inhibitor (QSI) in *S. aureus*, can be loaded into degradable polymer nanofibers by electrospinning, and that this approach can deposit QSI-loaded nanofiber coatings onto model non-woven mesh substrates. QSI was released over ~3 weeks when these materials were incubated in physiological buffer, and retained its biological activity and strongly inhibited agr-based QS in a GFP reporter strain of *S. aureus* for at least 14 days without promoting cell death. These materials also inhibited production of hemolysins, a QS-controlled virulence phenotype, and reduced the lysis of erythrocytes when placed in contact with wild-type *S. aureus* growing on surfaces. This approach is modular, and can be used with many different polymers, active agents, and processing parameters to fabricate nanofiber coatings on surfaces important in healthcare contexts. *S. aureus* is one of the most common causative agents of bacterial infections in humans, and strains of this pathogen have developed significant resistance to conventional antibiotics. The QSI-based strategies reported here thus provide springboards for the development of new anti-infective materials and novel treatment strategies that target virulence as opposed to growth in *S. aureus*. This approach also provides porous scaffolds for cell culture that could prove useful in future studies on the influence of QS modulation on the development and structure of bacterial communities.

6.2 Introduction

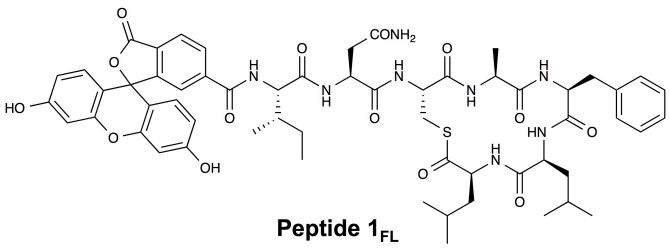
Bacterial fouling and infection remain a persistent challenge confronting the use of interventional devices, implanted objects, dressings, and a wide range of other materials used in healthcare-related applications *(1, 2)*. One useful strategy to prevent or treat these infections is to design materials and surface coatings that release agents that can prohibit or attenuate bacterial cell proliferation or the upregulation of virulent behaviors *(3-5)*, such as biofilm formation *(2)*. These 'surface-mediated' approaches to release and delivery have several practical advantages relative to the systemic administration of antimicrobial agents, including reducing the likelihood of host cell toxicity and other side effects by enabling the local delivery of reduced concentrations of antimicrobial agents directly to areas that are more prone to bacterial infection (e.g., near the surface of an indwelling device or topical dressing) *(3, 4)*.

Regardless of the approach used for delivery, the use (and over-use) of conventional antimicrobial agents has lead to a sharp increase in the prevalence of antibiotic-resistant strains of many common human pathogens—a problem that is the result, at least in part, of the bactericidal nature of those agents, which can contribute to evolved resistance *(6, 7)*. A frightening statistic in this regard is that methicillin-resistant strains of the Gram-positive pathogen *Staphylococcus aureus* (i.e., MRSA) kill more people in the U. S. annually than Parkinson's disease, HIV/AIDS, emphysema, and homicide combined *(8)*. In view of this rapidly emerging threat, new methods for treating or preventing bacterial infections that move beyond conventional antibiotics and other biocidal strategies are urgently needed *(9, 10)*. One potential alternative to these biocidal strategies is the use of agents that can interfere with or inhibit bacterial 'quorum sensing' (QS) circuits that govern many infection phenotypes in common pathogens *(11)*, including virulence factor production and biofilm formation, but do not promote bacterial cell death *(12-14)*. This new 'anti-virulence' approach has been demonstrated to be promising in many clinically relevant bacteria, including *S. aureus (15-17)* and the Gram-negative pathogens *Pseudomonas aeruginosa (18, 19)* and *Acinetobacter baumannii (20)*.

Recent studies by our group *(21-25)* and others *(26-36)* have demonstrated that synthetic inhibitors of bacterial QS (QSIs) can be imbedded in or immobilized onto a variety of materials, and that this approach can be used to design surfaces and coatings that inhibit QS and reduce virulent behaviors in human pathogens. Of particular relevance to the work reported here, we recently reported materials-based approaches to the release of a highly potent synthetic mimic of the auto-inducing peptide (AIP) signal that regulates the accessory gene regulator (*agr*) QS system in *S. aureus* (peptide **1**) *(23, 24)*. Peptide **1** inhibits QS at sub-nanomolar concentrations in all four specificity groups of *S. aureus* (including group-I and group-III *S. aureus*, which are the groups commonly associated with methicillin resistance and toxic shock syndrome, respectively) *(15)*. This peptide acts via competitive inhibition of the native AIP signal by binding its cognate transmembrane receptor, AgrC. Inhibition of *S. aureus* AgrC activity blocks the downstream transcription of an arsenal of virulence factors that are critical for infection, including proteases, hemolysins, enterotoxins, immunomodulatory peptides,



Peptide 1



Peptide 1_{FL}

regulatory RNAs, and surface factors, and modulates the production and maturation of biofilms *(37)*. Accordingly, AgrC represents a central and attractive target for infection control in *S. aureus (38)*. In our past work, we developed peptide **1**-loaded coatings using either conventional solvent-casting approaches *(23)* or new methods for the fabrication of porous

superhydrophobic materials *(24)* to promote the release of biologically-active peptidic QSIs rapidly (e.g., within ~5 min) or over prolonged periods (e.g., over ~8 months), respectively, when exposed to aqueous environments. In this study, we sought to explore new materials design strategies that could (i) permit control over the release of peptidic QSIs at intermediate time scales (e.g., over several days or several weeks) that are relevant in many healthcare contexts, and (ii) provide robust QSI-eluting materials using methods of fabrication that are scalable and more amenable to deposition on complex substrates than methods used in our past studies (i.e., dip-coating *(23)* or layer-by-layer assembly methods *(24)*). Our approach is based on the electrospinning of porous, non-woven mesh coatings (or 'mats') of degradable QSI-loaded polymer nanofibers.

The electrospinning of polymer solutions is widely used to produce non-woven meshes or mats of randomly aligned polymer nanofibers *(39-41)*. These materials are fabricated by using a strong electrical potential to extrude a concentrated solution of polymer from a needle to form extremely thin (nanometer-scale) fibers that can be deposited onto electrically grounded surfaces or collected onto other objects. This electrospinning approach is compatible with the use of many different types of natural and synthetic polymers, and it provides multiple means to tune the physical properties of the resulting fibers (e.g., by control over solution concentrations, flow rates, and other process variables) *(39-41)*. In the specific context of drug delivery, this approach also enables the fabrication of nanofibers loaded with active agents simply by adding those agents directly to the polymer solutions prior to electrospinning *(42, 43)*. This combination of features, combined with the ability to deposit materials over large areas and on topologically complex objects, renders electrospinning attractive for the design of fiber-based coatings of potential utility in many biomedical contexts, including the controlled release of small-molecule and macromolecular agents *(42-44)* and the design of new functionalized or drug-eluting porous polymer platforms for cell culture and tissue engineering *(43, 45)*. Depending on the type of polymer, agent, and processing conditions used, this approach can be used to produce drug-

loaded nanofiber mats and coatings that release embedded agents by diffusion, by polymer degradation, or by a combination of the two, over a broad range of time scales *(43, 44)*. Such mats and coatings have broad potential in the context of combating acute and chronic infections *(46-48)*.

Here, we report the design and fabrication of non-woven and hydrolytically degradable nanofiber mesh coatings that release peptidic QSIs active in *S. aureus* when exposed to physiologically relevant environments. We demonstrate that solutions of peptide **1** and poly(lactide-*co*-glycolide) (PLGA) can be electrospun onto planar surfaces and other non-woven supports to produce coatings that release peptide **1** for approximately three weeks, and that objects coated with these peptide-loaded mats can modulate *agr*-type QS signaling in *S. aureus* using a GFP reporter. We demonstrate further that these materials can be used to strongly inhibit the production of bacterial toxins (i.e., hemolysins) that are under the control of QS in *S. aureus*, both in suspensions of wild-type planktonic bacteria and when fiber-coated materials are placed into contact with wild-type bacteria growing on surfaces. Our results provide the basis of a new and highly adaptable approach that could be used to tune the release of QSIs from the surfaces of topologically complex objects, including fabric-based dressings or gauzes, interventional devices, and implantable objects. With further development, we anticipate that this electrospinning approach could contribute to the development of new and non-bactericidal anti-virulence approaches that provide novel strategies for combatting bacterial infections, with the potential to side-step, or at least substantially delay, issues associated with the development of evolved resistance that currently plague approaches based on bactericidal agents.

6.3 Results and Discussion

*6.3.1 Fabrication of Nanofiber Mats Containing Synthetic Peptidic QSIs **1** and $\mathbf{1_{FL}}$*

Our approach to the design of non-woven nanofiber mats that can inhibit bacterial QS is based upon the electrospinning of polymer solutions containing peptide **1**. As outlined above,

peptide **1** is a potent synthetic inhibitor of agr-type QS in the four groups of *S. aureus*, with an IC_{50} of 0.485 nM against MRSA-associated group-I strains and an IC_{50} of 0.0506 nM against toxic shock syndrome-associated group-III strains *(15)*. strains that are of importance in the context of bacterial infections. To explore the feasibility of this new approach and demonstrate proof of concept, we selected the commercially available polyester PLGA (with a 50:50 ratio of lactide and glycolide repeat units) as a model degradable polymer for several reasons: (i) this polymer is FDA-approved and has a long history of use for drug delivery and other biomedical applications *(49-51)*, (ii) the structure and composition of this polymer can be easily manipulated to exert useful control over the release of encapsulated agents *(52, 53)*, and (iii) the use of this polymer as a basis for the electrospinning of degradable polymer nanofibers using a range of solvents and processing parameters is well established *(43, 45, 54-56)*.

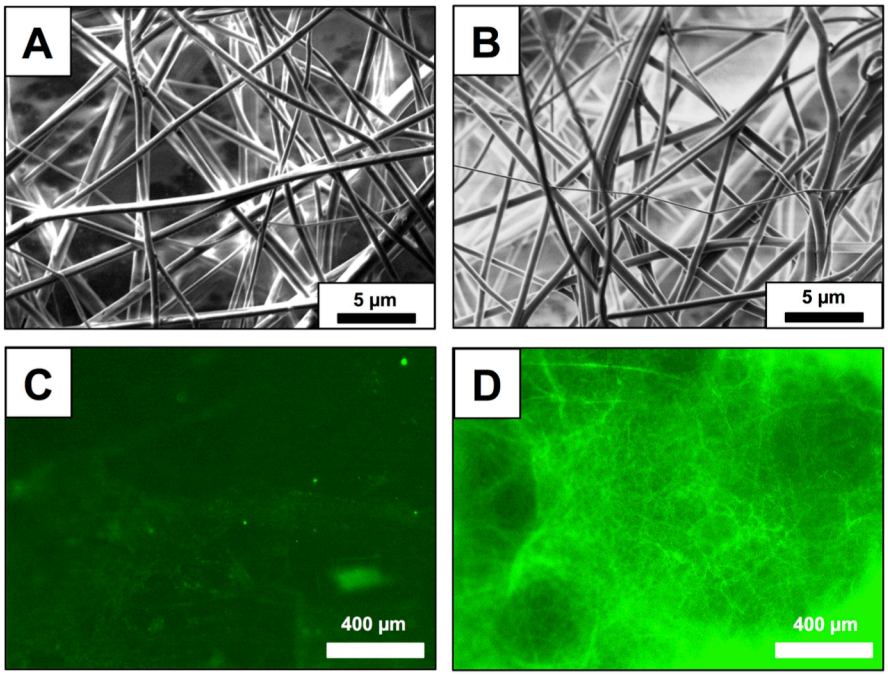


Table 1: Measurements of Fiber Diameters

Material	Average (nm)	Median (nm)	St. Dev. (nm)
PLGA	930	830	380
PLGA+Peptide 1	860	780	410
PLGA+Peptide 1_{FL}	830	770	330

Figure 6.1: (A,B) Representative SEM images of electrospun PLGA nanofibers loaded with peptide **1** (A) or peptide $\mathbf{1}_{FL}$ (B). (C,D) Representative fluorescence microscopy images of electrospun PLGA nanofibers loaded with non-fluorescent peptide **1** (C) or fluorescently-labeled peptide $\mathbf{1}_{FL}$ (D).

For all experiments described below, PLGA nanofibers were fabricated by electrospinning solutions of PLGA containing 0.25 mM of peptide **1** onto model non-woven mesh substrates composed of poly(ethylene terephthalate) and polyethylene fibers (see Methods for additional details of electrospinning process parameters used in these experiments). For experiments designed to characterize the loading and release of the peptide from the nanofibers, we used PLGA solutions containing peptide $\mathbf{1}_{FL}$, a fluorescein-labeled derivative of peptide **1** *(24)*, to facilitate characterization by both fluorescence microscopy and

solution fluorometry. Figure 6.1A-B shows SEM images of nanofiber mats electrospun from PLGA solutions containing peptide **1** (A) and peptide $\mathbf{1}_{FL}$ (B). These images reveal a network of smooth and randomly aligned nanofibers with median diameters of approximately 780 nm (± 410 nm) and 770 nm (± 330 nm), respectively (see also Table 1; results for PLGA nanofibers alone (no QSI) are shown for comparison; additional characterization of nanofiber distributions is shown in Figure 6.5 of the Supplementary Information). We did not observe substantial non-uniformities or the presence of beaded fiber morphologies *(40, 43, 54)* in PLGA/QSI fibers fabricated under the conditions used in this study. Figure 6.1D shows a representative fluorescence microscopy image of a fiber mat fabricated using a PLGA solution containing peptide $\mathbf{1}_{FL}$. The green fluorescent network of filamentous structures in this image is consistent with the encapsulation of this fluorescently-labeled QSI in the electrospun fibers (Figure 6.1C shows an image of fibers electrospun using polymer solutions containing non-fluorescent peptide **1**, and is dark by comparison).

6.3.2 Characterization of QSI Release Profiles

We characterized the release of peptide $\mathbf{1}_{FL}$ from the PLGA nanofiber mats described above by incubating small swatches of fiber-coated mesh substrates in PBS at 37 °C. Figure 6.2 reveals peptide release to occur over a period of approximately three weeks (~210 pmol/cm^2 of peptide $\mathbf{1}_{FL}$ was released over the first 24 h, with ~350 pmol/cm^2 released over the course of the first 24 days). This period of release was followed by a plateau, after which very little of the peptide (~0.56 pmol/cm^2 per day) was released. This general behavior is consistent with the release profiles of other small molecules from PLGA-based polymer/drug matrices *(53)*, including similar PLGA electrospun nanofiber-based materials *(57, 58)*.

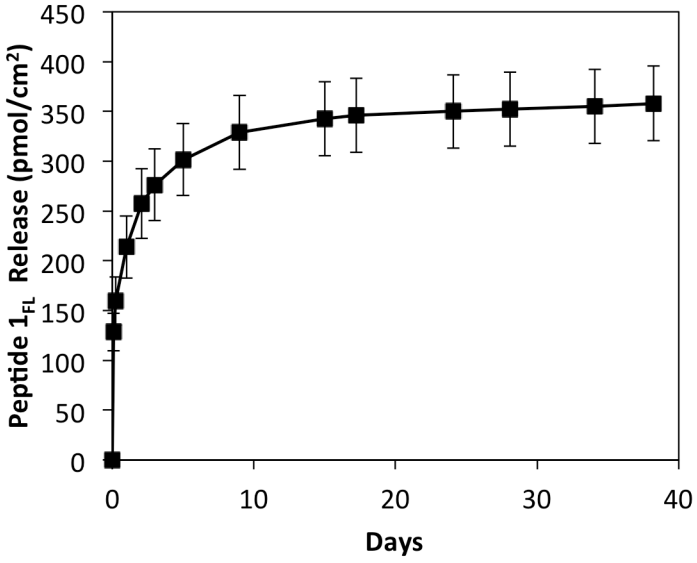


Figure 6.2: Plot showing the release of peptide $\mathbf{1_{FL}}$ from PLGA nanofiber mats versus time upon incubation in PBS at 37 ºC. Each point represents the mean values obtained from four different replicates with error bars representing standard error. Total release is normalized to the surface area of the fiber-coated substrates used in these experiments.

Upon more extended incubation, we visually observed segments of the nanofibers to detach from the mats (we note that at least some portion of this mass loss was likely promoted by repeated stresses associated with the physical manipulation and transfer of these fiber-coated substrates during experiments designed to characterize release profiles). In view of these observations, we restricted proof of concept characterization of the biological activities of QSI-loaded coatings in the studies described below to periods of no more than 14 days, over which no potentially confounding mass loss was observed. Notably, this shorter time frame is relevant in the context of infection control, and the amounts of peptide released during this 14-day period (Figure 6.2) were substantially higher than those needed to inhibit QS in *S. aureus* using peptide **1** (IC_{50} of 0.485 nM in group I *S. aureus (15)*; as described below).

6.3.3 QSI-Loaded Nanofiber Mats Inhibit QS in S. aureus

One potential limitation of peptide **1** in the context of integration into materials-based

strategies for extended release in aqueous environments is that this QSI contains a water-labile thioester bond that maintains the peptide in a macrocyclic conformation that is critical to its biological activity *(16, 59, 60)*. Hydrolysis of this thioester bond renders peptide **1** completely inactive as a QSI and occurs with a half-life of ~72 h at neutral pH *(61)* (and with a half-life of ~4 h in alkaline media *(61)*). In past studies, we demonstrated that embedding this peptide in extremely non-wetting 'superhydrophobic' coatings that limit contact between the peptide and bulk water can preserve the biological activities of peptide **1** (e.g., the ability to inhibit QS and regulate biofilm formation in *S. aureus*) for at least 40 days *(24)*. Past studies establish, however, that the transport of bulk water into PLGA matrices occurs rapidly *(53, 62)*. Thus, although the total amount of fluorescent peptide released in the above experiments was high relative to the IC_{50} of peptide **1**, it was not clear at the outset of these studies (because no distinction between intact and hydrolyzed peptide is made in the fluorescence detection method) that this PLGA-based approach could be used to sustain the release of biologically-active peptide in quantities sufficient to inhibit QS.

To determine whether peptide was released from QSI-loaded PLGA fiber mats in a bioactive form following electrospinning and incubation in aqueous environments, we conducted a series of experiments in which aliquots of released peptide were collected at pre-determined time points and incubated with cultures of group-I *S. aureus*. In initial experiments, we used a reporter strain of *S. aureus* that produces GFP when QS is activated *(63)*, thus permitting quantification of QSI-induced reductions in QS by fluorometry. These and all other biological studies reported here were performed using PLGA nanofiber mats loaded with peptide **1**; fibers loaded with peptide $\mathbf{1_{FL}}$ were not used in these experiments because this fluorescently-labeled derivative has a lower activity than peptide **1** and the presence of the fluorescein tag would complicate the characterization and quantification of GFP production. We used an experimental design in which strips of nanofiber-coated substrates were incubated initially in PBS for a defined period, and then incubated in assay media during the 24 h immediately prior to

characterization of biological activity (see Materials and Methods for additional details related to these biological assays). This overall experimental design permitted characterization of the biological activity of only that peptide released during the most recent preceding 24-hour period.

Figure 6.3 shows a plot of percent fluorescence, relative to results obtained using media alone (black bars), in cultures of *S. aureus* incubated with aliquots collected from nanofiber-

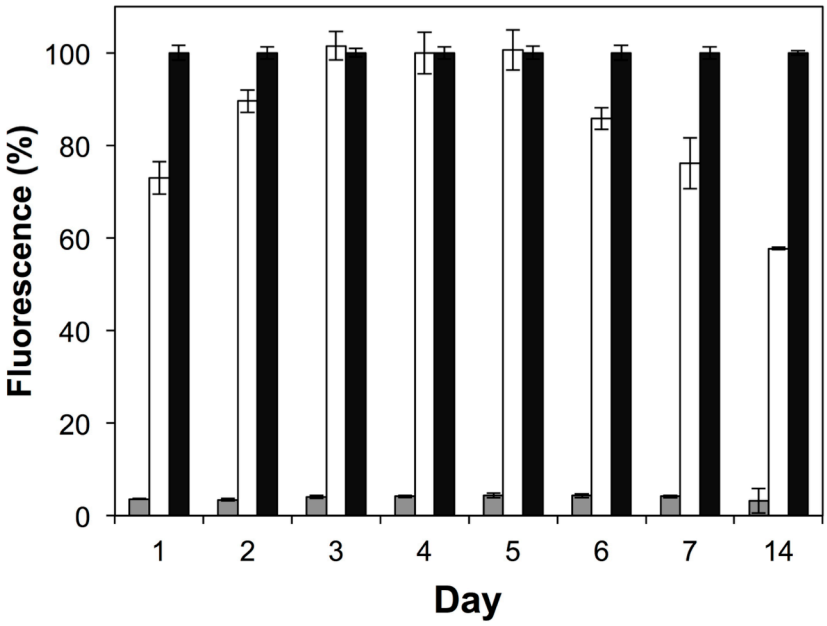


Figure 6.3: Plot showing the fluorescence of a GFP reporter strain of *S. aureus*, normalized to positive media controls, versus time for the incubation of substrates coated with nanofiber mats (see main text for additional details). Gray bars show the average normalized fluorescence for peptide **1**-loaded PLGA nanofiber mats; white bars show average normalized fluorescence for control PLGA nanofiber mats (no peptide); black bars show average normalized fluorescence for positive media controls. All experiments were performed in three sets of four replicates; error bars represent standard error. All results obtained for peptide-loaded nanofiber mats were significant at the 95% confidence interval ($p < 0.05$) versus control PLGA mats and positive media controls.

coated substrates for up to 14 days of incubation. Inspection of these results reveals samples obtained from peptide **1**-loaded mats (gray bars) to inhibit the production of GFP by >95% at all time points [in contrast, levels of GFP production were >70% for at least 7 days in experiments conducted using otherwise identical PLGA-only nanofiber mat control that were free of peptide **1** (white bars)]. Further, bacterial cultures incubated with samples obtained from the incubation of peptide **1**-loaded mats exhibited no decrease in optical density (OD_{600}) over these time periods

(see Figure 6.6 of the Supplementary Information), suggesting that, as expected, neither the peptidic QSI nor the PLGA have biocidal effects. These results, when combined, demonstrate that this degradable nanofiber approach can be used to sustain the release of peptide **1** in a form that remains biologically active, and at concentrations that are able to strongly inhibit QS in a model *S. aureus* strain, after incubation in bulk aqueous media for at least 14 days. These results also hint that the hydrolysis of the thioester bond in peptide **1**, which, as noted above, is critical to its biological activity, may occur more slowly upon exposure to water than it does when dissolved in pH neutral media. Although additional analyses will be required to understand processes that could lead to the inactivation of peptide **1** upon incorporation or long-term encapsulation in these materials, it is possible that the preservation of biological activity observed here could be aided, at least in part, by the presence of an acidic microclimate in the PLGA nanofiber matrix (which has been demonstrated in past studies to stabilize or prolong the activities of other hydrolytically-labile agents under certain conditions) *(64-66)*.

6.3.4 QSI-Loaded Nanofiber Mats Inhibit QS-Controlled Hemolysis in Solution and at Surfaces

Further studies demonstrated that, in addition to being able to inhibit the artificial QS reporter system described above, these QSI-loaded nanofiber mats are also capable of modulating QS phenotypes relevant to *S. aureus* virulence in wild-type cells. As noted above, inhibition of AgrC receptor activity has been demonstrated to inhibit the production of many toxins that play important roles in infection. One particularly salient AgrC-controlled phenotype of *S. aureus* is the production of hemolysins (e.g., alpha-toxin), which promote extensive lysis of mammalian host red blood cells *(67-69)*. Hemolysin production can be readily monitored using straightforward and robust assays in the laboratory, and we have previously shown that peptide **1** can strongly inhibit hemolysin production in prior studies *(15)*. We thus chose to characterize the ability of our peptide **1**-loaded nanofiber mats to prevent or reduce hemolysis of red blood cells as a first proof-of-concept experiment to demonstrate the ability of these materials to block

an AgrC-controlled QS phenotype. We first investigated the potential of our peptide **1**-loaded mats to inhibit hemolysis using a liquid culture assay. Using an experimental design similar to that used in the GFP-reporter assays described above, we incubated wild-type *S. aureus* in media obtained during peptide **1** release experiments for 6 hr before using those cells in quantitative solution-based red blood cell hemolysis assays. As shown in Figure 6.4A, hemolysis was inhibited, relative to media controls, by an average of 65% over a period of 14 days (gray bars). In comparison, PLGA-only (no peptide) control samples promoted an average inhibition of ~7% under otherwise identical conditions (white bars). The differences in the levels of inhibition exhibited by the peptide **1**- loaded mats relative to these PLGA controls was statistically significant ($p < 0.05$; 95% confidence interval) at all time points. It is likely that these levels of inhibition could be improved further by manipulation of peptide loading levels or through changes to polymer structure or electrospinning parameters to tune release profiles; further optimization of this solution-based analytical assay was not pursued as part of the proof of concept studies reported here. In addition, we note that, as observed during the GFP assays above, bacterial densities (OD_{600} values) did not change significantly during these experiments (see Figure 6.7 of the Supplementary Information). On the basis of these results, we again conclude that the decreases in hemolytic activity observed in Figure 6.4A are the result of the inhibition of agr-type QS by the released peptide, and not a result of cell death.

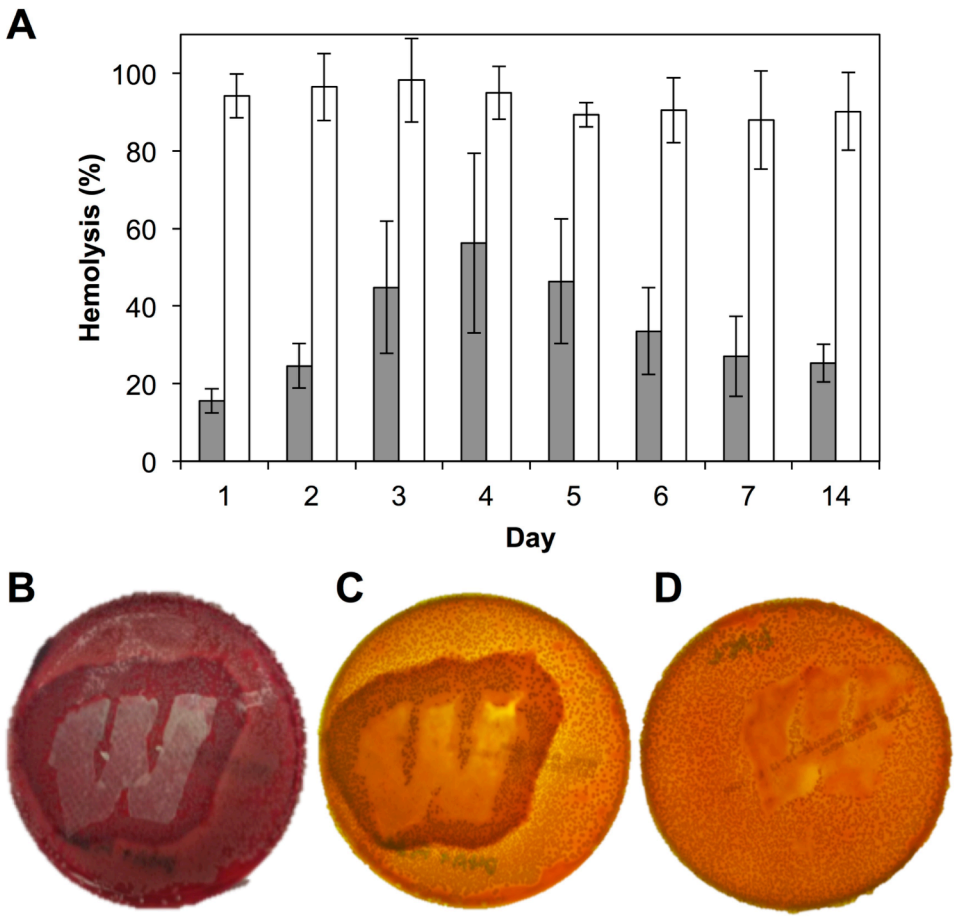


Figure 6.4: Inhibition of hemolysis by group-I *S. aureus* promoted by QSI released from substrates coated with electrospun PLGA nanofiber mats. (A) Inhibition of hemolysis by *S. aureus* in liquid-culture assays over 14 days. Gray bars: peptide **1**-loaded mats; white bars: control PLGA nanofiber mats (no peptide). Data are presented as averages of three biological replicates; error bars represent standard error. All results were significant at the 95% confidence interval ($p < 0.05$). (B-D) Representative images of hemolysis inhibition as observed on a solid blood agar plate inoculated with *S. aureus*. (B) Zone of hemolysis inhibition (dark red) observed around a non-woven substrate coated with a peptide **1**-loaded mat; photographed from above under ambient lighting; the lighter red background indicates active hemolysis by *S. aureus* colonies in areas not adjacent to the substrate. (C) The same plate as in (B), but photographed when backlit to enhance contrast (see text); the yellow-orange background indicates active hemolysis by *S. aureus* colonies in areas not adjacent to the substrate. (D) No inhibition of hemolysis was observed in experiments using an otherwise identical uncoated mesh substrate; the plate was also photographed when backlit for clarity.

To supplement the liquid culture hemolysis assay, we also characterized the ability of our QSI-loaded nanofiber coatings to inhibit hemolysis by wild-type *S. aureus* when placed in direct contact with each other on a surface, thus better mimicking interactions that would occur between bacteria and a nanofiber coating at an infection site. To test for this function, we

characterized the ability of peptide **1**-loaded mats to inhibit hemolysis in *S. aureus* grown on blood agar plates. These experiments were performed by manually placing samples of nanofiber-coated mesh substrates on top of a blood agar plate inoculated with *S. aureus* and incubating these two contacting surfaces for 24 h (see Methods for additional details). Over this time frame, *S. aureus* grows to cover the entire plate surface, reaches a (presumably) quorate population, and produces hemolysins to promote a change in the color of the underlying blood agar plate from dark red (a color indicative of intact red blood cells) to light red/orange (a color indicative of lysed red blood cells) *(70)*. This change in color can thus be used to visualize and characterize qualitative changes in the production of hemolysins by *S. aureus* growing on a solid surface *(70)*.

Figure 6.4B-D shows representative results of this assay 24 h after the incubation of inoculated blood agar plates with non-woven mesh substrates coated with peptide **1**-loaded nanofibers (B-C) or control PLGA nanofibers electrospun in the absence of peptide **1** (D). The image in panel B shows a plate imaged under normal light prior to removal of the coated substrate (approximately 2.5 x 3.8 cm, shown in white); the images in panels C and D show plates imaged using backlighting and after the removal of the coated substrate for clarity. As anticipated, we observed a zone of inhibition of hemolysis surrounding substrates coated with peptide **1**-loaded nanofibers (darker red color in Figure 6.4B and darker orange color in Figure 6.4C, corresponding to regions with intact red blood cells; the apparent differences in color in these images arise from differences in the lighting used to acquire these two images, as noted above). Beyond this zone of inhibition, the remainder of the plate was lighter in color (e.g., lighter red in Figure 6.4B and light orange/yellow color in Figure 6.4C), consistent with extensive hemolysis of the red blood cells in areas remote from the coated substrates *(70)*. The spatial extent of the zone of inhibition observed in these studies reflects, in part, the rate and extent of the lateral diffusion of peptide **1** on the surface of these agar plates after it is released from the nanofibers. In contrast, when similar experiments were performed using substrates coated with

PLGA-only (no peptide) nanofiber controls, the entire plate appeared light orange/yellow (Figure 6.4D), indicative of uniform red blood cell hemolysis in all areas surrounding the substrate. Bacterial colonies were visible on the plates, both within and around the zones of inhibition, suggesting no decreases in cell viability as a result of presence of peptide **1** (bacterial colonies were not observed in the areas directly beneath the film-coated substrates in either the peptide-loaded or the PLGA control cases under the conditions used in these assays; bacterial colonies were, however, observed to be attached to the plate-facing sides of the removed substrates, suggesting preferential growth on the nanofiber mats in those regions). When combined, these results demonstrate that peptide **1**-loaded PLGA nanofibers can be used to inhibit the production of a critical, QS-controlled virulence factor in wild-type *S. aureus*, both in liquid-culture and when placed directly in contact with bacteria growing on a soft surface. Because AgrC controls the production of numerous other virulence factors and biofilm growth in *S. aureus*, we anticipate that these peptide **1**-loaded coatings should also modulate the production of these other phenotypes, thereby expanding the potential future utility of these materials beyond the proof-of-concept results reported here.

6. 4 Summary

We have reported the fabrication, characterization, and biological evaluation of degradable polymer nanofiber mats that release potent peptide-based inhibitors of bacterial QS and promote the localized, surface-mediated inhibition of a salient, QS-controlled bacterial virulence phenotype in the pervasive human pathogen *S. aureus*. This study is, to our knowledge, the first to evaluate the use of electrospun polymer nanofiber mats for the distribution and dissemination of small-molecule or peptidic QSIs, and has implications for the development of new anti-infective materials, coatings, and treatment strategies that target bacterial virulence rather than bacterial growth. Our results demonstrate that peptide **1**, a synthetic macrocyclic QSI that is active against *S. aureus*, can be readily loaded into PLGA

nanofiber mats using conventional polymer electrospinning techniques, and that this approach can be used to readily deposit nanofiber-based coatings on the surfaces of model non-woven mesh substrates. Peptide **1** was released over a period of approximately three weeks when nanofiber mats were incubated in physiologically relevant media. Liquid-culture cell-based reporter assays revealed released peptide to retain its biological activity and strongly inhibit agr-based QS in an *S. aureus* strain containing a GFP reporter for periods of at least 14 days. We also demonstrated that these QSI-loaded nanofiber mats can inhibit the production of hemolysins, a QS-controlled phenotype in *S. aureus* that is relevant in bacterial infections *(71)*. Our results reveal that the QSIs released from these materials not only reduce levels of hemolysis in red blood cells in liquid cultures of wild-type *S. aureus*, but also strongly block hemolysis when placed in direct contact with wild-type *S. aureus* growing on the surface of a blood agar plate, an experimental geometry designed to more closely mimic interactions that would occur between bacteria and a nanofiber mat at an infection site. In view of the central role of the agr-QS system in the production of virulence factors and biofilm formation in *S. aureus*, it is likely that these materials could also modulate other associated virulence phenotypes pertinent in both acute and chronic infections.

S. aureus is a causative agent of life-threatening infections in burn wounds, diabetic ulcers, and other skin lesions, and strains of this pathogen have developed substantial resistance to conventional antibiotic treatments (e.g., MRSA) *(72)*. Our findings, and this general non-bactericidal approach to the design of anti-infective materials, are thus timely and provide a useful springboard for the continued development of new QSI-based strategies to assist in the prevention or treatment of infectious diseases. In this specific context, we note that the electrospinning approach reported here is modular, and can be used with many different types of polymers, active agents (or combinations of agents), and processing parameters to deposit nanofiber coatings with tunable physical or chemical properties on a broad range of topologically complex objects important in healthcare-related applications (including indwelling

interventional devices, implants, wound dressings, and even the surfaces of open wounds) *(43, 46-48)*. More broadly, the overall approaches and materials reported here could also provide novel porous scaffolds for bacterial cell culture useful for fundamental studies of the influence of QS modulation (either inhibition or activation) on the development of bacterial communities.

6.5 Methods

6.5.1 Materials

Poly(D,L-lactide-*co*-glycolide) (PLGA; 50:50, MW = 30,000–60,000), *N,N*-dimethylformamide (DMF; ACS reagent grade), and tetrahydrofuran (THF; HPLC grade) were purchased from Sigma-Aldrich (Milwaukee, WI) and used as received. Peptide **1** and fluorescently labeled peptide $\mathbf{1}_{\mathbf{FL}}$ were synthesized and purified as described previously *(15, 24)*. Blood agar plates (tryptic soy agar, with 5% sheep blood) were purchased from Fisher Scientific (Hanover Park, IL). Pooled rabbit blood cells were purchased from Lampire Biological Labs (Piperville, PA). Non-woven bonded carded web mesh composed of fibers of poly(ethylene terephthalate) and polyethylene (Vliesstoffwerk Sandler 12 gsm Sawabond NW Cover – Velvet; calendared) was obtained from Sandler AG (Schwarzenbach/Saale, Germany).

6.5.2 Instrumentation and Related Considerations

Fluorescence microscopy images were acquired using an Olympus IX70 microscope and analyzed using the Metavue version V7.7.8.0 software package (Molecular Devices). Top-down scanning electron micrographs were acquired using a LEO-1550 VP field-emission SEM operating with an accelerating voltage of 2.00 kV. Samples were coated with a thin layer of gold using a Hummer Junior Sputtering (Technics) system operating at 10 mA under a vacuum pressure of 70 mTorr for 60 s prior to imaging. Fiber diameters were measured using the ImageJ version 1.49r software package. Solution fluorescence was measured using a Jobin Yvon FluoroMax-3 fluorometer with DataMax version 2.2 software. A Biotek Synergy 2

microplate reader with Gen5 software was used to measure the absorbance and fluorescence of bacterial cultures.

6.5.3 Biological Reagents and Strain Information

All biological reagents, with the exception of Brain-Heart Infusion (BHI) medium, were purchased from Sigma-Aldrich and used according to enclosed instructions. *S. aureus* strains AH1677 (methicillin-resistant group-I with a P3-*gfp* reporter plasmid) and RN6390B (wild-type group-I) were grown in BHI medium purchased from Teknova (Hollister, CA). Bacterial cultures were grown in a standard laboratory incubator at 37 ºC with shaking (200 rpm) unless otherwise noted.

6.5.4 Fabrication of Non-Woven Nanofiber Mats

A 300 mg/mL solution of PLGA was prepared using a THF:DMF solvent mixture (3:1, v/v) and stirred overnight. For fabrication of nanofibrous mats containing peptide **1** or peptide $\mathbf{1}_{\mathbf{FL}}$, these solutions were prepared using DMF having a 1 mM concentration of the peptide instead of neat DMF. Electrospinning was conducted using a custom-built electrospinning device with a digital syringe pump (Harvard Bioscience Company) at a flow rate of 0.2 mL/h. A 15 cm working distance separated the blunt 20G needle and the 10 x 10 cm grounded collector covered with the non-woven mesh substrate. A 20 kV potential was applied between the needle tip and collector. All materials used in release experiments were fabricated by electrospinning 0.25 mL of solution. The resulting electrospun mats were stored in the dark at room temperature until further use.

6.5.5 Characterization of Peptide Release Kinetics

Experiments used to characterize the release of imbedded peptides were conducted using PLGA mats containing peptide $\mathbf{1}_{\mathbf{FL}}$. Strips of non-woven mesh coated with electrospun

nanofibers (0.8 x 2.0 cm; 1.6 cm^2) were incubated in 1 mL of PBS buffer (pH = 7.4) at 37 °C. At designated time points, the buffer was removed for analysis and replaced with fresh buffer. Removed buffer was briefly centrifuged to pellet and remove any solid polymer debris that may have dislodged from the mats and could complicate analysis of the peptide release. Concentrations of released peptide $\mathbf{1}_{FL}$ were measured using a fluorometer. All release experiments were conducted with n = 4.

6.5.6 Release of Peptides for Liquid Culture Assays

Characterization of the biological activities of released peptides was conducted using PLGA mats containing peptide **1**. Small strips of non-woven mesh coated with electrospun nanofibers (0.6 x 1.5 cm; 0.9 cm^2) were cut and UV sterilized by exposure to UV light for 15 min in a biological safety cabinet. In the 24 h immediately prior to a designated time point in the biological assay, the strips were incubated statically in 500 µL of either BHI media (for GFP reporter assays) or Tryptic Soy Broth media (TSB; for hemolysis assays) at 37 °C. At all other times prior to the 24 h period before a measured time point, the strips were maintained statically in 500 µL of 7.4 pH 1x PBS buffer at 37 °C. PLGA mats fabricated without peptide **1** were used as controls for the biological assays. Each release experiment was conducted with n = 4, and three release experiments were performed for each biological assay to generate three biological replicates. All manipulations of sterilized samples were performed using flame-sterilized forceps.

6.5.7 GFP Reporter Assays

GFP reporter assays in *S. aureus* were performed using our previously reported protocol *(15)*. In brief, an overnight culture of the GFP-reporter strain *S. aureus* AH1677 *(63)* was diluted 1:50 to a total volume of 200 µL with BHI medium used in peptide release experiments and placed into the wells of a black 96-well polystyrene microtiter plate (Costar). Dilution with fresh BHI medium was used as a control. The plates were incubated at 37 °C for 24 h with shaking.

The fluorescence and OD_{600} of each well were then measured using a plate reader, with fluorescence values normalized to the fresh BHI control.

6.5.8 Hemolysis Assays

For liquid culture hemolysis assays, an overnight culture of the wild-type strain *S. aureus* RN6390B was diluted 1:100 to a total volume of 200 µL with TSB medium used in peptide release experiments and placed into the wells of a clear 96-well polystyrene microtiter plate (Costar). Dilution with fresh TSB medium was used as a control. The plates were incubated statically at 37 °C for 6 h, and OD_{600} values were then measured using a plate reader. A 13 µL aliquot of rabbit red blood cells (10%, suspended in PBS) was then added to each well, and the plate was incubated statically at 37 °C for 15 min. The plate was centrifuged at 2000 rpm at room temperature for 4 min, and a 150 µL aliquot of the supernatant from each well was transferred to wells of a clean, clear 96-well plate to measure absorbance at 420 nm using a plate reader. For blood agar plate assays, an overnight culture of *S. aureus* RN6390B was diluted 1:$2x10^5$ with fresh BHI. A 500 µL aliquot of the diluted culture was added to the blood agar plate and spread evenly over the surface using a sterilized Pasteur pipette that was bent at a 90° angle using a flame. Segments of non-woven mesh coated with electrospun nanofibers, fabricated both with and without peptide **1**, were UV sterilized for 15 min and placed on top of the agar plate such that the nanofiber-coated side was facing the agar surface. The agar plate was then incubated at 37 °C for 24 h, after which digital images of the plate were acquired.

6.6 Supplementary Information

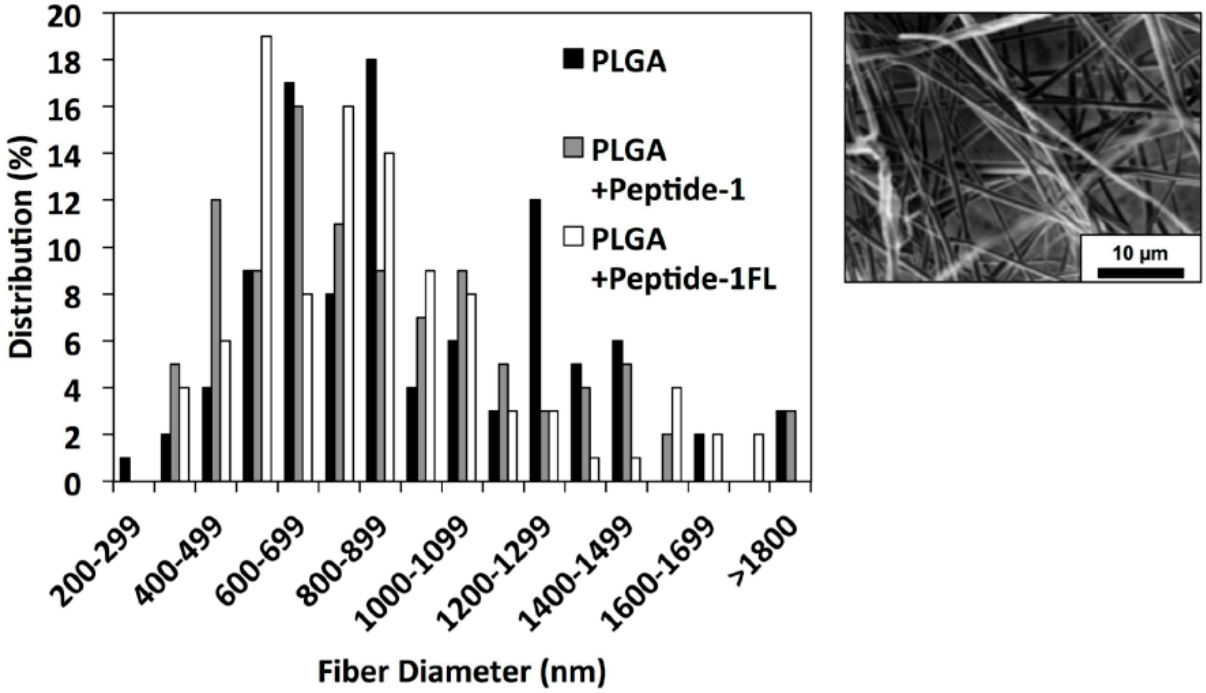


Figure 6.5: (Left) Histogram showing the distribution of fiber diameters for samples of electrospun nanofiber mats, showing results for: PLGA nanofibers alone (no peptide; black), peptide 1-loaded nanofibers (gray), and nanofibers loaded with peptide 1_{FL} (white); the number of fibers characterized in each case was 100). These results show that the distribution of diameters is roughly similar for each experimental condition evaluated in this study. (Right) Representative SEM image of control PLGA nanofibers (no peptide), revealing a non-woven, nanofibrous morphology similar to those of mats produced using solutions of PLGA and either peptide 1 or peptide 1_{FL} (see main text).

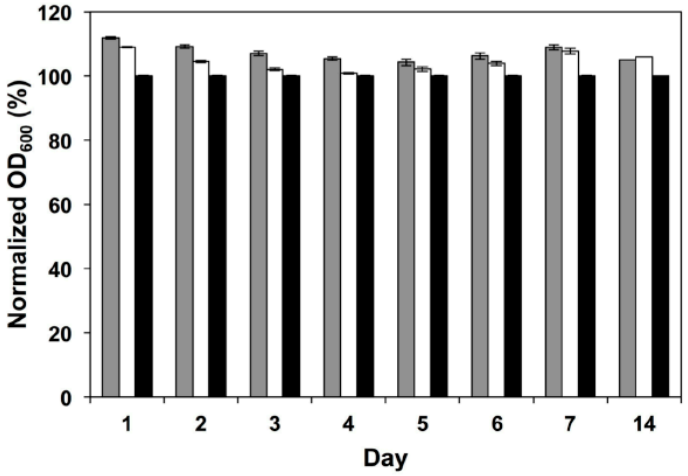


Figure 6.6: Plot showing the optical densities of bacterial cultures in the GFP reporter assays used to obtain the results shown in Figure 6.3 of the main text. Results were obtained following treatment with samples collected during the incubation of peptide 1-loaded mats (gray bars) or control PLGA mats (no peptide; white bars) and are shown normalized to culture media controls (black bars); error bars represent standard error.

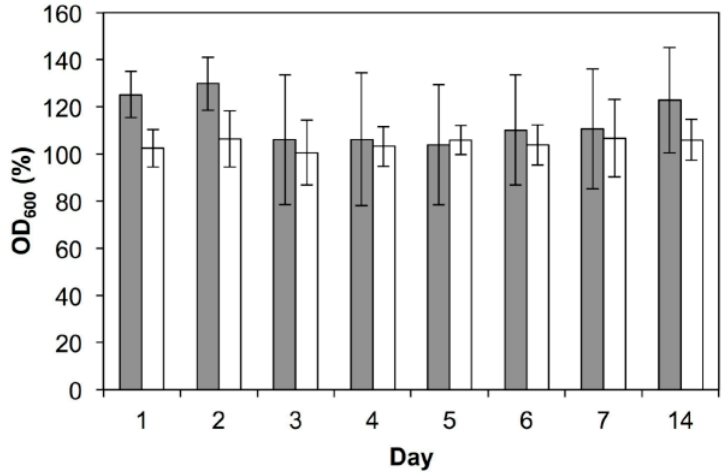


Figure 6.7: Plot showing the optical densities of bacterial cultures in the liquid-phase hemolysis inhibition assays used to obtain the results shown in Figure 6.4A of the main text. Results were obtained following treatment with samples collected during the incubation of peptide 1-loaded mats (gray bars) or control PLGA mats (no peptide; white bars); error bars represent standard error.

6.7 Acknowledgments

Financial support for this work was provided by the Office of Naval Research (N00014-16-1-2185), the NSF (through a grant to the UW-Madison Materials Research Science and Engineering Center; MRSEC; DMR-1121288), and the Burroughs Wellcome Fund, and made use of NSF-supported facilities (DMR-1121288). M. J. K. acknowledges the UW-Madison Biotechnology Center for a Morgridge Biotechnology Fellowship. T. Y. acknowledges support from the UW-Madison NIH Biotechnology Training Program (T32 GM08349). We thank Prof. Tom Turng for providing access to electrospinning instrumentation, and acknowledge support for those facilities provided by the Wisconsin Institutes of Discovery and the Vice Chancellor for Research and Graduate Education at UW-Madison. We also thank Dr. Matthew C. D. Carter for assistance with the acquisition of SEM images of nanofiber mats, and Eric Codner for assistance with the laser cutting of substrates used in hemolysis blood agar assays.

6.8 References

1. Percival, S. L., Suleman, L., Vuotto, C., and Donelli, G. (2015) Healthcare-associated infections, medical devices and biofilms: risk, tolerance and control, *J. Med. Microbiol. 64*, 323-334.

2. Hall-Stoodley, L., Costerton, J. W., and Stoodley, P. (2004) Bacterial biofilms: From the natural environment to infectious diseases, *Nat. Rev. Microbiol. 2*, 95-108.

3. Wu, P., and Grainger, D. W. (2006) Drug/device combinations for local drug therapies and infection prophylaxis, *Biomaterials 27*, 2450-2467.

4. Hetrick, E. M., and Schoenfisch, M. H. (2006) Reducing implant-related infections: active release strategies, *Chem. Soc. Rev. 35*, 780-789.

5. Zilberman, M., and Elsner, J. J. (2008) Antibiotic-eluting medical devices for various applications, *J. Control. Release 130*, 202-215.

6. Wright, G. D. (2012) The origins of antibiotic resistance, *Handbook of experimental pharmacology*, 13-30.

7. Walsh, C. T., and Wright, G. D. (2009) Antimicrobials, *Curr. Opin. Microbiol. 12*, 473-475.

8. Ventola, C. L. (2015) The antibiotic resistance crisis: part 1: causes and threats, *P. T. 40*, 277-283.

9. Rasko, D. A., and Sperandio, V. (2010) Anti-virulence strategies to combat bacteria-mediated disease, *Nat. Rev. Drug Disc. 9*, 117-128.

10. Curtis, M. M., Russell, R., Moreira, C. G., Adebesin, A. M., Wang, C., Williams, N. S., Taussig, R., Stewart, D., Zimmern, P., Lu, B., Prasad, R. N., Zhu, C., Rasko, D. A., Huntley, J. F., Falck, J. R., and Sperandio, V. (2014) QseC inhibitors as an antivirulence approach for Gram-negative pathogens, *mBio 5*, e02165.

11. Rutherford, S. T., and Bassler, B. L. (2012) Bacterial quorum sensing: its role in virulence and possibilities for its control, *Cold Spring Harbor perspectives in medicine 2*, a012427.

12. Njoroge, J., and Sperandio, V. (2009) Jamming bacterial communication: New approaches for the treatment of infectious diseases, *EMBO Mol. Med. 1*, 201-210.

13. Cegelski, L., Marshall, G. R., Eldridge, G. R., and Hultgren, S. J. (2008) The biology and future prospects of antivirulence therapies, *Nat. Rev. Microbiol. 6*, 17-27.

14. Clatworthy, A. E., Pierson, E., and Hung, D. T. (2007) Targeting virulence: a new paradigm for antimicrobial therapy, *Nat. Chem. Biol. 3*, 541-548.

15. Tal-Gan, Y., Stacy, D. M., Foegen, M. K., Koenig, D. W., and Blackwell, H. E. (2013) Highly Potent Inhibitors of Quorum Sensing in *Staphylococcus aureus* Revealed

Through a Systematic Synthetic Study of the Group-III Autoinducing Peptide, *J. Am. Chem. Soc. 135*, 7869–7882.

16. Wang, B., and Muir, T. W. (2016) Regulation of Virulence in *Staphylococcus aureus*: Molecular Mechanisms and Remaining Puzzles, *Cell chemical biology 23*, 214-224.

17. Sully, E. K., Malachowa, N., Elmore, B. O., Alexander, S. M., Femling, J. K., Gray, B. M., DeLeo, F. R., Otto, M., Cheung, A. L., Edwards, B. S., Sklar, L. A., Horswill, A. R., Hall, P. R., and Gresham, H. D. (2014) Selective chemical inhibition of agr quorum sensing in *Staphylococcus aureus* promotes host defense with minimal impact on resistance, *PLOS Pathog. 10*, e1004174.

18. Welsh, M. A., Eibergen, N. R., Moore, J. D., and Blackwell, H. E. (2015) Small Molecule Disruption of Quorum Sensing Cross-Regulation in *Pseudomonas aeruginosa* Causes Major and Unexpected Alterations to Virulence Phenotypes, *J. Am. Chem. Soc. 137*, 1510-1519.

19. O'Loughlin, C. T., Miller, L. C., Siryaporn, A., Drescher, K., Semmelhack, M. F., and Bassler, B. L. (2013) A quorum-sensing inhibitor blocks *Pseudomonas aeruginosa* virulence and biofilm formation, *Proc. Natl. Acad. Sci. U.S.A. 110*, 17981-17986.

20. Stacy, D. M., Welsh, M. A., Rather, P. N., and Blackwell, H. E. (2012) Attenuation of quorum sensing in the pathogen *Acinetobacter baumannii* using non-native N-Acyl homoserine lactones, *ACS Chem. Biol. 7*, 1719-1728.

21. Breitbach, A. S., Broderick, A. H., Jewell, C. M., Gunasekaran, S., Lin, Q., Lynn, D. M., and Blackwell, H. E. (2011) Surface-mediated release of a synthetic small-molecule modulator of bacterial quorum sensing: gradual release enhances activity, *Chem. Commun. 47*, 370-372.

22. Broderick, A. H., Breitbach, A. S., Frei, R., Blackwell, H. E., and Lynn, D. M. (2013) Surface-mediated release of a small-molecule modulator of bacterial biofilm formation: a non-bactericidal approach to inhibiting biofilm formation in *Pseudomonas aeruginosa*, *Advanced healthcare materials 2*, 993-1000.

23. Broderick, A. H., Stacy, D. M., Tal-Gan, Y., Kratochvil, M. J., Blackwell, H. E., and Lynn, D. M. (2014) Surface Coatings that Promote Rapid Release of Peptide-Based AgrC Inhibitors for Attenuation of Quorum Sensing in *Staphylococcus aureus*, *Advanced healthcare materials 3*, 97-105.

24. Kratochvil, M. J., Tal-Gan, Y., Yang, T., Blackwell, H. E., and Lynn, D. M. (2015) Nanoporous Superhydrophobic Coatings that Promote the Extended Release of Water-Labile Quorum Sensing Inhibitors and Enable Long Term Modulation of Quorum Sensing in *Staphylococcus aureus*, *ACS Biomat. Sci. Eng. 1*, 1039-1049.

25. Kratochvil, M. J., Welsh, M. A., Manna, U., Ortiz, B. J., Blackwell, H. E., and Lynn, D. M. (2016) Slippery Liquid-Infused Porous Surfaces that Prevent Bacterial Surface Fouling and Inhibit Virulence Phenotypes in Surrounding Planktonic Cells, *ACS Infect. Dis. 2*, 509-517.

26. Hume, E. B. H., Baveja, J., Muir, B. W., Schubert, T. L., Kumar, N., Kjelleberg, S., Griesser, H. J., Thissen, H., Read, R., Poole-Warren, L. A., Schindhelm, K., and Willcox, M. D. P. (2004) The control of *Staphylococcus epidermidis* biofilm formation and in vivo infection rates by covalently bound furanones, *Biomaterials 25*, 5023-5030.

27. Baveja, J. K., Wilcox, M. D. P., Hume, E. B. H., Kumar, N., Odell, R., and Poole-Warren, L. A. (2004) Furanones as potential anti-bacterial coatings on biomaterials, *Biomaterials 25*, 5003-5012.

28. Melander, C., Moeller, P. D. R., Ballard, T. E., Richards, J. J., Huigens, R. W., III, and Cavanagh, J. (2009) Evaluation of dihydrooroidin as an antifouling additive in marine paint, *Int. Biodeterior. Biodegradation 63*, 529-532.

29. Ho, K. K. K., Cole, N., Chen, R., Willcox, M. D. P., Rice, S. A., and Kumar, N. (2010) Characterisation and in vitro activities of surface attached dihydropyrrol-2-ones against Gram-negative and Gram-positive bacteria, *Biofouling 26*, 913-921.

30. Ho, K. K. K., Chen, R., Willcox, M. D. P., Rice, S. A., Cole, N., Iskander, G., and Kumar, N. (2014) Quorum sensing inhibitory activities of surface immobilized antibacterial dihydropyrrolones via click chemistry, *Biomaterials 35*, 2336-2345.

31. Nowatzki, P. J., Koepsel, R. R., Stoodley, P., Min, K., Harper, A., Murata, H., Donfack, J., Hortelano, E. R., Ehrlich, G. D., and Russell, A. J. (2012) Salicylic acid-releasing polyurethane acrylate polymers as anti-biofilm urological catheter coatings, *Acta Biomater. 8*, 1869-1880.

32. Gomes, J., Grunau, A., Lawrence, A. K., Eberl, L., and Gademann, K. (2013) Bioinspired, releasable quorum sensing modulators, *Chem. Commun. 49*, 155-157.

33. Nafee, N., Husari, A., Maurer, C. K., Lu, C., de Rossi, C., Steinbach, A., Hartmann, R. W., Lehr, C.-M., and Schneider, M. (2014) Antibiotic-free nanotherapeutics: Ultra-small, mucus-penetrating solid lipid nanoparticles enhance the pulmonary delivery and anti-virulence efficacy of novel quorum sensing inhibitors, *J. Control. Release 192*, 131-140.

34. Shenderovich, J., Feldman, M., Kirmayer, D., Al-Quntar, A., Steinberg, D., Lavy, E., and Friedman, M. (2015) Local sustained-release delivery systems of the antibiofilm agent thiazolidinedione-8 for prevention of catheter-associated urinary tract infections, *Int. J. Pharm. 485*, 164-170.

35. Lu, H. D., Spiegel, A. C., Hurley, A., Perez, L. J., Maisel, K., Ensign, L. M., Hanes, J., Bassler, B. L., Semmelhack, M. F., and Prud'homme, R. K. (2015) Modulating *Vibrio cholerae* Quorum-Sensing-Controlled Communication Using Autoinducer-Loaded Nanoparticles, *Nano Lett. 15*, 2235-2241.

36. Wu, Y. C., Quan, X. C., and Si, X. R. (2015) Incorporation of brominated furanone into Nafion polymer enhanced anti-biofilm efficacy, *Int. Biodeterior. Biodegradation 99*, 39-44.

37. Thoendel, M., Kavanaugh, J. S., Flack, C. E., and Horswill, A. R. (2011) Peptide signaling in the staphylococci, *Chem. Rev. 111*, 117-151.

38. Wang, B. Y., and Muir, T. W. (2016) Regulation of Virulence in *Staphylococcus aureus*: Molecular Mechanisms and Remaining Puzzles, *Cell chemical biology 23*, 214-224.

39. Huang, Z. M., Zhang, Y. Z., Kotaki, M., and Ramakrishna, S. (2003) A review on polymer nanofibers by electrospinning and their applications in nanocomposites, *Compos. Sci. Technol. 63*, 2223-2253.

40. Li, D., and Xia, Y. N. (2004) Electrospinning of nanofibers: Reinventing the wheel?, *Adv. Mater. 16*, 1151-1170.

41. Greiner, A., and Wendorff, J. H. (2007) Electrospinning: A fascinating method for the preparation of ultrathin fibres, *Angew. Chem. Int. Ed. 46*, 5670-5703.

42. Zamani, M., Prabhakaran, M. P., and Ramakrishna, S. (2013) Advances in drug delivery via electrospun and electrosprayed nanomaterials, *Int. J. Nanomedicine 8*, 2997-3017.

43. Sill, T. J., and von Recum, H. A. (2008) Electrospinning: Applications in drug delivery and tissue engineering, *Biomaterials 29*, 1989-2006.

44. Chou, S. F., Carson, D., and Woodrow, K. A. (2015) Current strategies for sustaining drug release from electrospun nanofibers, *J. Control. Release 220*, 584-591.

45. Li, W. J., Laurencin, C. T., Caterson, E. J., Tuan, R. S., and Ko, F. K. (2002) Electrospun nanofibrous structure: A novel scaffold for tissue engineering, *J. Biomed. Mater. Res. 60*, 613-621.

46. Dong, R. H., Jia, Y. X., Qin, C. C., Zhan, L., Yan, X., Cui, L., Zhou, Y., Jiang, X. Y., and Long, Y. Z. (2016) In situ deposition of a personalized nanofibrous dressing via a handy electrospinning device for skin wound care, *Nanoscale 8*, 3482-3488.

47. Mele, E. (2016) Electrospinning of natural polymers for advanced wound care: towards responsive and adaptive dressings, *J. Mater. Chem. B 4*, 4801-4812.

48. Zahedi, P., Rezaeian, I., Ranaei-Siadat, S. O., Jafari, S. H., and Supaphol, P. (2010) A review on wound dressings with an emphasis on electrospun nanofibrous polymeric bandages, *Polymer. Adv. Tech. 21*, 77-95.

49. Anderson, J. M., and Shive, M. S. (1997) Biodegradation and biocompatibility of PLA and PLGA microspheres, *Adv. Drug Deliv. Rev. 28*, 5-24.

50. Ikada, Y., and Tsuji, H. (2000) Biodegradable polyesters for medical and ecological applications, *Macromol. Rapid Commun. 21*, 117-132.

51. Panyam, J., and Labhasetwar, V. (2003) Biodegradable nanoparticles for drug and gene delivery to cells and tissue, *Adv. Drug Deliv. Rev. 55*, 329-347.

52. Makadia, H. K., and Siegel, S. J. (2011) Poly Lactic-co-Glycolic Acid (PLGA) as Biodegradable Controlled Drug Delivery Carrier, *Polymers 3*, 1377-1397.

53. Fredenberg, S., Wahlgren, M., Reslow, M., and Axelsson, A. (2011) The mechanisms of drug release in poly(lactic-co-glycolic acid)-based drug delivery systems-A review, *Int. J. Pharm. 415*, 34-52.

54. Katti, D. S., Robinson, K. W., Ko, F. K., and Laurencin, C. T. (2004) Bioresorbable nanofiber-based systems for wound healing and drug delivery: Optimization of fabrication parameters, *J. Biomed. Mater. Res. Part B Appl. Biomater. 70B*, 286-296.

55. Kim, K., Luu, Y. K., Chang, C., Fang, D. F., Hsiao, B. S., Chu, B., and Hadjiargyrou, M. (2004) Incorporation and controlled release of a hydrophilic antibiotic using poly(lactide-co-glycolide)-based electrospun nanofibrous scaffolds, *J. Control. Release 98*, 47-56.

56. Luu, Y. K., Kim, K., Hsiao, B. S., Chu, B., and Hadjiargyrou, M. (2003) Development of a nanostructured DNA delivery scaffold via electrospinning of PLGA and PLA-PEG block copolymers, *J. Control. Release 89*, 341-353.

57. Puppi, D., Piras, A. M., Detta, N., Dinucci, D., and Chiellini, F. (2010) Poly(lactic-co-glycolic acid) electrospun fibrous meshes for the controlled release of retinoic acid, *Acta Biomater. 6*, 1258-1268.

58. Sofokleous, P., Stride, E., and Edirisinghe, M. (2013) Preparation, Characterization, and Release of Amoxicillin from Electrospun Fibrous Wound Dressing Patches, *Pharm. Res. 30*, 1926-1938.

59. Tal-Gan, Y., Ivancic, M., Cornilescu, G., Cornilescu, C. C., and Blackwell, H. E. (2013) Structural Characterization of Native Autoinducing Peptides and Abiotic Analogs Reveals Key Features Essential for Activation and Inhibition of an AgrC Quorum Sensing Receptor in *Staphylococcus aureus*, *J. Am. Chem. Soc. 135*, 18436-18444.

60. Thoendel, M., Kavanaugh, J. S., Flack, C. E., and Horswill, A. R. (2011) Peptide signaling in the staphylococci, *Chem. Rev. 111*, 117-151.

61. Tal-Gan, Y., Ivancic, M., Cornilescu, G., Yang, T., and Blackwell, H. E. (2016) Highly Stable, Amide-Bridged Autoinducing Peptide Analogues that Strongly Inhibit the AgrC Quorum Sensing Receptor in *Staphylococcus aureus*, *Angew. Chem. Int. Ed. 55*, 8913-8917.

62. Batycky, R. P., Hanes, J., Langer, R., and Edwards, D. A. (1997) A theoretical model of erosion and macromolecular drug release from biodegrading microspheres, *J. Pharm. Sci. 86*, 1464-1477.

63. Kirchdoerfer, R. N., Garner, A. L., Flack, C. E., Mee, J. M., Horswill, A. R., Janda, K. D., Kaufmann, G. F., and Wilson, I. A. (2011) Structural basis for ligand recognition and discrimination of a quorum-quenching antibody, *J. Biol. Chem. 286*, 17351-17358.

64. Zhu, G. Z., Mallery, S. R., and Schwendeman, S. P. (2000) Stabilization of proteins encapsulated in injectable poly (lactide-co-glycolide), *Nat. Biotechnol. 18*, 52-57.

65. Fu, K., Pack, D. W., Klibanov, A. M., and Langer, R. (2000) Visual evidence of acidic environment within degrading poly(lactic-co-glycolic acid) (PLGA) microspheres, *Pharm. Res. 17*, 100-106.

66. Shenderova, A., Burke, T. G., and Schwendeman, S. P. (1999) The acidic microclimate in poly(lactide-co-glycolide) microspheres stabilizes camptothecins, *Pharm. Res. 16*, 241-248.

67. Recsei, P., Kreiswirth, B., O'Reilly, M., Schlievert, P., Gruss, A., and Novick, R. P. (1986) Regulation of exoprotein gene expression in *Staphylococcus aureus* by agar, *Mol. Gen. Genet. 202*, 58-61.

68. Pragman, A. A., and Schlievert, P. M. (2004) Virulence regulation in *Staphylococcus aureus*: the need for in vivo analysis of virulence factor regulation, *FEMS Immunol. Med. Microbiol. 42*, 147-154.

69. George, E. A., and Muir, T. W. (2007) Molecular mechanisms of agr quorum sensing in virulent staphylococci, *Chembiochem : a European journal of chemical biology 8*, 847-855.

70. Burnside, K., Lembo, A., de los Reyes, M., Iliuk, A., BinhTran, N. T., Connelly, J. E., Lin, W. J., Schmidt, B. Z., Richardson, A. R., Fang, F. C., Tao, W. A., and Rajagopal, L. (2010) Regulation of Hemolysin Expression and Virulence of *Staphylococcus aureus* by a Serine/Threonine Kinase and Phosphatase, *PLOS One 5*, e11071.

71. Bantel, H., Sinha, B., Domschke, W., Peters, G., Schulze-Osthoff, K., and Janicke, R. U. (2001) alpha-toxin is a mediator of *Staphylococcus aureus*-induced cell death and activates caspases via the intrinsic death pathway independently of death receptor signaling, *J. Cell Biol. 155*, 637-647.

72. Tong, S. Y., Davis, J. S., Eichenberger, E., Holland, T. L., and Fowler, V. G., Jr. (2015) *Staphylococcus aureus* infections: epidemiology, pathophysiology, clinical manifestations, and management, *Clin. Microbiol. Rev. 28*, 603-661.

CHAPTER 7:

Thesis Summary and Future Directions

7.1 Summary

The common pathogens *S. aureus* and *S. epidermidis* are the leading causing agents for nosocomial infections and represent a significant burden on public health *(1-3)*. With growing concerns over the rise of antibiotic resistant and hypervirulent strains, new approaches to combating staphylococcal infections are needed *(2, 3)*. The *agr* QS systems play important roles in staphylococca*l* virulence and are likely heavily involved in colonization, making the *agr* systems attractive target for developing new anti-virulent strategies to attenuate infectivity of these pathogens *(2, 3)*. However, the roles of the *agr* systems in staphylococci are complex, and more in-depth investigations are needed to better understand these roles and to better assess the viability of the *agr* systems as a therapeutic target *(2-4)*. Chemical modulators can serve as powerful tools for such investigations, and our work summarized in this thesis contribute to the development of new and improved *agr* modulators that can be used to probe the role of QS in *S. aureus* and *S. epidermidis*.

Our SAR analyses of *S. epidermidis* native AIPs (AIP-I–III) in Chapter 2 and 4 provided the first systematic characterization of the AIP:AgrC interactions in *S. epidermidis*. Not only did we identified key residues for receptor binding and activation, we also uncovered a number of potent AgrC modulators, including the first set of potent, non-native pan-group inhibitors for AgrC receptors in *S. epidermidis*. We provided the first structural support for the SARs of *S. epidermidis* AIPs derived from the cell-based reporter assay in Chapter 3, by visualizing three-dimensional structures of agonists and antagonists of the receptor AgrC-I. The structural analyses allowed us to propose a model for AgrC-I activation and inspired us to attempt the design of pan-group agonists against all three AgrC receptors in *S. epidermidis*. As shown in Chapter 4, we successfully identified the first known pan-group agonists against all three AgrC receptors in *S. epidermidis*, and they represent, to the best of our knowledge, the first AIP analogs with this type of activity (pan-group agonism) towards the *agr* systems of a single staphylococcal species.

We also contributed to the efforts of facilitating the application of *agr* modulators in more biologically relevant settings to better study the function of the *agr* systems in *S. aureus* infections. The development of AIP analogs with enhanced hydrolytic stability and solubility, while maintaining the high inhibitory potencies typically observed for AIP-derived inhibitors, in Chapter 5 is a step forward in enabling the application of AIP-derived modulators for long-term studies of QS in *S. aureus* infections. Using a material-based approach for delivering *agr* modulators, our work in Chapter 6 provides a different avenue for applying AIP-derived *agr* modulators for future *in vivo* studies. In particular, nanofiber materials used in Chapter 6 protected the *agr* modulator from significant hydrolysis over at least 2-weeks, allowing for sustained release of bioactive compounds capable of inhibiting *agr*-regulated phenotypes in *S. aureus*.

Taken together, the *agr* modulators developed in the work summarized here, along with the material-based approach for delivering them, represent novel and valuable tools for probing the complex roles of the *agr* system in *S. aureus* and *S. epidermidis* infections and evaluating the impact of targeting QS on the infectivity of both pathogens. A number of future studies built on the work presented here can be carried out.

7.2 Development of *S. epidermidis* pan-group agonists with improved efficacy

While the pan-group agonists uncovered in Chapter 4 are novel and important for demonstrating feasibility, they are not equally effective against all three AgrC receptors in *S. epidermidis*. The set of AIP analogs designed for screening pan-group agonists in Chapter 4 were based on preliminary SARs for AIP-II and AIP-III, and were therefore limited in scope. More in-depth SAR characterization, along with structural analyses of potent AgrC-II and AgrC-III modulators, like those done with AIP-I and AgrC-I, will provide a better understanding of chemical features important to AgrC-II and AgrC-III activation. Combined with the pan-group agonism SARs described in Chapter 4, this information will allow for the design and evaluation

of additional AIP analogs that could yield more potent and effective pan-group agonists. Such compounds, in conjunction with the previously described material-based approach for delivering them, can be powerful tools for assessing the effectiveness of targeting *agr* systems for reducing biofilm growth *in vitro* and *in vivo*.

7.3 Application of QS inhibitor embedded electrospun nanofiber coatings in animal models of *S. aureus* infections.

Our work with material-based delivering of QS modulators in Chapter 6 represents a new strategy for applying QS modulators to study *S. aureus* infections. Excitingly, the nanofibers generated from the electrospinning procedure can be deposited on a variety of surfaces, including the gauze-like non-woven mesh used in our study. We envision the electrospun nanofibers coated materials being used like a dressing for wounds, and the embedded *agr* modulators can be released to limit the infectivity of *S. aureus* that might colonize the open wounds. To test this proposal, in collaboration with groups from the Veterinarian school as a part of a UW2020 project, we are actually in the process of establishing a protocol for using a mouse skin wound infection model to assess the effect of QS inhibitor loaded nanofiber coatings on the progression of *S. aureus* infections. Although the QS inhibitor currently embedded in the nanofiber coatings contains a thiolactone, we are strongly considering substituting in the more hydrolytically stable and soluble QS inhibitors that were developed in Chapter 5, as the improved properties of these inhibitors may allow for greater effect in physiological settings. We expect the results from this study to better inform us on the practicality of using AIP-derived QS inhibitors to attenuate *S. aureus* infections.

7.4 Expansion into other Gram-positive organisms

While the *agr* system in *S. aureus* is well characterized and the *agr* systems of both *S. aureus* and *S. epidermidis* have received considerable attention, *agr* systems in commensal

staphylococci and the *agr*-like systems in other Gram-positive pathogens have not been investigated as in-depth *(3, 5)*. Pathogens like *Listeria monocytogenes, Clostridium difficile, and Enterococcus faecalis* all have *agr*-like QS systems and AIP-like signals. Methods used in the work reported here can be applied to the study of the QS systems in those pathogens to better understand how their QS systems regulate virulence. Similarly, given that the commensal staphylococci of the human skin microflora can offer protection of the host from colonization of *S. aureus* and that *agr* systems may be important for colonization and competition *(3, 6, 7)*, chemical modulators of the *agr* systems in the commensal staphylococci can be valuable for evaluating the *agr* systems as a target for a probiotic approach to limit *S. aureus* infections.

7.5 References

1. Otto, M. (2009) *Staphylococcus epidermidis*--the 'accidental' pathogen, *Nat. Rev. Microbiol. 7*, 555-567.

2. Le, K. Y., and Otto, M. (2015) Quorum-sensing regulation in staphylococci-an overview, *Front. Microbiol. 6*, 1174.

3. Kavanaugh, J. S., and Horswill, A. R. (2016) Impact of Environmental Cues on Staphylococcal Quorum Sensing and Biofilm Development, *J. Biol. Chem. 291*, 12556-12564.

4. Paharik, A. E., and Horswill, A. R. (2016) The Staphylococcal Biofilm: Adhesins, Regulation, and Host Response, *Microbiol. Spectr. 4*.

5. Gray, B., Hall, P., and Gresham, H. (2013) Targeting agr- and agr-Like quorum sensing systems for development of common therapeutics to treat multiple gram-positive bacterial infections, *Sensors (Basel) 13*, 5130-5166.

6. Canovas, J., Baldry, M., Bojer, M. S., Andersen, P. S., Grzeskowiak, P. K., Stegger, M., Damborg, P., Olsen, C. A., and Ingmer, H. (2016) Cross-Talk between *Staphylococcus aureus* and Other Staphylococcal Species via the agr Quorum Sensing System, *Front. Microbiol. 7*, 1733.

7. Paharik, A. E., Parlet, C. P., Chung, N., Todd, D. A., Rodriguez, E. I., Van Dyke, M. J., Cech, N. B., and Horswill, A. R. (2017) Coagulase-Negative Staphylococcal Strain Prevents *Staphylococcus aureus* Colonization and Skin Infection by Blocking Quorum Sensing, *Cell Host Microbe 22*, 746-756 e745.

APPENDIX I:

Investigation of the Role of *agr* Interference in Competition between *Staphylococcus aureus* and *Staphylococcus epidermidis* in Lab Media

Contributions: T.Yang planned and carried out the experiments and prepared the Appendix.

H.E. Blackwell guided the research and assisted in writing.

Appendix I.1 Abstract

The *agr* QS systems in human pathogen *S. aureus* and *S. epidermidis* have been shown to play vital roles in their infectivity. Important to the activation of the *agr* system is the binding of the receptor AgrC and its cognate AIP signal. To date, four and three different receptor-signal pairs have been identified for *S. aureus* and *S. epidermidis*, respectively. These different pairs are categorized as *agr* specificity groups, and the AIP of one group can exhibit cross-group or cross-species inhibitory activities towards non-cognate AgrC receptors. This phenomenon, dubbed *agr* interference, is hypothesized to play a role in establishing infections and colonization, but the *in vivo* studies have not provided conclusive support for the hypothesis. In Chapter 2, we reported AIP analogs capable of inhibiting AgrC receptors from selective specificity groups or staphylococcal species. In Appendix I, we document the attempt to use the species-selective AgrC inhibitors to probe whether *agr* interference plays a role in competition between *S. aureus* and *S. epidermidis*. Our initial attempt shows that, in lab media, *agr* interference does not appear to have an impact. However, investigation of *agr* interference in settings where *agr* systems likely play important roles is needed to better test the hypothesis on *agr* interference.

Appendix I.2 Introduction

Quorum sensing (QS) is a process by which the bacteria sense their local population density using secreted small chemical signals and coordinate their gene expressions at high cell density *(1, 2)*. QS-regulated genes tend to be beneficial to the bacteria colony and can vary widely *(3)*. For pathogens, these genes also include virulence factors *(4)*. Consequently, QS has received considerable interest as a target for developing anti-virulence strategies to attenuate infections *(3-5)*.

The opportunistic Gram-positive pathogens *Staphylococcus aureus* and *Staphylococcus epidermidis*, the leading causative agents for nosocomial infections *(6, 7)*, also use QS for virulence regulation and establishing infections *(4, 8-10)*. The primary QS circuit in these pathogens is the accessory gene regulator (*agr*) system, which is first characterized and best studied in *S. aureus (8, 11, 12)*. Central to the activation of the *agr* system is the interaction between the peptide signal (called the autoinducing peptide, or AIP) and its cognate receptor AgrC *(8, 11, 12)*. AIP accumulates in the extracellular milieu as the population density increases. Once sufficient concentration of AIP is reached, AIP can bind effectively to AgrC and trigger the signaling cascade that leads to changes in gene expression.

A hypervariable region between the 3' end of the *agrB* gene and the 5' end of the *agrC* gene has resulted in the identification of multiple variants of the *agr* systems within a staphylococcal species, such that any strain of a staphylococcal species only uses one variant of the *agr* systems *(8)*. These variants are categorized into *agr* specificity groups based on the unique sequence of the cognate AIP. For *S. aureus*, four *agr* groups (Group I-IV) have been identified (Figure Appendix I.1A) *(8)*, while three groups (Group I-III) have been conclusively established for *S. epidermidis* (Figure Appendix I.1B) *(8, 13, 14)*. Interestingly, these *agr* systems are not completely "blind" to the non-cognate AIPs produced by other group of the same species or by a different species. Instead, cross-group or cross-species inhibitory activities are often observed for the different *agr* systems, where an AIP not only activates the cognate AgrC receptor but

also can inhibit non-cognate AgrC receptors *(8)*. Although the biological significance of this phenomenon, dubbed *agr* interference, is not well established *(8, 15, 16)*, the observations that specific *agr* groups are found to be associated with different types of infections and that staphylococcal species often colonize similar environment niches on the host has led to the hypothesis that *agr* interference plays a role in competition for colonization and establishing infections *(8, 17-19)*. More in-depth investigation is needed to better understand the physiological relevance of *agr* interference, if any. Chemical modulators capable of selectively activating or inhibiting specific *agr* systems without affecting other *agr* systems would serves as valuable tools for investigating the significance of *agr* interference.

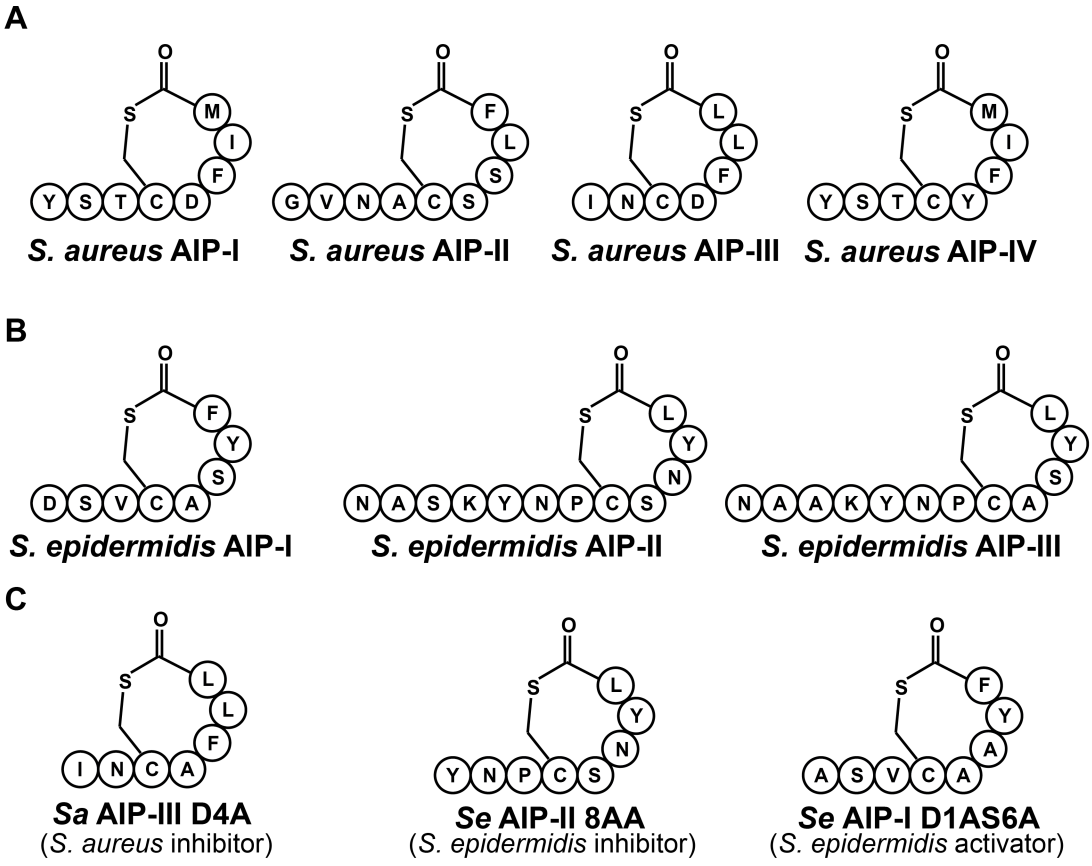


Figure Appendix I.1: Primary structures of the native AIPs identified in (A) *S. aureus* and (B) *S. epidermidis* and the (C) AIP analogs used in this work.

We recently reported the identification of a number of *S. epidermidis* AIP analogs that have shown selective inhibition of AgrC receptors from specific group in *S. epidermidis* or from specific *agr* systems in either *S. aureus* or *S. epidermidis (20)*. In the Appendix, we document our attempt to utilize the species-selective *agr* inhibitors to investigate the impact of *agr* interference on planktonic and biofilm growth of *S. aureus* and *S. epidermidis* in co-cultures of the two bacteria grown in lab media.

Appendix I.3 Results and discussion

To investigate whether *agr* interference is involved in competition between *S. aureus* and *S. epidermidis*, we set up co-culture experiments with *S. aureus* Group I and *S. epidermidis* Group I in Tryptic Soy Broth (TSB), a rich lab medium. Previous studies have shown that the *agr* system *S. aureus* Group I is inhibited by *S. epidermidis* AIP-I, but *S. epidermidis* Group I is not affected by *S. aureus* AIP-I *(17-20)*. Therefore, if *agr* interference were to play a role, we would expect growth *S. aureus* Group I to be affected by the presence of *S. epidermidis* Group I. Since *S. epidermidis* is a ubiquitous colonizer of the human skin and *S. aureus* is likely to face an established colony of *S. epidermidis* when trying to colonize the same niche *(6)*, we placed *S. aureus* Group I at an disadvantage by inoculating the co-culture experiments with a ten-fold excess of *S. epidermidis* overnight culture. We also divided the bacteria into planktonic population and biofilm population, as the *agr* system is implicated in biofilm growth, and measured the growth of each population using colony forming unit (cfu) counts. Lastly, to distinguish *S. aureus* and *S. epidermidis* from the co-cultures, we used the phenol red mannitol salt agar plate to selectively grow *S. aureus* within 24 hours and determine the cfu counts. Although *S. epidermidis* is reportedly also capable of growing on mannitol salt agar plates *(21)*, in our experience no *S. epidermidis* colonies can be detected on the agar plates after 24-hour growth at 37 °C. As an estimate of *S. epidermidis* growth, we determined the total cfu counts of

both species from the co-cultures on a TSB agar plate and substract the *S. aureus* cfu counts from the total cfu counts.

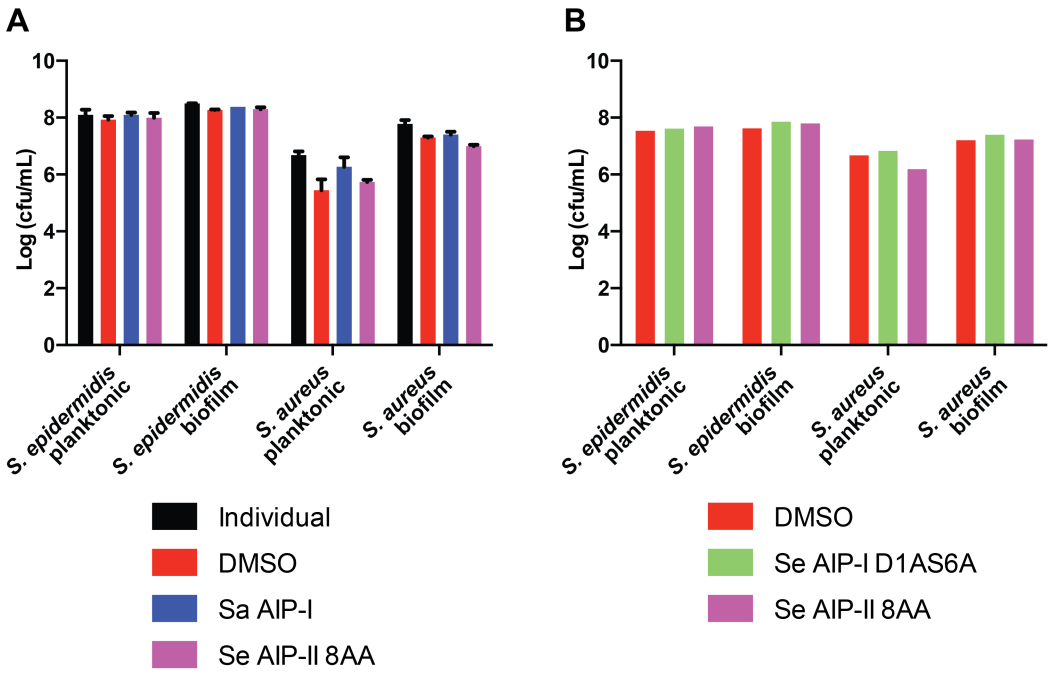


Figure Appendix I.2: Cfu counts of *S. aureus* and *S. epidermidis* planktonic and biofilm growth from co-culture experiments. (A) Co-cultures were set up by diluting *S. epidermidis* overnight culture by 1:1000 and diluting *S. aureus* overnight culture by $1:10^4$ (10-fold excess of *S. epidermidis*) with TSB. Individual = grown by itself. (B) Co-cultures were set up by diluting overnight cultures of both *S. aureus* and *S. epidermidis* by 1:1000 with TSB.

Comparison of growth of both bacteria in DMSO-treated co-culture to that of each bacterium cultured individually suggests that the planktonic growth of *S. aureus* was reduced in the co-culture, while biofilm growth was less affected (Figure Appendix I.2A). This observation is in agreement with the proposed role of the *agr* system in biofilm growth, where inhibition of the *agr* system is typically associated with stronger biofilm growth *(22)*. Since *S. epidermidis* AIP-I is an inhibitor of the *agr* system in *S. aureus* Group I, *S. aureus* Group I is more likely to form biofilm in the co-culture. In contrast, *S. epidermidis* growth is not affected by the presence of *S. aureus*. We then treated the co-culture with either an activator of *S. aureus* Group I (Sa AIP-I) or a selective inhibitor of *S. epidermidis* Group I (Se AIP-II 8AA) (Figure Appendix I.1C). In both cases, activation of the *agr* system in *S. aureus* Group I should be promoted. Although the

addition of Sa AIP-I seemed to promote more planktonic growth of *S. aureus* Group I, the inhibition of the *agr* system in *S. epidermidis* Group I did not impact the growth of *S. aureus* in the co-cultures. Regardless of the treatment with *agr* modulators, growth of *S. epidermidis* was not affected. Overall, the impact of selectively modulating the *agr* systems on bacterial growth in co-cultures is at most minimal.

Since the first set of co-culture experiments had *S. aureus* Group I at a disadvantage, we wanted to test whether *agr* systems would have an impact on bacterial growth when neither species has an advantage. To do so, we set up co-culture experiments where the same dilution of the overnight cultures of each species was used for inoculation of the co-cultures. We then treated the co-cultures with either DMSO, Se AIP-I D1AS6A an activator of the *agr* system in *S. epidermidis* (Figure Appendix I.1C), or Se AIP-II 8AA. The addition of neither the activator nor the inhibitor caused any significant difference in planktonic and biofilm growth of either species (Figure Appendix I.2B).

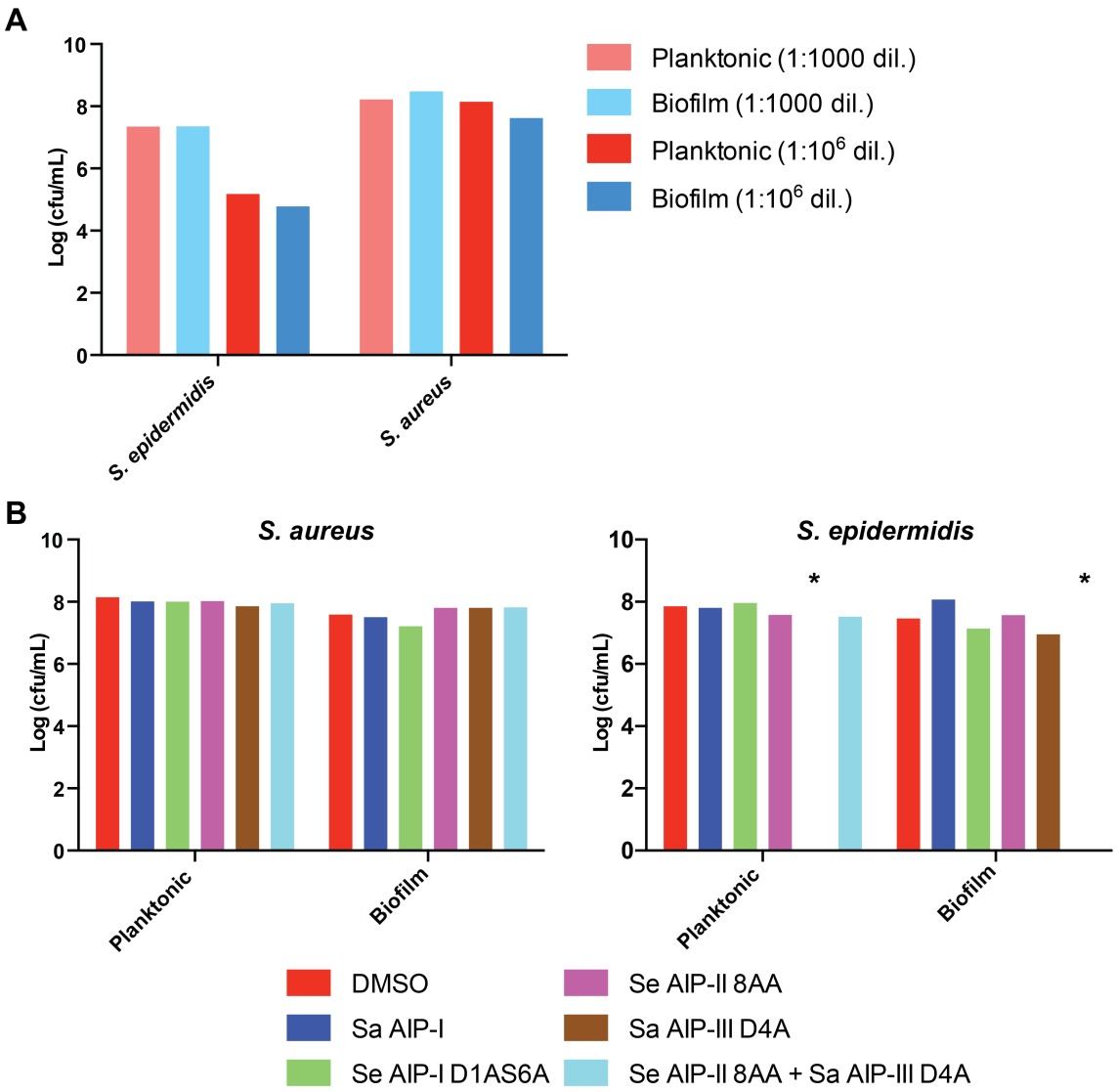


Figure Appendix I.3: Cfu counts of *S. aureus* and *S. epidermidis* planktonic and biofilm growth from co-culture experiments performed in minimal media. (A) Growth of *S. epidermidis* and *S. aureus* individually in minimal media. Two different dilutions of the overnight cultures with minimal media were performed (1:1000 and $1:10^6$). (B) Cfu counts of *S. aureus* and *S. epidermidis* from co-cultures in minimal media treated with different *agr* modulators (DMSO was included as a control). * Negative cfu counts were calculated for *S. epidermidis* and not graphed. See text for explanation.

Since TSB is nutrient rich, we reasoned that the activity of the *agr* system could be inconsequential to bacterial growth, as *agr* systems are not required for growth and nutrients are sufficiently abundant. In a minimal medium, competition for resources could be more important, and the *agr* systems could have stronger impact, especially since the *agr* systems are shown to alter expression levels of metabolic genes *(23, 24)*. Before performing co-culture experiments

with minimal media, we first examined the ability of *S. aureus* and *S. epidermidis* to grow in minimal media (Figure Appendix I.3A). While inoculating minimal media with overnight culture of *S. epidermidis* diluted at 1:1000 showed no effect on *S. epidermidis* growth, the dilution of *S. epidermidis* overnight culture into minimal media at $1:10^6$ caused a two-order of magnitude decrease in final cfu counts. Such effect was not observed for *S. aureus*. To account for the influence of minimal media on *S. epidermidis* growth, we set up the co-culture experiments by inoculating the minimal media with a 100-fold excess of the *S. epidermidis* overnight culture compared to *S. aureus* overnight culture. We then treated the co-cultures with DMSO (control), Sa AIP-I (activator for *S. aureus agr*), Se AIP-I D1AS6A (activator for *S. epidermidis agr*), Se AIP-II 8AA (selective inhibitor of *S. epidermidis agr*), Sa AIP-III D4A (selective inhibitor of *S. aureus agr*), and Se AIP-II 8aa + Sa AIP-III D4A (inhibitors of both *agr* systems). None of the treatments led to any significant change of bacterial growth in planktonic state and biofilm state for either species (Figure Appendix I.3B). The lack of *S. epidermidis* cfu counts from a couple growth conditions is due to the method of distinguishing *S. aureus* and *S. epidermidis* from co-cultures. Specifically, the cfu counts for *S. epidermidis* were estimated by subtracting cfu counts of *S. aureus*, which selectively grew on phenol red mannitol salt agar plates, from the total cfu counts of both *S. aureus* and *S. epidermidis*, which grew on TSB plates indiscriminately. Since cfu counts are not precise, negative cfu counts were calculated for *S. epidermidis* for a couple growth conditions.

Appendix I.4 Conclusion and future direction

Overall, our initial attempt of investigating the role of *agr* interference in competition between *S. aureus* and *S. epidermidis* suggested that *agr* interference did not have any impact. We would like to note, however, that our method of estimating the bacterial growth of *S. epidermidis* is inexact and is not suitable for measuring subtle differences in growth. Furthermore, we performed the co-culture experiments using either rich media or lab minimal media. Neither

growth condition necessarily requires the presence of an active *agr* system. Therefore, to better test the hypothesis of *agr* interference playing a role in the competition for colonization and establishing infections by staphylococci, experimental settings where *agr* activation is important are necessary. A recent study found an active *agr* system to be important for *S. epidermidis* colonization using a skin colonization model *(14)*. Such model would provide a better environment for assessing the effect of *agr* interference on staphylococcal competition.

Appendix I.5 Methods

All reagents were purchased from commercial sources and used according to enclosed instructions. *S. aureus* Group I strain (RN6390B) and *S. epidermidis* Group I strain (RP62A) were cultured in TSB and grown at 37 °C with shaking (200 rpm) unless noted otherwise. Co-cultures were set up by diluting overnight cultures of *S. aureus* and *S. epidermidis* with either TSB or minimal media (1X M9 salt solution, 2 mM $MgSO_4$, 0.1 mM $CaCl_2$, 1% glucose, 1% casamino acids, 1 mM thiamine-HCl, 0.5 mM nicotinamide; filter sterilized). Dilution factors are 1:1000, $1:10^4$, $1:10^5$, or $1:10^6$ depending on the experiments. Each co-culture was incubated in 35 x 10 mm petri dishes at 37 °C without shaking for 24 hours. After 24 hours, liquid culture was collected, and the petri dish was gently rinsed with 1X PBS once. The rinse was added to the liquid culture and the bacteria in the solution were labeled as planktonic population. The remaining bacteria in the petri dish were scraped off and resuspended in 2 mL of 1X PBS; these bacteria are labeled as biofilm population. Both populations were serially diluted and plated on either TSB agar plate or phenol red mannitol salt agar plate. The plates were incubated overnight and the cfus were counted. Cfu counts from phenol red mannitol salt agar plate represent bacterial growth of *S. aureus*, cfu counts from TSB agar plate represent total bacterial growth. *S. epidermidis* growth was estimated by subtracting *S. aureus* cfu counts from total cfu counts.

Appendix I.6 References

1. Waters, C. M., and Bassler, B. L. (2005) Quorum sensing: cell-to-cell communication in bacteria, *Annu. Rev. Cell Dev. Biol. 21*, 319-346.

2. Camilli, A., and Bassler, B. L. (2006) Bacterial small-molecule signaling pathways, *Science 311*, 1113-1116.

3. Popat, R., Cornforth, D. M., McNally, L., and Brown, S. P. (2015) Collective sensing and collective responses in quorum-sensing bacteria, *J. R. Soc. Interface 12*.

4. Rutherford, S. T., and Bassler, B. L. (2012) Bacterial quorum sensing: its role in virulence and possibilities for its control, *Cold Spring Harb. Perspect. Med. 2*.

5. Joint, I., Allan Downie, J., and Williams, P. (2007) Bacterial conversations: talking, listening and eavesdropping. An introduction, *Philos. Trans. R. Soc. Lond. B. Biol. Sci. 362*, 1115-1117.

6. Otto, M. (2009) *Staphylococcus epidermidis*--the 'accidental' pathogen, *Nat. Rev. Microbiol. 7*, 555-567.

7. Wang, B., and Muir, T. W. (2016) Regulation of Virulence in *Staphylococcus aureus*: Molecular Mechanisms and Remaining Puzzles, *Cell Chem. Biol. 23*, 214-224.

8. Thoendel, M., Kavanaugh, J. S., Flack, C. E., and Horswill, A. R. (2011) Peptide signaling in the staphylococci, *Chem. Rev. 111*, 117-151.

9. Gray, B., Hall, P., and Gresham, H. (2013) Targeting agr- and agr-Like quorum sensing systems for development of common therapeutics to treat multiple gram-positive bacterial infections, *Sensors (Basel) 13*, 5130-5166.

10. Le, K. Y., and Otto, M. (2015) Quorum-sensing regulation in staphylococci-an overview, *Front. Microbiol. 6*, 1174.

11. Lyon, G. J., and Novick, R. P. (2004) Peptide signaling in *Staphylococcus aureus* and other Gram-positive bacteria, *Peptides 25*, 1389-1403.

12. Novick, R. P., and Geisinger, E. (2008) Quorum sensing in staphylococci, *Annu. Rev. Genet. 42*, 541-564.

13. Carmody, A. B., and Otto, M. (2004) Specificity grouping of the accessory gene regulator quorum-sensing system of *Staphylococcus epidermidis* is linked to infection, *Arch. Microbiol. 181*, 250-253.

14. Olson, M. E., Todd, D. A., Schaeffer, C. R., Paharik, A. E., Van Dyke, M. J., Buttner, H., Dunman, P. M., Rohde, H., Cech, N. B., Fey, P. D., and Horswill, A. R. (2014) *Staphylococcus epidermidis* agr quorum-sensing system: signal identification, cross talk, and importance in colonization, *J. Bacteriol. 196*, 3482-3493.

15. Lina, G., Boutite, F., Tristan, A., Bes, M., Etienne, J., and Vandenesch, F. (2003) Bacterial Competition for Human Nasal Cavity Colonization: Role of Staphylococcal agr Alleles, *Appl. Environ. Microbiol. 69*, 18-23.

16. Fleming, V., Feil, E., Sewell, A. K., Day, N., Buckling, A., and Massey, R. C. (2006) Agr interference between clinical *Staphylococcus aureus* strains in an insect model of virulence, *J. Bacteriol. 188*, 7686-7688.

17. Otto, M., Sussmuth, R., Vuong, C., Jung, G., and Gotz, F. (1999) Inhibition of virulence factor expression in *Staphylococcus aureus* by the *Staphylococcus epidermidis* agr pheromone and derivatives, *FEBS Lett. 450*, 257-262.

18. Otto, M. (2001) *Staphylococcus aureus* and *Staphylococcus epidermidis* peptide pheromones produced by the accessory gene regulator agr system, *Peptides 22*, 1603-1608.

19. Otto, M., Echner, H., Voelter, W., and Gotz, F. (2001) Pheromone cross-inhibition between *Staphylococcus aureus* and *Staphylococcus epidermidis*, *Infect. Immun. 69*, 1957-1960.

20. Yang, T., Tal-Gan, Y., Paharik, A. E., Horswill, A. R., and Blackwell, H. E. (2016) Structure-Function Analyses of a *Staphylococcus epidermidis* Autoinducing Peptide Reveals Motifs Critical for AgrC-type Receptor Modulation, *ACS Chem. Biol. 11*, 1982-1991.

21. Parisi, J. T., and Hamory, B. H. (1986) Simplified method for the isolation, identification, and characterization of *Staphylococcus epidermidis* in epidemiologic studies, *Diagn. Microbiol. Infect. Dis. 4*, 29-35.

22. Paharik, A. E., and Horswill, A. R. (2016) The Staphylococcal Biofilm: Adhesins, Regulation, and Host Response, *Microbiol. Spectr. 4*.

23. Yao, Y., Vuong, C., Kocianova, S., Villaruz, A. E., Lai, Y., Sturdevant, D. E., and Otto, M. (2006) Characterization of the *Staphylococcus epidermidis* accessory-gene regulator response: quorum-sensing regulation of resistance to human innate host defense, *J. Infect. Dis. 193*, 841-848.

24. Queck, S. Y., Jameson-Lee, M., Villaruz, A. E., Bach, T. H., Khan, B. A., Sturdevant, D. E., Ricklefs, S. M., Li, M., and Otto, M. (2008) RNAIII-independent target gene control by the agr quorum-sensing system: insight into the evolution of virulence regulation in *Staphylococcus aureus*, *Mol. Cell 32*, 150-158.